DIRECT AND INVERSE PROBLEMS FOR THREE- DIMENSIONAL INERIOR ACOUSTIC WAVE SCATTERING

Bushra Abdul-Lateef Hassan

Department of Electronic Engineering/college of Engineering

Diyala University/ Iraq

Receiving Date: 2011/10/18 - **Accept Date:** 2012/1/30

Abstract:

The first aim of this research to solve the direct interior problem in a given region D in three space $\mathcal{R}^3$ of a non-homogeneous and homogeneous Helmholtz's equation with boundary conditions. Secondly, using the Direct Variation method which is used successfully to solve the inverse problem for determining a form of region in space $\mathcal{R}^3$ over which the Helmholtz's equation is defined or main about the solution of this equation is available in space $\mathcal{R}^3$. Numerical simulation for this case is utilized. Some of the results tabulated, indicated that the direct variation method is reliable in solving mathematical inverse problems.

المستخلص:

الهدف الاول في هذا البحث هوحل المسالة المباشرة لمعادلة Helmholtz غير المتجانسة وعلى منطقة داخلية في الفضاء الثلاثي $\mathcal{R}^3$. والثاني استخدام طرق التغاير المباشرة لحل المسالة العكسية لايجاد شكل المنطقة المعرفة عليها معادلةHelmholtz عندما تكون بعض معلومات حل المعادلة متوفرة في منطقة ما في الفضاء الثلاثي$\mathcal{R}^3$.وتمت مناقشة هذه المسالة عدديا وجدولت بعض النتائج التي توضح ان طرق التغاير تكون مناسبة جدا.

DIRECT AND INVERSE PROBLEMS FOR

THREE- DIMENSIONAL INERIOR ACOUSTIC WAVE SCATTERING

M.s. Bushra Abdul-Lateef Hassan

Introduction:

The direct interior problem which is concerned here to determine the solution of the non-homogeneous Helmholtz equation in a region D in space $\mathcal{R}^3$ with homogeneous boundary conditions. This problem can be solved by using the variation method (Ritz Method) as an inverse problem of calculus of variation [3, 4].

While the inverse interior problem that has also been considered here is to determine the shape of a region D in space R^3 in which the non-homogeneous Helmholtz equations is defined when the values of the solution of this equation are given at a finite number of a given points which lie in the unknown region and some of these points lie on its inverse problem is solved by using the direct variation method which is first used to solve an inverse eigenvalue problem, [5] and secondly used to solve the inverse acoustic scattering problem to determine a region D in space R^3, [6].In this method the problem of determining the unknown region is transformed to determine unknown parameters of the unknown region. Such parameters are determined by using a discrete form at least square approximation which named by representing a nonlinear optimization problem, the constrained Hook and Jeeves method becomes efficient in solving that problem, [1, 7].

2-The direct interior problem for Helmholtz equation with its solution

2.1 The Statement of the problem:-

Let the region D be defined in three-dimensions as:

$$D=\{(x,y,z): -a \le x \le a, -h(x) \le y \le h(x), -g(x,y) \le z \le g(x,y),\}.$$

The non-homogeneous Helmholtz equation in three-dimensions is;

$$(\nabla^2 + k^2)u = f \quad on\ region\ D \tag{1}$$

where $u : D \to \mathcal{R}, u \in C^2(D) and\ f : D \to \mathcal{R}, f \in C\ (D).$

L is a linear operator defined by:

$$\nabla^2 = \frac{\partial^2}{\partial x^2} + \frac{\partial^2}{\partial y^2} + \frac{\partial^2}{\partial z^2} \tag{2}$$

$\nabla^2$is a Laplacian in three dimensional coordinate in the interior region D k= wave number, where k^2is not an eigenvalue of the associated homogeneous problem and k^2∈R,D is a bounded regular domain in the three space (R3).

Assume that the bounded condition associated with equation (1) is

$$u = 0 \text{ on } \partial D . \tag{3}$$

The direct problem is to find the solution of equations (1) and (3) in the region D.

2.2 Variational Formulation of the problem:-

Before solving equation (1) &(3) in the region D, it is very important to mention that problem has a unique solution, since k^2 is not an eigenvalue for the associated homogeneous equation [4].

For solving this problem using the variational method (Ritz Method), it must be formulated as a variational problem. To make such formulation, first let $< u, v >$ be the symmetric, non degenerate, classical, bilinear form defined by:

$$< u, v >= \iiint_D uvdzdydx, \tag{4}$$

where $u : D \to \mathcal{R}$ and $v : D \to \mathcal{R}$.

The linear operator L in (2) is symmetric with respect to the non-degenerate classical bilinear form (4), that is to say:

$$< Lu_1, u_2 >=< Lu_2, u_1 > , \tag{5}$$

Where $u_1 = u_1(x, y, z)$ and $u_2 = u_2(x, y, z)$, both satisfying the boundary condition (3), and both belong to the domain of definition of L. Consequently, the critical points of the functional

$$J[u] = \frac{1}{2} < Lu \ , u \ >=< f, u > \tag{6}$$

are solutions of the boundary value equations [1,3] and [4].

Equation (6) can be formed as:

$$J[u] = \frac{1}{2}\iiint_D \left(u_{xx} + u_{yy} + u_{zz} + k^2u^2\right) dzdydx - \iiint_D fu \; dzdydx. \quad (7)$$

Upon using divergent theorem, and vanishing of u on the boundary, equation (7) becomes

$$J[u] = -\frac{1}{2}\iiint_D \left(u_x^2 + u_y^2 + u_z^2 - k^2u^2 + 2fu\right) dzdydx. \quad (8)$$

2.3 Solution of the variational problem:-

To find the solution of u which is the critical point of equation (8), the Ritz method will be used[3]. The procedure utilized here, can be described by using the following steps:

Step 1: The solution of u is approximated by a linear combination of elements of a complete sequence of functions $\{Q(x,y,z)\}$ defined over the region D and each function vanishes on ∂D.In other words,

$$u_N(x,y,z) = \sum_{n=1}^{N} a_n Q_n(x,y,z) \quad (9)$$

where $a_1, a_2, a_3, \ldots, a_N$ coefficients to be determined. These functions can be defined as follows

$Q_1 = (z^2, g^2(x,y), Q_2 = xQ_1, Q_3 = yQ_1, Q_4 = zQ_1, Q_5 = x^2Q_1,$
$, Q_6 = xyQ_1, , Q_7 = xzQ_1 \; , Q_8 = y^2Q_1, , , Q_9 = yzQ_1, , Q_{10} = z^2Q_1$, where $Q_i = Q_i(x,y,z)$
$\forall i = 1,2,\ldots,10.$ (10)

It should be mentioned that the above procedure can used to define other elements of the sequence of functions defined over the region D, and each of these functions vanishes along the boundary D. However, in this work N is taken to be in equation (10).

Step 2: Substituting u as given by expression (9) and its first partial derivatives with respect to x,y and z for their corresponding terms of u in equation (8), one obtains the following function for the unknown parameters a_n:

$$J[u] = -\frac{1}{2}\iiint_D \left(\left(\sum_{n=1}^{N} a_n \frac{\partial Q_n}{\partial x}\right)^2 + \left(\sum_{n=1}^{N} a_n \frac{\partial Q_n}{\partial y}\right)^2 + \left(\sum_{n=1}^{N} a_n \frac{\partial Q_n}{\partial z}\right)^2 - k^2\left(\sum_{n=1}^{N} a_n Q_n\right)^2 + 2f\sum_{n=1}^{N} a_n Q_n\right) dzdydx. \quad (11)$$

where $\bar{a} = (a_1, a_2, a_3, \dots, a_N)$, $Q_a = Q_n(x,y,z)$ $and\ f = f(x,y,z)$.

Step 3: To find the critical points of equations (10), one must determine the unknown parameters such that at such values equation (10) has a minimum value. The problem is thus reduced to find the minimum of function (10) with respect to $\bar{a}$, such problem is a non linear optimization problem. In this work it is solved by using unconstrained Hook and Jeeves method,

Step 4: Substitute the resulting values for $a_1, a_2, a_3, \dots, a_N$ from the last step in equation(9) to obtain the approximate solution $u_n(x,y,z)$ of equations (1)and(3) in the region D.

2.4 Numerical Example:

Consider the direct interior problem for Helmholtz equation that have been discussed before, let a Helmholtz equation is given by:

$$u_{xx} + u_{yy} + u_{zz} + k^2u^2 = f(x,y,z) \quad on\ region\ D$$

where

$$f(x,y,z) = 2\left(c^2 - \frac{c^2}{a^2}x^2 - \frac{c^2}{b^2}y^2\right)\left(\frac{2c^2b^2+2c^2a^2}{a^2b^2}\right) + 2\left(1 - \frac{2c^2}{a^2}x^2 - \frac{c^2}{b^2}y^2\right) + k^2\left(z + c^2 - \frac{c^2}{a^2}x^2 - \frac{c^2}{b^2}y^2\right)\left(z - c^2 - \frac{c^2}{a^2}x^2 - \frac{c^2}{b^2}y^2\right) \tag{12}$$

$a = 1; b = 1.5; c = 2\ and\ k = 2.1.$

associated with the boundary condition,

$u = 0 \ \ on\ \partial D.$

The region D in section 1.1 is used, where,

$$h(x) = \sqrt{b^2 - \left(\frac{bx}{a}\right)^2} \quad and\ g(x,y) = c^2\left(1 - \frac{1}{a^2}x^2 - \frac{1}{b^2}y^2\right) \tag{13}$$

DIRECT AND INVERSE PROBLEMS FOR

THREE- DIMENSIONAL INERIOR ACOUSTIC WAVE SCATTERING

M.s. Bushra Abdul-Lateef Hassan

A computer program is written and is used to solve the direct interior problem for Helmholtz equation which is considered above. The problem is solved by using the unconstrained Hook and Jeeves method optimization method to minimize function (10) with respect to the unknowns $a_n(n = 1,2,3,\dots,N)$ which are the coefficients of the approximate solution (9) where N=10 are tabulated below:

Table (1), The results of solution by computer program for Helmholtz's equation for different value of a,b and c. b and c

n	x_n
1	0.99927
2	0
3	-1.94289×10^{-16}
4	1.94289×10^{-16}
5	7.87×10^{4}
6	1.99429×10^{-16}
7	1.94289×10^{-15}
8	-3.89999×10^{-4}
9	0
10	8.39999×10^{-4}

3-The iInverse interior problem for Helmholtz equation in $\mathcal{R}^3$

3.1Description of the problem:-

The previous part (section 1) us devoted to the solution of the interior direct problem for Helmholtz equation in space$\mathcal{R}^3$in which the solution of the equation is found over the interior of a given region. Determination of the inverse of this problem is the region D when the solution of Helmholtz equation is given over a subset Γ (at discrete points or otherwise) of the region D. In both cases (direct and inverse) it is assumed that the solution vanishes over the boundary (known or unknown) of region D.

Before indulging in the details of the steps for finding the solution too worthwhile to mention that the unknown region may not be cubic; hence it is assumed that the boundary ∂D of the region D can be expressed by:

$$\partial D=\begin{cases} \left.\begin{matrix} y=a_1(x)\ where\ y<0 \\ y=a_2(x)\ where\ y>0 \end{matrix}\right\} for\ -a<x<a \\ \left.\begin{matrix} z=b_1(x,y)\ where\ z<0 \\ z=b_2(x,y)\ where\ z>0 \end{matrix}\right\} for\ a_1(x)<y<a_2(x) and\ -a<x<a \end{cases} \tag{14}$$

3.2Mathematical Statement of the Inverse Interior Problem of Helmholtz Equation:-

Before using the direct variational method, the boundary of the unknown region must be approximated by functions with unknown coefficients.

From the definition of ∂D as is given in equation (14) it seems that to determine the region D it suffices to determine the unknown interval (-a,a) and the continuous functions:

$$\left.\begin{matrix} h_1:(-a,a)\longrightarrow \boldsymbol{R^-}, h_2:(-a,a)\longrightarrow \boldsymbol{R^+}, \\ g_1:(-a,a)\times(-b,b)\longrightarrow \boldsymbol{R^-}, g_2:(-a,a)\times(-b,b)\longrightarrow \boldsymbol{R^+}, \end{matrix}\right\} \tag{15}$$

where b∈ $\boldsymbol{R}$

Such that:

$$h_n(-a) = h_n(a) = 0 \quad for \quad n = 1,2,$$

and

$$g_n(-a,0) = g_n(a,0) = g_n(0,-b) = g_n(0,b) = 0 \quad for \quad n = 1,2,$$

Now, assume that:

$$\left.\begin{aligned} h_1(x,\bar{\alpha}) = \sum_{r=0}^{L} \alpha_r x_r \,, h_2(x,\bar{\beta}) = \sum_{r=0}^{L} \beta_r x_r \,, \\ g_1(x,y,\bar{\gamma}) = \in \sum_{t=0}^{N}\sum_{s=0}^{M} \gamma_{st} x^s y^t \quad and \quad g_2(x,y,\bar{\eta}) = \sum_{t=0}^{N}\sum_{s=0}^{M} \eta_{st} x^s y^t \end{aligned}\right\} \qquad (16)$$

For all x∈(-a,a),y ∈ $(-b,b)$ where $\bar{\alpha} = (\alpha_0, \alpha_1, \dots, \alpha_L)$, $\bar{\beta} = (\beta_0, \beta_1, \dots, \beta_L)$,

$$\bar{\gamma} = (\gamma_{00}, \gamma_{01}, \dots, \gamma_{m0}, \gamma_{01}, \gamma_{11}, \dots, \gamma_{M1}, \dots, \gamma_{0N}, \gamma_{1N}, \gamma_{2N}, \dots, \gamma_{MN})$$

$$\bar{\eta} = (\eta_{00}, \eta_{01}, \dots, \eta_{m0}, \eta_{01}, \eta_{11}, \dots, \eta_{M1}, \dots, \eta_{0N}, \eta_{1N}, \eta_{2N}, \dots, \gamma_{\eta MN})$$

And $\alpha_r, \beta_r, \gamma_{st}, \eta_{st}$ are unknown real numbers (for r=0,1,…,L;s=0,1,…,M; t=0,1,…,N) which will be determined.

The unknown region can be approximated by the region as well as

D(a, $\bar{\alpha}, \bar{\beta}, \bar{\gamma}, \bar{\eta}$) = $\{(x,y,z) | x \in (-a,a), y \in (h_1(x,\bar{\alpha}), h_2(x,\bar{\alpha})), z \in (g_1(x,y,\bar{\eta}), g_1(x,y,\bar{\eta}))\}$

To make the analysis easier it is assumed that:

i-The unknown region is convex.

ii-The unknown region in xy-plane is symmetric about the both x-axis and y-axis.

iii-The unknown region is symmetric about xy-plane.

If the unknown region is convex, it is advisable to assume that the approximate region D(a, $\bar{\alpha}, \bar{\beta}, \bar{\gamma}, \bar{\eta}$) must likewise be convex. This is insured if one assumes that the polynomials approximating the functions $h_1(x,\bar{\alpha})$ and $h_2(x,\bar{\beta})$ in the definition of the unknown region D

must at most of order 2, that is L=2. From conditions (15.a) and assumption(ii) one can be obtained that the functions h_1 and h_2 can be defined in the form

$$h_1(x,a,b) = -\sqrt{b^2 - \frac{a^2}{b^2}x^2} \text{ and } h_2(x,a,b) = -\sqrt{b^2 - \frac{a^2}{b^2}x^2} \quad (17)$$

where a and b are unknown real numbers, to be found. From conditions (15.b) and assumption (iii), it follows that the functions h_1 and h_2 can be defined in the form

$$g_2(x,y,a,b,c) = c^2(1 - x^2/a^2 - y^2/b^2) \text{and } g_1(x,y,a,b,c) = -g_2(x,y,a,b,c) \quad (18)$$

where c is unknown real number to be determined of the unknown region D(a, $\bar{\alpha}, \bar{\beta}, \bar{\gamma}, \bar{\eta}$) becomes in the form

$$D(Z) = \{(x,y,z) | x \in (-a,a), y \in (h_1(x,a,b), h_2(x,a,b)), z \in (g_1(x,y,a,b,c), g_2(x,y,a,b,c)) \; x,y,z \in \mathcal{R}\}, \quad (19)$$

where $\bar{\tau}$=(a,b,c) and a,b, and c are unknown real numbers to be determined.

The essence of the direct variational method for solving the inverse problem is to determine the unknown parameters a,b and c using the discrete least-square approximation:

$$Min \; H(\bar{\tau}) = \sum_{i=1}^{I}\sum_{j=1}^{J}\sum_{k=1}^{K}\left[u(x_i,y_j,z_k) - u_a(x_i,y_j,z_k,\bar{\tau})\right]^2 \quad (20)$$

where $u(x_i,y_j,z_k)$ are the given values of the solution of problem (1)-(3) in the region D at the point (x_i,y_j,z_k) *in the set* Γ, while $u_a(x_i,y_j,z_k,\bar{\tau})$ are the values of the approximate solutions of the same problem, but in the region D($\bar{\tau}$) evaluated at the same point (x_i,y_j,z_k) *of* Γ.

Relation (20) is unconstrained non-linear optimization problem for the unconstrained Hooke and Jeeves method used (3) & (4).

3.3 The direct variational method for solving the Inverse Interior Problem of Helmholtz Equation:-

The direct variational method is used for solving the inverse interior Helmholtz equation. In this case to calculate the objective function H($\bar{\tau}$), one must solve the linear partial differential equation

$$u_{xx} + u_{yy} + u_{zz} + k^2 u^2 = f \quad in\ D(\bar{\tau}), \tag{21}$$

where f= f(x,y,z) is defined in (12),with the boundary condition

$$u=0 \text{ on } D(\bar{\tau}). \tag{22}$$

The variational method as discussed in section (1) for the solution of the direct problem is used for solving equation (21)-(22),at any iteration $\ell$of the Hooke and Jeeves method given solution $u_\alpha(x_i, y_j, z_k, \bar{\tau}^\ell)$ in the region D($\bar{\tau}^\ell$). This solution together with the given solution u(x,y,z) are evaluated at each point (x_i, y_j, z_k) in the set $\Gamma \subset$ D. To calculate the objective equation (20) at $\bar{\tau} = \bar{\tau}^\ell$, It is important to mention that the Hooke and Jeeves method is used in this work.

Firstly it is used to minimize the objective equation (20),to find the vector of the unknowns $\bar{\tau} = (a, b, c)$, at any iteration ℓ of this method. Secondly the method is also used simultaneously to find the solution $u_\alpha(x_i, y_j, z_k, \bar{\tau}^\ell)$ of equation (21)-(22) in the region D($\bar{\tau}^\ell$).

It is too important to refer here for the Hooke and Jeeves method (to find the unknown coefficients in the solution u_α,at any initial ℓ in the first use of the Hooke and Jeeves method for solving the optimization equation (20).

3.4 Numerical Simulation:

To avoid the need for experimental measurements, that is hard to achieve, the following numerical simulation is used to check the usefulness of any new technique.

The results of the direct problem which is considered in section (2.4) are used as a given values of the solution (measurements) at each point of the set Γ which is defined in the form:

$$\Gamma = \{(x_i, y_j, z_k) | -1 \le x_i \le 1, h_1(x_i) \le y \le h_2(x_i), -g_1(x_i, y_j) \le z_k \le g_2(x_i, y_j) \quad for$$

$$i = 1,2,..,I, j = 1,2,...,J, k = 1,2,...,K\}$$

where $h_2(x_i) = \sqrt{2.25 - 1.125{x_i}^2}$, $h_1(x_i) = -h_2(x_i)$

$g_2(x_i, y_j) = 4(1 - {x_i}^2 - {y_j}^2/2.25)$ and $g_1(x_i, y_j) = --g_2(x_i, y_j)$.

To solve the inverse the unknown region D is approximated by the unknown region $\mathbf{D}(\vec{\tau})$ defined in equation (19) where $\vec{\tau} = (a, b, c) and\ a, b$ unknowns to be determined.

These unknown parameters are determined by using the direct variational method that depends on minimizing (20) with respect to these unknown, and which are solved by using the unconstrained Hooke and Jeeves method.

A computer program is used to solve the interior problem. In this program the non-linear optimization equation (20) is solved for different initial values of the unknowns a,b and c with each initial values the initial step lengths h=0.1,h=0.5 and h=1 are used 9in the method of Hooke and Jeeves.

Table (2), The results for a,b and c the approximate values of the coefficients a_n,(n=1,2,…,N) in the approximation solution equation (9) with N=10 are tabulated below:

a=1,b=1.5,c=2,$x_n = \sqrt{b^2 - \left(\frac{bn}{a}\right)^2}$

n	x_n
1	0.998968
2	5.420926×10^{-8}
3	2.9417344×10^{-8}
4	1.853727×10^{-7}
5	8.5010249×10^{-3}
6	$-4.1453167 \times 10^{-5}$
7	$-2.9147264 \times 10^{-5}$
8	-4.298106×10^{-4}
9	$-1.7257731 \times 10^{-3}$
10	1.2229377×10^{-3}

4. Remarks and Conclusions:

1.The initial values of the unknown parameters can be chosen such that the region which is obtained using these initial values contains the given points that the solution of this problem.

2. The convergence of the numerical method is ensured by the convergence of the direct Ritz method for variational problem, and by the convergence of the algorithm used to solve the non-linear programming problem.

3. The numerical integration method in the problem has been carried at using the Gaussian quadrature integration method of order 7.

4. The inverse problem is solved for different initial values of the unknown a, b &c and for each such initial values, different step lengths in the optimization method of Hooke and Jeeves are used. The approximate values of the above unknown coincide with their corresponding exact values. And for simplicity, we give the results of one execution.

4. References:

1. Bazaraa, M.S."Non-Linear Programming, Theory and Algorithms",John Wiely and Sons Inc,1979 .

2. Cheser, C.R."Techniques in partial differential equations".2001

3. Gelfand, F."Calculus of Variations",Prentice-Hall Inc,2000.

4. Magri, F.," Variational Formulation for Every Linear Equation", Inc.J.Engng.Sci, Vol.12, pp.537-549, 1994

5. Mahlol, S.Mahmod," Inverse problems in differential equations with an Application to Localizing Brain Tumors",Ph.D ,thesis, University of Baghdad.1991.

6. Makky, S.M. and Ali, J.A.," "Direct and Inverse Scattering Problems for Acoustic Waves", Accepted for publication in Mu'tah Journal for Research and Swdies,1994.

7. Rao,S.S., "Optimization and Application",2nd ed.,Wiely,2005.

8. B.M. Podlevskyi, Newton's method as a tool for finding the eigenvalues of certain two-parameter (multiparameter) spectral problems, compute., Math., Vol.12,pp.537-549.1993.

9. B.M. Podlevskyi, and V.V. Khlobystov, About one approach to finding eigenvalue curves of linear, mathematical methods and physics mechanical, Fields,51,No.4,pp. 86-93.2009.

Fast Image Steganography Using Affine Mapping

Loay E. George * Ahmed H. Ali **

* Computer Science Department\ College of Science\University Of Baghdad
** Computer Science Department\ Studies, Planning and Follow up Directorate\Ministry Of Higher Education and Scientific Research

Receiving Date: 2011/6/12 - **Accept Date:** 2011/10/4

Abstract

One of the most important characteristics of using fractal image coding in hiding images is the encoding process that involves very long time complexity. In this paper new hiding system is proposed that hide secret image (color or gray) into cover image (color) with reducing the time of encoding process 10 times less than classical systems that use block indexing as descriptor with fractal coding. Affine transform is used in matching process to find the closer cover block for each secret block and least significant bit method to embed the coefficient affine transform. The results indicated that the encoding time is actually reduced and hiding rate reach to 100% and the quality of extracted secret image is still within the acceptable level.

المستخلص

يعتبر عامل الوقت من الخصائص المهمة التي تميز عملية ترميز الصور الكسورية والذي يكون طويل جدا، لذا يقترح هذا البحث نظام اخفاء جديد يقوم باخفاء الصورة السرية (ملونة او رمادية) في الصورة الغطاء (ملونة) حيث يقوم هذا النظام بتقليل الوقت الذي تحتاجة عملية التشفير الى ١٠ مرات اقل من الانظمة التقليدية (والتي تستخدم عملية ترميز الصور الكسرية فقط) باستخدام طريقة (فهرسة البلوك) . تم استخدم التحويل الافيني في عملية المطابقة لايجاد اقرب بلوك من بلوكات الصورة الغطاء لكل بلوك من بلوكات الصورة السرية وطريقة اخفاء اصغر بت في عملية اخفاء معاملات التحويل واظهرت النتائج الى ان وقت الترميز تم انقاصة فعليا وان نسبة الاخفاء قد تصل الى ١٠٠% بدون تغيير على كفاءة الصورة السرية .

KeyWords: FBC (Fractal Block Indexing), PIFS (Partition Iteration Function System), (CATs), Contractive Affine Transformations FIC (Fractal Image Coding)

Fast Image Steganography Using Affine Mapping

Dr. Loay E. George, Ahmed H. Ali

Introduction

Image coding based on fractal theories and techniques are recently developed and received a great deal of attention [1]. Jacquin proposed the (FBC) scheme to automatically convert an image into a partitioned iteration function system, which is a set of (CATs) [2]. The small range block R and large domain block D used in CAT both are partitioned from an image. The coefficients represent the best-match transformation which minimizes

error. A number of papers on fractal image encoding have been published since the pioneering idea of Barnsley and Sloan in 1988 [3].

All attempts to speed-up PIFS encode method dealt with encoding the gray-scale images (or images consist of only one color plane) [3]. Many researchers studied the implementation of FIC on color images in ways different than that followed in JPEG or JPEG 2000 [4,5]. Also many studies apply moment features in FIC to speeding color and gray image compression by using different method [6, 7].

Proposed System

Proposed system hides secret image (color or gray) into cover image (color) that use affain mapping with block indexing as descriptor with fractal coding.

Block Indexing

In this paper we adopt block indexing techniques that are used to reduce exhaustive search in matching process. The blocks are classified into classes depending on equation (1) each class have sever

$$F = \left| \frac{m_{01}^{\ 2} - m_{10}^{\ 2}}{m_{01}^{\ 2} + m_{10}^{\ 2}} * N \right| \qquad \text{... (1)}$$

Where

F= { 0 . . 100}

N={50,100,200,…,800}

F class and N no. of classes

$$m_{01} = \sum_{y=0}^{blocksize-1} \sum_{x=0}^{blocksize-1} x \times image(x, y) \quad \text{....(2)}$$

$$m_{10} = \sum_{y=0}^{blocksize-1} \sum_{x=0}^{blocksize-1} y \times image(x, y) \quad \text{....(3)}$$

Affain Mapping

Affine transform is a set of coefficients that used to build the constructed image from the cover image so that each block in secret image can be obtained from blocks of cover image by applying the suitable rotation and reflection operations after partitioning the secret image into blocks of fixed size [8].

For each cover block an approximation must be obtained from equation (4)

$$s \approx L\, c + F \quad \text{... (4)}$$

Where

s scale block

c cover block

L scale

F offset

The computation needs the following steps

-For each *s* block make the suitable symmetry and compute an optimal approximation as follow:

- Calculate the values of scaling (*L*) and offset (*F*) coefficients by using the least square optimization as equation (5),(6)

$$L = \frac{n(\sum_{x,y} c_i s_i) - (\sum_{x,y} c_i)(\sum_{x,y} s_i)}{n(\sum_{x,y} c_i^2) - (\sum_{x,y} c_i)^2} \quad \text{... (5)}$$

And

$$F = \frac{1}{n}(\sum_{x,y} s_i) - n(\sum_{x,y} c_i) \quad \text{... (6)}$$

Where s is secret block and c cover block and n no. of pixels.

- use the quantized coefficients (L) and (F) to compute the error $Err(c,s)$ equation(7):

$$\text{Err}^2 = \frac{1}{n}[\sum_{x,y} s^2 + L(L\sum_{x,y} c_i^2 - 2\sum_{x,y} c_i s_i + 2F\sum_{x,y} c_i) + F(Fn - 2\sum_{x,y} s_i)] \quad \text{... (7)}$$

- Find the c blocks with minimal error.

- The output is the set of quantized coefficient (L and F) and symmetry index and the c blocks.

The symmetry matching done as follow:

-identity

- Reflection around Y-axis

- Reflection around X-axis

- 180^o rotation.

- Reflection around the diagonal Y=X

- 90^o rotation

- 270^o rotation

- Reflection around the diagonal Y=-X

Fast Image Steganography Using Affine Mapping

Dr. Loay E. George, Ahmed H. Ali

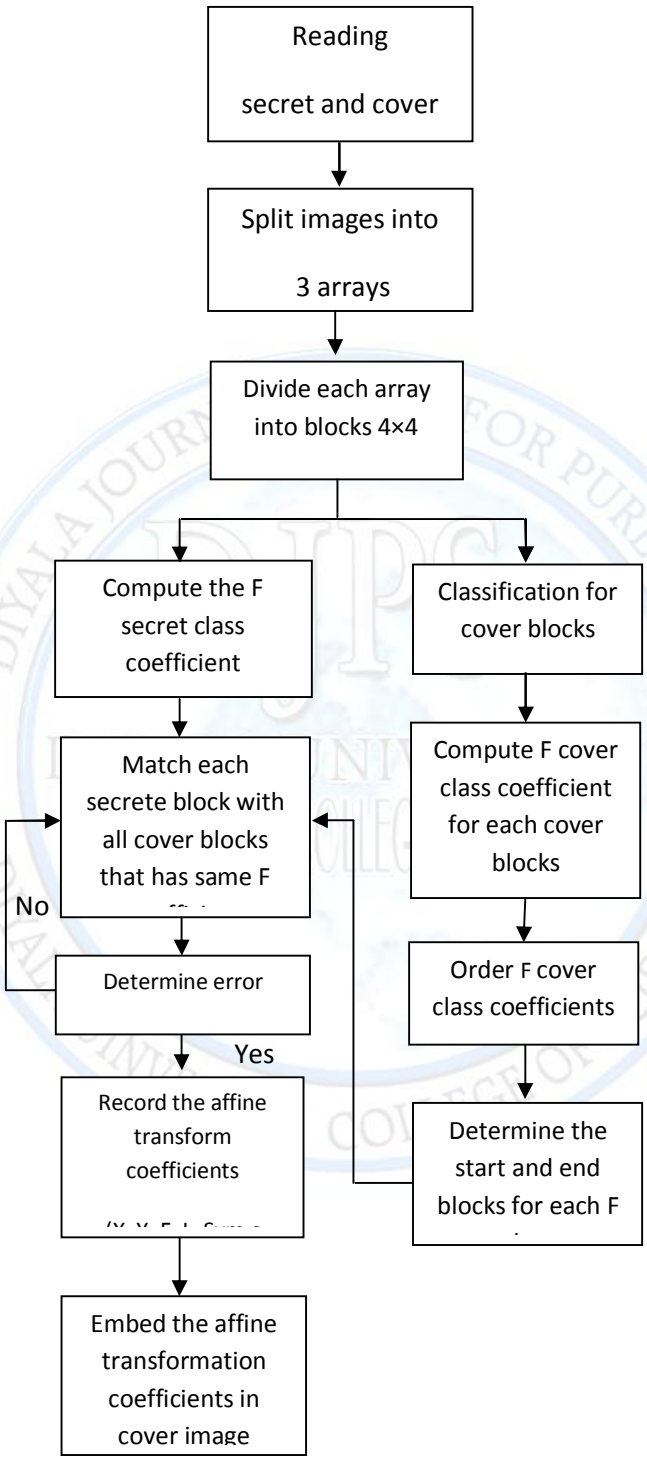

Figure (1) The Proposed System

Encoding process

Encoding process begin by reading secret_ images, divide the images into 3 arrays, and into blocks (4×4) then we use block indexing method to improve (speed up) the secret search task. Instead of compare all cover blocks with each affine transformed secret block, we need only to test the cover blocks whose F class values are similar to that of the tested secret block. To implement this idea the following block indexing algorithm is built as shown in Figure (1):

1. Load BMP images (Secret and Cover) and put it in (R,G,B) array (three 2D arrays).
2. For each cover block:
   a. Compute F cover class values (equation 1).
   b. Store the position (*Xs, Ys*) of the cover block and its F cover class values in array *T*.
2. Sort the records of the array *T* in ascending order according to their F value.
3. Establish start and end of each block of records that have same F cover class value.
4. for each secret block:
   a. Determine F secret class values (equation 1).
   b. depend on the array *T*, match only the cover blocks whose *Fs* values equal to F cover class. In each matching instance determine the *L* and F and *Err* (equations 5,6,7) for all possible symmetry cases (sym=0,1,…,7).
   c. Compare the result (*Err*) of each matching instance with the minimum Err registered during the previous matching instances. If *Err* is smaller then put its value in minimum Err register values of (L, F, Sym, Xs , Ys).
   d .In the case that the new registered minimum *Err* is less than error between matched blocks then stop the search process, and output the set (L, F, Sym, Xs , Ys) as best match, and go to step (4e).
   e. Otherwise, start test another cover blocks until either the registered minimum error become less than (Err_{max}) or all the cover blocks are tested.
   f. Output the set of IFS code (L, F, Sym, Xs , Ys) for the tested secret block.
5. After the affine transformation coding of all secret blocks, apply the coding method to encode the sequence of affine transformation coefficients.

Extraction process

In this process we built the secret image from cover image by:

1- For each layer of cover image:
   a- Retrieve the array of coefficient from cover image by collect the least significant bit from each byte from cover image.
   b- Apply the coefficient on cover block to obtain secret block depend on the equation (4).
   c- Put the secret block in the right position in the reconstruction image (secrete image).
2- Merge the 3 layers of the reconstructed image to built the secrete image.

Test Result

The proposed methods are tested on cover image (Lena image 256 x 256, 24 bits) and secret image (Lena image 128 x 128, 8 or 24 bits) Figure (2),(3). The size of secret blocks is 4 x 4 pixels; the search step size is 1, the number of bits allocated for the scaling and offset factor is 13 bits, and for the symmetry factor 3 bits. So the hiding rate would be 100%. All methods were programmed using visual basic 6.0 and implemented on a Dell laptop with Intel Core 2 Due 2.0 GHz CPU.

Figure (2)

Cover Image

Figure (3)

Secret Image

The results listed in Table (1,2,3,4,5) illustrate the effect of using step size, block length and no. of classes only the error threshold (Err) as a stopping search condition with time of encoding (T_E), *(MSE)* and *(PSNR)* as a descriptor to measure the quality of the secret image.

$$MSE = \frac{1}{w \times h}\sum_{x,y}(I_{x,y} - I`_{x,y})^2$$

$$PSNR = \frac{w \times h \times 255^2}{(I_{x,y} - I`_{x,y})^2}$$

Where *w, h* is height and width of the image.

I, I` represent pixel in two image.

Step size	Time in Minute	MSE	PSNR
1	83.85	9	38.5
5	5.5	11	37.6
8	2.2	11.6	37.4
10	1.4	12	37.3

Table (1) Effect of step size on classical system with block length=4 and hiding rate 0.35

Step size	Time in Minute	MSE	PSNR
1	6.86	10.3	38
5	0.45	12.8	37
8	0.2	13.4	36.8
10	0.14	13.7	36.7

Table (2) Effect of step size on proposed system where block length=4 and no of classes 100 and hiding rate 0.35

Block length	Time in Minute	Hiding rate	MSE	PSNR
4	1.4	0.35	12	37.3
5	1.1	0.5	20	35
6	1	0.8	19.3	35.2
7	0.8	1.08	20.2	35

Table (3) Effect of block length on classical system with step size=10

Block length	Time in Minute	Hiding rate	MSE	PSNR
4	0.14	0.35	13.7	36.7
5	0.11	0.5	20.8	34.9
6	0.1	0.8	20.6	34.9
7	0.08	1.08	21	34.8

Table (4) Effect of block length on proposed system with step size=10 and no of classes=100

No Of Classes	Time in Minute	MSE	PSNR
50	0.15	13.2	36.9
100	0.14	13.7	36.7
300	0.1	14.5	36.4
500	0.06	14.7	36.4

Table (5) Effect number of classes on proposed system with step block length=4 and size=10 and hiding rate=0.35

Conclusion

As seen in the result that the classical system using FIC only uses: step size 10, hiding rate (0.35) and the required time(1.4) minute, *PSNR is* (37.5) dB as shown in table (1) while the proposed system uses: step size 10, hiding rate(0.35) and the required time (0.14) minute, *PSNR is* (36.7) dB as shown in table (2) this indicates that the encoding time is reduced by 10 times and hiding rate reach to 100% using 1-least significant bit in hiding method and the quality of extracted secret image is still within the acceptable level.

References:

[1] Fisher Y. " Fractal Image Compression: Theory and Application", Springer-Verlag, New York, 1995.

[2] Jacquin A.E. "Fractal image coding: a review," Proceedings of the IEEE, vol. 81, pp. 1451–1465, October 1993.

[3] Jacquin, A.," *Image Coding based on a Fractal Theory of Iterated Contractive Image Transformations"* IEEE trans. Image processing, vol. 1, pp.18-30, 1992.

[4] Hurtgen, B., Mols, P., and Simon, S., "Fractal Transforms Coding of Color Images", Visual Communications and Image Processing, SPIE 94, Chicago, pp.1683-1691, 1994.

[5] Zhaohuili, Zhao, L., Soma, Y. ,"Fractal Color Image Compression", IEEE, 0-7695-0878-2/00, 2000

[6] Loay A. George, "IFS coding for zero-mean image blocks", Iraqi J. Sci., vol. 47, no. 1, pp. 190-194, 2006.

[7] Loay E. George, and Eman A. Al-Hilo, "Speeding-up Fractal Colored Image Compression Using Moments Features", ICCCE08, International Conference on Computer and Communication Engineering, International Islamic University Malaysia (IIUM), Kuala Lumpur, Malaysia, ISBN: 978-1-4244-1691-2, pp. 1303-1307, 2008.

[8] Saud Kakil, "Image in Image Hiding System Using Affain Transform", University of Sulaimani/ College of Science, 2009.

Study of Toxoplasma infection in women recurrent abortion in First trimester of pregnancy by Indirect immunoflurescent antibody test (IFAT)

Rana Talib AL-Ani, Department of Biochemistry, Medicine College, AL_Anbar University, Ramadi , IRAQ

Receiving Date: 2011/2/1 - **Accept Date:** 2011/5/2

ABSTRACT

During a period of six months, 50 blood samples were collected from women the occupation were Housewife in First trimester of pregnancy who were referred to the Maternity and Child Hospital in Ramadi , in addition to 50 samples from healthy women as control. All women were screened for *Toxoplasma* antibodies by latex agglutination test to study the positive rate of toxoplasmosis in the community and to investigate the effect of the risk factors on the positive rate of the disease.

Toxoplasma -IgM antibodies were demonstrated by using IFAT to distinguish between acute and chronic infections. The overall seroprevalence of toxoplasmosis was 50%. The *Toxoplasma* antibodies increased with age especially in the age groups (26-30-31-35) years. Most of the positive women showed the highest titers 320 IU/ml especially in age group 26-30, 31-35 years. Were recorded high number for abortion (30) from total number (50) .

IFAT test was evaluated for specific IgM when testing 50 sera, 15 cases were with acute infection and 25with chronic toxoplasmosis using IFAT .

Key words:- *Toxoplasma*, *First trimester*, *Indirect immunoflurescent antibody test , abortion*

Rana Talib AL-Ani,

Introduction

Toxoplasmosis is a parasitic disease caused by the protozoan Toxoplasma gondii.[1] The parasite infects most genera of warm-blooded animals, including humans, but the primary host is the felid (cat) family. Animals are infected by eating infected meat, by ingestion of feces of a cat that has itself recently been infected, or by transmission from mother to fetus. Although cats are often blamed for spreading toxoplasmosis, contact with raw meat is a more significant source of human infections in many countries, and fecal contamination of hands is a greater risk factor [2,3] .

During the first few weeks post-exposure, the infection typically causes a mild flu-like illness or no illness. Thereafter, the parasite rarely causes any symptoms in otherwise healthy adults. However, those with a weakened immune system, such as AIDS patients or pregnant women, may become seriously ill, and it can occasionally be fatal. The parasite can cause encephalitis (inflammation of the brain) and neurologic diseases, and can affect the heart, liver, inner ears, and eyes (chorioretinitis) [4,5].

During acute toxoplasmosis, symptoms are often influenza-like: swollen lymph nodes, or muscle aches and pains that last for a month or more. Rarely, a patient with a fully functioning immune system may develop eye damage or nasal lesions from toxoplasmosis. Young children and immunocompromised patients, such as those with HIV/AIDS, those taking certain types of chemotherapy, or those who have recently received an organ transplant, may develop severe toxoplasmosis. This can cause damage to the brain (encephalitis) or the eyes (necrotizing retinochoroiditis). Infants infected via placental transmission may be born with either of these problems, or with nasal malformations, although these complications are rare in newborns [1].

Most patients who become infected with Toxoplasma gondii and develop toxoplasmosis do not know it.[citation needed] In most immunocompetent patients, the infection enters a latent phase, during which only bradyzoites are present, forming cysts in nervous and muscle tissue. Most infants who are infected while in the womb have no symptoms at birth but may develop symptoms later in life [5,6] .

While rare, skin lesions may occur in the acquired form of the disease, including roseola and erythema multiforme-like eruptions, prurigo-like nodules, urticaria, and maculopapular lesions. Newborns may have punctate macules, ecchymoses, or “blueberry muffin” lesions. Diagnosis of cutaneous toxoplasmosis is based on the tachyzoite form of T. gondii being found in the epidermis. It is found in all levels of the epidermis, is about 6 µm by 2 µm , bow-shaped, the nucleus being one-third of its size. It can be identified by electron microscopy or by Giemsa staining tissue where the cytoplasm shows blue, the nucleus red [7] .

Detection of Toxoplasma gondii in human blood samples may be achieved by using the polymerase chain reaction (PCR) [5].

Toxoplasmosis can't be detected with immunostaining. Lymph nodes affected by toxoplasma have characteristic changes, including poorly demarcated reactive germinal centers, clusters of monocytoid B cells and scattered epithelioid histiocytes [8,9]

Congenital toxoplasmosis is a special form in which an unborn child is infected via the placenta. A positive antibody titer indicates previous exposure and immunity and largely ensures the unborn baby's safety. A simple blood draw at the first pre-natal doctor visit can determine whether or not the woman has had previous exposure and therefore whether or not she is at risk. If a woman receives her first exposure to toxoplasmosis while pregnant, the baby is at particular risk. A woman with no previous exposure should avoid handling raw meat, exposure to cat feces, and gardening (cat feces are common in garden soil). Most cats are not actively shedding oocysts and so are not a danger, but the risk may be reduced further by having the litterbox emptied daily (oocysts require longer than a single day to become infective), and by having someone else empty the litterbox. However, while risks can be minimized, they cannot be eliminated. For pregnant women with negative antibody titer, indicating no previous exposure to T. gondii, as frequent as monthly serology testing is advisable as treatment during pregnancy for those women exposed to T. gondii for the first time decreases dramatically the risk of passing the parasite to the fetus [6,10].

Materials & Methods:

1- Patients: -

A total of 50 patients , the occupation were Housewife in First trimester of pregnancy were investigated in Al-Ramadi Maternity and Child Hospital during the period from 10th to January 10th July 2009. The age ranged between 18-45 years. In addition to 50 serum samples were collected from healthy women as a control. The age of this group is similar to the group of patients studied.

Materials

1-Kits :-

A-Kits used for identification of Toxo-antibodies by latex agglutination . Linear (Spain)

B-Kits used for IgM IFAT Bio-Merieux (France)

2-method

1-Latex agglutination test:

Direct agglutination test on the slide for the determination of toxoplasmosis .

Reagent :

1- Toxoplasmosis latex: suspension of latex particles coated with *T. gondii* antigen, sodium azaide 0.1%.
2- Positive control: human serum, sodium azaide 0.1.%
3- Negative control: non-reactive human serum, sodium azaide 0.1.%

Procedure:

1- Bring the reagents and the samples to room temperature. Prepare the sample dilution tubes as in the following table:

Tubes	1	2	3	4	5	6
Saline sol.	-	50 µl	50 µl	50 µl	50 µl	50 µl
Sample	100 µl	Serial dilution of 50 µl				
Dilution	1:1	1:2	1:4	1:8	1:16	1:32
Iu/ml	10	20	40	80	160	320

Placed 50 µl of each sample dilution into the individual circles of the control.Added into each circle one drop of the toxoplasmosis latex reagent, near the sample to be tested. Helped with the little stirrer mix the components covering all the surface of the circle. Rotated the slide slowly either by hand or by means of a mechanical rotator (80 r.p.m) for a period of 5 minutes.

2- Indirect immunoflurescent antibody test (IFAT) for determination of IgM antibodies:

Principle of the method:

The IFAT is based on the use of antiglobulins labeled with fluorescent dyes such as fluorescein isothiocyanate. These fluorochromes emit visible light after excitation by ultraviolet light.

Reagents:

1-Test kit with *toxoplasma* suspension, formalin killed, lyophilized *toxoplasma* suspension medium. Anti-human globulin IgM from rabbits for the *toxoplasma* test, fluorescein- conjugated.

2-Test kit *toxoplasma* controls sera, control serum (human), positive, control serum (human), negative.
3-Phosphate buffer solution concentrate PH=7.2.

4- Packing with 10 glass slides with 12 reaction fields each and 12 cover glasses, ready for use, grease-free.

5- Further reagents:

Glycerol, buffered with phosphate buffer solution (9+1) PH=7.2, distilled water.

Test procedure:

1-Dissolved toxoplasma suspension, lyophilized in 1ml suspension medium, homogenized well a tuberculin or record syringe by drawing and pushing out contents against the flask bottom.

2-Placed approximately 0.01 ml toxoplasma suspension with a syringe or capillary tube on the reaction fields of the grease-free slides which are ready for use. The suspension is not storable.

3-Allowed preparation to dry completely for 60 to 120 minutes in the incubator at 370C. If the prepared slides are kept at about -200C to -300C the toxoplasma preparations are stable for several weeks.

4-Diluted phosphate buffer-solution concentrate, PH 7.2, with distilled water 1+19 (100ml concentrate will give 2000 ml phosphate-buffered saline solution.

5-Prepared a geometric dilution series of the patient's serum with phosphate buffer-solution and load from dilution 1:64 on wards the prepared slide with approximately 0.01-ml of each serum dilution.

6-Placed slide for about 30 minutes in moist chamber.

7-Rinsed slide with phosphate buffer-solution PH=7.2 and adjust for 10 minutes in cuvette with phosphate buffer solution changing the rinsing liquid several times.

8-Placed slide between filter paper and dry up (nowiping) carry on immediately.

9-Anti-human globulin (Anti-IgM) for the toxoplasma test, fluorescien-conjugated. The globulin lyophilized with an admixture of Evans blue is dissolved with 1 ml phosphate buffer solution.
10-Overlay reaction fields with about 0.01 ml each of anti-human globulin (Anti-IgM) for the toxoplasma test.

11-Kept slide for 30 minutes at room temperature or placed in moist chamber at +370C.
12-Rinsed slide with phosphate buffer solution and adjust in cuvette with phosphate buffer solution.

13-Placed slide between filter paper and dry up (no wiping), carry on immediately.

14-Applied as little buffered glycerol as possible to the dried preparations and close with a cover glass.

15-Left preparation standing for 15 minutes at room temperature.

16-Examined preparations under the microscope.

Result and discussion

The results presented in this study were based on the analysis of a total number of 50 blood samples collected from women suffering from abortion and 10 healthy individuals as controls.

Table 1: Number and percentage of positive, negative, and control groups.

I. Group	N	%
Positive	30	30%
Negative	20	20%
Control	50	50%
Total	100	100%

The prevalence of *T.gondii* antibody was measured by latex agglutination test. Among the total 60, 30 were found positive, while 20 cases were negative (Table 1).

Table 2: Results of Latex agglutination according to age groups.

Age groups	No. Exam	Positive Group(%)	Negative Group(%)	Control Group(%)
15-20	5	2	2	5
21-25	10	5	3	10
26-30	12	8	3	5
31-35	20	11	6	15
36-40	13	4	6	15
Total	60	30	20	100

The correlation between age groups and positive antibody titers is shown in Table 2. The highest rate of infection as recorded in the age groups (31-35) years respectively while the age group (15-20) showed the lowest rate.

Table 3: Distribution of toxoplasmosis according to Latex titer and age groups with regard to all samples.

Age groups	Total Exam.	Positive		Latex titer IU/ml									
		No.	%	20		40		80		160		320	
				No.	%	No.	%	No.	%	No.	%	No.	%
15-20	5	2	40%	0	0	0	0	0	0	0	0	0	0
21-25	10	5	50%	0	0	0	0	0	0	2	2	2	20
26-30	12	8	66.7%	1	8.3	2	16.6	3	25	4	33.3	4	33.3
31-35	20	11	55%	0	0	2	10	1	5	0	0	3	15
36-40	13	4	30.8%	1	7.6	0	0	2	15.3	2	15.3	1	7.6
Total	60	30	50%	2	3.3	4	6.6	6	10	8	13.3	10	16.6

Table(3) shows the percentage of infected women corresponding to each titer with respect to the total number of sampled women in the three groups. The antibody titer ranges from 20 IU/ml (1:2) to 320 IU/ml (1:32).The lowest number 2 (3.3 %) was recorded with titer 20 IU/ml and the highest number was 10 (16.6 %) in the titer 320 IU/ml.

Table 4: Distribution of total sample individuals according to the various toxoplasmosis tests.

Sample	Test					
	Latex			IFAT (IgM)		
	Total	+ve	%	Total	+ve	%
Positive	30	30	100	30	15	50
Suspected	20	0	0	15	0	0
Control	50	0	0	50	0	0
Total	100	30	30	95	15	15.8

The diagnosis of a recently acquired *T.gondii* infection was based on the detection of specific IgM antibody. Sample groups were screened by the latex agglutination test and the positive cases were confirmed by indirect Immune Fluorescent Antibody Test (IFAT) Regarding positive results 15(50%) of cases were in IFAT, see the table (4 **).**

Table 5: Cross-classification of the categories of the latex test with the categories of the IFAT **test**

Latex categories	IFAT categories			Total
	0	32	64	
20	2	0	0	2
40	2	0	0	2
80	3	2	1	6
160	3	3	2	8
320	5	5	2	12
Total	15	10	5	30

II. In table 5 , The cross classification of the categories of the latex test with those of the IFAT showed that infected women in the categories (20 and 40) of the latex test are recorded as negative cases in IFAT . In latex agglutination test the positive cases were 30 (50%) cases positive from 60 while the IFAT revealed 15 positive cases out of those latex positive .

In table 6, These results indicated that the total abortions (50) are more likely to occur in age group 31-35 (17) years with high titer 160 and 320 IU/ml 50 while the age group 15-20 years showed the lowest rate(4). In addition to that some women suffered from many abortions during life.

Table 6: Correlation between age, positive antibody titers and number of abortion.

Age groups	Total abortions	Latex titer IU/ml									
		20		40		80		160		320	
		No.	%	No.		No.	%	No.	%	No.	%
15-20	4(8)	0	0	0	0	0	0	1	25	3	75
21-25	7(14)	0	0	1	14.3	2	28.6	2	28.6	2	28.6
26-30	13(26)	1	7.6	2	15.4	2	15.4	4	30.8	4	30.8
31-35	17(34)	3	17.6	2	11.8	3	17.6	4	23.5	5	29.4
36-40	10(20)	0	0	1	10	2	20	3	30	4	40
Total	50100)	4	8	6	12	9	18	14	28	18	36

III. The result of this study revealed that toxplasmosis is highly endemic in Ramadi city among aborted women since the seropositivity of disease was 30(50%) which is much higher than that recorded in Kirkuk 24.5% [11].and some similar result was found by Al Dulaimi[12] .who found that prevalence was 69.74% in Al-Anbar.while less than in Egypt(81.4%) [13].

IV. Al-Dulaimi, (2004) has reported similar results, he found that toxoplasma antibodies increased with age especially in the age groups 21-25,26-30 years (85.7%,81.1%) respectively. Similar results were recorded by many authors [14 , 15, 16,17] Other studies recorded contrast results [18,19].These results were similar to that reported [20].who used ELISA and IFAT in Northern Tunisia.

Women with positive antibodies showed a significant association between age groups and titers with respect to the number of abortions.

Thus women in high age groups are more likely to get abortion if they were in acute stage of the disease (titers 160 and 320 IU/ml). found that the risk of acute infections and abortions seems to be higher in the youngest ones as showed by the proportion of high antibodies titers observed in(31-35) years age group compared to that observed after 30 years using ELISA and IFAT. [20].All the patients under test (60) who were diagnosed previously by latex agglutination test (Table 5) in IFAT showed different results depending on the stage of the disease revealing variable picture of sensitivity and specificity of those tests.

This level decreased when the disease was resolved by treatment or limited itself [21]. Acute toxoplasmosis was detected during this study by measurement of specific IgM in 55 of women. IFAT showed (15) positive , while The IgM antibodies appear faster than IgG (as early a five days after

infection) and disappear sooner than IgG antibodies. It was found that IgM - IFAT antibody was increased rapidly and fall to low titers [22].

The specific immune response to parasite leads to the production of antibody, infection by *T.gondii* is associated with the production of the immunoglobulins IgG and IgM. Antibodies can bind to the surface of parasites and cause direct damage, or by interacting with complement lead to cell lysis [23].

References:-

1. Ryan KJ; Ray CG (editors) (2004). *Sherris Medical Microbiology* (4th ed.). McGraw Hill. pp. 723–7.
2. Torda A (2001). "Toxoplasmosis. Are cats really the source?". *Aust Fam Physician* **30** (8): 743–Montoya J, Liesenfeld O (2004). "Toxoplasmosis". *Lancet* **363** (9425): 1965–76.
3. Jones JL, Kruszon-Moran D, Sanders-Lewis K, Wilson M (2007). "*Toxoplasma gondii* infection in the United States, 1999-2004, decline from the prior decade". *Am J Trop Med Hyg* **77** (3): 405–10.
4. Paul M. (1999). "Immunoglobulin G avidity in diagnosis of toxoplasmic lymphadenopathy and ocular toxoplasmosis". *Clin. Diagn. Lab. Immunol.* **6** (4): 514–8.
5. M. De Paschale, C. Agrappi, P. Clerici, P. Mirri, M. T. Manco, S. Cavallari and E. F. Viganò: Seroprevalence and incidence of Toxoplasma gondii infection in the Legnano area of Italy. *Clinical Microbiology and Infection* Volume 14 Issue 2 (2007), Pages 186 - 189.
6. Torrey EF, Yolken RH (2003). "Toxoplasma gondii and schizophrenia". *Emerging Infect. Dis.* **9** (11): 1375–80.
7. M. De Paschale, C. Agrappi, P. Clerici, P. Mirri, M. T. Manco, S. Cavallari and E. F. Viganò: Seroprevalence and incidence of Toxoplasma gondii infection in the Legnano area of Italy. *Clinical Microbiology and Infection* Volume 14 Issue 2 (2007), Pages 186 - 189.
8. Ho-Yen DO, Joss AW, Balfour AH, Smyth ET, Baird D, Chatterton JM. "Use of the polymerase chain reaction to detect Toxoplasma gondii in human blood samples". *J. Clin. Pathol.* **45** (10): 910–3
9. Torrey EF, Yolken RH (2003). "Toxoplasma gondii and schizophrenia". *Emerging Infect. Dis.* **9** (11): 1375–80.
10. Kadir, M.A.; Abdul-Latif, B.M. and Jaffar, A. (1992). Prevalence of toxoplasmosis among women in Kirkuk-Iraq. J.Fac. Med. Baghdad. 34:279-285.
11. Al-Dulaimi, S.S.(2004).Seroepidemological study of toxoplasmosis among aborted women in Al-Anbar. J. Scie. Geom. 4: 1-3.
12. Soliman, M.; our-Eldin, M.; Elnaggar, H. El-Chareb, M.,& Ramadan, N. (2001). *Toxoplasma* antibody in normal and complicated pregnancy. J.Egyptian. Soc. Paras. 31:37-46.
13. Kimball, A.C.; Kean, B.H. and Fouchs, F. (1971). The role of toxoplasmosis in abortion. Ame . J. Obstet. Gynecol. 111:219-226.

14. Beach, G.P. (1979). Prevalence of antibodies to *T.gondii* in pregnant women in Oregon. J. Infect. Dis. 140:780-783.
15. Broadbent, E.; Ross, R. and Hurloy, R. (1981). Screening for toxoplasmosis in pregnancy. J. Clin. Pathol. 34:659-664.
16. Abbas, M.M. (2002). Seroepidemological studies on toxoplasmosis among women with history of abortion. M.Sc. Thesis College of Medicine. University of Saddam.
17. Romia, S.A.; Makhlouf, L.M.; ElMalky, S.A.; Handoussa, A.E. and Abou-Zakham, A.A. (1988). Sero-epidemologic observations on human toxoplasmosis in Dakahlia Governotrage. J.Egypt. Soc. Parasitol. 18: 481-493.
18. Mohammed, H.N.; Bener, A.; Ueluman, S. and Al-Karme, M. (1998). *Toxoplasma* antibody prevalence among healthy adults in United Arab Emirates. Saudi Med. J. 19:3.
19. Bouratbine, A.; Siala, E.; Chahed M.; Aoun, K. and Ismail, R. (2001). Seroepidemological profile of toxoplasmosis in Northern Tunisi. Parasite. 8:61-66.
20. Remington, J.S.; Mc caba, R.E.; Brooks, R.G. and Dorfman, R.F. (1987). Clinical spectrum in 107 cases of toxoplasmic lymphadenopathy. Rev. Infect. Dis. 9: 754.
21. Bertozzi ,L.C.; Suzuki, L.A. and Rossi, C.L. (1999). Seriological diagnosis of toxoplasmosis : usefulnesss of IgA detection and IgG avidity determination in patient with a persistant IgM antibody response of *T. gondii* . Rev. Inst. Med. Trop. Paulo. 41: 175-177.
22. Greenwood, D. ; Slack R.C.B. ; Peutherer, J.F. (1997).Medical Microbiology. Churchill Livingstone. 15ed.

V. دراسة داء المقوسات في النساء ذات الإجهاض المتكررفي الثُلث الأول من الحمل بطريقة الاستشعاع المناعي غير المباشر

رنا طالب محسن /قسم الكيمياء الحياتية-كلية الطب،جامعة الانبار،العراق

VI. الخلاصة

جمع ٥٠ نموذجا من دم نساء تعرضن للإجهاض خلال فترة ستة أشهر من اللواتي راجعن مستشفى النسائية و الأطفال في مدينة الرمادي، أضافه إلى ٥٠ نموذج جمعت من النساء الأصحاء واعتمدت مجموعة كسيطرة (Control) .

فحصت النماذج بطريقة التلازن المباشر Latex agglutination test للكشف عن الأجسام المضادة لمقوسات كوندي *Toxoplasma gondii* واستخدمت طريقة الاستشعاع المناعي غير المباشر IFAT لقياس مستوى الكلوبيولين المناعي IgM للكشف عن الحالات الحادة Acute و المزمنة Chronic .

وجدت الأجسام المضادة للطفيلي في ٣٠ عينة وتركزت أعلى إلاصابات عند الفئة العمرية(٢٦-٣٠-٣١-٣٥) وأظهرت غالبية النساء أعلى معيارية 32:1 (320 وحدة دولية /مل) وخصوصا في الفئات العمرية 26-31,30-35 سنة حيث سجل أعلى عدد للإجهاض من العدد الكلى (٥٠) .

ولأهمية قياس الكلوبيولين المناعي IgM تم استخدام IFAT حيث تم فحص ٣٠ امرأة وأظهرت النتائج فحصا موجبا للعينات باستخدام IFAT بنسبة ٥٠% أي إن15 مريضة كانت أصابتهم من النوع الحاد Acute و25 مريضة من النوع المزمن .

Calculation the Cross Sections and Neutron Yield for $^{50}Cr(p,n)^{50}Mn$ Reaction

Dr. Khalid H. Mahdi **Shaemaa Akram Abbas**

Physics Department – College of Ibn Al-Haytham – University of Baghdad

Baghdad – Iraq

Receiving Date: 2011/6/5 **- Accept Date:** 2011/9/21

Abstract:

In this study intermediate elements ^{50}Cr , ^{50}Mn for $^{50}Cr(p,n)^{50}Mn$ reaction as well as proton energy from (3.4576) MeV to (148.0) MeV with threshold energy (8.8179)MeV are used according to the available data of reaction cross sections. The more recent cross sections data of $^{50}Cr(p,n)^{50}Mn$ reaction is reproduced in fine steps and by using (Matlab-7.6)program and get the equation from 10-degree for plotted .By using inverse reaction principle also get mathematical equation to calculate the cross section of $^{50}Mn(n,p)^{50}Cr$. We deduced that the high probability to produced ^{50}Cr by bombard ^{50}Mn by neutron. These cross sections together with the stopping powers calculated from the Zeigler formula have been used to calculate the n-yield for reaction.

1.Introduction

When two charged nuclei, overcoming their Coulomb repulsion, a rearrangement of the constituents of the nucleus may occur. Similar to the rearrangement of atoms in reacting molecules during a chemical reaction this may result as a nuclear reaction. Nuclear reactions are usually produced by bombarding a target nucleus with a nuclear projectile , in most cases a nucleon (neutron or proton) or a light nucleus such as a deuteron or an α-particle ***[1]***.

At low excitation energies (< 10 MeV), the majority of nuclear reactions involve the formation of two nuclei, one nearly equal in charge and mass number to the target nucleus. Such reactions are represented by an equation of the type :

$$X + a \rightarrow Y + b \quad \text{------ (1)}$$

Or $X\,(a,b)\,Y$

Where (a) is the light projectile nucleus (proton , neutron, deuteron, ^{3}H, ^{3}He, or ^{4}He) and (*X)* is the target nucleus at rest in the laboratory system. (*Y)* is the produced nucleus and (b) is a light nuclear particle which carries away the major share of the kinetic energy. If the product nucleus (*Y*) is left in an excited state after the emission of the light particle (b), it usually subsequently decays by radiating one or more gamma rays. Alternatively if *(Y*) is beta unstable, it decays at some later date by electron or positron emission followed by gamma emission ***[2]***.

Nuclear reactions of low excitation energies include the following types : *(n,γ)* , *(n,p)* , *(n,α)* , *(α,n)* , *(p,γ)* , *(p,n)* , *(d,n)* , *(d,p)* , …..etc.

$$X + a \longrightarrow \begin{cases} X + a, \\ X^{*} + a, \\ Y + b, \\ Y^{*} + b, \end{cases} \quad \text{---------- (2)}$$

In the first two reactions of the set (2) the outgoing particle is of the same kind as the incident particle, and the process is called scattering. The first reaction represents elastic scattering and the second reaction represents inelastic scattering in which the target nucleus (X) is raised into an excited state (X^*). The other reactions of the set represent different possible nuclear transmutations in which the product nuclei may be found in their ground states or, more often, in excited states. The excited product nucleus usually decays very quickly to the ground state with the emission of γ-rays.

2. Cross Sections Of Nuclear Reactions:

To characterize the probability that a certain nuclear reaction will take place, it is customary to define an effective size of the nucleus for that reaction, called a cross section ***[1]***. The reaction cross section data provides information of fundamental importance in the study of nuclear systems. The cross section is defined by ***[3]***:

$$\sigma = R / I \quad \text{------ (3)}$$

where (σ) is the cross section,

(R) is the number of reactions per unit time per nucleus.

(I) is the number of incident particles per unit time per unit area,

The cross section has the units of area and is of the order of the square of nuclear radius and a commonly used unit is the barn:

$$1 \text{ barn} = 10^{-24} \text{ cm}^2$$

In general, a given bombarding particle and target can react in a variety of ways producing a variety of light reaction products per unit time. The total cross section is then defined as ***[4]***:

$$\sigma_{tot} = \sum_i \sigma_i \quad \text{------- (4)}$$

Where σ_i is the partial cross section for the process.

3. Stopping Power:

The stopping power is define a measure of the effect of a substance on the kinetic of a charged particle passing through it. Stopping power is often quoted relative to that of a standard substance, usually air or aluminum ***[5]***.

4. Proton Stopping Power :

For hydrogen projectiles, the nuclear stopping power is very small for all energies of interest ***[6]***. The electronic stopping power is found to be proportional to projectile velocity, the specific dependence ***[7]*** being given by:

$$S_e = Z_1^{1/6} \times 8\pi e^2 a_o \frac{Z_1 Z_2}{(Z_1^{2/3} + Z_2^{2/3})^{3/2}} \times \frac{\upsilon}{\upsilon_o}, \quad \text{-- (5)}$$

where $\upsilon < \upsilon_o Z_1^{2/3}$ and (Z_1), (Z_2) are the atomic numbers of projectile and target respectively .

(υ) is the projectile velocity,

(a_o), (υ_o) are the Bohr radius of the hydrogen atom and the Bohr velocity.

In the present work ,by using the formulas proposed by Varelas and Biersack sited in Ziegler ***[6]***

$$S_e = \frac{S_{Low} S_{High}}{(S_{Low} + S_{High})} \quad \text{------ (6)}$$

Where S_{Low} (Low energy stopping) is

$$S_{Low} = B_1 E^{1/2} \quad \text{------ (7)}$$

And S_{High} (High energy stopping) is

$$S_{High} = \frac{B_2}{E}\ln(1+\frac{B_3}{E}+EB_4) \text{ ----- (8)}$$

where B_1, B_2, and B_3 are fitting constants

$B_4 = 4\ m / I\ M$

where (m) is the electron mass,

(I) is the mean ionization potential,

(M) is the projectile mass

Eq.(6) asymptotically agree with eq.(5) at low energy , and with Bethe formula [6] at high energy .

5. Neutron Yields :

For an accelerating beam traversing a target, the occurred nuclear reactions produce (N) light product particles per unit time. Referring to Fig. (1) the yield is given by

$$Y(x) = I_o\ N_d\ \sigma\ x \quad \text{------ (9)}$$

Experimentally, the yield of neutrons detected per incident particle, Y_n, for an ideal, thin and uniform target and mono-energetic beam of energy (E) is given by

$$Y_n = (N_d\ x)\ \sigma(E_b)\ \eta(E_b) \quad \text{----- (10)}$$

where $(N_d\ x)$ is the a real number density of target atoms, and $(\eta)$is the neutron-detection efficiency.

For a target which is not infinitesimally thin, the beam loses energy as it passes through the target, and the yield is then given by ***[8]***

$$Y_n = \int_{E_t}^{E_b} \frac{\sigma(E`)\eta(E`)\ fdE`}{\frac{dE}{dx}(E`)} \text{ --- (11)}$$

in which $E_t = E_b - \Delta E$, where (ΔE) is the energy loss of the beam in the target, f is the number of target atoms in each target molecule, and $\frac{dE}{dx}(E`)$ is the stopping power per target molecule, If the target is sufficiently thick, and there exist one atom per each molecule (i.e., $f = 1$) and taking $\eta(E`) = 1$, then the resulting yield is called the thick-target yield which is given by

$$Y(E_b) = \int_{E_{thr}}^{E_b} \frac{\sigma(E)dE}{dE/dx} \quad \text{------ (12)}$$

where E_{thr} is the reaction threshold energy.

Thus, by measuring the yield at two closely spaced energies (E_1) and (E_2), one can determine the average value of the integrand over this energy interval as follows ***[9]***:

$$[\frac{\sigma(E)}{dE/dx}]_{E_b} = \frac{Y(E_2) - Y(E_1)}{E_2 - E_1} \quad \text{---- (13)}$$

Where (E_b) is the average of (E_1) and (E_2). If $\sigma(E)$ are available in the literature as a function of projectile energy (E_b) for natural elements, then the neutron yield can be calculated using eq.(13). If neutron yield is available as a function of projectile energy (E_b), then eq. (13) can be used to calculate $\sigma(E)$ as a function of (E_b). Thus, consequently one can calculated the neutron yield by using eq. (13).

For natural elements and if only one stable isotope is available in nature, then ***[10]***

$Y_o = Y(E)$ ------ (14)

where (Y_o) is the neutron yield per 10^6 bombarding particle for the natural element.

If $\sigma(E)$ is calculated for a certain isotope whose concentration (enrichment) is C %, then ***[10]***

$$Y_o = \frac{a}{c} Y(E) \quad \text{------ (15)}$$

where (a)is the abundance of the isotope in the natural element. If there exist more than one isotope that can be involved in the nuclear reaction and the cross sections are calculated as a function of incident energy for each isotope, then ***[10]***.

$$Y_o = \frac{a_1}{c_1} Y_1(E) + \frac{a_2}{c_2} Y_2(E) + ... \quad \text{---- (16)}$$

6. Results and Discussion

These data have been plotted, spline interpolated and recalculated in fine steps for proton energy from (3.4576) MeV to (148) MeV ***[11]*** by using Matlab program as shown in table (1). The reproduced cross sections by authors Chiba S., Chadwick M., Young P. ***[11]*** and declared by EXFOR-Library, we get the equation from 10-degree for plotted shown in Fig.(2) as fallows:

$Y = -4.3*10^6*x^7 + 2.6*10^6*x^6 - 6.5*10^5x^5 + 8.6*10^4 * x^4 - 6.1*10^3*x^3 + 1.9*10^2*x^2 + 2.6*x + 0.1$ By using the compound theory we derive the mathematical formula for ^{50}Mn(n,p)^{50}Cr reaction for first exited state :

$$\sigma_{n,p} = 0.45417 \frac{T_p}{T_n} \sigma_{p,n} \quad \text{----- (17)}$$

Using semi empirical formula the evaluated cross sections as a function of neutron energy from (0.1821)MeV to (113.184)MeV of present work are listed in table (2). From these data which were plotted and we get the mathematical equation representing the cross sections distribution in the indicated range of neutron energy Fig.(3) as follows :

$$y = -4.1*10^{-19}*x^{10} + 3*10^{-16}*x^9 - 9.5*10^{-14}*x^8 + 1.7*10^{-11}*x^7 - 1.9*10^{-9}*x^6 + 1.4*10^{-7}*x^5 - 6.7*10^{-6}*x^4 + 0.00021*^{x3} - 0.0039*x^2 + 0.038*x + 0.36 \quad \text{----- (18)}$$

These cross sections together with the stopping powers calculated from the Zeigler formula (12) have been used to measure the n-yield for reaction as shown in Fig.(4).

Calculation the Cross Sections and Neutron Yield for $^{50}Cr(p,n)^{50}Mn$ Reaction

Dr. Khalid H. Mahdi Shaemaa Akram Abbas

حساب المقاطع العرضية والحصيلة النيوترونية لتفاعل $^{50}Cr(p,n)^{50}Mn$

خالد هادي مهدي شيماء أكرم عباس

جامعة بغداد كلية التربيه – ابن الهيثم قسم الفيزياء

الخلاصة

في هذه الدراسة اعيد حساب المقاطع العرضية للنوى المتوسطة ^{50}Mn , ^{50}Cr للتفاعل $^{50}Cr(p,n)^{50}Mn$للبيانات المتوفرة في الادبيات العالمية وللمدى الطاقي من (3.4576) MeV الى (148.0) MeV وبطاقة عتبه مقدارها (8.8179)MeV كدالة للمقاطع العرضية .بأستخدام نظرية التعاكس تم اشتقاق معادلة لحساب المقاطع العرضية لتفاعل $^{50}Mn(n,p)^{50}Cr$ وذلك بالاعتماد على المقاطع العرضية لتفاعل $^{50}Cr(p,n)^{50}Mn$. تم رسم وجدولة النتائج بالاضافة الى مناقشة النتائج وتحديد نوع النيوترون لأنتاج ^{50}Cr .أستخدمت هذه المقاطع العرضيه المستحدثة مع قدرة الايقاف المحسوبة من معادلات Zeigler لحساب الحصيلة النيوترونية للتفاعل المذكور.

Reference

1. Meyerhof W.E., **(1967)** "Elements of Nuclear Physics" , McGraw- Hill Book Co.
2. Smith C. M. H., **(1964)** , "Nuclear Physics " .
3. cottingham W.N. and Greenwood D.A., **(2001)**," An Introduction to nuclear physic", 2nd ed. S Cambridge univ . press.
4. Jean L.B., James R., and Michel S., **(2005)** ,"Fundamentals in Nuclear physics" springer, p.14- 6 .
5. Arora E.D. , **(2003)** ; "Dictionary of Physics" ," Low Cost Text Book Publishers", Delhi, India.
6. Anderson H.H. and Ziegler J.F., **(1977)** , "Hydrogen: Stopping Powers and Ranges in all elements " vol.3, Pergamon Press, Oxford .
7. Linhard J. and Scharff M., **(1961)** , Phys. Rev. 124, 128 .
8. Wrean P.R., Ph.D. Thesis, California Institute of Technology, **(1998)**.U.S.A.
9. Norman E.B., Chupp T.E., Lesko K.T., Grant P.J., & Woodruff G.L. **(1984)** : Phys. Rev. C 30, 1339.
10. Abdulla R. H., **(1999)**, Ph.D. thesis, University of Baghdad .
11. Chiba S., Chadwick M. , Young P. , **(1999)** ," The evaluation is based on nuclear model calculations that have been benchmarked to experimental data" , ENDF/B-VII

Table (1):The cross sections of $^{50}Cr(p,n)^{50}Mn$ reaction as a function of proton energy with threshold energy (8.8179)MeV

p -energy (MeV)	Cross sections (mbarn)	p -energy (MeV)	Cross sections (mbarn)	p -energy (MeV)	Cross sections (mbarn)
3.4576	0.0554	30.1084	0.9495	73.0000	0.7698
4.0000	0.1189	30.2599	0.9484	74.0000	0.7667
5.0000	0.2638	31.0000	0.9423	75.0000	0.7637
6.0000	0.4073	29.0000	0.9570	76.0000	0.7608
7.0000	0.5375	30.0000	0.9503	77.0000	0.7578
8.0000	0.6597	32.0000	0.9328	78.0000	0.7550
8.5842	0.7201	32.0715	0.9321	79.0000	0.7521
8.7296	0.7331	33.085	0.9224	80.0000	0.7493
9.0000	0.7553	34.0000	0.9144	81.0000	0.7465
9.7838	0.8082	35.0000	0.9078	82.0000	0.7438
10.0000	0.8197	35.3458	0.9060	83.0000	0.7411
10.9934	0.8627	35.3992	0.9058	84.0000	0.7384
11.0000	0.8629	35.4093	0.9057	85.0000	0.7358
11.8652	0.8881	35.6683	0.9045	86.0000	0.7332
12.0000	0.8916	36.0000	0.9029	104.0000	0.6941
13.0000	0.9156	36.0311	0.9027	106.0000	0.6908
14.0000	0.9356	36.9437	0.8986	108.0000	0.6875
15.0000	0.9520	37.0000	0.8984	110.0000	0.6845
15.4051	0.9577	37.0052	0.8983	112.0000	0.6816
16.0000	0.9652	38.0000	0.8942	114.0000	0.679
16.6785	0.9722	38.7228	0.8913	116.0000	0.6765
16.7206	0.9726	39.0000	0.8903	118.0000	0.6743

16.7686	0.9730	39.8840	0.8869	120.0000	0.6723
16.8945	0.9741	40.0000	0.8865	122.0000	0.6705
17.0000	0.9750	41.0000	0.8828	124.0000	0.6689
18.0000	0.9814	42.0000	0.8791	126.0000	0.6675
19.0000	0.9849	42.4270	0.8776	128.0000	0.6664
19.2834	0.9855	43.0000	0.8755	130.0000	0.6654
19.9169	0.9863	43.1451	0.8749	132.0000	0.6646
20.0000	0.9864	44.0000	0.8718	134.0000	0.664
21.0000	0.9862	44.4436	0.8701	136.0000	0.6637
21.9342	0.9852	45.0000	0.8680	138.0000	0.6636
22.0000	0.9851	45.3450	0.8667	140.0000	0.6638
23.0000	0.9831	46.0000	0.8641	142.0000	0.6643
23.2553	0.9825	46.2916	0.8630	144.0000	0.665
23.2777	0.9825	48.0000	0.8564	146.0000	0.6661
24.0000	0.9805	48.3759	0.855	148.0000	0.6675
24.2476	0.9798	49.0000	0.8526	----	----
25.0000	0.9773	50.0000	0.8488	----	----
26.0000	0.9733	51.0000	0.8450	----	----
26.2704	0.9721	51.2295	0.8441	----	----
26.3120	0.9719	52.0000	0.8412	----	----
26.3378	0.9718	53.0000	0.8375	----	----
27.0000	0.9686	54.0000	0.8338	----	----
27.3797	0.9666	55.0000	0.8301	----	----
28.0000	0.9631	55.7216	0.8275	----	----
28.3553	0.9611	56.0000	0.8265	----	----
28.4858	0.9603	57.0000	0.8229	----	----

28.5676	0.9598	57.8851	0.8197	----	----

Table (2): The cross sections of $^{50}Mn\ (n,p)^{50}Cr$ reaction as a function of neutron energy.

n -energy (MeV)	Cross sections (mbarn)	n -energy (MeV)	Cross sections (mbarn)	n -energy (MeV)	Cross sections (mbarn)
0.1821	0.3822	24.1824	0.4671	54.1828	0.4058
0.9659	0.4089	24.2675	0.4667	55.1828	0.4041
1.1821	0.4148	25.1824	0.4627	56.1828	0.4024
2.1755	0.4365	26.1824	0.4594	57.1829	0.4007
2.1821	0.4366	26.5282	0.4585	58.1829	0.3991
3.0473	0.4494	26.5817	0.4583	59.1829	0.3975
3.1821	0.4511	26.5918	0.4583	60.1829	0.3958
4.1822	0.4633	26.8507	0.4577	61.1829	0.3942
5.1822	0.4734	27.1825	0.4569	62.1829	0.3926
6.1822	0.4817	27.2136	0.4568	63.1829	0.3911
6.5873	0.4846	28.1262	0.4547	64.1829	0.3895
7.1822	0.4884	28.1825	0.4546	65.183	0.388
7.8607	0.4919	28.1877	0.4546	66.183	0.3865
7.9028	0.4921	29.1825	0.4525	67.183	0.385
7.9508	0.4924	29.9053	0.451	68.183	0.3835
8.0767	0.4929	30.1825	0.4505	69.183	0.382
8.1822	0.4933	31.0665	0.4488	70.183	0.3806
9.1822	0.4966	31.1825	0.4486	71.183	0.3791
10.1822	0.4984	32.1825	0.4467	72.1831	0.3777
10.4657	0.4987	33.1825	0.4448	73.1831	0.3763

10.4827	0.4987	33.6095	0.4441	74.1831	0.375
11.0991	0.4991	34.1826	0.443	75.1831	0.3736
11.1822	0.4991	34.3276	0.4427	76.1831	0.3723
12.1823	0.499	35.1826	0.4411	77.1831	0.371
13.1165	0.4985	35.6261	0.4403	78.1831	0.3697
13.1823	0.4985	36.1826	0.4392	79.1831	0.3685
14.1823	0.4975	36.5276	0.4385	80.1832	0.3672
14.4375	0.4972	37.1826	0.4373	81.1832	0.366
14.46	0.4971	37.4742	0.4367	82.1832	0.3648
15.1823	0.4962	38.1826	0.4353	83.1832	0.3636
15.4299	0.4958	39.1826	0.4334	84.1832	0.3625
16.1823	0.4945	39.5585	0.4326	85.1832	0.3613
17.1823	0.4925	40.1826	0.4314	86.1832	0.3602
17.4528	0.4919	41.1826	0.4295	87.1833	0.3591
17.4943	0.4918	42.1827	0.4276	88.1833	0.3580
17.5201	0.4917	42.4122	0.4271	89.1833	0.3570
18.1823	0.4901	43.1827	0.4257	90.1833	0.3560
18.5620	0.4891	44.1827	0.4238	91.1833	0.3550
19.1824	0.4874	45.1827	0.4219	93.1833	0.3531
19.5377	0.4863	46.1827	0.4200	95.1834	0.3512
19.6682	0.4859	46.9044	0.4187	97.1834	0.3495
19.7500	0.4857	47.1827	0.4182	99.1834	0.3479
20.1824	0.4843	48.1827	0.4164	101.183	0.3463
21.1824	0.4808	49.0678	0.4148	103.184	0.3449
21.2908	0.4805	49.1828	0.4146	105.184	0.3436
21.4423	0.4799	50.1828	0.4128	107.184	0.3423

22.1824	0.4768	51.1828	0.4110	109.184	0.3412
23.1824	0.4720	52.1828	0.4093	111.184	0.3402
23.2539	0.4717	53.1828	0.4075	113.184	0.3393

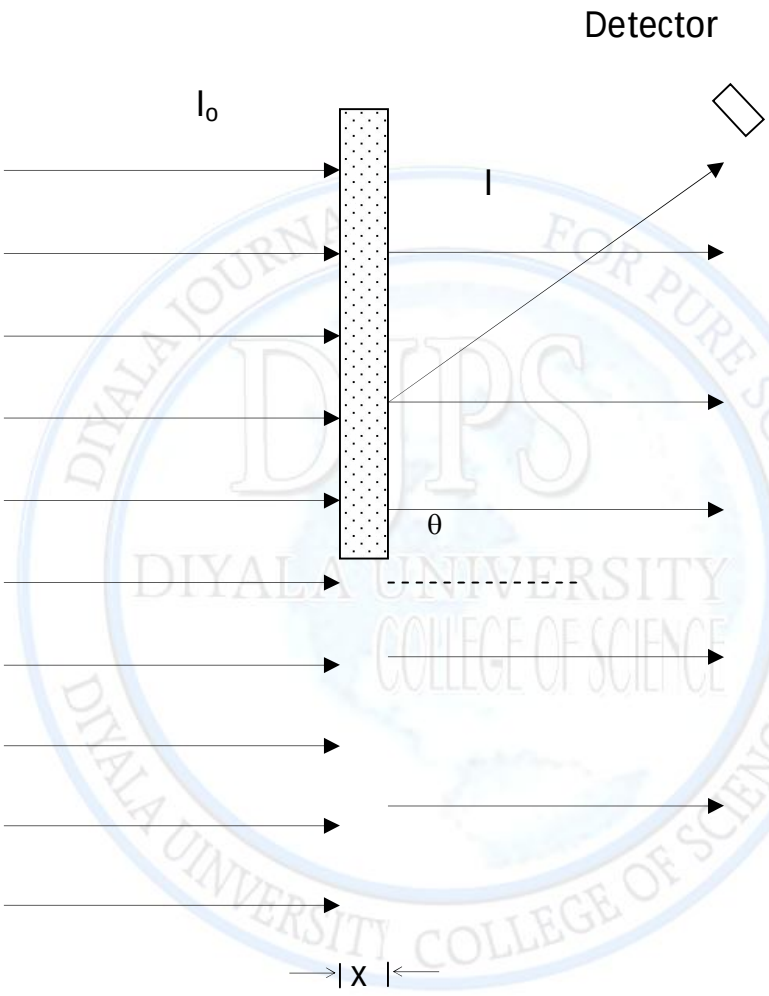

Figure (1): A schematic diagram illustrating the definition of total cross section in terms of the reduction of intensity***[8]***

Calculation the Cross Sections and Neutron Yield for $^{50}Cr(p,n)^{50}Mn$ Reaction

Dr. Khalid H. Mahdi Shaemaa Akram Abbas

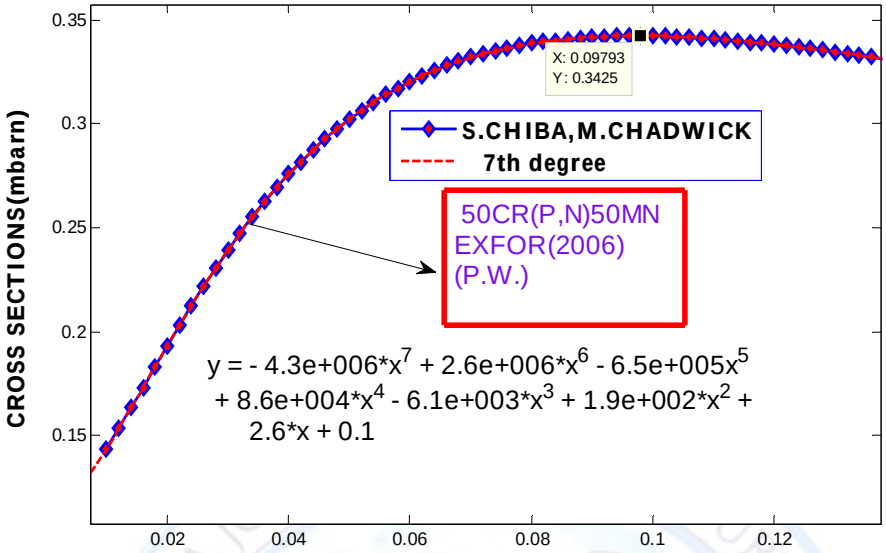

Figure (2):Cross Sections for 50Cr(p,n)50Mn

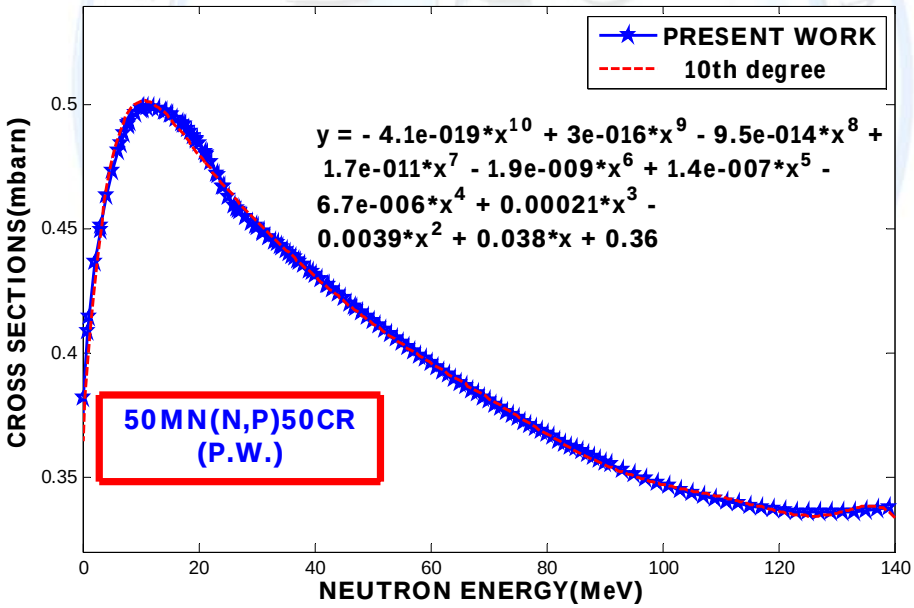

Figure(3):Cross Sections of 50Mn(n,p)50Cr

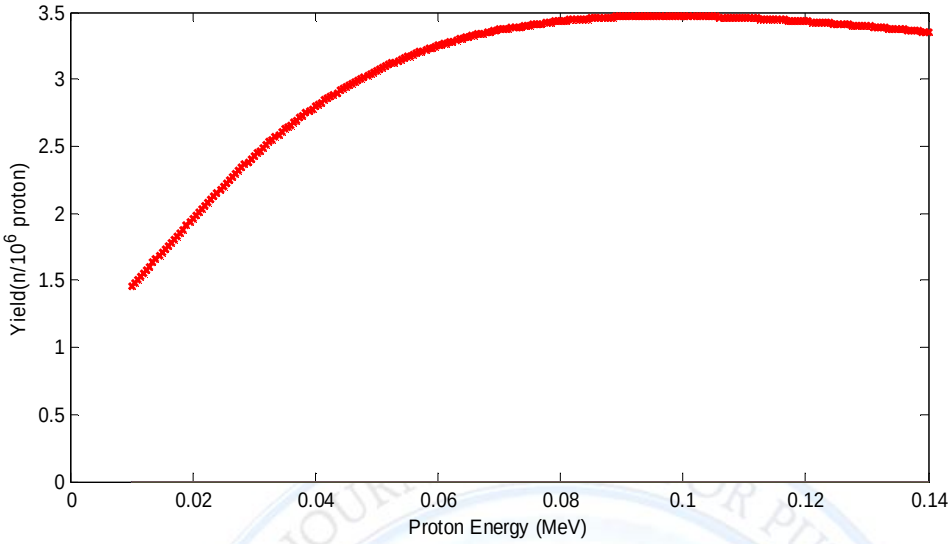

Fig.(4) : Neutron Yield for $^{50}Cr(p,n)^{50}Mn$ reaction

Effect of irradiation on the optical properties of PbSe thin film prepared by thermal evaporation method

Jasim Mohammed Abid Al-Leteef
University of Diayla College of science - Physics department

Receiving Date: 2011/9/18 - **Accept Date:** 2012/2/7

Abstract:

In this research, the effect of γ -rays from (Cs^{137}) source a time period (21) days on optical properties such as energy gap (E_g) , the optical Transmittance (T%) spectra , optical Absorption spectra (A), optical reflectance spectra (R %), absorption coefficient (α) ,Urbach energy (E_u), extinction coefficient (k) , refractive index(n) and dielectric constants for the lead selenide (PbSe) thin films prepared by the thermal evaporation on a glass substrate in 5×10^{-5} mbar pressure at room temperature of thickness (7000 Å) and rate of deposition (1.46 nm/s) . it were seen that all the parameters under investigation affected by gamma irradiation.

تأثير أشعة كاما على الخصائص البصرية لأغشية PbSe الرقيقة المحضر بطريقة التبخير الحراري في الفراغ

جاسم محمد عبد اللطيف

جامعة ديالى ، كلية العلوم، قسم الفيزياء

الملخص:

تم في هذا البحث دراسة تأثيرالتشعيع بأشعة كاما لمصدر(Cs^{137}) لمدة (21) يوم على الخواص البصرية المتمثلة بفجوة الطاقة البصرية(E_g) ، طيف النفاذية البصرية ، طيف الامتصاص البصري (A) ، طيف الانعكاسية البصري (R %) ، معامل الامتصاص(α) ، طاقة اورباخ(E_u) ، معامل الخمود (k) ، معامل الانكسار(n) وثابت العزل بجزأيه الحقيقي والخيالي لأغشية سلايند الرصاص(PbSe) المحضرة بطريقة التبخير الحراري على قواعد زجاجية في ضغط (5×10^{-5} mbar) عند درجة حرارة الغرفة بسمك(7000 Å) ومعدل ترسيب (1.46 nm/s) . ولقد وجد أن جميع المعلمات التي تمت دراستها قد تأثرت بأشعة كاما.

Effect of irradiation on the optical properties of PbSe thin film prepared by thermal evaporation method

Jasim Mohammed Abid Al-Leteef

1. Introduction

It is now a well known fact that the exposure of any solid material to ionizing radiations (such as X-rays, gamma rays, beta particles, alpha particles, fission fragments, etc) produces changes in the microstructural properties of the material, which in turn affects the optical and electrical properties.[1]

Studies on the changes in optical properties of thin films irradiated with ionizing radiations yield valuable information's regarding the electronic processes in these materials. High-energy radiations, such as γ -rays, change the physical properties of the materials they penetrate. The changes are strongly dependent on the internal structure of the absorbed substances. It is believed that ionizing radiation causes structural defects (called colour centres or oxygen vacancies in oxides) leading to their density change on the exposure to γ-rays [2].

The presence of such colour centres in a thick film matrix gives rise to changes in both the optical and electrical properties of the material, which can be utilised to assess the radiation dose absorbed [3].

The influence of radiation depends on both the dose and the parameters of the films including their thickness: the degradation is more severe for the higher dose and the thinner films [4].

Lead chalcogenides (PbSe, PbTe, and PbS) are IV-VI narrow band-gap semiconductor over several decade have been motivated by their importance for applications such as IR detectors, photographic plates, photo resisters ,lasers, light-emitting device, photovoltaic's, and high temperature thermoelectric [5-6]. Among the group compounds, Lead selenide (PbSe) thin film is used as a target material in infrared sensor, grating, lenses and various optoelectronic devices [7]. It has a cubic crystal structure (FCC) type ,a lead-grey ,somewhat bluish substance and a direct band gap of 0.27 eV in room temperature ,the refraction index at (3 μm) is (4.54) and the dielectric constant is (280). [8-10] Thus, the PbSe thin films attract attention of many researchers because they are cheap, abundant and they posses semiconducting properties. In the past, several techniques such as thermal evaporation electrodeposition , chemical bath deposition, , photochemical , sputtering, spray pyrolysis, sonochemistry , sonoelectrochemistry , microwave heating, molecular beam epitaxy , electrochemical atomic layer epitaxy and pulsed laser deposition method have been used in the deposition of PbSe thin films.[11,12]

Among the thermal evaporation method is one of the oldest and still most widely used techniques for depositing thin films because of it is cheap, non poisonous, easy method to produce films of extreme purity and , a certain extent of pre-selected structure . [13,14]

The aim of this experimental work is to investigate the changes in the optical properties of PbSe thin film structures under the influence of γ -radiation.

2. Experimental

The deposition process of PbSe thin films were done on commercial glass slides with 1mm thick and 2.5 × 7.5 cm^2 size. Before the deposition they were washed with detergent and a piece of gauze then rinsed many times in distilled water then cleaned by detergent solution then washed by distilled water and finally they were cleaned by using ethanol solution then The ultrasonic was used to clean glass substrates using isopropyl alcohol and finally the substrates were dried by blowing air. Thin films PbSe with weight percentage (0.5) of Pb and Se were grown with a thickness of 0.7 µm on glass substrates at a substrate temperature (T_s) equal to RT by thermal evaporation method using the Edward E306A coating system. The molybdenum boat which was used for film deposition with a high purity (99.999%) and covered with baffle. since the vacuum pressure during evaporation was about 2×10^{-5} torr and the deposition rate is about 1.46 nm/s.

The distance between the boat and substrate was kept at 15 cm. The substrate temperature was measured and controlled using digital thermometer.

A disc-type Cs^{137} gamma radiation source was used to expose PbSe thin films under Investigation for seven days to dose of about 18 Gy at room temperature.

The optical transmission and absorption spectra for unirradiated and irradiated PbSe films deposited at room temperature were obtained in infrared region with 2.5 µm to 5 µm using PYE UNICAM(Philips) , UV- spectrophotometer (Model: PU 9712). The measurements were done in the wavelength scanning mode under the infrared radiation(IR).

3. Results and discussion

The optical properties of a semiconductor can be defined as any property that involves the interaction between electromagnetic radiation or light and the semiconductor, including absorption, diffraction, polarization, reflection, and scattering effects. The best values of the band gap are obtained by the measurement of optical absorption[15]**.** Knowledge of optical constant of a film from a given material is basic importance in determining the characteristics of light transmission of the film. Such knowledge of the optical parameters of the material is of importance when designing devices through which electromagnetic radiation absorbed or transmitted[16].Therefore, the optical Transmittance (T%) and optical Absorption (A) spectra of unirradiated and irradiated PbSe films deposited at R.T in the spectral range(2.5-5 µm) are shown in Figure (1).

The percentage of transmittance peak for unirradiated and irradiated PbSe films deposited at R.T are decreases from 32% to 25% in infrared region respectively . We notice also that the transmittance (for both curves) decreases with uniform on the exposure to γ -rays and shifted toward longer wavelengths. This behavior could be explained as follows ; an increasing roughness of the irradiated thin films contributed to the drastic decrease of optical transmittance[17].

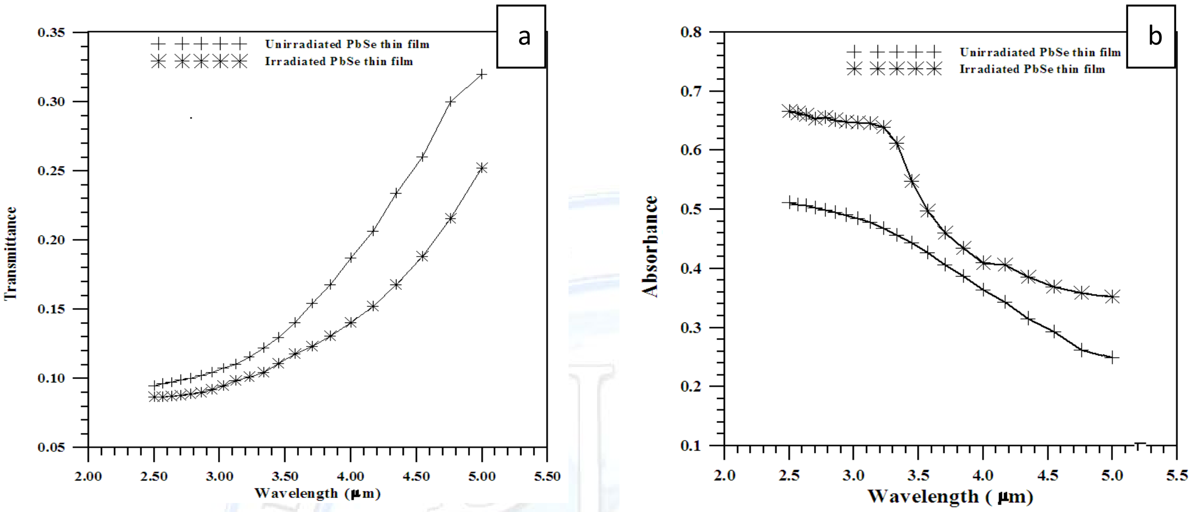

Figure(1) (a) Transmittance[%] versus Wavelength. (b) Absorbance versus Wavelength

It is observed that the Absorbance e (for both curves) decreases at the spectral region of fundamental absorption as a function of wavelength (μm) from (2.5 to 5μm).

The spectral behavior of these films shows that the absorption edge shift to shorter wavelength (higher energy) for the irradiated thin films. In this region the incoming photons have sufficient energy to excite electrons from the valence band to the conduction band and thus these photons are absorbed within the material to decrease the transmittance.[18]

Fig. 1c is a plot of reflectance as a function of wavelength for PbSe thin films in this work. In general the film shows the reflectance is below 43.3% and decreases with irradiation. This is occurs as a result to transmittance decreasing according to the relation[19]:

$R=1- T-A$ .... (1)

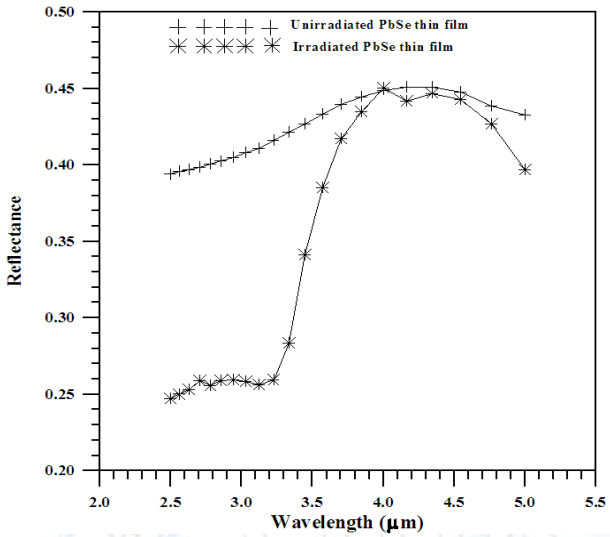

Fig. 1c. Reflectance vs. wavelength for PbSe

The variation of absorption coefficient(α) with wavelength is shown in the Fig.(2). Both films show higher absorption(or shift) on the shorter wavelength(or higher energy) side, this is attributed to increase the defect states which leads to increase absorption coefficient.

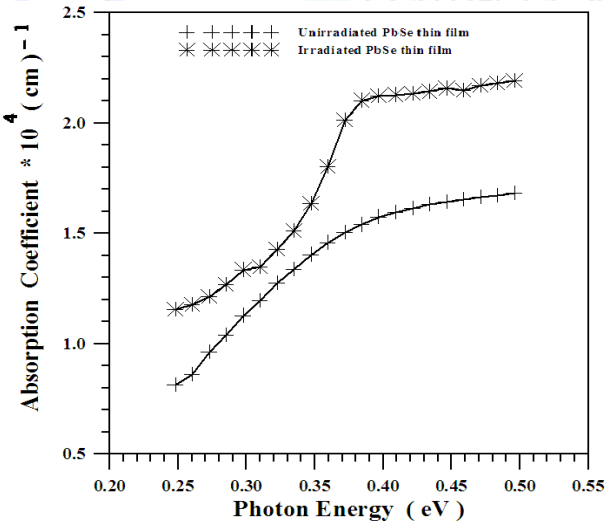

Figure (2) Absorption Coefficient as a function of Photon Energy (eV).

Clearly, exposure to gamma radiation produces considerable change in the shape of the optical absorption spectrum around the absorption edge. From an optical absorption curve, the

values of the absorption coefficient, α_ν, for different values of the photon frequency, were calculated using the relationship[20]:

$$\alpha_\nu = 2.303\ A_\nu / t \quad \text{……………………………………………………..…… (2)}$$

where A_ν denotes the absorbance corresponding to the photon frequency(ν) and (t) the thickness of the thin film. The absorption coefficient near the band edge shows an exponential dependence on the photon energy and obeys the Urbach's empirical formula [21] :

$$\alpha_\nu = \alpha_o\ e^{h\nu/\Delta E} \quad \text{………………………………………………………... (3)}$$

where α_o is a constant, h the Planck's constant and Δ E the energy width of the band tails of localized states. The graphs of lnα vs photon energy(hν) were plotted for unirradiated and irradiated PbSe films deposited at R.T and the values of Δ E were calculated from the reciprocal of the slopes of the straight-line portions of these plots as shown in figure 3. The energy width of the band tails of localized states (Δ E) has been found to increase with the gamma radiation from(0.137 eV to 0.183 eV) for unirradiated and irradiated films respectively . This increase in the energy width of the band tails of localized states can be attributed to the induced defects due to the exposure to gamma radiation.

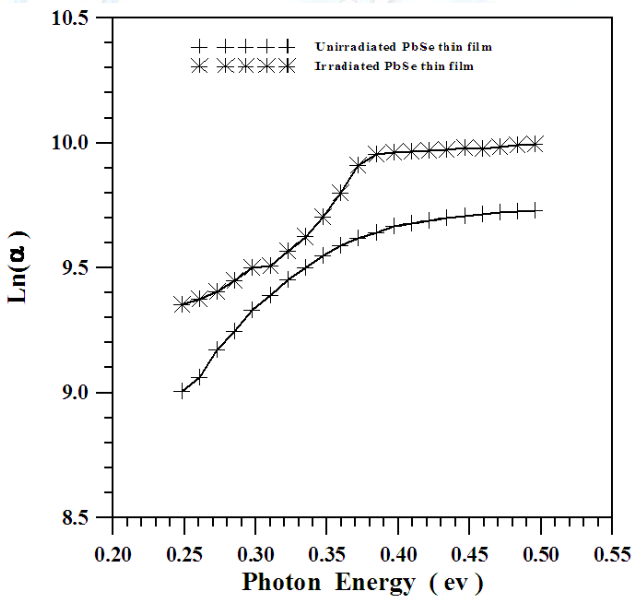

Figure (3) Ln(α) as a function of Photon Energy (eV).

The optical band gap was calculated using the Tauc [22] relation given by the formula

$$\alpha h\nu = A(h\nu - Eg)^n \quad \text{……………………………………………………..…… (4)}$$

Here hν is the photon energy, α is the absorption coefficient , Eg is the optical band gap, A is a constant and n =1/2 for direct band gap material. We plotted $(\alpha h\nu)^2$ vs. photon energy in the wavelength range 2.5–5 μm , the values of the optical band gap are determined by extrapolating the linear part of $(\alpha h\nu)^2$ vs. energy axis for direct allowed transitions, as shown in figure(4).

.

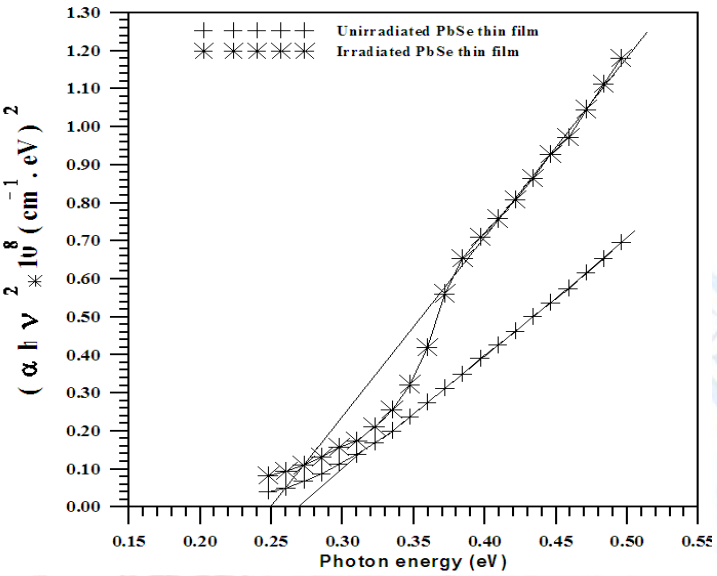

Figure(4) Band gap E_g estimation for PbSe films.

The optical band gap was shifted from 0.27 eV to 0.25 eV due to irradiation . Gamma doses cause the breaking of bonds, leading in turn to the increase of dangling bonds and of defects, as well as the trapping of the generated carriers. This may be the cause for the increase in band tail width(Δ E), and then decrease energy gap.

Refractive index is one of the fundamental properties for an optical material, because it is closely related to the electronic polarizability of ions and the local field inside materials. The evaluation of refractive index of optical material is important for many applications especially in optical devices .It is clear from figure (5) for the irradiated film ,that there are two regions of refractive index (n) spectrum. The first region occurs at (λ=2.5-4 μm) and the second region starts where λ exceeds(4 μm).The refractive index (n) increases in the first region ,results from the electronic transitions of valence band and the impurities(or increase of the compactness of the films) and the transitions of energy bands. These values are reduced sharply with increasing in wavelengths. In the second region of spectrum, the variation of refractive index (n) with wavelengths becomes slight decreases and its values are very close at cut-off wavelength. It can be calculated from the following equation [23,24]:

$$n = \left[\left(\frac{1+R}{1-R} \right)^2 + (k^2 + 1) \right]^{1/2} + \frac{1+R}{1-R} \quad \text{.....(5)}$$

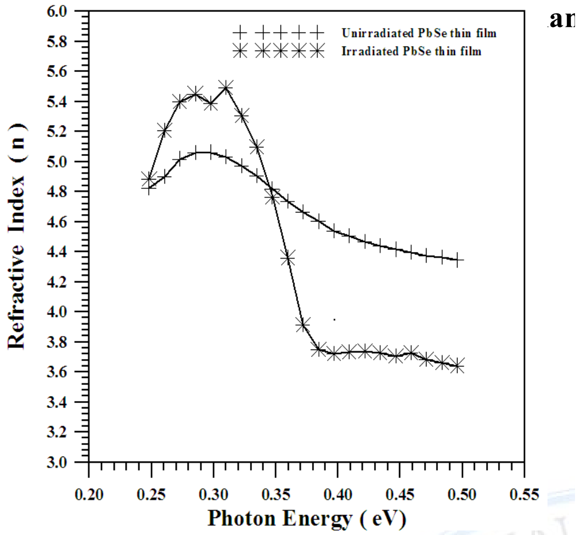

Figure(5) Refractive Index vs. Photon energy.

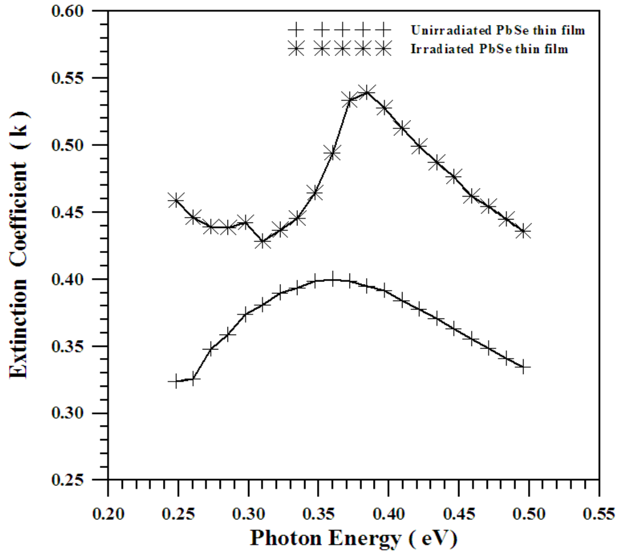

Figure(6) Extinction coefficient vs. Photon energy.

The extinction coefficient (k) represents the imaginary part of the refractive index , which is related to the exponential decay of the wave as it passes through the medium can be determined by using equation [25,26]

$$k = \frac{\alpha\lambda}{4\pi} \quad \text{.......(6)}$$

λ: is the wavelength of the incident photon.

The figure (6) shows the extinction coefficient (k) as a function of photon energy, the (k) for the unirradiated PbSe films less than (or decreases) the irradiated PbSe films ;This is attributed to the same reason mentioned previously in the absorption coefficient because the behavior of k is similar to α.

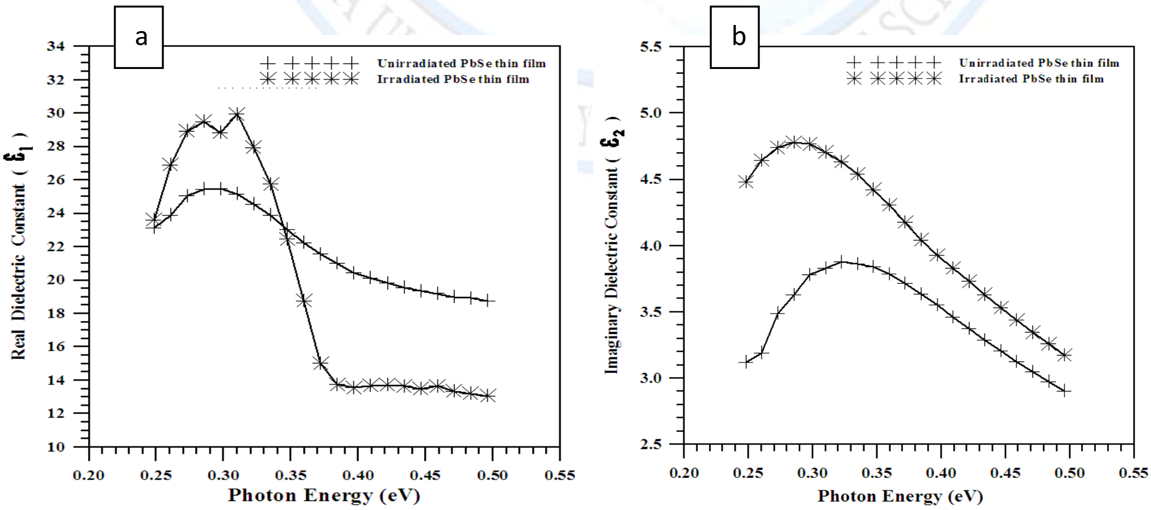

Figure (7-a&b)The (ε_1) **and** *The (ε_2) as a function of Photon Energy (eV).*

The dielectric constants consists of real part (ε_1) and imaginary part (ε_2) ,the variations of them with photon energy as shown in figure (7-a&b) and can be calculated by using equations[27]:

$$\varepsilon_1 = n^2 - k^2 \quad \text{.....(7)}$$

$$\varepsilon_2 = 2nk \quad \text{.....(8)}$$

The variation of ε_1 and ε_2 with the increase of the wavelength of the incident radiation is due to the change of reflectance and absorbance [28]. The behavior of ε_1 is similar to that of the refractive index because of the smaller value of k^2 compared with n^2, while ε_2 mainly depends on the k value, which are related to the variation of absorption coefficient. ε_2 represents the absorption of radiation by free carriers[29]. It is observed that ε_1 increases and decreases with irradiation, and this attributed to the same reason mentioned previously for the refractive index, while ε_2 increases with increasing the irradiation and this is due to the similar interpretation discussed previously for the extinction coefficient.

Conclusions

We can arrive at the following conclusions after the irradiation by gamma ray on PbSe thin film:

- Decreasing the transmittance spectral and the reflectance spectral caused by increasing the defect states which leads to the two spectral curve shifted toward the longer wavelengths,
- Increasing the Absorbance caused by increasing the defect states which leads to the position of the fundamental absorption edge shifted toward the shorter wavelength (higher energy),
- Increasing the absorption coefficient and the extinction coefficient,
- Increasing the energy width of the band tails of localized states (Δ E) this is attributed to increase the defect states which leads to decreasing the energy gap from 0.27 eV to 0.25 eV ,
- In general , decreasing the dielectric constants consists of real part (ε_1) and imaginary part (ε_2).

References

[1] A. M. Ibrahim and L. I. Soliman,"Rad. Phys. & Chem.", 53 ,469 ,(1998).
[2] R.Y.Zhu, 413, 297-311,(1998).
[3] A. Arshak, S. Zleetni and K. Arshak," Sensors",2, (2002)
[4] E. Tanassova, A. Paskaleva , R. Konakova , D. Spassov, V. F. Mitin ,32,553-562, (2001).
[5] Khang Hoang ,S.D.Mahanti, and Puru Jena,"Phys.Rev.",B76,115432,(2007).

[6] S.Prabahar,N.Suryanarayanan,K.Rajasekar,S.Srikanth,"Chalcogenide Letter", Vol.6,No.5,P.203-211.(2009).
[7] M.S. Ali, K.A. Khan, M.S.R. Khan, Phys. Status. Solidi. (a) 149,611, (1995).
[8] R. A. Smith , " Semiconductors " , 2nd edition , Cambridge University Press , (1987)
[9] D.M. Chizhikov and V.P. Shchastlivyl ," Selenium and Selenides",Collets(1968).
[10] D .R. Lide , ((Handbook of Chemistry and Physics)) , LRC Press , Boca Raton , Florida USA ,77th edition , (1996-1997).
[11] A. Kassim., .T .W. Tee, D.K.Abdullah, M. J. Haron, H. S.Min, S., Monohorn and N. Saravanan ," J.Kimia",Vol.4,No.1,P.1-6,(2010).
[12] K.W. Li, X.T. Meng, X. Liang, H. wang, H. Yan,"J. Sol. Stat. Elect.", Vol.10, P.48- 53,(2006).
[13] L. Eckertova , ((Physics of Thin Films)) , Plenum presses, New York and London (1977).
[14] R. W. Berry , P. M. Hall & M. T. Harris , ((Thin Film Technology)) , New York , Cincinnati , Toronto , London , Melbourne , (1979).
[15] C. Kittel, "Introduction to Solid State Physics", 8th ed., John Wiley and Sons, Inc., New York, (2005).
[16] R. J. Elliot and A. I. Gibson, "An Introduction to Solid State Physics and Application", 1st ed., Macillian Inc. (1974).
[17] N. Tigau , V. Ciupina , G. Prodan , G. I. Rusu , C. Gheorghies , E. Vasile , J. Optoelectron. Adv. Mater., 5, 907 ,(2003).
[18] A.N. Banerjee1, C.K. Ghosh & S. Das, K.K. Chattopadhyay .Physica B 370 , 264–276. (2005).
[19] G. Hass , ((Physics of Thin Films)) , Volume 1, Academic Press, 1963.
[20] T.K.Malty & S.I.Sharam ,"Bull. Mater . Sci.",Vol.31 ,No.6 ,pp.841-846 ,(2008).
[21] F. Urbach , " Phys. Rev." ,92 ,1324,(1953).
[22] J Tauc, "Amorphous and liquid semiconductrors" edited by J Tauc (Plenum Press, New York, p. 159,(1974).
[23] J. C. Mainfacier, J. Gasiot and J. P. Fillard, "J. Phys. E. Sci. Instrum.", 9, (1989).
[24] K. L. Chopra, "Thin Film Phenomena", McGraw-Hill, Inc., New York, (1969).
[25] J. I. Pankove, "Optical Processes in Semicoductors", Prentice – Hall, Inc., Englewoodcliffs, New Jersy (1971).
[26] R. A. Grenier "Semiconductor Device", Electronic Energy Series, McGraw-Hill, Book Co. Inc. (1961).
[27] A. H. Clark, "Polycrystalline and Amorphous Thin Films and Devices", Academic Press, New York, (1980).
[28] G.I. Rusu, P. Prepelita and N. Apetraoei, “Journal of Optoelectronics and Advanced Materials”, Vol.7, No.2, P. 829, (2005).
[29] P. Burrows and S. Forrest, “J. Appl. Phys.”, 79, 10, 7991, (1996).

THE EFFECT OF VINEGAR SOLUTION ON THE BACTERIA THAT CAUSE IMPETIGO

Anfal Shakir Motib

College of Medicine/ Diyala University

ABSTRACT

Out of fourty six samples collected from impetigo patients, fourty-two bacterial isolates were obtained, *Staphylococcus aureus* was constitute 24 isolates, *Streptococcus pyogenes* was *14 isolates and Proteus mirabilis* was only 4 isolates . The sensitivity of these bacterial isolates were tested against 7 different antibiotics . It was shown that the highest sensitivity of there isolates were against Erythromycin and Mithicillin , were as both Ciprofloxacin and Piperacillin were the most active inhibitors of the tested bacteria . On the other hand , the activity of vinegar solution of different concentration were tested against the different bacterial species isolated from impetigo cases, The results showed that the majority of bacterial isolates were sensitive to concentration between 2-32 mg\ml. The MIC and MBC of vinegar solutions toward the three bacterial species were as follows ; for *Proteus mirabilis* were 0.5-1.0 mg\ml , for *Streptococcus pyogenes* were 0.5-*0.75 mg\ml* and for *Staphylococcus aureus* were 0.15-0.25 mg\ml respectively . .

Key words:- Impetigo, Bacteria, Antibiotics, Vinegar.

THE EFFECT OF VINEGAR SOLUTION ON THE BACTERIA THAT CAUSE IMPETIGO.

Anfal Shakir Motib

الخلاصة

أجريت هذه الدراسة لاختبار فعالية محلول الخل في تثبيط نمو البكتريا المسببة لمرض القوباء، أذ جمعت 46 عينة من الأشخاص المصابيين بالمرض و تم الحصول على 42 عزلة بكتيرية وبواقع 24 عزلة من بكتريا العنقودية الذهبية و 14 عزلة من بكتريا المسبحية القيحية و4 من البكتريا المتقلبة. أختبرت حساسية العزلات البكترية تجاه سبعة من المضادات الحيوية أذ أبدت العزلات البكتيرية مقاومة عالية تجاه مضاد الارثرومايسين و الميثيسيلين بينما كان مضاد الببراسيلين و السبروفلوكساسين هما الأكثر فعالية في تثبيط نمو العزلات البكتيرية أختبرت فعالية محلول الخل على الأنواع المرضية المعزولة،و أظهرت النتائج أن أغلب العزلات كانت حساسة لمحلول الخل بالتراكيز من (2-32)ملغم \مل; ثم حددت التراكيز المثبطه والقاتله الدنيا لمحلول الخل تجاه العزلات المختلفة وكانت قيم التركيز المثبط الأدنى والتركيز القاتل الأدنى للبكتريا المتقلبه (0,5-1)ملغم\مل ولبكتريا المسبحية القيحية (0,5-0,75)ملغم\مل والبكتريا العنقودية الذهبية (5 1,0-0,25)ملغم\مل على التوالي. الكلمات المفتاحية:- القوباء، البكتريا، المضادات الحيوية، الخل.

INTRODUCTION

Impetigo is a contagious superficial pyogenic infection of the skin. It is of two main clinical forms; non bullous impetigo (impetigo contagiosa of Tilburg fox) and bullous impetigo (1).

Bacteriology:- Non-bullous impetigo may be caused by both *Staphylococcus aureus* and *Streptococcus pyogens* but there has been controversy as to the relative importance of the two genera, this may be partly depend on geographical variations. The *streptococcal* form being more prevalent in warmer climits (2,3). *Staphylococcus aureus* may be seconday invader in *streptococcal* impetigo and in some cases, it may be the predominant or the the only isolate, and the evidence for *Streptococcal* involvement may be rest on serology . Red lake Indian reservation in northern Minnesota detected both *Staphylococcus aureus* and streptococci, each alone in a sizeable minority, but both together in 58% of cultures, he concluded that in many of the mixed culture cases, the disease was primarily *streptococcal* with *Staphylococcus aures* as secondary colonizer (4). Recent European publications suggest that the *Staphylococci* may be the predominant infectious agent in most cases (5).

In *streptococcal* impetigo, lance field group A is by far the commonest, but there are occasional infections with group G and C organisms (4). Bullous impetigo is accepted as a *Staphylococcal* disease (predominantly phage group II) which produce epidermolytic toxin locally, and induce epidermal splitting and blister formation in bullous impetigo, while in generalized *Staphylococcal* scalded skin syndrome , the toxin is disseminated haematogenously (2,5).

Clinical features:- non bullous impetigo occurs more commonly in preschool age children, the initial lesion is a very thin-walled vesicle or pustule on an erythematous base, that ruptures quickly and evolving to yellowish-brown (honey-camp) crusted plaque, which show gradual irregular peripheral extension, without central healing up to (2cm) and multiple lesions were coalesce, usually there are no constitutional symptoms excepted in sever cases, but regional lymphadenopathy may be present in up to 90% of patients with sever prolonged untreated

infection. The face and the limbs are the sites more commonly affected, but lesions may occur anywhere on the body (1,5,6). Bullous impetigo occure commonly in newborn and in older infants, and is characterized by rapid progression of vesicles to flaccid bullae, which are less rapidly ruptured and become much larger(up to 1-2cm in diameter) and may persist for 2-3 days. Although the face is often affected, the lesions may occur anywhere on the skin, and the buccal mucous membrane may also be involved, but commonly, rather few lesions are present and regional lymphadenitis are rare(5,6). .

Diagnosis: is made by clinical criteria and confirmed by gram stain and culture of exudates from lesion (6).

Treatment: in mild and localized infection, a topical antibiotic alone may be suffice (e. g imupicrocin, fucidic acid, bacitracin) for both *staphylococcus* and *streptococcus* impetigo. If the infection is wide spread or sever or accompanied by lymphadenopathy or there is a reason to suspect a nephritogenic streptococcus, an oral antibiotic (flueloxacillin or erythromycin is indicated), also(azithromycin,cephalexin,cefaelor,cefprozol, and clindamycin) are alternative therapies(7,8). Black tea (as topical ointment) ,also give good result in treatment (9). Vinegar has been used in one form or another for over 10,000 years. It is used for many purposes and throughout the ages has served as a preservative, condiment, beauty aid, cleaning agent, and in medicine. The word vinegar comes from the Latin word venom meaning wine and Acer meaning sour. These two words eventually became one word and is now as vinegar. In 5000 B.C, the Babylonians fermented the fruit of date palms and created date vinegar. The roman made vinegar from grapes, figs, dates and rye. The armies of Julius Caesar would drink vinegar and water for its antiseptic properties (10). Many ancient cultures used vinegar and valued it for its medical benefits. It was used for disinfecting wounds and for insect bites and snake bites. Vinegar compresses were useful for healing bruises (11). The vinegar is a sour and astringent liquid consisting mainly from acetic acid, resulting from fermentation of an alcoholic beverage mainly whites and red wines. This product is cheap, easily found in the markets, and seems to have antimicrobial potential (12).The aim of this study is to test the effect of vinegar solution on the bacteria that cause impetigo .

MATERIAL AN D METHODS

Sample collection: Forty six patients were examined attending the out clinic of Baquba teaching hospital for the period, 30th of April to the 31st of July 2010. There were 28 males and 18 females, their age of 2-6years. They complained of rash on the skin, which was diagnosed clinically as impetigo. They were interrogated regarding the age, sex, address, chief complain, previous and present history of any associated disease. Sterile cotton swabs were taken from the lesions, under full aseptic conditions.

. **Bacterial species isolation and identification** : the samples were cultured on blood and MacConkeys agar for 24 hours at under aerobic condition for bacteriological studies, the isolation and diagnosis of types of bacteria was done according to the ideal methods (13 , 14).

THE EFFECT OF VINEGAR SOLUTION ON

THE BACTERIA THAT CAUSE IMPETIGO.

Anfal Shakir Motib

Bacterial sensitivity test to antibiotics : The sensitivity of bacterial isolates were determined against 7 different antibiotics (cefalexin, cefotaxime, methicilin, erythromycin, gentamycin, piperacillin, ciprofloxacin) using the method of kerby and bauer , according to this method , bacterial suspension of 0.1 x 10^6 CFU concentration was distributed on the surface of Muller-Hinton agar media for all bacterial species except *Streptococcus pyogenes* use blood agar instead of Muller-Hinton agar, then the antibiotic disc were put on the surface of culture media by sterile forceps . the plates were incubated under aerobic condition at 37C° for 24 hours, then the results were read by measuring the inhibition zones in mm (15).

. **Vinegar preparation**: Industrial vinegar solution prepared from local Iraqi date of has been used. Concentration of 5% acetic acid (50 mg\ml) stock solution was used and graduated concentration(32, 16, 8, 4, 2) mg\ml were prepared according to (16).

. **Bacterial sensitivity to vinegar solution**: The bacterial isolates against different antibiotics were chosen to test their sensitivity to vinegar by agar well diffusion method (17) . The activity of different concentrations of vinegar solution were determined by measuring the inhibition zone.On the other hand the minimum inhibitory concentration and minimum bactericidal concentration (MIC,MBC) of the vinegar solution by agar dilution method were also determined (18) and the used dilutions were (0.15, 0.25, 0.5, 0.75, 1, 1.5, 2.5)mg\ml .

RESULTS

Table (1) - The percentage of the bacterial isolates resistant to different antibiotics.

Proteus mirabilis	*Strept.pyogenes*	*Staph.aureus*	*Antibiotics*
50%	71.4%	50%	Cephalexin
25%	42.9%	37.5%	Cefotaxime
50%	71.4%	70.8%	Methicillin
75%	78.6%	62.5%	Erythromycin
25%	42.9%	33.3%	Gentamycin
0	35.7%	41.7%	Piperacillin
0	35.7%	33.3%	ciprofloxacin

THE EFFECT OF VINEGAR SOLUTION ON

THE BACTERIA THAT CAUSE IMPETIGO.

Anfal Shakir Motib

Table (2)- The effect of different concentration of vinegar solution on growth of different bacterial species in (mm).

Bacteria Species	Concentration of vinegar solution in mg /ml .					Mean
	2	4	8	16	32	
Staphylococcus aureus	38.3	42.27	45.23	46.33	47.3	43.80
Streptococcus pyogenes	29.1	31.2	33.3	35.3	38.4	33.46
Proteus mirabillis	15.1	18.23	21.2	24.3	26.4	21.04
Mean	27.51	30.56	33.24	35.31	37.37	
L.S.D	Concentration		Bacteria		Concentration x Bacteria	
0.05	1.300		1.679		Non Significant	
0.01	1.892		2.366		Non Significant	

Table (3)- MIC and MBC of vinegar solution on different bacterial growth measured in (mg/ml)

Bacteria	MIC	MBC
Staphylococcus aureus	0.15	0.25
Streptococcus pyogenes	0.5	0.75
Proteus mirabilis	0.5	1

THE EFFECT OF VINEGAR SOLUTION ON

THE BACTERIA THAT CAUSE IMPETIGO.

Anfal Shakir Motib

DISCUSSION

Table No (1) describe the sensitivity of bacterial isolates from impetigo patient . Forty-two bacterial isolates (24 isolates of *Staphylococcus aureus*, 14 isolate of *Streptococcus pyogens* and 4 of *Proteus mirabilis*) were tested against 7 antibiotics, by measuring the inhibition zone in mm (15). This table explain that the majority of bacterial isolates show resistant to more than one antibiotics. *Staphylococcus aureus* show resistant to (cephalexin, methicillin, erythromycin),the (50%, 70.8%, 62.5%),while *Streptococcus pyogenes* show resistance by (71.4%, 71.4%, 78.6%) and *Proteus mirabilis* by (50%, 50%, 75%) . On the other hand, the cefotaxime and gentamycin antibiotics show good activity toward *Proteus mirabilis* when the percentage of bacterial isolates resistant reach (25%, 25%) respectively and the percentage of resistant to cefotaxime antibiotic for *Staphylococcus aureus* and *Streptococcus pyogenes* found to be (37.5%, 42.9%) respectively while the percentage of resistant to gentamycin antibiotic reach (33.3%, 42,9%) respectively. The ciprofloxacin, piperacillin antibiotics show good activity toward the bacterial isolates mentioned above when the resistant of *Staphylococcus aures* to these antibiotics reach (33.3%, 41.7%) respectively and reach (35.7%, 35,7%) respectively for *Streptococcus pyogenes*, while the *Proteus mirabilis* show no resistant to both antibiotics. The cause of high bacterial resistant to the used antibiotics was the widely used of these antibiotics (14) , in addition , the development of the bacterial resistant due to change in the site of antibiotic activity and bacterial membrane permeability or may be enzymatic resistant (19,20). Three bacterial isolates were taken from each bacteria which show high resistant to antibiotics for testing their sensitivity to vinegar solution. All concentration of vinegar solution show effect on bacteria in comparison with distal water in different percentage, while the statistic analysis show no significant differences between the concentration of vinegar solution in their effect on growth of bacteria and in probability of 0.05 and 0.01. .
Table (2) show that *Staphylococcus aureus* was the highly sensitive to vinegar solution from other types of bacteria when the means of inhibition zones reach (38.3, 42.27, 45.23, 46.33, 47.3)mm for the concentrations (2,4,8,16,32) mg\ml respectively and the cause of this may be due to the vinegar solution contain high concentration of acetic acid (10), while the ratio of inhibition zones for *Streptococcus pyogenes* was (29.1, 31,2, 33.3, 35.3, 38.4) mm respectively for the same concentration , on the other hand, the *Proteus mirabilis* was the highly resistant to vinegar solution when the means of inhibition zones reach (15.1, 18.23, 21.2, 24.3, 26.4) mm respectively for the same concentration .

However, many of studies refer that the antimicrobial effect of vinegar solution may be due to prop ionic acid, acetic acid, pectin (fibers), and important minerals (such as potassium, calcium, magnesium, sulphur, chlorine, phosphorus, iron, silicon and other trace minerals), vitamins which are bioflavonoid {vitamin p},beta carotenes {precursors to vitamin A }, vitamin {C, E, B1, B2, and B6}(12). .
The MIC and MBC of vinegar solution described in table (3) refer to the activity of vinegar solution on different bacteria, the MIC of *Staphylococcus aureus* reach 0.15 mg/ml while that of *Streptococcus pyogenes* and *Proteus mirabilis* reach o.5mg/ml and the MBC of

Staphylococcus aureus reach 0.25 mg/ml while that of *Streptococcus pyogenes* and *Proteus mirabilis* reach (o.75,1) mg/ml respectively, and so, the decrease in MIC and MBC of vinegar solution on different bacterial types refer to the activity of vinegar on bacteria that cause impetigo. This effect may be due to the contents of vinegar(organic acids and oxidizing compounds) that lead to denaturizing of outer cell wall of the bacteria that lead to death (21) .

CONCLUSIONS

1.The *Staphylococcus aures* Bacteria is the main bacteria that cause impetigo.

2.The ciprofloxacin and piperacillin have the highest activity (from other antibiotics) on different bacteria that cause impetigo.

3.The *Staphylococcus aures* Bacteria was the most sensitive to the action of vinegar solution while the *Proteus mirabilis* was the lest sensitive to it.

REFERENCES

1.Tony, B. ; Stephen, B. ; Neil, C. and Christopher, G. Impetigo. Rook textbook of dermatology-7th ed,2004; volume 2- Ch 27, 13- 15.
2. Watkins, P. Impetigo aetiology , complications and treatment options, Nursing standard, 2005 ; 19 (36,) 50-54. {Abstract}, {NHS Athens Full- text}.
3. Sladden, M. J. and Johnston, G.A . Common skin infections in children, British medical Journal. 2004; 329 (7457), 95-99.
4. George, A. and Rubin, G. Asystematic review and meta-analysis of treatments for impetigo. Br J Gen Pract, 2003 Jun ;53 (4,1): 480-7.
5.Koning,S.;Verhagen,A.P.and Vansuijlekom-Smit, L.W.Interventions for impetigo(Cochrane Review).The Cochrane library.Issue 2.chichester,UK. 2003.

6. Klaus, W. ; Lowell, A. ; Barbara, A. and David, J. Impetigo. Fitzpatriks Dermatology inGeneral Medicine-7th ed,2008; volume 2 ,1695-1705.
7.British National Formulary (BNF).Medical Association and Royal Pharmaceutical Society of Great Britain. London,British. 50th ed,2005.
8.Jones,G.R. Principles and practice of antibiotic therapy for cellulitis . CPD Journal Acute Medicine. 2002;1(2) : 44-49 .

9.Sharquie,kh.and Al-Turffy ,Eh. Treatment of impetigo bytopical black tea. Post gradute thesis, college of medicine , Baghdad University. Iraq .1999 .

10. Pinto, T.M.. ;Neves,A.C. and Leao, M.V. Jorge vinegar as antimicrobial agent for control of candida spp. J Apple oral sci.2008;16(6) :385-90.

11.Bernardini, J. ; Bender, F. ; Florio ,T. ; Sloand, J. ; Palmmontalbang ,L. and Piraino, B. Randomized double-blind L, prevention of antibiotic exit sitye cream for patient, Jam Soc Nephrol, 2005; 16(2): 539-45.

12. Estrela , C.; Holland , R.; Bernabe ,P.; Souza,V.and Estrela, C. Antimicrobial potential of medicaments used in healing process in dogs teeth with apical periodontitis . Braz Dent J.2004; 15 (3) :181-5.

13. Tony ,H.M. and Paul,S.M. Color Atlas of Medical Microbiology .2nd ed. Mosby, London. 2008.

14.Jawetz,E.;Melnick,J.K.;Adelberg,E.A.;Brocks,J.F.;Butel,J.S. and Morse,S.A.Medical Microbiology ..Hill, NewYork. 23rd ,2004

15.National Committee For Clinical Laboratory Standards (NCCLS).. Performance standards for Antimicrobial disk susceptibility test. Twelfth information supplement . 2002;Document M 100- S12, Vol.22 , No. 1 .

16. Douglas, A, S. and Donald, M. ,W. ;Fundamentals of analytical chemistry. Japan, 4th ed,1982.

17.Boyanova,L.;Derejian ,S.;koumanova ,R.;Katsanov ,N.; Gergova ,G.; Mitov, I.; Nikolov , R.; krastev,Z. Inhibition of *Helicobacter pylori* growth 1`

report. J. Med. Microbiol. 2003; 52(5):417-9 .

18. Stocks , E.J. & Ridgway , G.. Handiling clinical speciment for Microbiological studies . Churchill Livingstone Edinburgh . 5th ed .1987 ;.P : 173 – 201. McGraw.

19.Myrvick, N. and weiser. S. Fundamentals of medical bacteriology and mycology, 2nd ed . Lea and febiger. Philadelphia. 1988

20.Kafaf, P.A. Genetic study on antibiotic resistance of some gram negative bacteria isolated from urinary tract infection .Athesis of Master, College of science, Al-Mustansiriya University. 2000.

21.Prescott's , L.M. ; Harley , J.P. and Klein , D.A.. Microbiology . The W.C. publishers . U.S.A . 1990.

Measurement of temperature distribution for "CO_2 laser –mild steel processing" By non-Contact methods

Jasim Hassan Rasheed
Physics department , science college,
University of Diyala

Receiving Date: 2011/7/17 **- Accept Date:** 2011/9/4

Abstract :

Measurement of temperature distribution by non- contact method (Digital camera Cyclops 52) are achieved . Outline to non-contact techniques is given Fundamental and basic terms of radiation laws are mentioned. Carbon dioxide laser Everlaser 525 (500w)is employed as a heat source to process mild steel under investigation **at different pressures and powers** .

خلاصة:

تم انجاز هدف البحث وهو قياس توزيع درجة الحرارة عن بعد بواسطة الكاميرا الرقمية (Cyclops 52) . واعطيت خلاصة عامة لتقنيات القياس عن بعد كما تمت الإشارة الى القوانين الاساسية للاشعاع .
واستخدم ليزر ثاني اوكسيد الكاربون (500واط) كمصدر حراري اثناء معالجة الفولاذ **تحت ضغوط وقدرات مختلفة .**

Measurement of temperature distribution for

"CO_2 laser –mild steel processing"

By non-Contact methods

Jasim Hassan Rasheed

1-Introduction :

The Sensation of heat or lack of it is very familiar. The human sensor mechanisms are calibrated by experience and these registered by touch (contact method) or by the Sensation relating to radiated heat (non contact method).

Colour on the other hands to be a guide for the higher temperatures. Colours used to assess the temperature both for the temperature required for the working of the metal and the resulting "temper" of the metal on gradient quenching .

There are means of determining temperature by two different colour method . One relating to the visual range of radiation emitted from hot metal surfaces at temperature above 500c, the other from the physical colour effect related to the passage of hight through an oxide film of varying thickness (12,15).

The oxide film "temper" indicator although reliable is only an instantaneous effect during the build up of the oxide film on the hot metal. with the time the oxide film formation continuous and if high temperatures are maintained considerable thermal gradients build up , due to heat transfer considerations, through the oxide film to the metal body underneath CO_2 laser is used as a heat of source during the present work to processes mild steel, and digital camera Cyclops 52 was adopted to measure temperature gradient .

2-Basic Concepts on thermal emission (2, 9 ,11)

All objects are continually emitting radiation at a rate and with a wavelength distribution that depends upon the temperature of the object and its spectral emissivity ε (λ).

A black body is an object that absorbs all incident radiation and , conversely is a perfect radiator .The energy emitted by a black body is the maximum for a given temperature.

The radiated power and its wavelength the distribution are given by the Blanks radiation law (2).

$$W_{(\lambda,T)} = \frac{2\pi hc^2}{\lambda^5}\left[\exp\left(\frac{hc}{\lambda kT}\right)-1\right]^{-1} \; W\,cm^{-2}\,\mu m^{-1}$$

\

(h) is Planck's constant (6.626*10^{-34} J.s).

(C) is the velocity of light (3 * 10^8 m / s) .

(K) is Boltzmann's constant (1.3805*10^{-23}J/k)

For most thermal radiation sources the total energy is approximately proportional to the fourth power of the temperature

$W = \sigma T^4$ (watts) …… (2)

Where σ is Stefan – Boltzmann constant (5. 67*10^{-8} wm^{-2} k^{-4}).

Figure (1) shows the variation in intensity as function of wavelength at various temperatures. The wavelength at which the intensity of radiated output is a maximum is shown by the broken line is given by wines law.

$\lambda_{max} T = 2.9*10^{-3}$ m.k (3)

i.e as the temperature increases the wavelength at which the maximum occurs becomes shorter and relatively more energy is radiated in the visible region.

Measurement of temperature distribution for

"CO_2 laser –mild steel processing"

By non-Contact methods

Jasim Hassan Rasheed

The radiated power output of practical sources is normally less than that for a black body , and they are referred to as non –black bodies .An emission coefficient which varies with the material and its surface condition is used so that the equation for the radiated output becomes:

$W = \varepsilon\sigma T^4$ (watt)……(3)

Where ε is the coefficient of emissivity and ($\varepsilon \leq 1$)

3- Emissivity (15) :

In practice , the emissivity of any sample will be affected by a number of factors those having a considerable influence being as follows:

a-Sighting angle : pyrometer measure radiation from a surface through a small solid angle . The emissivity of a surface is usually a function of the angle between the line of sight and the normal to the surface . Metals, because the polarization , effect , have a minimum emissivity normal to the surface and these effects become important at angle greater than 60 . On the other hand , the emissivity of insulating material is a maximum when viewed normal to the surface . Pyrometers should not , in general , be sighted at more than 45 to the normal of the surface .

b-Wavelength :when measured over all wavelengths of radiation emitted by a material the property concerned is "total emissivity". when measured over a small wave band, usually at short wavelengths ,the term is "spectral emissivity ".

c-Temperature :spectral emissivity doesn't vary greatly with temperature though it is usually wavelength dependent. For metals and alloys , emissivity is higher at short wavelengths than long one so that , as the temperature increases and more energy is emitted at short wavelengths, total emissivity increases.

Non-metal , if they are opaque at all wavelengths generally have spectral emissivity's which are not greatly dependent on wavelength and hence emissivity does not change with a rise in temperature.

d-Surface conditions : Surface roughness and oxide layers generally increases the emissivity of a sample.

For metals with smooth , un oxidized surface , emissivity's are usually in range (0.05 to 0.5) and are usually wavelength dependent (5).

Howeever if we ignore the emissivity altogether and infer temperature from the thermometer output ,we shall get a temperature lower than the true temperature by an amount depending on the values of emissivity and the characteristics of the thermometer . This temperature is known as the "apparent" or "brightness" temperature of the surface if the emissivity is constant this temperature rises and falls in exactly the same way as the true temperature and this may be sufficient for some purposes . To obtain the true surface temperature we must divide the actual output by the emissivity value (ε) before we convert to temperature.

Measurement of temperature distribution for

"CO_2 laser –mild steel processing"

By non-Contact methods

Jasim Hassan Rasheed

4- Interaction between CO_2 laser and metals (1 , 2 ,10)

a-CO2 laser work in the infrared radiation at wavelength of (10-6) µm and one powerful enough for metal processing such as ; hardening , welding and cutting .The absorption of CO_2 laser beam in metal is not high enough due to their high reflectivity. Increasing the absorption of the laser leads to change in physical and mechanical properties of the worked material. These changes are largely a function of the thermal properties of the material and can be controlled to some extent by adjustment of the laser power output , spots size and mode (Cw or pulses).figure (2) shoes the vibration energy levels diagram of CO_2 and N_2.

b- Basic characteristics of the laser metal processing (3 , 5 , 7)

The laser processer is characterized by three main parameters (figure 3) .

i-The laser beam : The laser include the beam related parameters as power , mode wavelength , divergence , beam diameter , etc……

These parameters are more or less fixed and present by the manufactures of the laser.

ii-The second parameter relates to the optical / nozzle system. Normally a lens fixed in a pressure chamber is used as a beam transmission and gas flow system .The optical system include parameters as focal length, focal spot diameter , depth of focus etc…. , which are parameters related to the quality of the optics and to the mechanical stability of the optical system . The nozzle system include parameters as type of system (coaxial, off-axial), nozzle shape(convergent, divergent), nozzle diameter , etc…, parameters which are related to the type gas flow and to the interaction between gas flow, laser beam and material .parameters in this case mainly fixed or preset by manufacturer or fixed for a certain type of system.

iii-The third parameter is related to the material includes optical properties as reflection , absorption depth etc…. , decide whether the material can be processes or not (14)

5-Non-Contact techniques for thermal detectors.

a-The Videocon , infrared camera , P 8092.

This Camera converts the thermal radiation to an electrical signal .This signal is proportional to the rate of change of the temperature at the target . It operates at room temperatures without cooling , The maximum operating temperature is 40c optimum sensitivity in the range of (8- 14) µm in which there is maximum radiant power from objects at temperature close to ambient .

b-Pyrometers :

i-The optical pyrometers (13): This is used to measure the radiance from the target within narrow band by filtering and is suitable for measuring only above 600 C. This pyrometer is employed to compare the intensity of radiant energy emitting from a target with the intensity of radiation from a body whose temperature in known .The band usually selected is 0.65 µm .

ii-Two colour Pyrometers (6)

The output of the detector is a chain of pulses which is amplified and then separated .The pulses are proportional to the energy transmitted .Determination the temperature from the ratio of the intensities at two wavelets is possible.

iii-Total radiation pyrometer (8) : This pyrometer is designed to take advantage of the dependence of the intensity of thermal radiation upon temperature .It consists an optical system for directing the energy to the detector which converts the radiation energy into an electrical signal .

iv-Band radiation pyrometer (4) .This pyrometer works in a wider band interval than the spectral pyrometer but with smaller range than the total radiation . All other principles are very similar.

c- Infrared cells : The infrared cell detects the near infrared by using suitable filter .This band of radiation needs to be detected because it appears at most temperatures. calibration with infrared emitter is necessary . The infrared cell need convenient amplifier to a void most noise.

d-Photo cells techniques : It is very similar to the infrared cells method .The only difference is that the photo cells detect the visible range as well as the very near infrared .

e-Digital Camera Cyclops 52(14) : It is possible to measure up to 3000c with certain very narrow wave band (0.8-1.1) µm temperatures . However , Cyclops 52 facilities can be summarized as follows (Fig 4 shows measuring distance and forget for Cyclops):

i-variable focus optical system allowing focusing from (1 m) to infinity.

ii-optional closes up lenses to allow measurements of targets as small as 0.4 mm by using lens no-110 and at maximum focus distance which is 205mm.

iii-precise definition of the target spot together with digital display of the target temperature in the view finder .

iv-Choice of measuring mode, continuous peak or valley hold.

v- Digital output suitable for deriving an optional digital printer.

However , this technique was employed to measure temperature for present work.

f-Temper colour (12) : The temper colour is due to slight oxidation of the surface . As the tempering temperature increases , the oxide film become thicker and a series of colour may be observed .However , temper color is first evident as a pale yellow at a bout 215C and there is a progressive change with rising temperature to blue .

6-Experimental work:

Everlase 525 model of CO_2 laser heat source (500w) was used through out this study to process mild steel of thickness 1.68 mm and 17mm length .The workpiece was oxidized due to air jet which is used throughout this work .However , laser power delivered through nozzle to hit the sample which was exposed as desired to the laser beam by means of the shutter . when the workpiece had completely passed the nozzle the shutter was closed . when the work table returned to its starting point and the shutter re-opened to continue the monitoring the power. However the experiment were carried out to investigate the temperature gradient at different pressures and powers by digital Camera Cyclops 52 as mentioned in previous section.

The sheet (workpiece) was not perfectly flat due to its being cut from a coil and buckling from previous heating runs which effect the focusing status .

Air is used for marking the sheet . Heating steel to or above 230C and quenching them in air, different colours are seen. It is assumed that there is a direct relationship between these colour and the maximum temperatures attained.

7- Results and Discussions:

a- Temperature variation along marking at different pressures:

Figure (5) shows the temperature variation along the marking path for two pressures , 5 and 20 psi , at a power of 170w , marking speed 5% of maximum speed(25mm/s) and material of 1.68mm thick .

Although the energy available at 20 psi is expected to be higher than that at 5 psi due to differences in rate reaction between mild steel and oxygen gas (exothermic reaction), the average temperature recorded along the marking path at a pressure of 5 psi is higher than that at 20 psi . lower temperature at higher pressure may be due to better efficiency in

ejecting the molten metal from the irradiated path . In other words more energy is taken a way at high pressure leaving the cut path cooler .

A second explanation to the pressure role is that as the pressure increases and other parameters (power and speed) are constant , a wider path is melted and more heat is dissipated through the material bulk . Again lower temperature is expected .

Widening the mark kerf and increasing the molten material reduces the efficiency of the clearing mark or cut path . The efficiency of ejecting the molten product can be related to the cut quality . It was found at a lower pressure the edge surfaces smoother .

b-Temperature distribution along marking path for different laser power.

The different temperature between the maximum and minimum points is proportional to the power(Fig 6).

Because the temperature fluctuation is large at higher laser power the condition of the edge cut should be worse . In other words the roughness is greater.

The average temperature along the marking path is also proportional to the laser power when all the other parameters are constant. The 5 psi may not be enough to remove the melted material from the path particularly when the power increases . Building up melted material with better efficiency in absorbing energy may be responsible for the higher temperature recorded as shown in figure (7) .

8- Conclusion :

mild steel was processed by carbon dioxide laser. An attempt to measure temperature distribution by non-contact method was achieved .Relateships between temperature and marking path at different power and pressures are given.

It was found that the average temperature along the marking path increases as the power is increasing due to higher energy consumed during processing operation , while it decreases as the pressure is increasing which may attributes to cooling effect in spite of presence of exothermic reaction between oxygen and mild steel.

Measurement of temperature distribution for

"CO_2 laser –mild steel processing"

By non-Contact methods

Jasim Hassan Rasheed

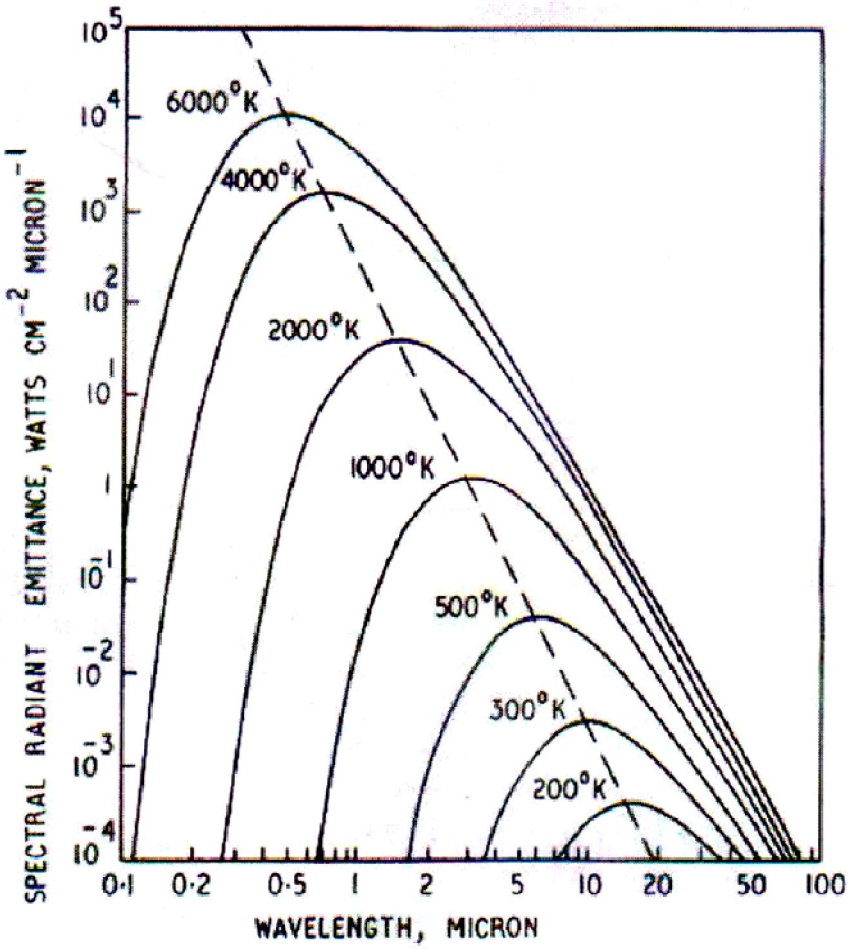

Fig. 1 The spectral radiant emittance of an ideal blackbody at various temperatures, as a function of wavelength in micron

Measurement of temperature distribution for

"CO_2 laser –mild steel processing"

By non-Contact methods

Jasim Hassan Rasheed

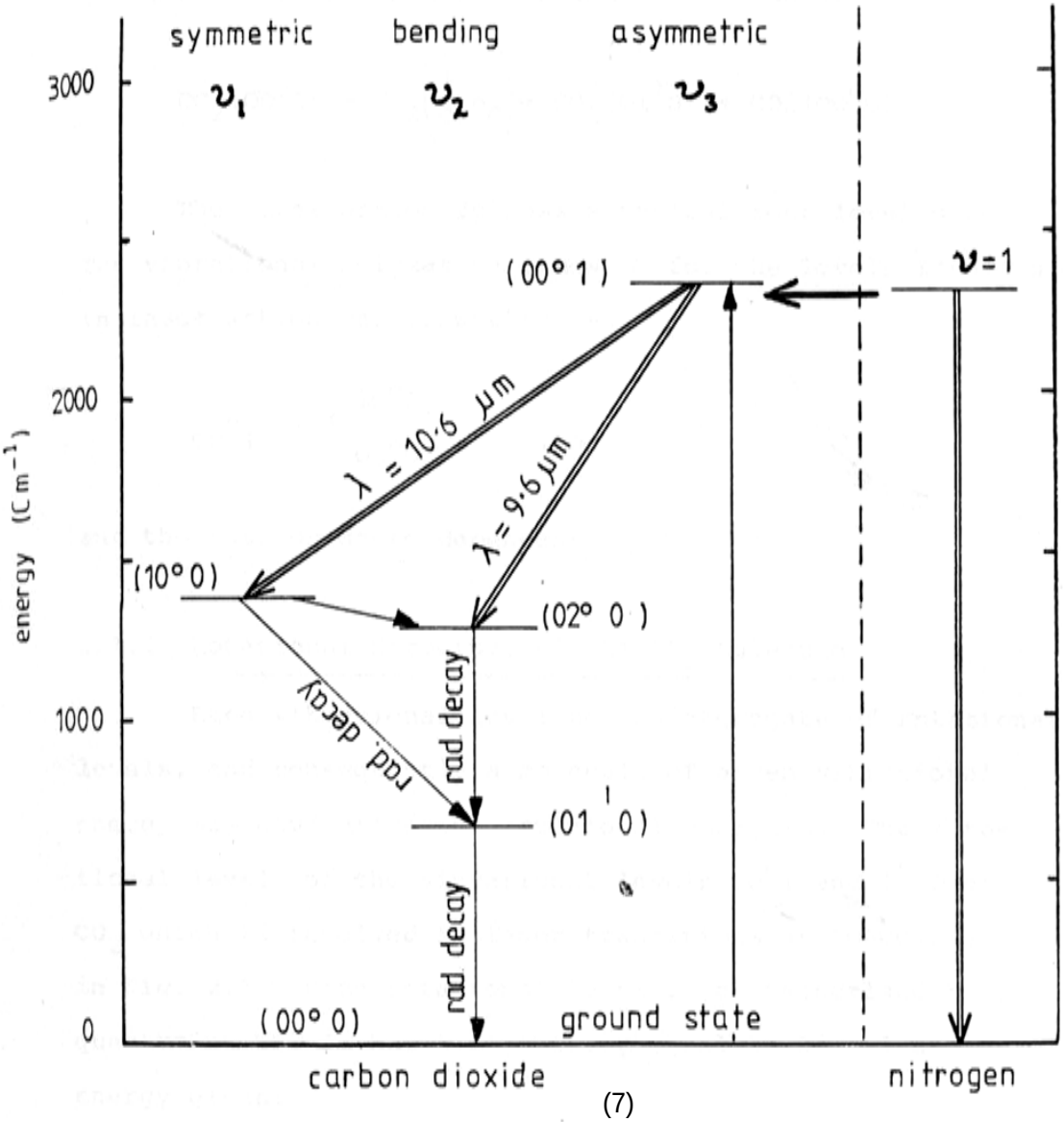

(7)

FIG. 2.2: Energy level diagram of lower vibrational levels of CO_2 and N_2.

Measurement of temperature distribution for

"CO_2 laser –mild steel processing"

By non-Contact methods

Jasim Hassan Rasheed

LASER CUTTING PROCESS PARAMETERS.

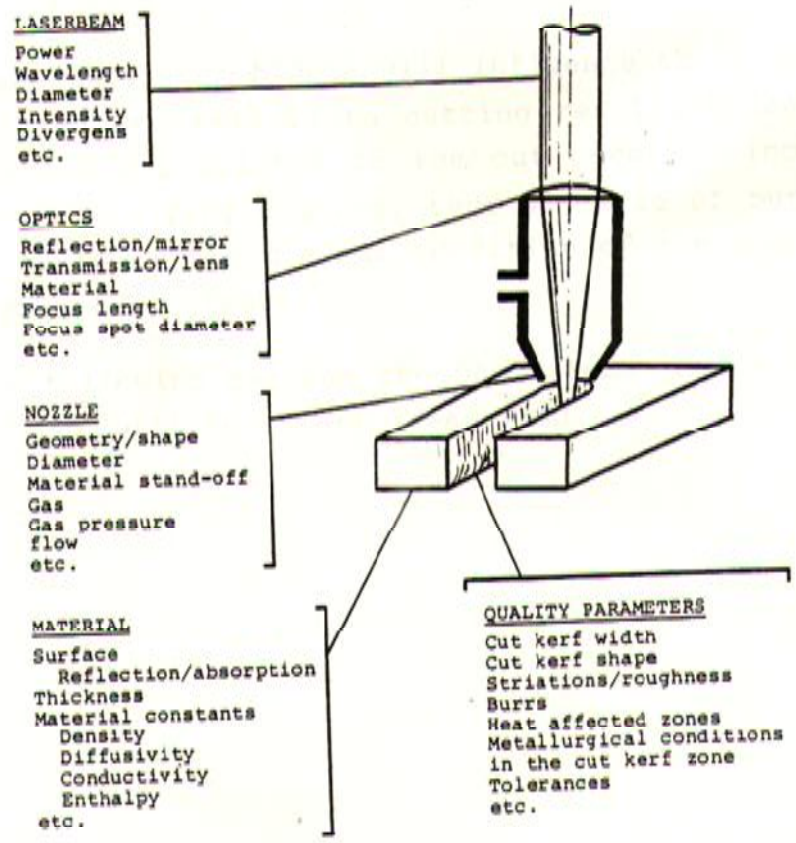

Figure 3-1: Main parameters in the laser cutting process

Measurement of temperature distribution for

"CO_2 laser –mild steel processing"

By non-Contact methods

Jasim Hassan Rasheed

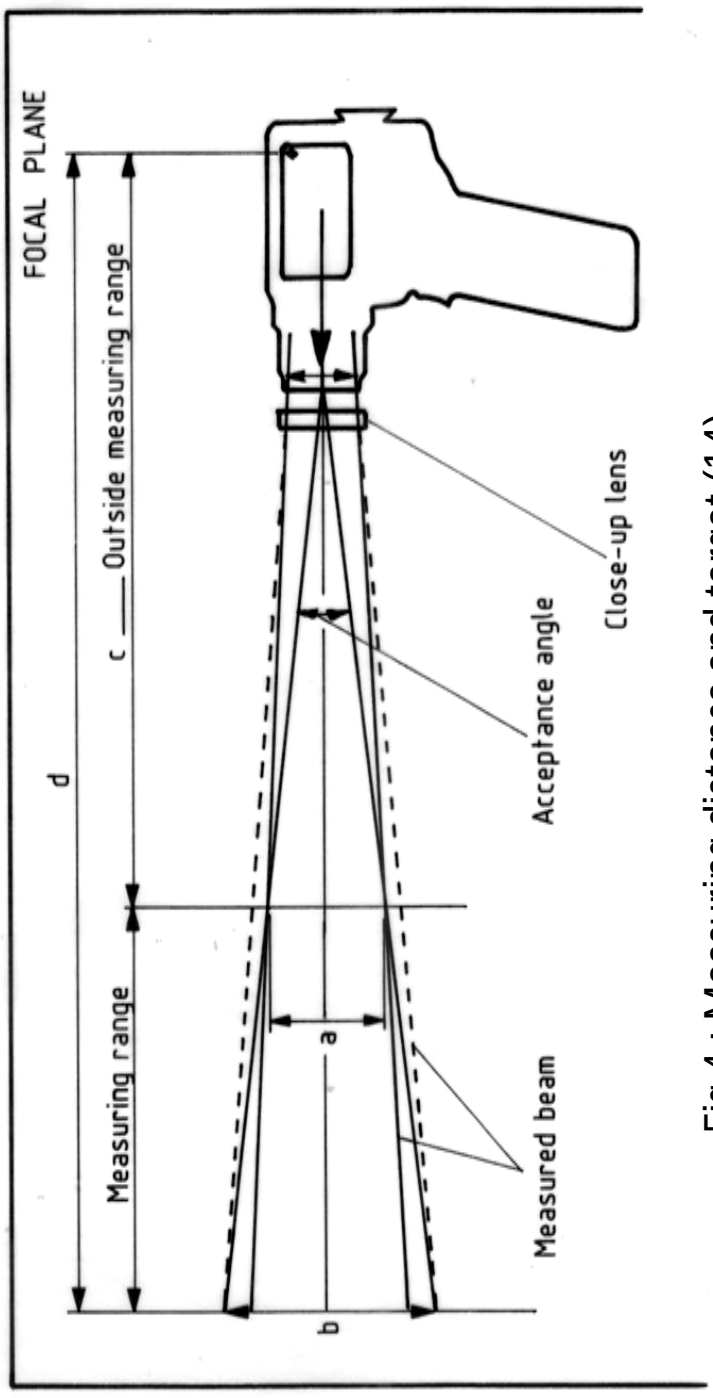

Fig 4 : Measuring distance and target (14)

Measurement of temperature distribution for

"CO_2 laser –mild steel processing"

By non-Contact methods

Jasim Hassan Rasheed

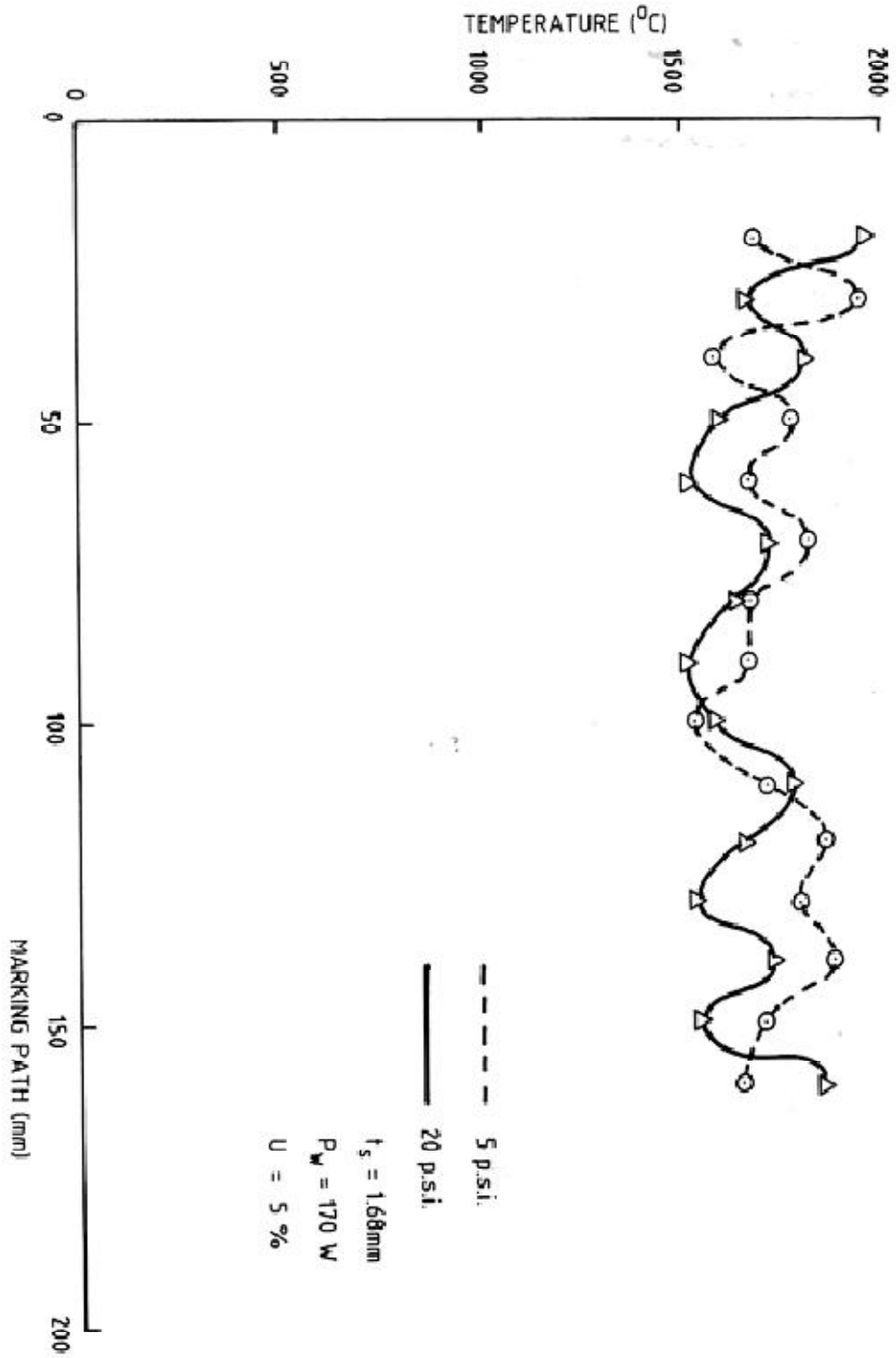

Fig.(5) Variation of temperature along marking path

Measurement of temperature distribution for

"CO_2 laser –mild steel processing"

By non-Contact methods

Jasim Hassan Rasheed

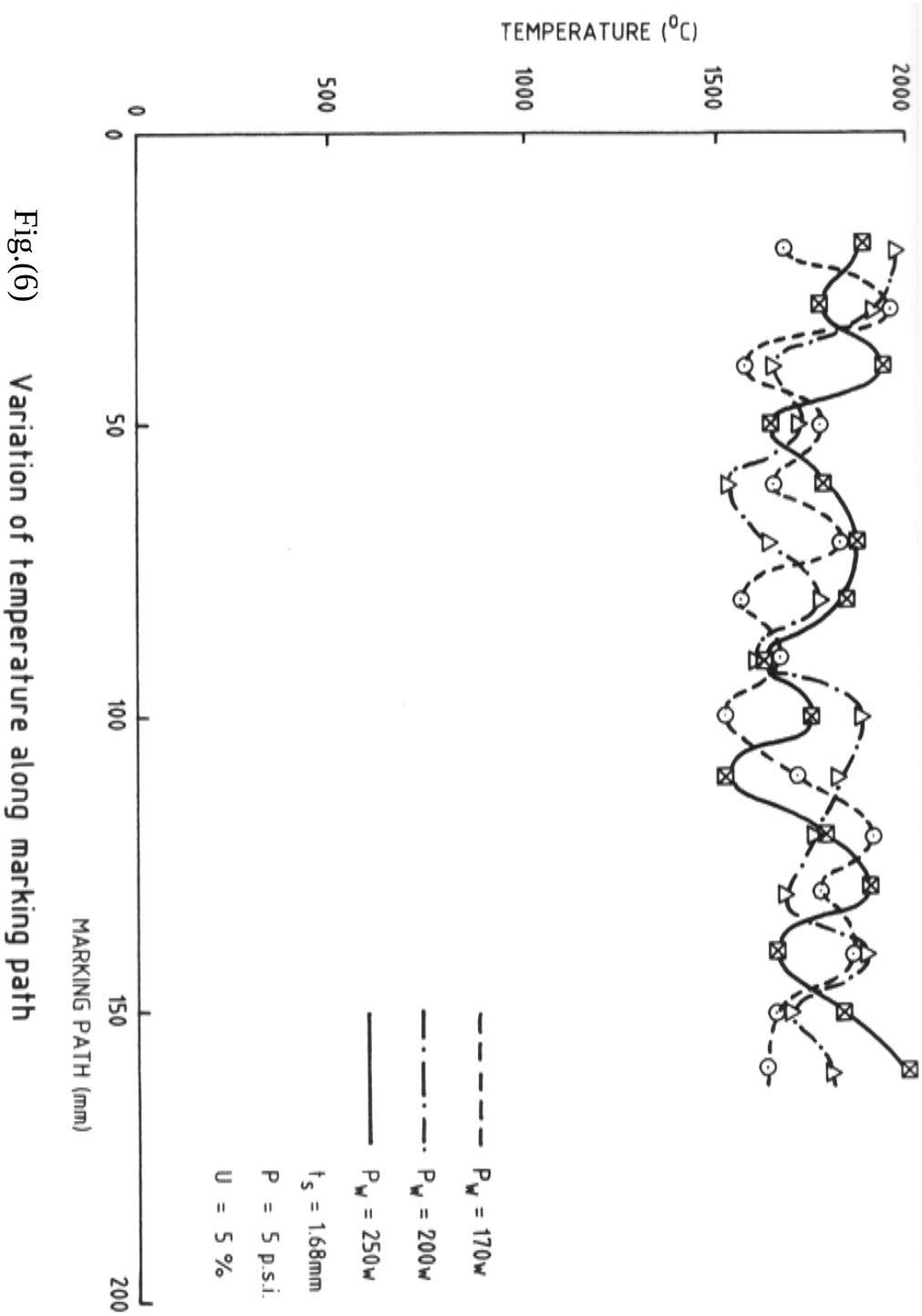

Fig.(6) Variation of temperature along marking path

Measurement of temperature distribution for

"CO_2 laser –mild steel processing"

By non-Contact methods

Jasim Hassan Rasheed

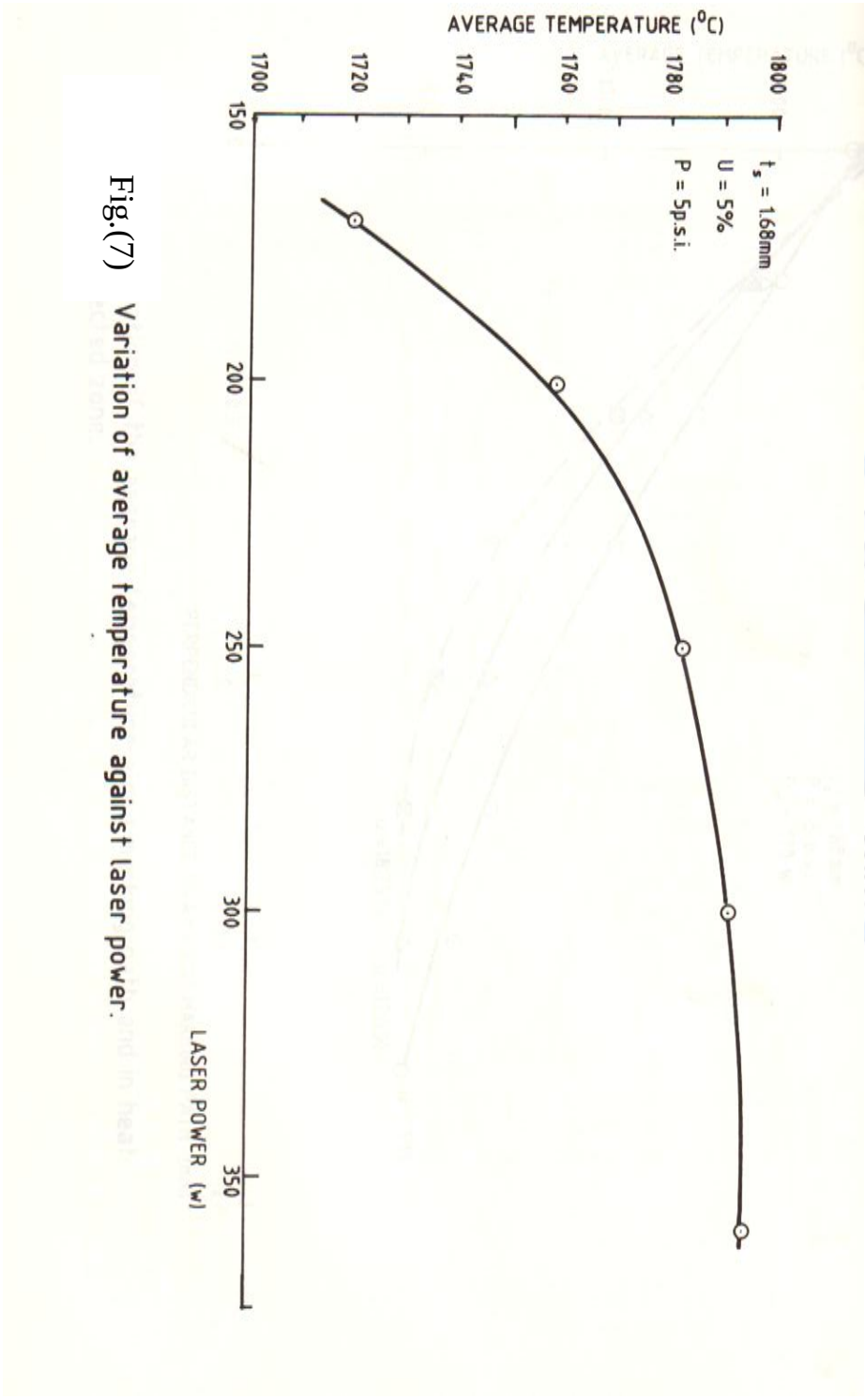

Fig.(7) Variation of average temperature against laser power.

References :

1-M.K.Chun. "Interaction of high intensity laser beam with metal" J. appl phys. V(41),pp614-620 ,1970.

2- J. Harry " Industrial laser and their applications"MrGraw Hill Book Company (U .K) Limited, 1974.

3-D. Roessler and V. Gregson "Reflectivity of steel at 10.6 µm wavelength" Appl- optics . C(17) pp992 -993 , 1978.

4-L.Coslovi; "Accurate pyrometry with microsecond time resolvtion" J. phys. V(12) , pp 216 – 223, 1979.

5-K. Park and W. Walter " metal reflectance changes during intense laser irradiation" Proc . conf . 1979. Washington.

6-F. Jorgenson "Two colour pyrometer measurement of the temperature" J. Appl. Phys. V(18), 486 – 491, 1985.

7-P .O. OLSEN , A . Bmmel , "Contribution to Oxygen assisted CO_2 laser cutting "Processing 6 th conf . laser in Manufacturing , may ,1981,U.K.

8-T.P.Jones "Radiation Pyrometers for temperature measurement during Aluminum processing" J. phys. V(20) pp 615 -619 , 1987.

9- I. B. Foldes "light absorption in laser heated cavities , Appl. Phys. B(43) , pp 117 -122, 1987.

10-Jasim .H. Rasheed ." private work. " mech. Eng., Loughborough univ ., UK, 1990.

11-G. Brigg "Temperature measurement" Dept. of metallurgy ,Sheffield city polytechnic, UK, 2002.

12-W. Heimunn "Non – Contact determination of temperature by measuring the infrared radiation emitted from the surface of a target . "Cont .Inst. of phys. Londan,and Bristol , 2003.

13- Loughborough Univ. Of technology , Dept . of phys .(U.K)"optical pyrometers" 2005.

14-Land infrared Cyclops 52 "division of land instruments international ltd"2007.

15-M. Wood "Temperature measurement of radiation" Sheffield polytechnic , 2009.

Effect of garlic (Allium sativum) extract on lipid profile in Rats

Hadeel Ahmad Hassan

Assiss Tecnelecturer

Institute of Medical Technology / Mansour

تأثير مستخلص الثوم في مستويات الدهون في الجرذان

هديل أحمد حسن

المعهد الطبي التقني / المنصور

Receiving Date: 2011/1/20 - **Accept Date:** 2011/6/21

Effect of garlic (*Allium sativum*) extract on lipid profile in Rats

Summary:

The effect of garlic (*Allium sativum*) on lipid profile in normal and hyperlipidimic rats was studied. Forty rats were allocated randomly into four groups, each of ten rats. The first group was received distilled water as acts as a control group. The second and the third group were given high cholesterol diet (2% cholesterol) for 4 weeks, one considered as a hyper cholesterolimic group and the other was hyper cholestermic which received alcoholic extract of garlic at a dose of 300mg/kg B.W for 4 weeks. The fourth group was given alcoholic extract of garlic at the same dose and the same duration. The serum lipid profile of the experimental animals in all groups was assayed and the resulting values statistically analyzed.

The values of total cholesterol (Tch), Triglyceride (TG) and low density lipoprotein (LDL) were significantly decrease in groups received garlic extract comparing with control and hyper cholesterolimic groups with non significant increase in high density lipoprotein (HDL) in all groups.

Garlic may be recommended as an anti atherogenic agent and is suggested to be used with food in patient with hyperlipidemia.

Effect of garlic (Allium sativum) extract on lipid profile in Rats

Hadeel Ahmad Hassan

تأثير مستخلص الثوم في مستويات الدهون في الجرذان

الخلاصة:-

درس تأثير الثوم في مستويات الدهون في الجرذان طبيعية التغذية والجرذان ذات التغذية عالية الكلستيرول. وزرعت أربعون جزذا بصورة عشوائية في أربع مجموعات احتوت كل منها ١٠ جرذان وكالاتي:

المجوعة الأولى التي أعطيت الغذاء الطبيعي وجرعت بالماء المقطر واعتبرت مجموعة سيطرة، المجموعة الثانية والثالثة والتي أعطيت عليقه غنية بالكستيرول(٢٪) لمدة أربع أسابيع حيث اعتبرت المجموعة الثانية المجموعة العالية الكلستيرول ولم تجرع بمستخلص الثوم في حين اعتبرت المجموعة الثالثة المجموعة عالية الكلستيرول وجرعت بمستخلص الثوم بجرعة مقدارها ٣٠٠ ملغم/كغم من وزن الجسم لأربعة أسابيع، أما المجموعة الرابعة فقد أعطيت العليقة الاعتيادية وجرعت بمستخلص الثوم بنفس الجرعة وللفترة الزمنية ذاتها.

أخضعت مستويات الشحوم في جميع الحيوانات المختبرية للمجاميع كافة للتحليل الكيمياوي وحللت النتائج إحصائيا. أظهرت النتائج انخفاض معنوي في مستويات الكلستيرول الكلي، الكليسرول الثلاثي والبروتين ألشحمي واطئ الكثافة في المجموعتين اللتان جرعتا بمستخلص الثوم المائي مقارنة بمجموعة السيطرة والمجموعة التي غذيت بمستوى عالي من الكلستيرول مع زيادة غير متوقعة في البروتين ألشحمي عالي الكثافة في المجاميع كافة مقرنة بمجموعة السيطرة.

يمكن التوصية ومن خلال نتائج هذه الدراسة باعتبار مستخلص الثوم الكحولي كعامل مضاد لتصلب الشرايين مع إمكانية استخدامه في غذاء المرضى الذين يعانون من ارتفاع مستوى الشحوم في الدم.

Introduction:

Atherosclerosis is the principal contributor to the pathogenesis of myocardial and cerebral infarction. Elevated plasma concentration of cholesterol, especially in LDL, is recognized as leading to the atherosclerosis [1].

Garlic (*Allium sativum*) belongs the plant Lily family which is a genus of 500 species. It has been grown a round the world for the flavoring cooking. The potency of garlic has been as knowledge for 7500 years. In ancient times, the Babylonian, Egyptian, Chinese, Greeks, and Hinds used garlic frequently [2]. Interest in the potential benefits of garlic has origins in antiquity and is one of the earliest documented example of plant used for maintenance of health and treatment of diseases [3]. It is possesses many healthful properties that are related to its bioactive compounds [4]. It widely used as an all-around treatment for prevention or slowing the progression of atherosclerosis [5].

More recently, attention has been focused an garlic 's ability to decrease blood cholesterol level in clinical trials in humans [6], as well as in experimental studies with animals [7].

The present study was carried out to investigate the effect of alcoholic extract of garlic on lipid profile in experimental rats.

Material and methods:

The materials:

1.The plant:

Garlic bulbs were purchased directly from local market. It is fully grinded by blender, the grinded garlic was put in light polyethylene bags and placed in freezer at -20 ˚C until used.

2.Animals:

Forty fertile male albino rats weighting approximately 200 – 210 gm body weight were obtained from animal house of physiology department in veterinary medicine, university of Baghdad. They kept under good ventilation with 12 house light and dark cycle. Experimental hyper cholesterolemic animals were fed a cholesterol – enriched high fat diet for four weeks. They were arranged into four groups (10 rats per group) as follow:-

a. Garlic group : was administered garlic extract at a dose of 300mg/kg B.W. with gastric tube for four weeks.

b. Hyper cholesterolemic group : fed a cholesterol – enriched fat diet for four weeks.

c. Garlic and hyper cholesterolemic group : was administered garlic extract at a dose at 300 mg/kg B.W. and fed a cholesterol – enriched fat diet for four weeks.

d. Control group : fed adlibitum on standard diet with distilled water.

The methods

1.Extraction by ethanol 95% :

To 18 gm of dry plant powder, 150ml oh ethyl alcohol 95% was added, left on magnatic starrier for 1 hours the whole mixture was filtered first by medical gauze followed by centrifugation at 3000 rpm/min for 15 seconds supernatant was collected and put in earthen bowl to dryness by oven at 40 ˚C, the crude extract was kept at -20 ˚C until use [8].

2.Preparation of alcoholic extract :

Three grams was weighted from primary crude extract by ethanol and dissolved in 10 ml of ethanol to prepare (300mg/ml), this concentration were put on vertex for 10 second, sterilize by Millipore filter (0.22hm), then put in sterile tubes for use.

3.Biochemical assessment :

The blood was collected in non heparinized tube from rats in each group, and centrifuged at 3000 rpm/min and the serum was collected. Serum levels of total cholesterol, triglyceride and HDL were determining according to [9] ,[10] and [11]. LDL was calculated from the total cholesterol [12].

Results

The serum lipid lowering effect of alcoholic extract of garlic in albino rats is presented in table (1). The mean total cholesterol, LDL and triglyceride levels were significantly decreased.

There is no significant differences in HDL levels of the different groups.

Table(1) : The effect of equeous extract of garlic on lipid profile in rats.

Groups	Total cholesterol mg/dl	Total triglyceride (mg/dl)	HDL (mg/dl)	LDL mg/dl
Control	74.2 ± 3.5	45.03 ± 5.1	52.7 ± 1.5	22.9± 2.2
Hypercholesterol	132*.7± 2.0	81*.5 ± 3.	45.4± 2.5	71*.2 ± 4.4
Garlic	68*.1 ± 1.3	33*.2 ± 1	57.2 ± 2.1	18*.3 ± 1.2
Hypercholesterolimic + Garlic	90*.5 ± 2.4	42.0± 1	50.4± 3.1	20.4 ± 1

-Data were expressed as mean± SE (n=10) by applying one way ANOVA and determined F test.
* The data significant at (P< 0.05)

Discussion

Hypercholesterolemia is an autosomal dominant disorder that cause sever elevations in total cholesterol which enhanced the development programming of atherosclerosis [13].

The most studied are reported health promoting effect of garlic is cardio protection [14]. However some authors claim that garlic is not effective in plasma lipid lowering and the use of garlic for treatment of hypercholesterolemia is of questionable value [15].

Other publications [16] , [17] suggested that not all preparations may be hypocholesterolemic which have caused confusion within both public and academic domains.

Although the reason for these inconsistencies remain unknown, it likely relates to preparation methods, stability and quantity of compounds occurring in the preparations quantity of the preparation provided and for the duration the study.

The cholesterol lowering action of garlic may be attribute to in part to depressed cholesterol synthesis by the liver. The triglyceride lowering effect of garlic might be explained in part by its inhibitory action of fatty acid synthesis. Furthermore there are several explanation for the result were obtained. The mechanism for cholesterol lowering effect of garlic has also been attributed to inhibition of specific activity of enzyme HMG-CoA reductase a rate- limiting enzyme in cholesterol biosynthesis. This enzyme has been reported to be significantly lowered in rat liver microcosms after garlic consumption [18]. The protective effects of garlic may be attributed to inhibition of enzymes involved in lipid synthesis, prevent lipid peroxidation and LDL increased antioxidant, these mechanism are however open to further studies [19].

Garlic decrease S.T.C And S.T.G in hyperlipidemic- garlic received rats compared with hyperlipidemic control, it is suggested that this effect may be due to action of allyl cystine And diallyl-disulfide present in garlic oil, these ingredients are potent inhibitor to mono oxygenase enzyme inhibition of this enzyme lead to cholesterol synthesis inhibition [20].

Further more garlic depress the hepatic activities of lipogenic and cholesterogenic enzyme, (Malic enzyme) and HMG- CoA reductase which is provide a possible explanation for reduction effect of garlic on S.TG [21], and the reduction in LDL may be due to the suppression of LDL oxidation [22].

It can be concluded that the garlic used as antiathrogenic agent by reducing the S.T.C. and S.TG and LDL.

References

1. **Shimokawa,H. &Vanhoutte, M. (1989)** . Impaired endothelium-decendent relaxation to aggregation platelets and related vascactive substances in porcine coronary arteries in hypercholesterol- emic and atherosclerosis . *Circ.Res.* ; 64:900-914.

2. **Block, E. (1985).** Chemistry of garlic and onions. *Sci. Am.* ; 252:94-99.

3. **Kahn, G. (1996)**. History of garlic.In: Garlic: The science and therapeutic application of (*Allium sativum*) L. and Related Species (Koch, H. P. & Lawson, L. D. eds.), pp. 25-36 Williams and Wilkins, New York, N.Y.

4. **Leelarungrayub, N. Rattanapanone,V. Chanarat,N. & Gebicki, M. (2006)** . Quantitative evaluation of the antioxidant properties of garlic and shallot preparations. *Nutr.* ;22:266- 74.

5. **Koscielny, J. Klussendorf, D. & Latza,R. (1999)**. The antiatheorsclerotic affect of *Allium satium*. Atherosclerosis. *et al.* ; 144:237-249.

6. **Adler, J. & Holub, J. (1997)** . Effect of garlic and fish-oil supplementation on serum lipid and lipoprotein concentrations in hypercholesterolemic men. *Am. J. Nutr.* ; 65:445-450

7. **Aouadi, R. Aouidet, A. Elkadhi, A. Ben Rayana ,C. Jaafoura, H. Tritar, B. Nagati, K.(2000).** Effect of fresh garlic (*Allium sativum*) on lipid metabolism in male rats. *Nutr. Res.* ; 20:273- 280.

8. **Fohri,B. Aiache, J. Memmi, A. Korbi, S. & Lamaison, J. (1994)**. Aypotension, Hypoglycemia, Hypouricemia recorded after repeated administration …... aqueous leaf Extract of oleaeuropeal. J. pharm. Belg. ; 49(2) : 101-8.

9. **Deeg, R. & Ziegenhorn, J. (1983).** Kinetic enzymic method for automated determination of total cholesterol in serum. *Clin Chem.* ; 29(10):1798–1802.

10. **Fossati, P. Prencipe, L. (1982)**. Serum triglycerides determined colorimetrically with an enzyme that proceduces hydrogen peroxide. *Clin Chem.* ; 28(10):2077–2080.

11. **Grove , H. (1979).** Effect of reagent PH on determination of the high-density lipoprotein cholesterol by precipitation with sodium phototungestate-magnesium. *Clin Chem.* ; 25(4):560–564.

12. **Friedewald ,T. Levy,I. & Fredrickson,S. (1972)**. Estimation of low density lipoprotein cholesterol in plasma without use preparative ultracentri-fuge. *Clin Chem* .;18(6):499- 502.

13. **Austin, A. Hutter, M. Zimmern, L.& Humphries ,E. (2004).** Familial hypercholesterolemia ancoronary heart disease: a HuGE association review. *Am J Epidemiol.* ;160(5):421–429.

14. **Lau , S. (2006)**.Suppression of LDL oxidation by garlic compounds is a possible mechanism of cardiovascular health benefit. *J Nutr*; 136:765S- 8S.

15. **Peleg , A. Hershcovici, T. Lipa, R. Anbar, R. Redler, M. Beigel,Y. (2003)**. Effect of garlic on lipid profile and psychopathologic parameters in people with mild to moderate hypercholesterolemia. *Isr Med Assoc J* ;9:637 - 40.

16. **Berthold, D. Sudhop, T. Bergmann, V. (1998)** . Effect of a garlic oil preparation on serum Lipoproteins and cholesterol metabolism. J. *Am. Med. Assoc.* ; 279:1900-1902.

17. **Breithaupt-Grögler, K. Ling, M. Boudoulas, H. Belz, G. (1997)**. Protective effect of chronic garlic intake on elastic properties of aorta in the elderly. *Circulation* ; 96:2649 - 2655.

18. **Merat, A. & Fallahzadeh, M. (1996)** . Effect of garlic on some blood lipids and HMG-CoA reductase activity. *Iran J. Med. Sc.* ; 21(3 & 4): 146-151.

19. **Rahman, K. & Lowe, M. (2006)**. Garlic and Cardiovascular Disease: A Critical Review. *J. Nutr.* ; 136(3):736S–740S.

20. **Gupta, N. Porter , D. (2001)**. Garlic and garlic derived compounds inhibit human squalene monooxygenase. *J. Nutr.* ;131: 1662- 1667.

21. **Yu Yan Yeh, L. & Liu, L. (2001)** . Cholesterol lowering effect of garlic extract and organosulfur compounds: Human and animal studies. *J. Nutr.*;131: 9895- 9935.

22. **Lau Benjamin, S. (2001)** . Suppression of LDL oxidation by garlic. *J. Nutr.* ;131: 9555-9585.

Study of proteins encoded by different fragments of C virus gene for detection hepatitis C infection

Mohammed A. Saleh
Biology Department, College of Science , Diyala University.

Receiving Date: 2011/5/2 - **Accept Date:** 2011/6/13

Abstract

This study was carried out to evaluate proteins encoded by different fragments of HCV genes for detection hepatitis C infection. Eighty eight Iraqi hepatitis C patients were involved in this study, these patients attended the Gastroenterology Department of Baghdad Teaching Hospital during the period from December 2009 to March 2011. These patients included 58 males and 30 females with ages ranged between (16-64) year. The results of this study showed that 88 specimens were immunoreactive to one or more of the 4 HCV recombinant proteins, besides that 34 serum samples were collected from apparently healthy individuals (included 21 males and 13 females) they served as a control group, all the samples obtained from control group didn't show any reactivity to hepatitis C virus.Additionally, the positive rates of anti-capsid ,anti-NS3,anti-NS4 and anti-NS5 were 77.2%,64.7%,55.6% and 46.5% respectively ,while 13.6 % reacted to capsid protein , 5.7% reacted to NS3 protein , in addition , 3.4% reacted to NS4 protein , furthermore , 2.3% only reacted to NS5 protein . Finally, all the 88 specimens (100%) were immuno-reactive to the mixed proteins. In conclusion , Our results sustain different immunoreactivity of the HCV recombinant proteins encoded by different fragments of C virus gene, therefore the mixture of all the protein derived from HCV different regions should be applied in further HCV diagnostic test to detect hepatitis C infection.

Key words: hepatitis C infection , C virus genome , NS proteins

DIYALA JOURNAL FOR PURE SCIENCES

Study of proteins encoded by different fragments of C virus

gene for detection hepatitis C infection

Mohammed A. Saleh

دراسة البروتينات المشفرة من القطع المختلفة لجين الفيروس ج للتحري

عن الإصابة بالالتهاب الكبد الفيروسي ج .

د. محمد عبد الدايم صالح

قسم علوم الحياة ، كلية العلوم، جامعة ديالى .

الخلاصة

أجريت هذه الدراسة لتقييم البروتينات المشفرة من القطع المختلفة لجين الفيروس ج للتحري عن الإصابة بالتهاب الكبد الفايروسي ج .

تضمنت الدراسة ٨٨ مريض عراقي مصابين بالتهاب الكبد الفايروسي ج من المراجعين لقسم الجهاز الهضمي في مستشفى بغداد التعليمي خلال الفترة الممتدة من كانون الأول ٢٠٠٩ إلى آذار ٢٠١١. المرضى مؤلفين من ٥٨ ذكر و٣٠ أنثى وبمعدل عمري يتراوح من ١٦-٦٤ سنة.أثبتت نتائج الدراسة بان ٨٨ نموذج أعطوا تفاعل مناعي لواحد أو أكثر من بروتينات فيروس ج الأربعة .من جانب أخر تم اخذ ٣٤ نموذج مصلي من أشخاص أصحاء ظاهريا وتم استخدامهم كمجموعة سيطرة ، جميع النماذج التي أخذت من مجموعة السيطرة لم تعطي أي نتيجة تفاعلية مع فيروس سي. من جهة أخرى أكدت نتائج الدراسة أن معدل الموجبية لكل منanti-capsid وanti-NS3 و anti-NS4 وanti-NS5 كان ٧٧.٢%، ٦٤.٧% ، ٥٥.٦%، ٤٦.٥ % على التوالي ، بينما ١٣.٦% أعطى نتيجة موجبة مع بروتين الغلاف capsid، ٥.٧ % أعطوا نتيجة موجبة مع بروتين NS3 و وبالإضافة إلى ٣.٤ % أعطوا نتيجة موجبة مع NS4 و ٢.٣% أعطوا نتيجة موجبة مع NS5 وأخيرا فان جميع النماذج ٨٨ (١٠٠%) أعطوا نتيجة موجبة مع البروتينات المخلوطة . نتائج الدراسة أثبتت وجود اختلاف مناعي تفاعلي لبروتينات الفيروس ج المشفرة من القطع المختلفة لجين الفيروس ج لذلك فان خليط البروتينات المشتقة من المناطق المختلفة لفيروس التهاب الكبد ج يجب أن يوضع ضمن الفحوصات التشخيصية لفيروس سي لغرض التحري عن الإصابة بالتهاب الكبد الفيروسي ج.

Introduction

Hepatitis C virus (HCV) infection has become a major public health problem, about 170 million people considered to be infected worldwide. The disease progresses slowly and a chronic infection develops in 85% of the cases. Among patients with chronic hepatitis, 20 to 30% develop cirrhosis that, once established, carries a poor prognosis, with a high risk of 1). Structural studies of the HCV genome have shown that the (developing hepatocarcinoma virus have a positive – strand RNA virus related to flaviviruses family , The high rate of mutation in the RNA genome of this RNA virus may cause the variability of the envelope protein (2,3). HCV has been linked to a blood – borne , e. g. patients receiving organ transplants , blood product , or intravenous drug use , born to an infected mother , and sexual practices (4) . Infection with acute HCV is usually subclinical, but the likelihood of chronic is high. Infection with HCV is most typically diagnosed in the chronic phase of infection (5).Patients may be diagnosed coincidentally during the investigation of fatigue or abnormal liver function test, or with manifestation of chronic liver disease. The initial screening test for HCV is detection of circulating anti-HCV antibodies, if present; confirmation is required either by more specific antibody testing using immunoblot, or more often by using Polymerase Chain Reaction (PCR) for viral RNA. Quantitative PCR and viral genotyping are

becoming more relevant as treatment strategies evolve (6). The HCV genome is a positive-stranded RNA molecule of approximately 10,000 nucleotides, which contains a single uninterrupted open- reading frame that encodes a protein of about 3,000 amino acids . The structural region consists of core and envelope (E1 and E2) proteins, and a 3' region codes the nonstructural proteins (NS2, NS3, NS4A, NS4B, NS5A and NS5B), which after processing constitute 10 mature viral proteins (7).The determining proteins which are encoded by different fragments of HCV genome are essential for diagnostic hepatitis C infection , therefore this research was aimed to study proteins encoded by hepatitis C virus gene for detection hepatitis C infection.

Subjects

Patients Study Group

Eighty eight Iraqi patients infected with hepatitis C were involved in this study , these patients attended the Gastroenterology Department of Baghdad Teaching Hospital during the period from December 2009 to March 2011. Their ages ranged between (16-64) year. These patients included 58 males and 30 females. They were sequentially selected from cases referred to the hospital at first presentation. They were diagnosis based upon the patient's medical history, physical examination and laboratory test.

Control group

Thirty four healthy individuals with age range from (21-62) year were studied as control group. This group included 21 males and 13 females. Samples were collected from those individuals only if they were not receiving any medication and did not had a history of a chronic or acute illness

Samples collection

From each individual included in this study, 5 ml of blood was drawn by vein puncture using disposable syringes. The blood was placed in plastic disposable tubes, it was left to stand at room temperature (20-25°C) to allow it to clot, then the sera was separated by centrifugation 10000 r.p.m for 5 minutes, and divided into aliquots (250 µl) and stored at -20°C till examination. Each aliquot of the serum was used once to avoid thawing and freezing. All sera and reagents were allowed to stand at room temperature before use in the test.

Methods

1-Enzyme Linked Immunosorbent Assay (ELISA):

Principle:

Employing a second-antibody sandwich principle, diluted patient sample or control were added to microtitre wells precoated with purified antigens mimicking the core, NS3, NS4 and NS5 gene segments of the HCV genome. These peptides have been shown to react and bind with the predominant classes of anti-HCV antibodies present in HCV positive serum. After incubation, peroxidase-conjugated anti-human IgG antibody was added to form a detectable complex. After washing, one shot substrate was added to form a colored complex. The intensity of the color that may consequently develop is proportional to the amount of anti-HCV present in the sample. The reaction was then stopped by the addition of acid and the resulting color intensity can be read spectrophotometrically at 450 nm (8).

Procedure :

The detailed procedure was carried out as has been suggested in the leaflet supplied with the test kit (Randox, U.K)

2-Recombinant Immunoblot Assay

Principle:

The RIBA HCV 3.0 is a three-stage test which utilizes individual recombinant HCV antigens and the synthetic peptides immobilized as individual bands onto the test strips. In the first stage, the specimen or assay control is diluted and incubated with the strip. Antibodies specific to HCV, if present, will bind to the corresponding recombinant antigen and / or synthetic peptide bands on the strip. In the second stage, the strip is incubated in the presence of a peroxidase-labeled coat anti-serum IgG conjugate. In the third stage, a colorimetric enzyme detection system composed of hydrogen peroxide and 4-chloro-1naphthol is added.. After the development of color on the strip, the reaction is stopped by removal of the reactants and final wash steps. The visual band patterns which develop on each individual strip are the result of specific antibody being bound to each of the individual recombinant antigens and/ or synthetic peptides on that strip. The reactivity of specimens towards each antigen band is determined by visually comparing the intensity of the individual antigen band with that of the low and high human IgG internal control bands plotted onto each strip. (9).

Procedure :

The detailed procedure was carried out as has been suggested in the leaflet supplied with the test kit (Chiron, Ireland).

Results and Discussion

Table 1 : Sex distribution of studied group

	hepatitis C Patients		Control group	
Sex	Number	%	Number	%
Male	58	65.9	21	61.7
Female	30	34.1	13	38.3
Total	88	100	34	100
M/F ratio	1.93:1		1.61:1	

Table 1 shows the majority of patients and control groups are males (65.9% and 61.7%) respectively rather than females (34.1% and 38.3%) respectively. The ratio between male to female among patients group was 1.93:1, whereas 1.61:1 among control group . This high frequency of infection with HCV among males may be attributed to socio-community nature of Iraqi people which makes men undergone the responsibility of working and eventually are in great contact with the pathogens rather than the women. Most studies denoted to the prevalence of HCV was among men rather than women which revealed that the male: female is (2:1) (10,11,12,13). Some observed an equal ratio of males: females (1:1) in Iraq (14,15).

Table 2 : Distribution of patients and control groups according to anti-HCV Ab and recombinant proteins

Patients number	Anti –HCV antibody		Immuno-reactive to one or more HCV recombinant protein		Control group	Anti –HCV antibody		Immuno-reactive to one or more HCV recombinant protein	
	+ve	%	+ve	%		+ve	%	+ve	%
88	88	100	88	100	34	0	0	0	0

Table 2 revealed the distribution of patients according to anti-HCV Ab and recombinant proteins. According to this table, It was found that 88 anti-HCV-positive specimens were immunoreactive to one or more of HCV recombinant proteins, while control group didn't show any positivity to anti –HCV antibody and recombinant protein . Additionally, these results agreed with (16) who reported seventy-five out of the 90 known anti-HCV-positive

were reactive to one or more of HCV recombinant antigens. Moreover (17) found that young adults, a considerable difference among anti –HCV antibody and HCV recombinant proteins for investigating hepatitis C infection .

Table 3: Frequency of patients and control groups according to antibody against viral recombinant proteins

Patients Number	Anti-capsid		Anti-NS3		Anti-NS4		Anti-NS5		Control group	Anti-capsid , Anti-NS3, Anti-NS4, Anti-NS5	
	+ve	%	+ve	%	+ve	%	+ve	%		+ve	%
88	68	77.2	57	64.7	49	55.6	41	46.5	34	0	0

The positive rates of anti-capsid ,anti-NS3,anti-NS4 and anti-NS5 were 77.2%,64.7%,55.6% and 46.5% respectively in comparison to control group (0%)(table 3) .

Table 4: Frequency of patients and control groups according to positivity to viral recombinant proteins

Patients Number	capsid protein		NS3 protein		NS4 protein		NS5 protein		Mixed proteins		Control group	Mixed proteins	
	+ve	%	+ve	%	+ve	%	+ve	%	+ve	%		+ve	%
88	12	13.6	5	5.7	3	3.4	2	2.3	88	100	34	0	0

while 13.6 % reacted with capsid protein besides , 5.7 % reacted with NS3 protein , in addition , 3.4% only reacted with NS4 protein , furthermore , 2.3 % only reacted with NS5

protein ,while control group didn't show any positivity to mixed proteins , finally, all the 88 specimens (100 %) were immuno-reactive to the mixed proteins as presented in table 4 . The result of the current study is comparable to that of the (16) which mentioned that there was high positivity among anti-capsid,anti-NS3,anti-NS4 and anti-NS5 were 70.0%,61.1%,52.2% and 44.4% respectively, as well as 13 % reacted with capsid protein , 5.9 % reacted with NS3 protein , 3.2% reacted with NS4 protein and 1.9 % reacted with NS5 protein .However, all the specimens were reactive to the mixed proteins. Moreover, The result appeared in concurrence with study done by (17 ,18) who recorded a lower detection level of capsid , NS3, NS4 and NS5 proteins among patients with hepatitis C ,whereas all patients gave positive reaction to the mixed proteins. Therefore the mixture of all the antigens derived from HCV different regions should be applied in further HCV diagnostic test to detect hepatitis C infection.

Reference

1- Lauer, G.M. and Walker, B.D. (2001).Hepatitis C virus infection. *N Engl J Med*.; 345: 41-52.
2- Kittleson, D.J.; Chianese-Bullock, K.A.; Yao, Z.Q.; Bracial, T.J.; and Hahn, Y.S. (2000). Interaction between complement receptor gC1qR and hepatitis C virus core protein inhibits T-lymphocyte proliferation. *J.Clin. Invest.;* 106(10): 1239-1249.
3- Gong, G.Z.; Lai, L.Y.; Jiang, Y.F.; He, Y.; and Su, X.S. (2003). HCV replication in PBMC and its influence on interferon therapy . *World J. Gastroentrol*.; 9 (2): 291-294.
4- Weltman, M.D.; and Tally, N.J. (2003). Chronic hepatitis C infection: a review and update on treatment strategies .*ADF Health*; 4(1): 27-33.
5- Saab, S.; and Martin, P. (2000). Tests for acute and chronic viral hepatitis. *The practical peer-Reviewed J. for primary care phycicians*; 107(2): 123-130.
6- Berry, V.; Arora, R. and Paul, P.(2005). Hepatitis C – Clinical outcome and diagnosis. *Ind. J. K. sci.;* 7(1): 129-32.
7- Dou, X.G.; Talekar, G.; Chang, J.; Dai, X.; Li, L.; Bonafonte, M.T.; Holloway, B.; Fields, H.A. and Khudyakov, Y.E. (2002). Antigenic heterogeneity of the hepatitis C virus NS5A protein. *J. Clin. Microbiol.*; 40: 61-67.
8- Banker, P.D. (2003) .Viral hepatitis. *Ind. J. Med. Sci.;*57: 461-68.
9- Damen, M.; Zoaijer, H. and Cuyper, H. (1995) . Reliability of the third-generation recombinant Immunoblot assay for hepatitis C virus. *Transf*.; 35: 745-749.
10- Anne, F.; Celona, M.C. and Macnish , P. (2004) Hepatitis C in Los Angeles public hepatitis clinic: Demographic and biochemical differences associated with Race-Ethnicity. *Clin. Gastroenterol. Hepatol.;* 2 :459-462.
11- Sabri ,H.J.A.(2003) .The diagnostic role of liver biopsy in grading ,staging and etiology of chronic hepatitis. A thesis for fellow ship Iraqi commission for Medical Specialization in Pathology .
12- Douraid, K.S. (1995).Prevalence of hepatitis C virus infection in a sample of Iraqi patients with chronic liver disease. A thesis for fellow ship Iraqi commission for Medical Specialization in Medicine.

13- Derek, P. ; Norah, A.; Terraul, T. (2005).Cost –effectiveness of Hepato cellular carcinoma surveillance in patients with hepatitis C virus –related cirrhosis. *Clini. gastro-entero. and Hepato.;*3: 75-84.

14- Rahi, S.J. (2003) .Cytokines profile in Iraqi patients infected with HCV. M. Sc. Thesis, College of Medicine, University of Baghdad .

15- Moatter, T.; Hussainy, A.S.; Hamid, S.; Ahmed, Z. and Siddiqui, S. (2002). Comparative analysis of viral titers and histologic features of Pakistani patients infected with hepatitis C virus type 3. *Int. J. Infect. Dis.;* 6: 272-276.

16- Weizhen ,Q.(2004).Significance of recombinant proteins encoded by different fragments of hepatitis C virus (HCV) gene for detection of anti-HCV antibodies. *J.clin.lab.sci.;*3:45-53.

17- Yang ,S. ; Jiao-jiao, L.; Ming, L. and You-ming,W. (2005). The Diagnostic Research of Hepatitis C with Recombinant Antigen. *J.Virologica.Sinica.;* 2:23-31.

18-Wang , Z.; Yang ,Y .; Han, G. and Yang, T. (2004). Molecular cloning, expression, purification and antigenicity analysis of NS3 gene of hepatitis C virus. *Chinese J. of Hepato.;* 11:67-78.

Dependence of electrons distribution function and the swarm parameters on the buffer gas (Xe) concentration in SF_6-Xe gas mixture

Raad Hameed Majeed

College of Education-Ibn-AL-Haitham/Department of physics

Receiving Date: 2011/3/27 **- Accept Date:** 2011/5/11

Abstract

The effect of concentration varying of the buffer gas Xenon (Xe) in a mixture of Sulphur hexafluoride and Xenon (SF_6-Xe) are considered to study the change in electrons distribution function and therefore the change of the electrons transport or swarm parameters such as the drift velocity , the main energy, characteristics energy, electrons mobility, …etc., in order to choose the suitable optimized calculated set of the electrons transport parameters for the mixture that have realty usage in many high voltage engineering purposes in industrial applications, by comparing with the recently published experimental results.

Dependence of electrons distribution function and the swarm parameters on the buffer gas (Xe) concentration in SF_6-Xe gas mixture

Raad Hameed Majeed

Introduction

The motion of particles for gas or plasma considered as pure or as a mixture is completely described by Boltzmann equation or sometimes called transport equation. By solving this equation numerically one can get the normalized distribution function which plays important roles in calculation the electrons swarm parameters.

Since inert gases are monatomic and their atoms are of closed shell structure, the collision of an electron with an inert gas atom is the most typical case of electron-atom collision processes [1]. Pure SF_6 is not poisonous, so that this gas is not dangerous to inhale, provided that the oxygen content is high enough. SF6is about 6 times heavier than air, it means that it may condensed in cable ducts or at the bottom of tanks. Because SF_6 is non flammable gas its used in electrical apparatus and also can be used as a fire extinguishing agent [2,3] .it is necessary to note that SF6 gas is used (pure or mixture) as an insulating medium in substations and as insulating and cooling medium in switchgear for high and intermediate voltage applications, and for these usage it required to cut off the power in case of a fault in order to protect people and equipments [4,5] . In our work, we use the mixture SF_6-Xe gases as a medium gas target.

The method for calculating the sparking potential of gases or gaseous mixtures is basically approach by calculating e the ionization and attachment coefficients from electron energy distribution functions and then applies the breakdown criterion, i.e.,

$\alpha/N = \eta/N$, (α is the ionization coefficient in cm^{-1}, η is the attachment coefficient in Cm^{-1}, N is the number of gas molecules at 0 ℃ = $3.54x10^{16}$ pcm^{-3}, p is the gas pressure in Torr). This approach relies only on the basic physical properties of the industrial gases which are available in some, but not in all, gases from fundamental research studies of the behavior of electron in gases [6].

Theory

The classical theory of transport processes is based on the Boltzmann transport equation; this equation can be driven simply by defining a distribution function and inspecting its time derivative. From this equation many important swarm parameters could be derived that it is still being used in many contemporary research projects to model transport phenomena.

The general form for the Boltzmann transport equation may be written as [7,8].

$$\left(\left(\frac{\partial}{\partial t}\right) + v \cdot \nabla_r + \left(\frac{eE}{m}\right) \cdot \nabla_v\right) f(r,v,t) = \left(\frac{\partial f}{\partial t}\right)_{collisions} \quad ----(1)$$ Or

$$\left(\frac{\partial f}{\partial t}\right) + v \cdot \nabla_r f + a \cdot \nabla_v f = \Sigma \iint [f(v',r,t) F_j(V_j',r,t) - f(r,v,t)\, F_j(V_j,r,t) * v_{r,j}\, \sigma_j(\theta, v_{r,j})\, d\Omega_j\, dV_j$$

Where, v is the velocity of charge particles

a is the acceleration of charges particles

$f(r,v,t)$ is the electrons distribution function

$F_j(V_j,r,t)$ is the neutral species distribution function

$v_{rj} = | v - V_j |$ is the relative velocity of charges particles

V_j is the velocity of neutral species

$\sigma_j(\theta, v_{rj})$ is the differential microscopic cross section of interaction the charges particles (electron) with neutral gas species j

$d\Omega_j = Sin\, d\theta d\phi$ is the element solid angle, where θ and ϕ are the polar and azimuthally angles, respectively.

The left and right hand sides describe the behavior changes of electrons distribution function by the Varity independent collisions and also the binary collisions of charges particles with the neutral gas species, respectively. The electron distribution function

$f(r,v,t)$ is approximated by $f(v)$, since it is assume that electrons fields is independent of space and time and the problems of electrons interactions are spatially uniform, so that the velocity dependence distribution function can be written by Legendre series expansion as follow.

$$f(r,v,t) \approx f + \sum f(\text{ v,r,t }) \text{ P (Cos } \theta \text{)} \text{-------(2)}$$

Or, in terms of the velocity dependence approximation

$$f(\text{v}) \approx f(\text{v}) + \sum f(\text{ v}) \text{ P (Cos } \theta \text{)} \text{ --------(3)}$$

The use of a Maxwellian electron energy distribution function is justifiable on the basis that the rotation and vibration excitation occur in molecular gases at the low electron energy ranges appropriate to a breakdown of gaseous insulation. From the electron energy distribution function we can calculate the swarm properties using the relations.

$$\omega = -\frac{1}{3} \text{E} \int_0^{\infty} \frac{\epsilon}{N\theta} \frac{d}{d\epsilon} \frac{F(\epsilon)}{\epsilon^{1/2}} \, d\epsilon \quad ----(4)$$

$$\mu = \frac{\omega}{E} \quad \text{----------(5)}$$

$$\bar{\epsilon} = \int_0^\infty \epsilon\, F(\epsilon)\, d\epsilon \text{ ---------- .(6)}$$

$$\frac{\alpha}{N} = \frac{1}{W}\int_{\epsilon_t}^\infty Q_i\, \epsilon^{1/2} F(\epsilon) d\epsilon --(7) \quad \frac{\eta}{N} = \frac{1}{W}\int_{\epsilon_a}^\infty Q_a\, \epsilon^{1/2} F(\epsilon) d\epsilon --(8)$$

Where W is the drift velocity (in m s^{-1}), θ the momentum transfer cross section (in cm^2), $\bar{\epsilon}$ the mean energy, μ the electrons mobility (in cm^2/V), α (in cm^{-1}) the ionization coefficient, η (in cm^{-1}) the attachment coefficient, Q_i (in cm^2) the ionization cross section, Q_a (in cm^2) the attachment cross section, ϵ_i the ionization potential. It is important to note that Eqs. (4)-(7) are applicable for all types of energy distribution function.

Substitution of the breakdown criterion of gases $\frac{\alpha}{N} = \frac{\eta}{N}$ gives the value $\frac{E}{N}$ at which breakdown occurs in highly electronegative gases.

Calculations and Results

To calculate the drift velocity of electrons and the others swarm parameters, a knowledge of the dependence of the momentum transfer cross section θ on the electron energy is essential. The drift velocity does not depend on electron energy distribution function significantly, particularly when the cross section does not vary rapidly with electron energy. Using the FORTRAN77 international computer code NOMAD, which solved the Boltzmann transport equation numerically by the finite difference techniques, can calculate the electrons distribution and therefore all the swarm parameters.

The gas density for pure gas or the concentration percentage for gases mixture can be calculated by using the following formulas

N =(m.AV)/ Mw for pure gas

N =((ρ1.V1+ ρ2.V2+ ρ3.V3+……).AV)/ Mw for gasous mixture

Where m=ρ.V, is the mass of the gas, AV,is the Avogadro number,

(V1, V2, V3,….) are the volume fraction for the gases mixture, Mw, is the molecular weight for the gas or gases mixture

Our results are tabulated and described pictorially as follow.

Dependence of electrons distribution function and the swarm parameters on the buffer gas (Xe) concentration in SF_6-Xe gas mixture

Raad Hameed Majeed

Table (1): swarm parameters of electrons in SF_6-Xe gaseous mixture for the case of concentrations percentage 50% SF_6, 50% Xe.

	N = 1.310 x 10^{19} cm^{-3}		
Electric field/gas density E/N (Td=10^{-17} $V.cm^2$)	Drift velocity V_d (cm/sec)	Characteristic energy D/μ (eV)	electron mobility μ (cm^2/V.sec)
150	10.300x10^6	7.200	320.600
200	13.200x10^6	8.85	278.410
300	19.400x10^6	14.20	183.200
400	25.500x10^6	21.50	124.840
500	31.600x10^6	30.80	88.820
600	35.900x10^6	42.00	65.810

The variation of number density of molecules for the gaseous mixture with the mixture concentration percentage is well described in the following table.

Table (2): Variation of number density with mixture concentration percentage in SF_6-Xe gaseous mixture.

No.	Mixture concentration percentage (SF_6/Xe)%	Number density N cm^{-3}	No.	Mixture concentration percentage SF_6/Xe%	Number density N cm^{-3}
1	**90/10**	**1.333 x10^{19}**	**6**	**40/60**	**1.304x10^{19}**
2	**80/20**	**1.327 x10^{19}**	**7**	**30/70**	**1.298 x10^{19}**
3	**70/30**	**1.321 x10^{19}**	**8**	**20/80**	**1.293 x10^{19}**
4	**60/40**	**1.315 x10^{19}**	**9**	**10/90**	**1.287 x10^{19}**
5	**50/50**	**1.310 x10^{19}**			

Dependence of electrons distribution function and the swarm parameters on the buffer gas (Xe) concentration in SF_6-Xe gas mixture

Raad Hameed Majeed

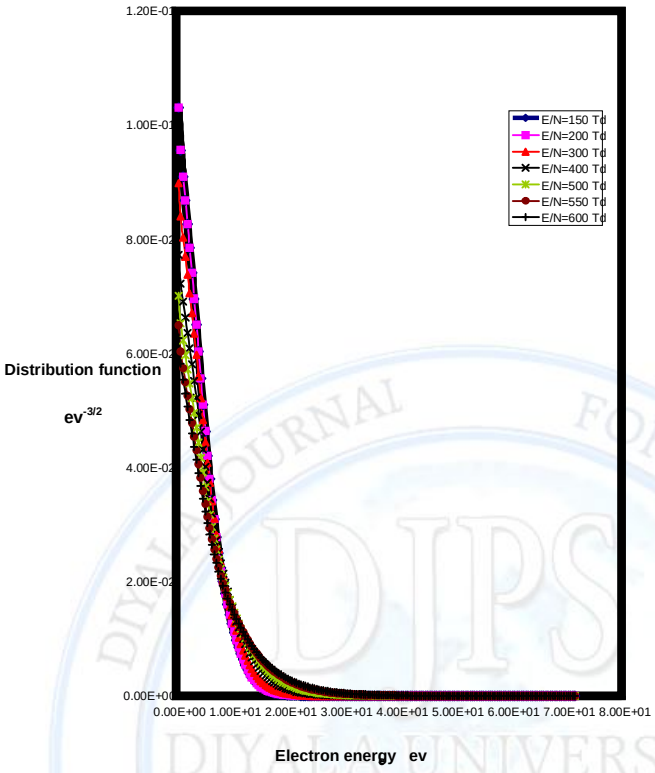

Fig.(1) The electron distribution function versus the electron energy in SF_6-Xe(50/50%) gaseous mixture

Dependence of electrons distribution function and the swarm parameters on the buffer gas (Xe) concentration in SF_6-Xe gas mixture

Raad Hameed Majeed

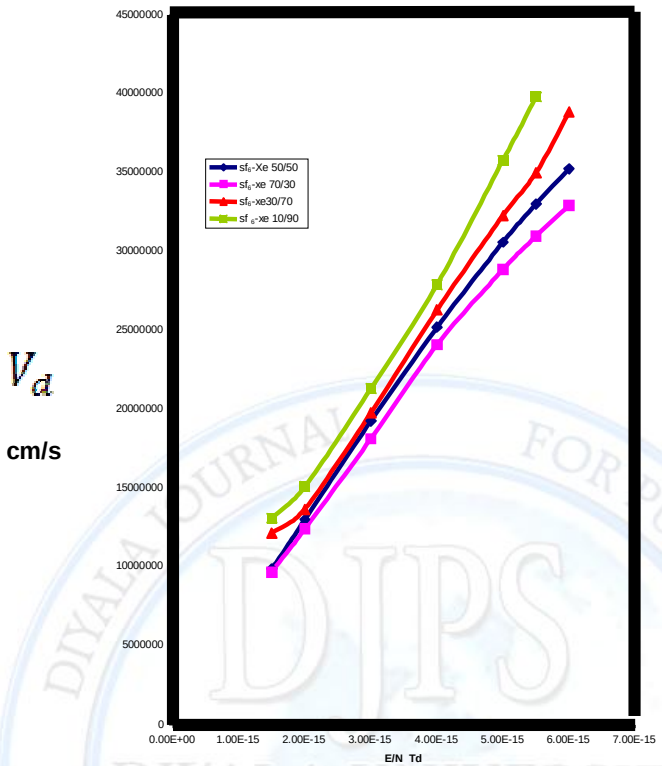

Fig.(2) The electrons drift velocity versus E/N in SF_6-Xe gaseous mixture various percentage

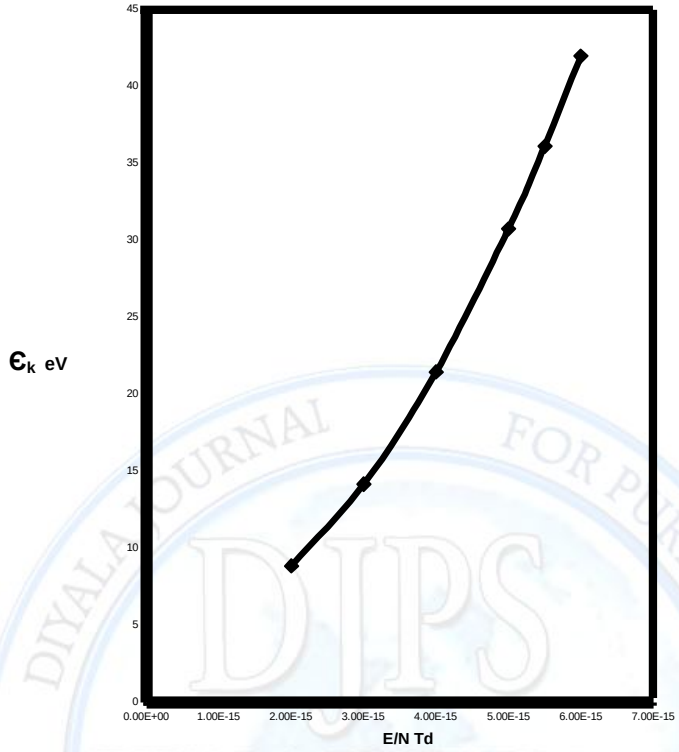

8

Fig.(3) The characteristic energy of electron as a function of E/N in SF_6 -Xe (50/50)% gaseous mixture

Dependence of electrons distribution function and the swarm parameters on the buffer gas (Xe) concentration in SF_6-Xe gas mixture

Raad Hameed Majeed

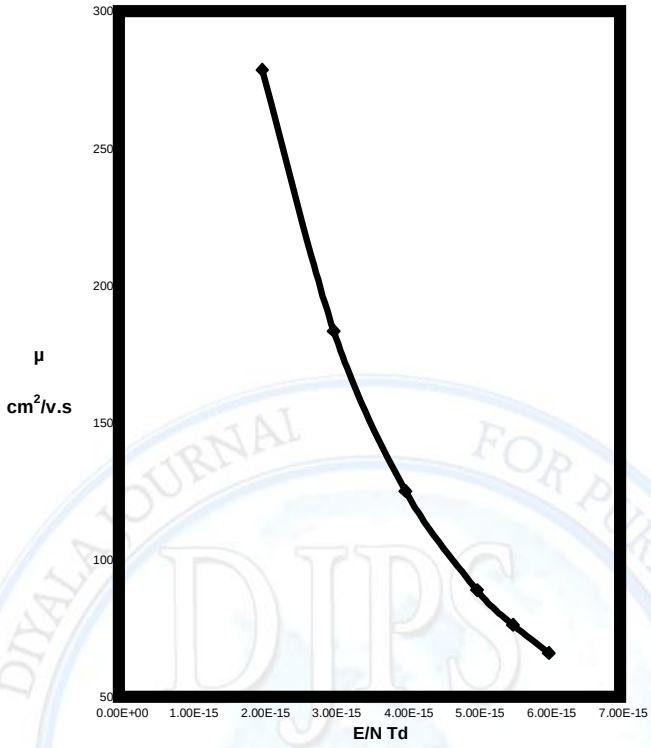

Fig.(4)The mobility of electrons as a function of E/N in SF_6 –Xe (50/50)% gaseous mixture

Dependence of electrons distribution function and the swarm parameters on the buffer gas (Xe) concentration in SF_6-Xe gas mixture

Raad Hameed Majeed

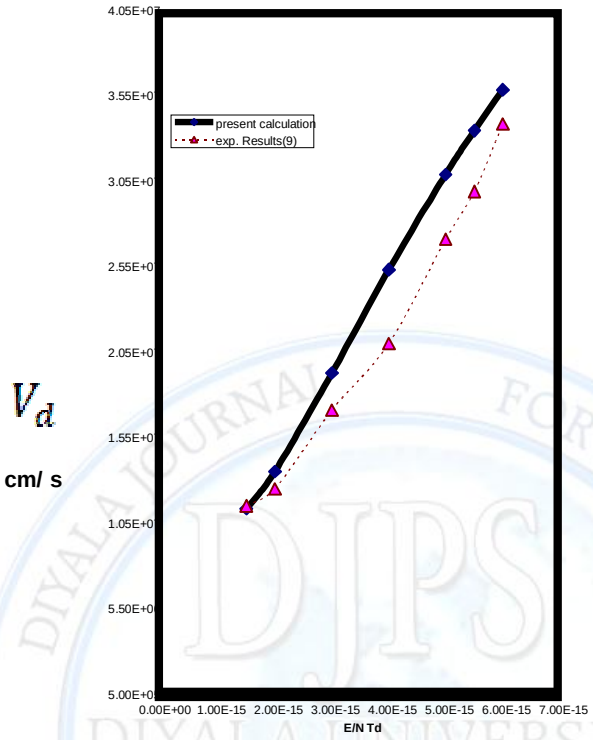

Fig.(5) The electron drift velocity as a function of E/N in SF_6 - Xe (50/50) gaseous mixture

Discussion and conclusion

In our work, the present calculation were focused on the concentration percentage value 50% for sulphur hexafluoride and xenon gaseous mixture, so for their measurement distinguished of the transport or swarm parameters in the applied research, and this case are more suitable for comparison with the published measured results.

Figure (1) show the behavior of the electrons energy dependence distribution function for different cases of the factor (E/N), which reflect the fact of the steady state form, and this can be explained theoretically that there are no mistake in the results. After avoiding the above point, figure (2) show the variety in the drift velocity of electrons and it is clearly appear the effect of adding the buffer gas xenon to the sulphur hexafluoride electronegative gas in increasing their drift velocity due to the change in the different types of collision processes.

It is necessary to note that from figure (5), which explain a brief comparison between our calculated results and a published experimental results [9] for the electrons drift velocity, that there are an increasing beehives in both values and one can explain the relation between the electrons drift velocity and the factor (E/N) as a linear function. In addition there exists a small shift between the two results for a given value of the factor (E/N), and this can be interpret that practically no one of the collision processes are neglected and also all the energy range are involved. In addition, theoretically we need to use a many set of published tables for the different types of cross sections, i.e., the momentum transfer, electronic excitations, electronic vibrations, electronic attachments, etc…in order to reduce the shift or the difference between the two values.

References

1- Xiao D.M., Zhu L.L., Li X.G., J. Of Phys. D: Appl. Phys., Vol.33, No.23, PP. L145-L147, 2000.
2- Maggon K.K., Drug of the future, Vol.19, No.12, PP. 1101-1107, 1994.
3- Lhle G.M., Bonneville Power Administration, 1983.
4- Gorur G.R., Gaseous Electronics, Theory And Practice, 2005.
5- Steve Offord, IEEE, Vol.6, Issue, 2008.
6- Govinda Raju G.R., Hackam R., J. Appl. Phys., Vol.53, No.8, PP. 5557-5564, Aug. 1982.
7- Edward A., Eral W. Mc Daniel, Transport properties of ions in gases, John Wiely and Sons, Inc., 1988.
8- Morgan W.L., Penetrane B.M., Computer physics communication CPC, Vol.58, PP. 127-152, 1990.
9- Hyuck Cho, Robert J. Gulley, Stephen J. Buckman, J. Phys. B:, At Mol. Opt. Phys. Vol.33, No.8, PP. L309-L315, 2000

Solar Energy Utilization Instead of Oil Energy

I. G. Faiadh*, F. L. Rashed*, S. A. Salman**

*Ministry of Science & Technology

** College of Science/ Department of Physics/ University of Diyala

Receiving Date: 2011/5/2 - **Accept Date:** 2011/6/19

Abstract:

In this work solar collector had been used as thermal collector for old oil system refrigerator driven by oil (spent gas) after developing it's diffusion-absorption hest pump.

Glycerin liquid boiling 290 °C was used instead of water in the pipe which surround the, generator with a pipe of 30 cm height and 5 cm in diameter. The ammonia vapor generator at fluid temperature of 140 °C up to 190 °C where the pipe near the condenser become hot, this mean that the ammonia vapor generator up to the condenser.

The requirement calculation were performance for this work are the volume of storage hot fluid required to operate the refrigerator for one day, the flow rate required to supply heat input to generator, and the solar collector absorber area.

Keywords:

Solar Energy, Gas circulation, Air-conditioning system, Power refrigerating system.

Solar Energy Utilization Instead of Oil Energy

I. G. Faiadh, F. L. Rashed, S. A. Salman

إستغلال الطاقة الشمسية بدل الطاقة النفطية

ابراهيم كيطان فياض*، فرحان لفتة رشيد*، د.صباح أنور سلمان**

*وزارة العلوم و التكنولوجيا

** كلية العلوم/ قسم الفيزياء/ جامعة ديالى

الخلاصة:

في هذا العمل، تم إستخدام خلية شمسية كمجمع حراري لمنظومة نفطية تعمل بالنفط بعد تحوير المضخة الحرارية امتصاصية-انتشارية لها.

تم إستخدام سائل الكليسرين بدل الماء في الانبوب المحيط بالمولد ذو درجة غليان عالية ٢٩٠ م وبانبوب ذي ارتفاع ٣٠ م وبقطر ٥ سم حيث قد تم تبخر الامونيا بمعدل درجة حرارة ١٤٠-١٩٠ م.

ان الحسابات المطلوب انجازها لهذا العمل هي كمية المائع المار مطلوب خلال مدة يوم واحد كامل، وبمعدل جريان الحرارة للمولد وكذلك الحسابات المتعاقة بالمساحة الامتصاصية للمجمع الشمسي.

الكلمات المفتاحية:

طاقة شمسية، تدوير الغاز، منظومة تكييف الهواء، منظومات تبريد قدرة.

I. G. Faiadh, F. L. Rashed, S. A. Salman

Introduction:

The significant milestones assumptions of solar energy as an energy resource to meet the needs of developing countries. Firstly, most of the countries called developing are in adjacent to the tropics and have good solar radiation available. Secondly, energy is a critical need of these countries but they do not have widely distributed, readily available supplies of conventional energy resources. Thirdly, most of the developing countries are characterized by arid climates, dispersed and inaccessible populations and a lack of investment capital and are thus faced with practically insuperable obstacles to the provision of energy by conventional means, for example, by electrification. In contrast to this solar energy is readily available and is already distribution to the potential users. Fourthly, because of the diffuse nature of solar energy the developments all over the world have been in smaller units which fits well into the pattern of rural economics. [1-8]

The important problem in this technique it's energy supply to refrigeration and air-conditioning systems. If solar radiation is high the cooling load is generally high. Together with existing technologies, solar energy can be converted to both electricity and heat, either of which can be used to power refrigeration systems. [9]

Cooling unit:

The absorption diffusion refrigerator machine is designed according to operation principles of the refrigeration machine mono pressure. This machine used three operation fluid, water (absorber), the ammonia (refrigerant), and hydrogen as inert gas used in order to maintain the total pressure constant, represented on left hand of the figure (1) is composed of the principle elements, such as boiler, condenser, evaporator, absorber, and fuse. [10]

Solar Collectors:

The major energy gains in the absorber in a solar collector are from the direct absorption of visible light from the sun and, additionally, the absorption of infrared radiation from the warm glass. Important energy losses are infrared radiation emission, convective heat due to natural convection between the absorber and glass, as well as conduction of heat through the rear and sides of the collector. Therefore, the efficiency of the solar collector depends on all of these factors. The efficiency of the solar collector sub-system can be defined as the ratio of useful heat output to the total incident solar radiation (isolation).

In the following efficiency definition,[11] it is assumed that radiation is in the hemispherical region, all rays reach the absorber, and the multiple reflections between the cover and absorber are neglected. The solar collector efficiency can be written as,

$$\eta = F_m\left(\eta_{opt} - \frac{U_L\left(T_{abs,avg} - T_a\right)}{I}\right) \qquad (1)$$

$\eta_{opt} = \tau_\alpha$ optical efficiency of solar collector.

U_L is over all heat loss coefficient ($W/m^2.°C$).

$T_{abs,avg}$ is average temperature of heat transfer fluid in receiver (°C).

T_a is ambient temperature (°C).

I is solar radiation (W/m^2).

F_m is called the collector efficiency factor or a heat transfer factor. The value of F_m depends on the type of the collector and operating conditions. Typical values of F_m is in the range of 0.8-0.9 for non-evacuated air collectors, 0.9-0.95 for non-evacuated liquid collectors, and 0.95-1 for evacuated collectors.

In essence, it is easier to measure the temperature of the heat transfer fluid than to measure the temperature of the absorber surface temperature. Therefore, the solar collector efficiency is often written in terms of the temperature of the inlet (T_i) and outlet (T_o) temperature of the heat transfer fluid. The average temperature of the absorber surface can be assumed to be:

$$T_{abs,avg} = \frac{T_i + T_o}{2}$$

The efficiency of the solar collector can be defined as:

$$\eta = F_R\left(\eta_{opt} - \frac{U_L(T_i - T_a)}{I}\right) \qquad (2)$$

or

$$\eta = F_R(\tau_\alpha)_e - F_R U_L \frac{(T_i - T_a)}{I} \qquad (3)$$

F_R is the collector heat removal factor. The later equation is based on the 'Hottel-Whillier-Bliss' Equation. The value of factors $F_R(\tau_\alpha)e$ and F_RU_L depend on the type of the collectors, layer of the cover glass and selective material. Typical values of these factors are shown in Table (1):

Table (١): The Value of $F_R(\tau\alpha)_e$ and F_RU_L for Some Type of Solar Collector

Solar Collector Type	$F_R(\tau\alpha)_e$	F_RU_L (W m^{-2} K^{-1})
Flat-Plate, Selective-Surface, Single-Glass Cover	0.80	5.00
Flat-Plate, Selective-Surface, Double-Glass Cover	0.80	3.50
Evacuated Tubular Collectors	0.80	Range 1-2
Parabolic-Through Concentrating solar collector (PTC)	**0.70**	**2.5**

Concentrating Solar Collectors:

Two types of line-axis concentrating solar thermal collectors are commonly used today: a Compound Parabolic Concentrating (CPC) and Parabolic-through Concen- trating (PTC).

The concentration ratio (C) describes the characteristics of the concentrating solar collector. It is the ratio of the incident solar radiation area (Ain) to the absorber area (A_{abs}).

$$C = \frac{A_{in}}{A_{abs}} \qquad (5)$$

The concentrating optical solar collector is suitable for high temperature applications (e.g. temperatures >150°C). The large absorber area induces high heat losses. By concentrating the radiation incident of the aperture onto a smaller absorber, the heat losses per absorber area can be reduced. Tracking system is necessary to follow the movement of the sun in order to maintain concentration. The compound parabolic concentrator (CPC) is however not necessary for tracking since the concentration ratio is quite low. The CPC can, therefore, play an important role in solar cooling in the future. The main contribution is the direct (not the diffuse) solar radiation which differs somewhat from the flat-plate solar collector.

Concentrators can be divided into two categories: non-imaging and imaging concentrators. The non-imaging concentrator does not produce a clearly defined image of the sun on the absorber; but distributes radiation from all parts of the solar disc onto all parts of the absorber. The values of the concentration ratio of linear non-imaging collectors are quite low, generally below ten. The imaging concentrator is similar to a simple camera lens, which can form images on the absorber.

For a concentrating collector with a reflectivity (ρ), the optical efficiency can be written as,

$$\eta = \rho\tau_\alpha \qquad (6)$$

Present Solar Driven Absorption System

Present design study is adapt gas fired diffusion-absorption heat pump 150 liter (5ft) refrigerator which available in the market and modify it by removing the original heat input

source (kerosene flam, chimney and the jacket of electrical heater) and substitute it with solar heat input source.

Two attempt were done, first with pipe of height 90 cm, the bottom section, 40 cm height with diameter of 5cm, and upper section, 50cm height with diameter of 4 cm, around the original generator pipe of refrigerator, using as heat Input generator, fill with hot water maintaining at temperature of 97°C ,but the refrigerator is not operate because the temperature of water is not enough to allow the ammonia–water mixture to boil and no temperature gradient along the pipe height where the heat pump occurs, and second attempt with a pipe 30 cm height and diameter of 5 cm around the bottom section of original generator pipe of refrigerator, using a fluid with high boiling point to reach the temperature at which ammonia vapor generation, this was observed when working fluid temperature inlet the external generator(pipe added) reach 140°C where the rectifier pipe becomes hot . In this work glycerin was used as a working fluid (boiling point 290°C).Figure(1) show the pipe added and all the parts of the cooling system.

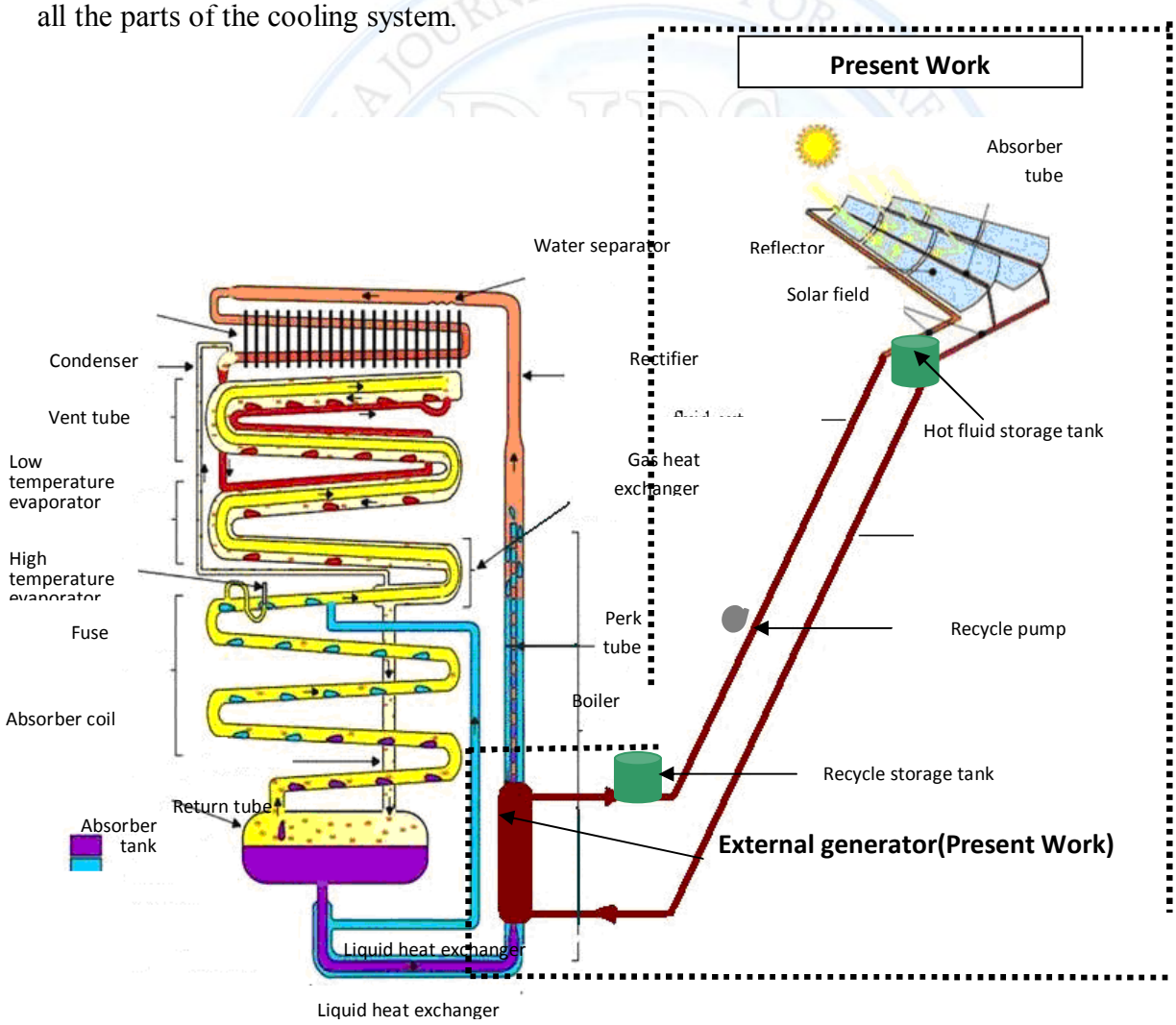

Figure (1) Solar Driven Platen-Munter Diffusion Absorption Refrigerator

The operating pressure of the cooling unit (150 liter (5ft)) is 23bar, concentration of rich solution is 33%, concentration of weak solution is 12%, and 1kg of ammonia vapor leave the generator toward the condenser need 649kcal [12].

From the T\Log diagram the boiling point of rich ammonia-water mixture (33%) is 130°C and the weak mixture (12%) temperature at 23bar is about 190°C .To operate the cooling unit with above condition, inlet generator temperature about 200°C, and outlet temperature about 140°C must be supplied from solar concentrator, then the flow rate of the working fluid required to achieve this operation is calculate as follow:

In this study 2.52hr was measured to generate 1kg of ammonia with 649kcal, the energy demand of the generator is:

$$Q_g = \frac{649}{2.52} = 257.5\ kcal\ hr^{-1}$$

$$= 257.5 \times 1.166667 = 300\,W$$

$$Q_g = \dot{m} C_p \Delta T \qquad (7)$$

The specific heat C_p of glycerin is 2.4J/g °C, which is define:

$$\dot{m} = \frac{Q_g}{C_p \Delta T}$$

then the mass flow rate of heat exchange fluid required (glycerin) can be calculated based on the proposed entrance and exit temperatures of the oil in the generator:

$$\dot{m} = \frac{300}{2.4 \times (200 - 140)} = 2.1\ g\ s^{-1}$$

$$= 7.56 \text{ kg hr}^{-1}$$

The density of glycerin is 1.26 g/cm^3 then:

The volumetric flow rate is:

$$\frac{7.56}{1.26} = 6 \text{ liter hr}^{-1}$$

The required hot fluid volume for 24hr is:

$$6 \times 24 = 144 \text{ liter perday}$$

Parabolic-through Concentrating (PTC) collector, shown in figure(1), was used in this study. The area of the solar collector required by the system was determined based on the

quantity of energy demanded and the mass flow of required heat exchange fluid. The energy demand of the generator is 300W (considering a safety factor of 15%, i.e Q_g=345W).

To determine the efficiency of the solar collector it is necessary to know the temperature difference and the solar radiation. The absorber inlet and outlet temperatures were obtained to be 130°C and 200°C, respectively, and the ambient temperature is 30°C.For an average of six hours of effective solar radiation, the value of 1000W/m^2, then from Equation(3),and table(1) the efficiency of the solar collector is:

$$\eta = 0.7 - 2.5\frac{130-30}{1000} = 0.45$$

Then the energy absorbed is:

$$Q_{abs} = 0.45 \times 1000 = 450\,W/m^2$$

This result in a total absorption (receiver) area of:

$$A_{abs} = \frac{345}{450} = 0.77\,m^2$$

The required outside wall temperature of the absorber is calculated from following equation:

$$Q_{abs} = U_a (T - T_{abs,ave}) \qquad (8)$$

$$T_{abs,ave} = \frac{T_i + T_o}{2} = \frac{130+200}{2} = 165^o C$$

Where T_i and T_o are inlet and outlet temperatures of absorber, respectively, and U_a is the heat conduction coefficient =8W/m^2°C.Then:

$$T = \frac{450}{8} + 165 = 221.25^o C$$

The thermal output Q_{out} of concentrating collector operating at temperature T is given by:

$$Q_{out} = Q_g = F_m(\tau\tau\alpha_e A_{in} q_{in} - F_m U_a A_{abs}(T - T_a) \qquad (9)$$

Dividing equation (9) by A_{abs} yield:

$$\frac{Q_g}{A_{abs}} = Q_{abs} = F_m(\tau\tau\alpha_e \frac{A_{in}}{A_{abs}} q_{in} - F_m U_a (T - T_a)$$

F_m=0.9, $(\tau\alpha)_e = 0.8$, and q_{in}=1000W/m^2 then:

$$\frac{A_{in}}{A_{abs}} = \frac{0.9 \times 8(221.25 - 30)}{720} + 450 = 2.54$$

Then:

$A_{in}=0.77\times2.54=2\ m^2$

Heat storage

Heat storage tank was shown in figure(1), allows a solar thermal plant to produce power at night and on overcast days. This allows the use of solar power for base load generation as well as peak power generation, with the potential of displacing both coal and natural gas fired power plants. Additionally, the utilization of the generator is higher which reduces cost.

Heat is transferred to a thermal storage medium in an insulated reservoir during the day, and withdrawn for power generation at night. Thermal storage media include pressurized steam, concrete, a variety of phase change materials, and molten salts such as sodium and potassium nitrate.

Heat transport refers to the activity in which heat from a solar collector is transported to the heat storage vault. Heat insulation is vital in both heat transport tubing as well as the storage vault. It prevents heat loss, which in turn relates to energy loss, or decrease in the efficiency of the system.

Results & Discussion

Solar cooling systems strongly depend on local conditions e.g. solar radiation, ambient temperature, or cooling load. Systems should therefore be specifically designed for each location, thereby obtaining the best performance. For thermally-driven systems, a solar cooling system requires less solar collector area per cooling demand (kWh. One severe restriction for solar cooling in general is the heat rejection temperature. Heat sink temperatures must be kept as low as possible in order to maintain a stable operation and high performance.

A good local heat sink such as a lake, a river or the sea or even a cooling tower can be used with additional parasitic energy consumption for the latter. The best solar cooling locations are therefore located near sufficient solar radiation and a good heat sink.

Solar driven absorption refrigerator need less initial operating time than gas fired refrigerator, when increase the working fluid flow rate at initial time. This refrigerator

is expensive compare with gas fired and electrical refrigerators but it is active when the house is complete work with solar energy(heating, washing, cooking, …etc) and in the remote areas (out of electrical grid).The refrigerator is not operate when the working fluid from collector pass along the whole boiler tube because no temperature gradient occurs.

The disadvantages of using solar instead of gas fired refrigerator:

- The efficiency of solar refrigerator will be approaches to minimum value with the presence of cloud, or at night.
- There are some difficults for the multi-components that connected with the solar refrigerator system.

References:

1- Kapar, J. C., Areport on Utitization of Solar Energy for refrigeration and air conditioning applications, Solar Energy, 4, (1960).
2- Development Trends in the Production of Energy Electrowatt Engineering Services Ltd. Zurich, (1979).
3- International Symposium Workshop Solar Energy, (16-22), June, Cairo, Egypt, (1978).
4- Transactions of the conference on the use of Solar Energy, the Scientific Basis Tuscan, University of Arizona Press, (1958).
5- Christopher Carroll, Lucas Growth model, 29, pp. 1-5 (2009).
6- Simth M. C. Geothermal Energy, Loss Alamos Report La-5289- Ms. 1973.
7- Solar Energy Research, Univ. of Wisconsin Press (1955).
8- Lucas, Rebert E., on the mechanics of Economic Development, J. Monetary Economics, 22, pp. 3-42, (1988).
9- Eisenstadt. M., Flanigan, M, & Farber, A., Solar Air conditioning with an Ammonia-water Absorption Refrigeration system, AM. SOC. Mec. Eng., (1959).
10- Key Issues for Renewable Heat in Europe (K4RES-H), Solar Assisted Cooling-WP3, Task, 3.5, European Solar thermal Idustry Federation (2006).
11- R. H. B. Exel, Principles of Solar thermal conversion, King Mongkut's University of Technology Thonburi (2000).
12- Carl G. Alimen Chapter 3 (The gas circulation), pp. 3-13, (2007).

Synthesis and characterization of mixed ligand complexes of some metals with 1-nitroso-2-naphthol and L-leucin

F.H, Ghanim
Chemistry Department .Ibn -Al-Haithem College of Education,
University of Baghdad-IRAQ

Receiving Date: 2010/12/23 - **Accept Date:** 2011/5/8

Abstract:

The mixed ligand complexes of Mn(II),Fe(II),Co(II),Cd(II), and Pb(II) with 1-nitroso-2-naphthol ($C_{10}H_7NO_2$), symbolized (NNPhH)] and amino acid [L-leucin **(** $C_6H_{13}NO_2$**),** symbolized (LeuH), were synthesized and characterized by: Melting points, Solubility, Molar conductivity, and determination the percentage of the metal in the complexes by flame(AAS), magnetic susceptipibility , Spectroscopic Method [FT-IR and UV-Vis], And Program [Chem office– CS.Chem.– 3D pro 2004] was used.

The results showed that the deprotonated two ligands acts as a bidentate ligand , (leu-) was coordinated to the metal ions through the oxygen of the carboxylic group and the nitrogen of the amine and the 1-nitroso-2-naphthol ligand was coordinated to the metal ions through the oxygen and nitrogen atoms . Octahedral geometry for M(II) are proposed.

تحضير وتشخيص معقدات مختلطة الليكاند من (1- نتروزو 2- نفثول وحامض الليوسين)

DIYALA JOURNAL FOR PURE SCIENCES

Synthesis and characterization of mixed ligand complexes of some metals with 1-nitroso-2-naphthol and L-leucin

F.H, Ghanim

مع بعض أيونات العناصر الانتقالية

فائزة حسن غانم
جامعة بغداد / كلية التربية ـ ابن الهيثم / قسم الكيمياء

تضمن هذا البحث تحضير وتشخيص معقدات ذات ليكاندات مختلطة للايونات الفلزية Pb(II) و من الليكاند (1- نتروز 2- نفثول) ($C_{10}H_7NO_2$) بالرمز (NNPhH)
Mn(II),Fe(II),Co(II),Cd(II)
مع حامض الليوسين($C_6H_{13}NO_2$) بالرمز (LeuH) .

المعقدات المحضرة بلورات صلبة درست من النواحي الآتية:
درجات الانصهار، التوصيلية الكهربائية المولارية، الذوبانية، الخواص المغناطيسية،تقدير النسبة المئوية للأيون الفلزي في المعقدات بوساطة مطيافية الامتصاص الذري، الدراسات الطيفية: وتضمنت أطياف (الأشعة تحت الحمراء، الأشعة فوق البنفسجية– المرئية، مع استعمال البرنامج (Chem. Office– Cs. chem– 3D pro 2004) في رسم أشكال المعقدات.

INTRODUCTION

1-nitroso-2-naphthol (IUPACName:1-nitrosonaphthalen-2-ol)
($C_{10}H_7NO_2$)
is crystalline solid, sparingly soluble in water and readily soluble in alcohol ,ether and common organic solvent. The melting point is equal to 103–106°C, Ortho-substituted nitrosonaphthols can undergo tautomerisation to give oxo-oximes. (Figure- 1) In the case of 1-nitroso-2-naphthol, the equilibrium is greatly displaced toward keto-form and the compound has, in the solid state and in solution, a predominately quinone which is a hybrid of resonance forms of the type [1-5]. Disodium 1-nitroso-2-naphthol-3,6-disulfonate (nitroso-R salt) was introduced in 1921 by Van Klooster for the detection of cobalt(II) and then subsequently used by various investigators for the determination of small quantities of metals in various samples. it is also a sensitive and specific reagent for Fluor metric determinations of tyrosine residues in proteins and peptides [6] Along with other phenols and naphthols, it belongs to biologically important com pounds, especially because of its cytotoxic action.

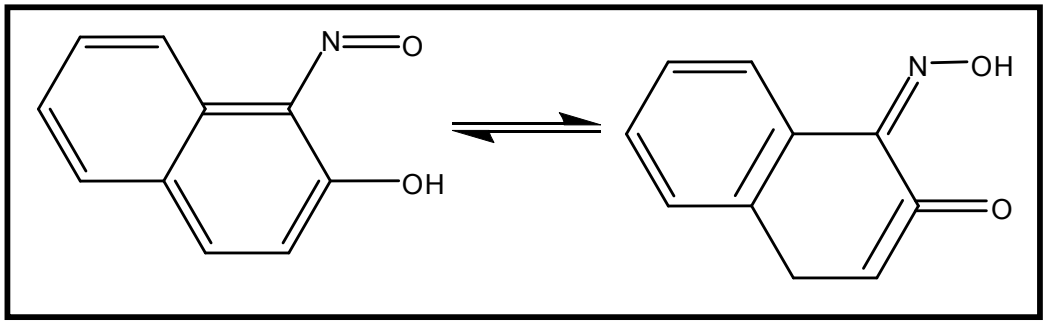

Figur-1:Tautomerisation in 1-nitroso-2-naphthol

(Figure - 1):Tautomerisation of 1-nitroso-2-naphthol

During the recent years , there has been significant interest in the coordination chemistry , the structural properties and the reactivity of metal complexes of amino acids . [7-10]

L-leucin is one of the twenty major amino acids and is considered an essential amino acid. Inorganic elements like transition metals are vital to the proper functioning of the body's processes. Metal ions have the ability to form strong bonds and be stable in more than one oxidation state.[11]

Experimental

a- Reagents and instruments: L-leucin was purchased from (Merck) ,1 -Nitroso-2-naphthol a Fluka Chemie AG, metals chloride and solvents from (B.D.H). The reagents were used without further purification .

b- Instruments: FT-I.R spectra were recorded as KBr discs using Fourier transform Infrared Spectrophotometer Shimadzu 24 FT-I.R 8400s. Electronic spectra of the prepared complexes were measured in the region (200- 1100) nm for 10^{-3}M solutions in ethanol at 25ºC using shimadzu-U.V-160. A Ultra Violet Visible-Spectrophotometer with 1.000 ± 0.001 cm matched quartz cell. While metal contents of the complexes were determined by Atomic Absorption (A.A)Technique using Japan A.A-67G Shimadzu. Electrical conductivity measurements of the complexes were recorded at 25ºC for 10^{-3} M solutions of the samples in Ethanol using pw 9527 Digital conductivity meter (Philips). Melting points were recorded by using Stuart melting point apparatus.

The proposed molecular structure of the complexes were determinated by using chem. office prog, 3DX (2004).

C- **General synthesis :**

a) Sodium leucinate(Na^+Leu^-) : L-leucin [0.131 gm, 1 mmol] was dissolved in 10 ml ethnol and added to 10 ml of ethnolic solution containing [0.04 gm (1mmol)] of the sodium hydroxide , the solution was deprotonated according to the following reaction (scheme -1)

b) sodium 1-Nitroso-2-naphthol ate (Na^+NNPh^-):

1-nitroso-2-naphthol ((NNPhH)**]**) [0.346 gm(2mmol)] was dissolved in 10 ml ethanol and added to (10) ml of ethanolic solution containing [0.08 gm (2mmol)] of the sodium hydroxide , the solution was deprotonated according to the following reaction (scheme -1)

c) Synthesis of complexes: The complexes were prepared by the addition of ethnolic solutions of the (Na^+NNPh^-) and (Na^+Leu^-) to warm stirred ethnolic solution of the respective metal (II) chloride in the stoichiometric ratio matel:ligand (M:2 NNPh: Leu) in (20 min). The mixture was stirred for half an hour at room temperature , crystalline precipitates was observed . The resulting precipitates were filtered off , recrystallized from ethanol and dried at 50C°. according to the following reaction (scheme -1).

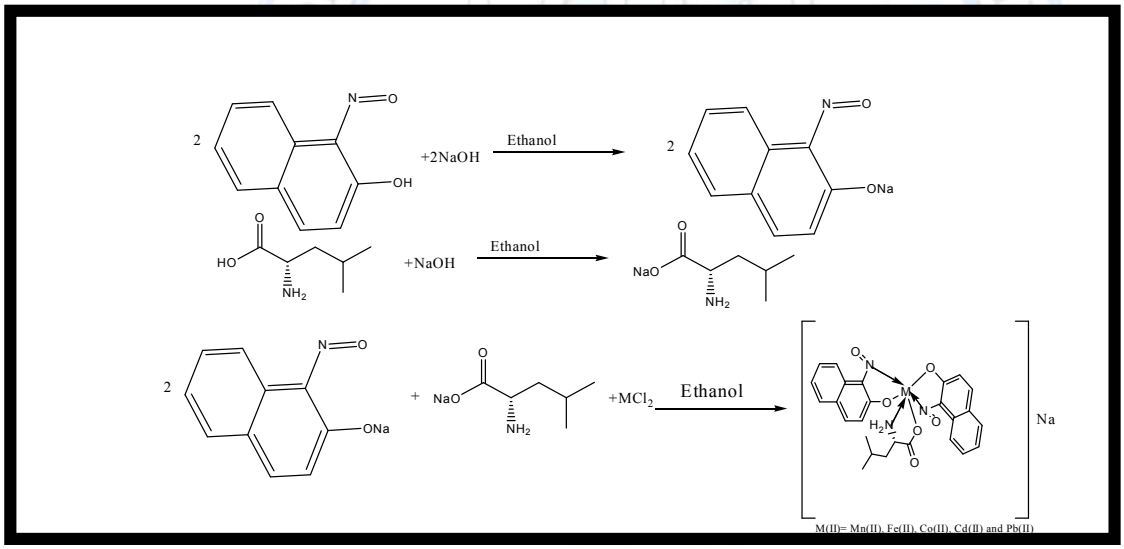

Scheme (1): Synthesis of the Na [M ($C_{26}H_{24}N_3O_6$)] complexes

Results and Discussion

All the complexes are colored, non-hygroscopic and thermally stable solids (Table 1), indicating a strong metal-ligand bond. The complexes are insoluble in water but soluble in common organic solvents such as ethanol, ethyl alcohol, acetone, chloroform ,DMF and DMSO .The observed molar conductance (Table 1) values measured in ethanol in 10^{-3}M solution lie in the (37-42) Ω^{-1} cm^2 mol^{-1} range, indicating their electrolytic nature with(1:1). [12-13]

The atomic absorption measurements (Table-1) for all complexes gave approximated values for theoretical values.

In conclusion, our investigation this suggest that the ligands L-leucin and 1-nitroso-2-naphthol coordinate with M (II) forming Octahedral geometry (Figur-2) .

Figure (3), Table (2), displays the (FT-IR) spectrum for the (L-leucin) exhibited a band around υ (3417) cm^{-1} that corresponds to the stretching vibration of υ (N-H) $_{+}$υ (O-H), while another strong absorption band at υ (3070) cm^{-1} is due to the υ(N-H_2)sym while the bands at (1585) cm^{-1} and (1415)cm^{-1} were assigned to the υ(-COO)asy and υ(-COO)sym respectively. υΔ (-COO)asy-sym =170 cm^{-1}. [14]

Figure (4) ,Table (2), displays the (FT-IR) spectrum for the(1-nitroso-2-naphthol) which exhibits very strong band at (1616)cm^{-1} due to υ(C=O) stretching vibration. [14-15] The band at (3425)cm^{-1} is due to the υ(O–H) stretching vibration [14]. The band at (1523)cm^{-1} is due to the υ(C=N) while the bands at (1450) and (2790)cm^{-1} were assigned to the υ(C=C) aromatic and υ(C–H) aromatic stretching respectively. The band at (3066)cm^{-1} were assigned to υ(HO---H) hydrogen bonding [15,16] and the band at (1153) cm^{-1} is due to the υ(N-O) stretching vibration.

The complexes show band at (590-520) and (470-489) cm-1 rang, due to the ν(M-N) and ν(M-O) vibrations respectively. [14-16]

Electronic spectra :

The electronic spectral data of the free ligands 1-nitroso-2-naphthol and L-leucin and their complexes are summarized in table-3. The u.v-vis spectra of the free ligand (1-nitroso-2-naphthol) in ethanol solvent appeared a high, intense absorption bands at (**304**nm) (**32894** cm^{-1}) (∈max=**937** $molar^{-1}$.cm-1) and at (**383**nm) (26109cm^{-1}) (∈max =**2238** $molar^{-1}.cm^{-1}$).

These bands are attributed to (π→π*)and (n→π*) transitions respectively. The electronic spectra of leucin show an absorption band at 305 nm (32786cm^{-1}) in ethanol . The (UV-Vis) spectra of the complexes displayed absorptions at (301-334) nm assigned for ligand field. the (UV-Vis) spectrum of $[Co(C_{26}H_{24}N_3O_6)]^-$ complex band observed at (412) nm are attributed to (d-d) transitions of type $T_{1g}(F) \rightarrow {}^4T_{2g}(P)$. [17-18]

The complex of $[Cd(C_{26}H_{24}N_3O_6)]^-$ complex exhibits two bands at (304 and 385) nm assigned to charge –transfer transitions [17]. Figures(7-10) From the above data ,we suggested that the geometry of the all complexes are octahydral.

Table 1-The physical properties of the complexes

Compound / Ligand	M.wt	Color	M.p°c (de) °c	Λm $\mu S.cm^2.Mol^{-1}$	Metal% theory	Metal% exp	Cl%
$C_6H_{13}NO_2$ (leu)	131.18	white	289	1.24	-	-	-
1-nitroso-2-naphthol ($C_{10}H_7NO_2$)	173.17	dark-Brown	106	1.77	-	-	-
$[Mn(C_{26}H_{24}N_3O_6)]Na$	529.45	dark-Brown	240 de	37	10.83	11.2	Nill
$[Fe(C_{26}H_{24}N_3O_6)]Na$	530.36	green	228 de	39	10.53	11	Nill
$[Co(C_{26}H_{24}N_3O_6)]$ Na	533.513	red	265 de	38	11.05	13	Nill
$[Cd (C_{26}H_{24}N_3O_6)]$ Na	586.92	green	206 de	42	19.15	21	Nill
$[Pb(C_{26}H_{24}N_3O_6)]$ Na	681.71	green	236 de	40	30.40	29	Nill

Λm = Molar Conductivity de = decomposition

Table (2) FT-IR spectral data of the Ligands and their complexes

Compound	υ(N-H)+ υ (O-H)	υ $(C-H)_{cy}$ $(C-H)_{ali}$	υ(C=O)	υ(C=N)	υ(N-O)	υ$(-COO)_{asy}$	υ $(-COO)_{sym}$	M-N	M-O
$C_6H_{13}NO_2$ (leu)	3417m	1580s	-	-	-	1585vs	1415vs	-	-
1-nitroso-2-naphthol ($C_{10}H_7NO_2$)	3425s-br-3066w	2790vw	1616vs	1523vs	1153m	-	-	-	-
[Mn($C_{26}H_{24}N_3O_6$)]Na	3471s 3062m	2931s 2870w	1616s	1589vs	1134vs	1508vs	1411s	532s	489s
[Fe($C_{26}H_{24}N_3O_6$)]Na	3402vs	2924m	1610vs	1550m	1139vs	1506vs	1355vs	590m	480vs
[Co($C_{26}H_{24}N_3O_6$)] Na	3444vs 3062w	2954w	1647m	1597s	1268m	1516vs	1357m	559m	489s
[Cd ($C_{26}H_{24}N_3O_6$)] Na	3444s 3259w	2954w	1616m	1593m	1246s	1543vs	1346s	578m	470s
[Pb($C_{26}H_{24}N_3O_6$)] Na	3448vs 3043w	2954w	1624s	1558s	1288s	1477m	1361 m	520m	470s

Table 3- Electronic Spectral data, magnetic moment, of the studied complexes and two ligands

Compounds	λ (nm)	υ′(cm^{-1})	ε(max) L.mol. cm^{-1}	μ_{eff} (BM)	Assignment
$C_6H_{13}NO_2$ (leu)	305	32786	310	-	$\pi \rightarrow \pi^*$
1-nitroso-2-naphthol ($C_{10}H_7NO_2$)	304 383	32894 26109	937 2238	-	$\pi \rightarrow \pi^*$ $n \rightarrow \pi$
$[Mn(C_{26}H_{24}N_3O_6)]Na$	301 417 827	33222 32980 12091	1134 1760 365	5.92	Ligand field $A^6_{1g} \rightarrow {}^4T_2g$ (G) $A^6_{1g} \rightarrow {}^4T_1g$ (G)
$[Fe(C_{26}H_{24}N_3O_6)]Na$	304 378 798	32894 26455 12531	470 798 176	4.90	Ligand field C.T $^5T_{2g} \rightarrow {}^5E_{2g}$
$[Co(C_{26}H_{24}N_3O_6)]$ Na	314 412	31847 24271	2242 2328	3.87	Ligand field $T_{1g}(F) \rightarrow {}^4T_{2g}(P)$
[Cd $(C_{26}H_{24}N_3O_6)]$ Na	304 385	3289 25974	1290 1865	Diamag	C.T C.T
$[Pb(C_{26}H_{24}N_3O_6)]$ Na	339 377	29498 26525	2475 2446	---	Ligand field C.T

C.T= Charge transfer

Proposed molecular structure :

Studying complexes on bases of the above analysis , the existence of hexa coordinated $[M(C_{10}H_6NO_2)_2 (C_6H_{12}NO_2)]^-$,were M(II)= Mn(II), Fe(II), Co(II), Cd(II) and Pb(II). proposed models of the species were built with chem3D shows in **Figure** -2.

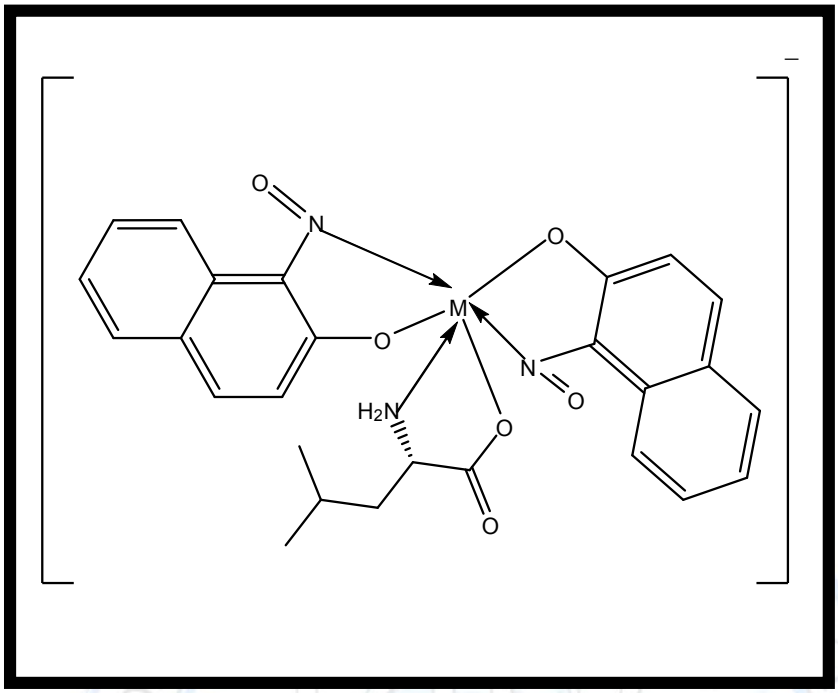

Figure (2):The suggested structure for the complexes $Na[M(C_{10}H_6NO_2)_2 (C_6H_{12}NO_2)]$
M(II)= Mn(II), Fe(II), Co(II), Cd(II) and Pb(II).

Nomenclature of prepared complexes:
Table (4) shows empirical formula and nomenclature (IUPAC) with abbreviated.

Table (4) Nomenclature of prepared complexes

Complexes	Nomenclature	Abbreviation
Na $[Mn(C_{26}H_{24}N_3O_6)]$	**Sodium(L-leucinato)bis(1-nitroso-2-aphtholato)manganese(II).**	**$[Mn(NNPh)_2(leu)$ Na**
Na $[Fe(C_{26}H_{24}N_3O_6)]$	**Sodium (L-leucinato) bis (1-nitroso-2-naphtholato) ferrate(II)**	**Na$[Fe(NNPh)_2(leu)]$**
Na $[Co(C_{26}H_{24}N_3O_6)]$	**Sodium (L-leucinato) bis (1-nitroso-2-naphtholato)cobalt (II)**	**Na$[Co(NNPh)_2(leu)]$**
Na $[Cd(C_{26}H_{24}N_3O_6)]$	**Sodium (L-leucinato) bis (1-nitroso-2-naphtholato)cadmium(II)**	**Na$[Cd(NNPh)_2(leu)]$**
Na $[Pb(C_{26}H_{24}N_3O_6)]$	**Sodium (L-leucinato) bis (1-nitroso-2-naphtholato)lead(II)**	**Na$[Pb(NNPh)_2$ (leu)]**

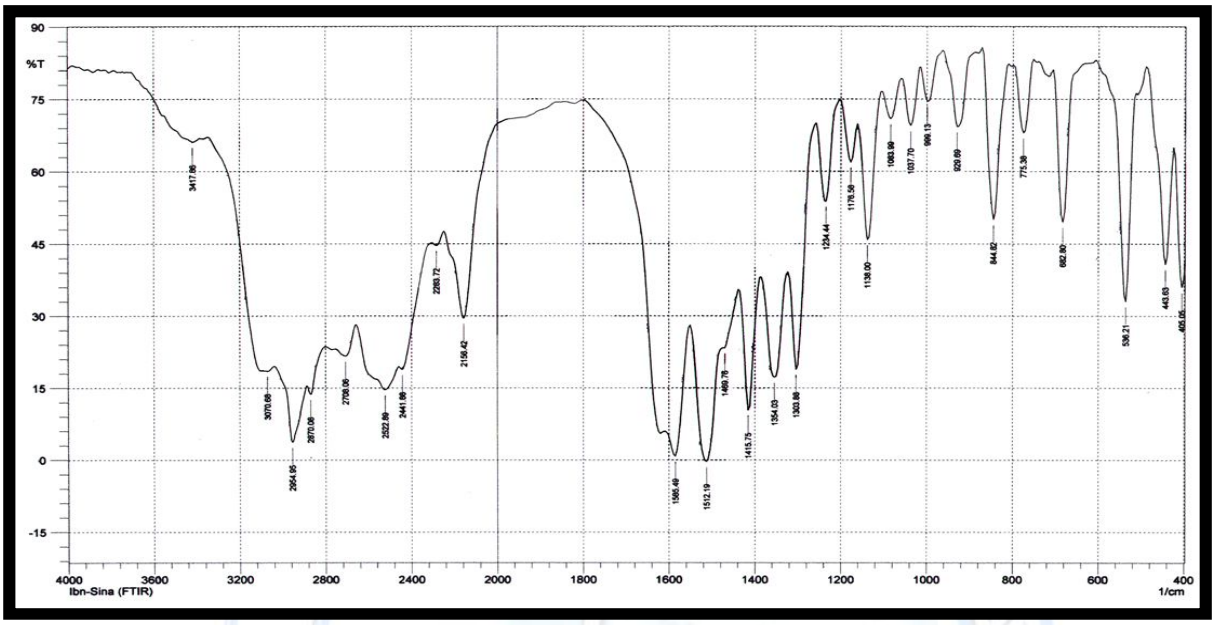

Figure .(3) FT- IR Spectrum of leucine $C_6H_{13}NO_2$

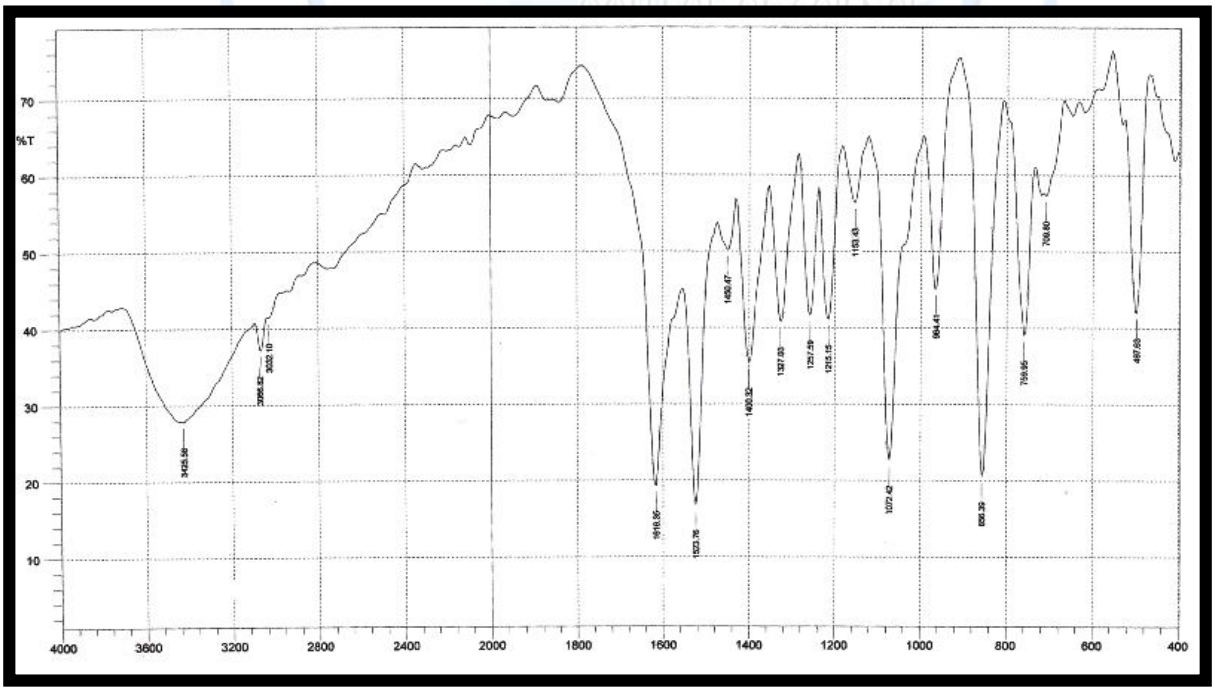

Figure .(4)FT- IR Spectrum of 1-nitroso-2-naphthol ($C_{10}H_7NO_2$)

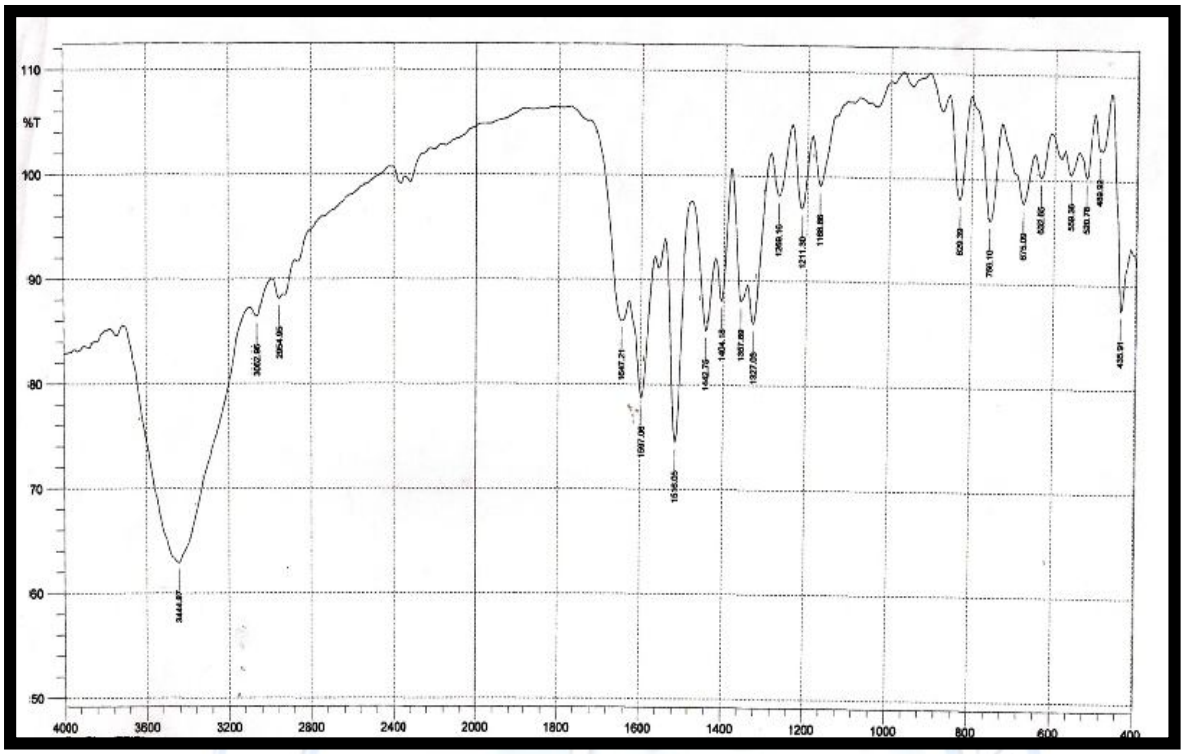

Figure .(5)FT- IR spectrum of $Na[Co(C_{26}H_{24}N_3O_6)]$

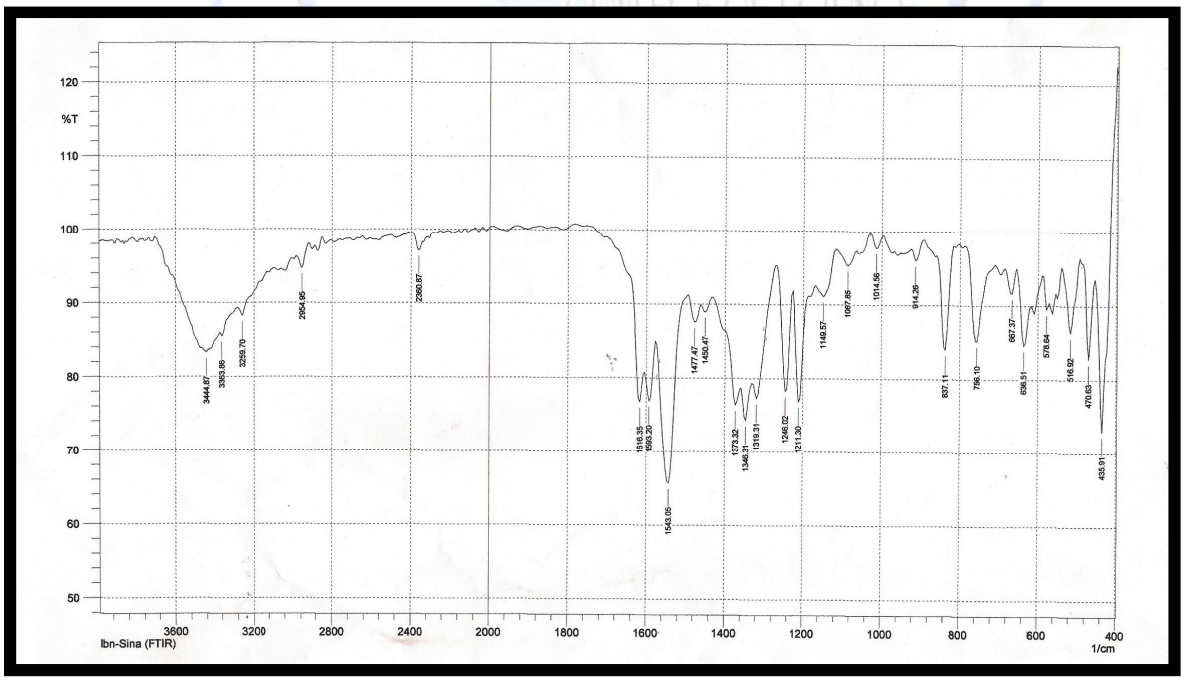

Figure .(6)FT- IR Spectrum of $Na[Cd(C_{26}H_{24}N_3O_6)]$

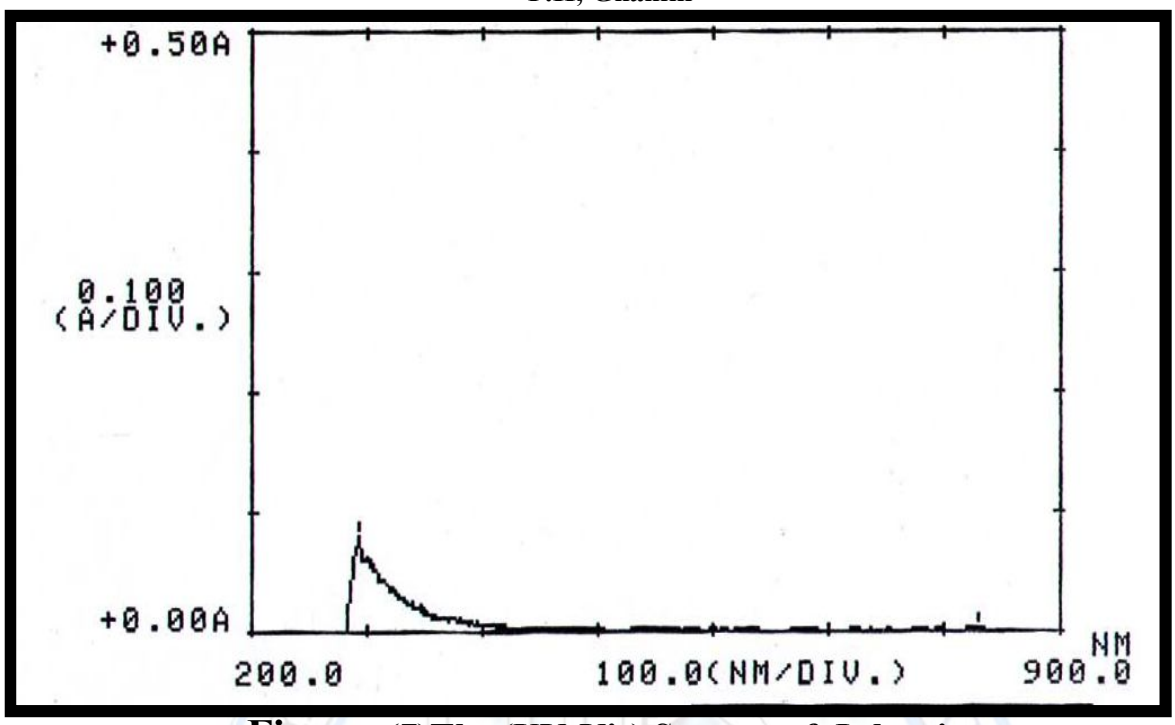

Figure. (7)The (UV-Vis) Spectra of L-leucin

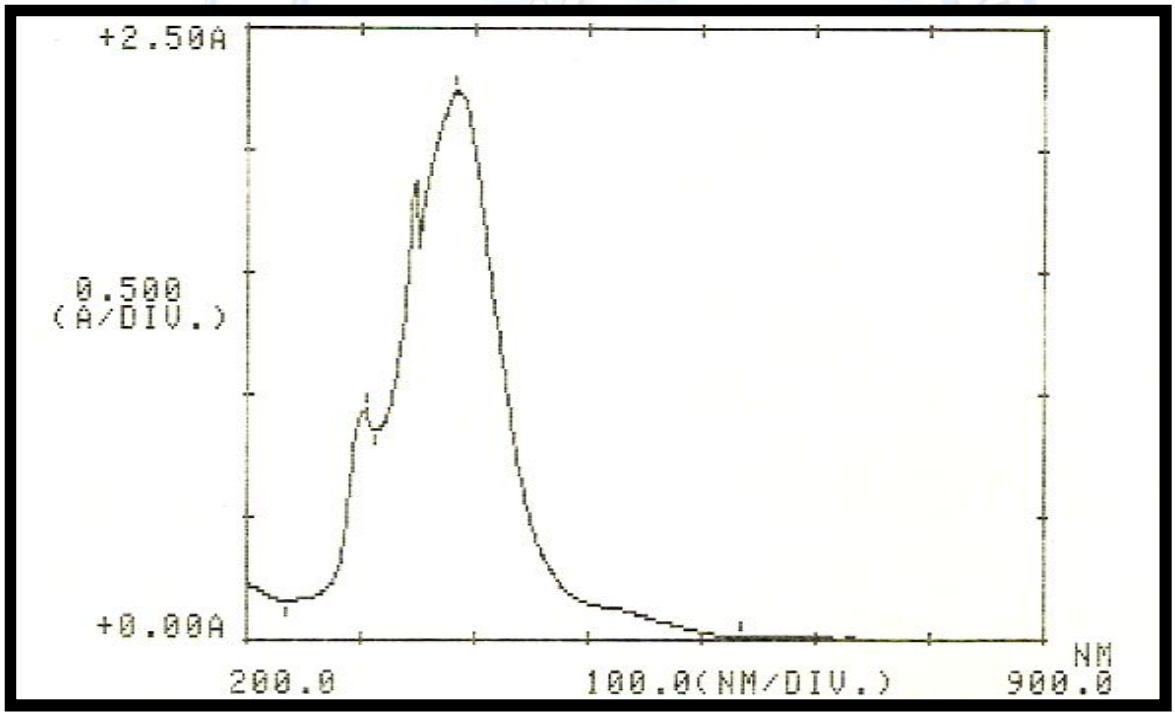

Figure.(8)The (UV-Vis) Spectra of 1-nitroso-2-naphthol

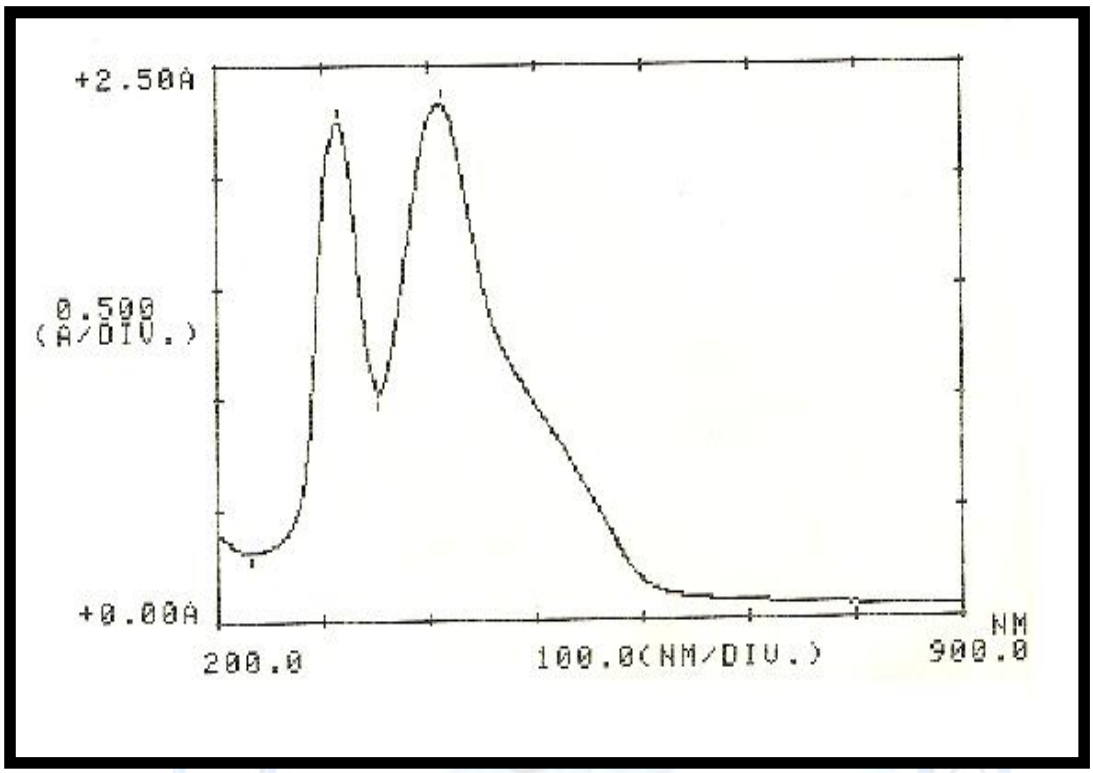

Figure.(9) The (UV-Vis) Spectra of Na[Co($C_{26}H_{24}N_3O_6$)]

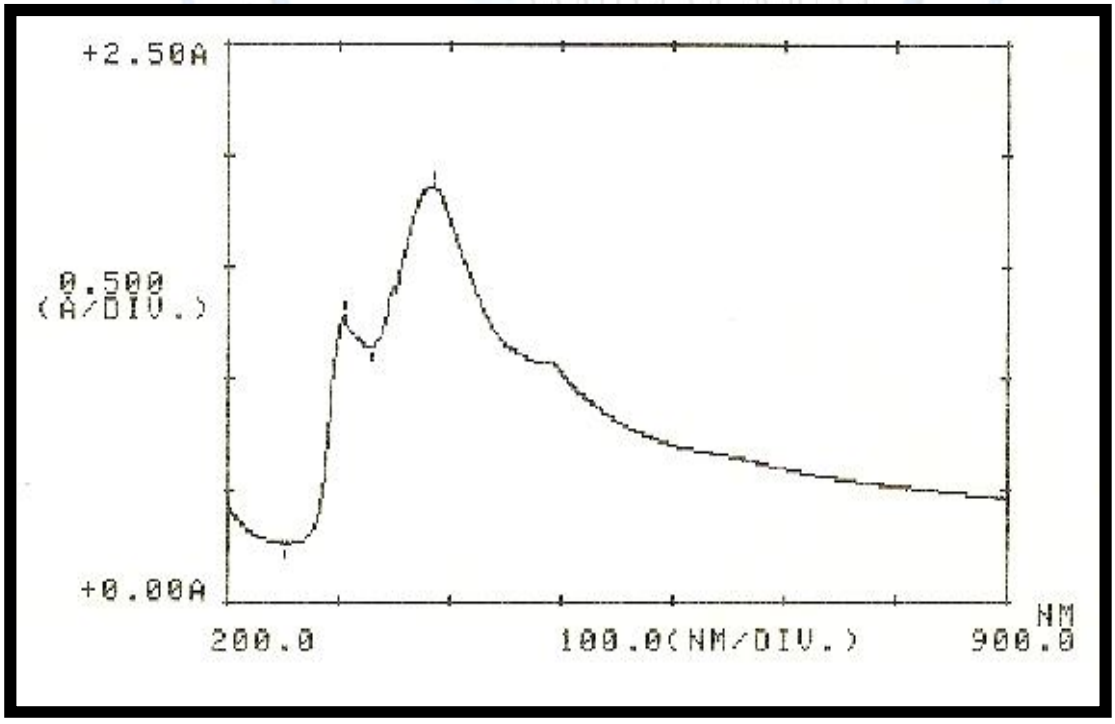

Figure.(10) The (UV-Vis) Spectra of Na[Cd ($C_{26}H_{24}N_3O_6$)]

REFERENCES

1- Bla`enka Foreti and Nicoletta Burger ,J Croatica Chemica Acta 75 (1) pp51-58 (2002)
2-M. Burawoy, M. Cais, J. T. Chamberlein, F. Liversedge, and A. R.Thompson, J Chem. Soc.pp 3727–.3733 (1955)
3- .K. K. Chatterjee, Anal. Chim. Acta 20 pp423–427 (1959) .
4-M.A. Taher, Anal. Sci. 16, pp501-506 (2000) .
5-M.A. Taher, Quimica Anal. (Spain). 19(3),pp 143-149 (2000).
6-F. Sundler, L. J. Larsson, and R. Hakanson, Histochemistry 50, pp39–46 (1976).
7-T.Huey Lu , P. hattopadhyay , F.L , Liao and J.Mau Lo , J.Analytical sciences , Vol. 17 pp 905-906 (2001) .
8-S.sharma , V.K.Srivastave , A.Kumar , Eur J.Med . chem , Aug ; 37(8) pp 689-697, (2005) .
9-P.Gurcan , N.Sari , N.J.Jnorg . chem., 38(12) pp 2807-2817 (1999) .
10-Y.yang , S.Zhang ., J.Spectro chim Acta. Mol Biomol spectrosc , 59(6) pp 1205-1209 (2003) .
11 -Tannistha Roy Barman and G n mukherjee, J. Chem. Sci., Vol. 118, No. 5, September, pp. 411–-418(2006).
12-W. J. Geary, Coord. Rev., 7, 81, (1971).
13-A .Ganesh. Thakur, V. Shrikant , Athlekarb, R.Sanjiv , Dharwadkr , Acta Poloniae Pharmaceutica ,Drug Research, 64 No. 1,. 9-15, (2007).
14-S. G. Mastrostamatis, M. S. Papadopoulos, I. C. Pirmettis, E. Paschali, A. D. Varvrigou, C. I. Sassinopoulou, C. P. Rapetopoulou, A. Teris and E. Chiotellis, J. Med. Chem., 37, 32112, (1994).
15-C. P. Prebhakaran and C. J. Patelc, J. Inorg. Nucl. Chem., 31, 3316, (1969).
16-K. Nakamoto*," Infrared Spectra of Inorganic and Coordination Compounds"* 4th Ed., J. Wiely nd Sons, New York, (1996).
17-M,Ketton, and A.B.P.Lever; Inorg. Chem; 10, No:1 (1971).
18. A.B.P. Lever.. "*Inorganic spectroscopy*" Elsverier publishing company London , New York. (1968).

Study of Molecular interactions in binary mixture of isobutanol with methyl acetate , ethyl acetate and normal propylacetate at different temperatures.

دراسة التداخلات الجزيئية لمزيج ثنائي من آيزوبيوتانول مع كل من خلات المثيل وخلات الاثيل وخلات البروبيل الاعتيادي في درجات حرارية مختلفة.

شيماء باسم خلف البغدادي

كلية التربية الرازي/ قسم الكيمياء /جامعة ديالى

Receiving Date: 2011/4/7 - **Accept Date:** 2011/5/10

Abstract

The properties associated with liquid mixtures; like density and viscosity,etc…..find several extensive applications , in chemical engineering ,design .

These properties are important from practical and theoretical point of view to understand liquid theory and provide informations about molecular interactions.

In this paper, we study the densities and viscosities for binary mixtures of isobutanol with methylacetae , ethylacetate, and n-propylacetate over the whole range of mixture composition at 298.15 , 303.15 and 308.15 K .Excess molar volumes v^E were calculated from precise density measurements at different temperatures. The viscosity deviation η^E where calculated from experimental viscosity values at different temperatures . The observed values of V^E,and η^E are discussed in term of molecular interactions in these binary mixture.The experimental results were fitted to the Redlich-Kister polynomial equation to evaluate the adjustable parameters and standard deviation for the ideal case .

Study of Molecular interactions in binary mixture of isobutanol with methyl acetate , ethyl acetate and normal propylacetate at different temperatures

شيماء باسم خلف

الخلاصة

ان الخصائص المرتبطة بالسوائل ومزيج السوائل مثل الكثافة و اللزوجة وغيرهما لها اهميتها ،حيث تجد هذه الخصائص المرتبطة تطبيقات في تصميم الهندسة الكيميائية.كما ان هذه الخواص مهمة من الناحية النظرية والعملية لفهم نظرية السؤال ودعم المعلومات بشأن التداخلات الجزيئية .و قد تم دراسة الكثافة و اللزوجة لمزيج من ايزوبيوتانول مع خلال المثيل وخلات الاثيل وخلات البروبيل الاعتيادي لمدى من الكسور المولية في درجات الحرارة (٢٩٨.١٥ ٣٠٣.١٥ و ٣٠٨.١٥) كلفن حيث تم حساب الحجم المولي الفائض V^E من قياسات الكثافة ولدرجات الحرارة المختلفة كما تم حساب اللزوجة الفائضة من قياسات اللزوجة ولدرجات الحرارة نفسها و كما تمت مناقشة النتائج وفق التداخلات بين الجزئيات وتكسر وتكوين الاواصر.تم تعيير القيم العملية لجميع الدوال الفائضة باستخدام معادلة Redlich – Kister متعددة الحدود وتم ايجاد الحدود المتعددة للمعادلة واستخدام النتائج لحساب الانحراف القياسي عن المثالية لهذه القيم.

Introduction:

The study of thermodynamic and transport properties of pure liquids and liquid mixtures are the subject of scientific research in many laboratories for many years. The thermodynamic excess functions such as molar volume, viscosity, molar enthalpy, molar Gibbs energy and refractive index are a source of information about interaction between molecules of the system components [1]

The systems alkanol + alkanoate are of great interest from a theoretical point of view because in mixing processes the breaking of H–bond structure of the alcohol occurs and the formation of new H–bonded molecular species between the alcohol and the ester takes place.[2.3]

The mixtures of isobutanol are used as a solvent for many purposes like printing inks, solubilizer in textile industry, extraction in the production of drugs antibiotics, hormones, vitamins extractor and as additives in polishes and cleaners [4].It is used in the production of many compounds. On the other hand, esters find applications as plasticizes in polymer–processing industries in order to impart favorable thermoplastic behavior.[5]

An understanding of the mixing behavior of isobutanol with esters is therefore important and has applications in many engineering areas and there was an earlier study on some of thermodynamic properties[6-9], we reported here the values of density, viscosity for the binary mixture of isobutanol with methylacetate , ethylacetate and n-propylacetate over the entire range of mixture composition at 298.15, 303.15, and 308.15K.

Experimental

Materials: High purity spectroscopic and analytical grade of methyl acetate and ethylacetate were produced from Aldrich chemical company. isobutanol and propylacetate were provided from E. Merck (Germany). All Samples were used without further purification because their purities exceeded 99% as tested by gas chromatography (HP 6890 series) using a flame ionization detector with a packed colum. Experimental values of ρ and η along with the

mol% purity of the liquids at 298.15 K are given in table (1). These results agreed well with the published data.

Mixtures were prepared in specially designed glass–stoppered bottles , and the measurements were performed on the same day. An electrical Sartorius balance (precision $1*10^{-5}$g) was used. The error in mole fraction is around ± 0.0002). (

Table-1-Densities, ρ, and Viscosities,η ,of pure components and those of literature at 298.15K

component	ρ/g.cm^{-3}		η/m.pa.s	
	exp	lit	exp	Lit
Isobutanol	0.7980	0.7998[10]	3.350	3.333[10]
Methylacetate	0.9284	0.9282[11]	0.384	0.385[11]
Ethylacetate	0.8946	0.8945[12]	0.424	0.426[12]
Propylacetate	0.8830	0.8830[12]	0.551	0.553[12]

Measurements:

All binary mixture of solvents were prepared by using determined volumes to obtain samples covering the whole range of mole fraction (o >x>1).

The mixtures were kept in tight stopper bottles to prevent any contamination with air. The mole fraction of each sample (mixture) of solvents was calculated from the following relation:

$$Xi=(Wi/Mi) \Big/ \sum_{s=i,j,k}^{m}(Ws/Ms) \text{ ----------(1)}$$

Where W_i and M_i are the weight in gram and the molecular weight of the component liquid. The possible error in the mole fraction is estimated be lower than 0.0001 respectively. Densities of pure liquids and their mixtures were measured by using a digital densimeter (Anton paar DMA 60/602). deionized and degassed water with a specific conductance of ($0.6*10^{-6}$ S.cm^{-1}) was used for calibration . For all mixtures and pure solvents, triplicate measurements were performed and the average is accurate to $\mp$ 0.0002 μg cm^{-3}.

Viscosities were measured by using a Cannon fenske viscometer (sige 75, ASTMD 445 supplied by Industrial Research Glassware Ltd ., Rosell, New Jersey). An electrical digital stopwatch with a readability of ± 0.01s was used for the flow time measurements. The measured viscosity values are accurate to $\mp$ 0.001µpa.s.

Results and Discusion

From the results of densities given in tables(2-4) excess molar volumes have been calculated from the following equation [13]

$V^E=V_m-V_1 X_1-V_2 X_2$ ---------- (2)

Where V_m is molar Volume of the mixture, V_1 and V_2 are the molar volumes of components 1 and 2 of the mixture, and X_i represents the mole fraction of the component in the mixture.

From the Values of η of the individual components as well as of the binary mixtures. The Δη have been calculated from [14]

$\Delta Y=Y_m-Y_1 C_1-Y_2 C_2$---------- (3)

For calculting η^E we have used the mole fractions X_i for C_i

Each set of excess functions have been fitted to the Redlich and Kister equation [15]

$$Y^E=X_1 X_2 \sum_{j=o}^{n} A_j(X_2-X_i)^j \text{ ----------(4)}$$

Where Y^E is the excess property, and n is the number of adjustable parameters Aj in each case for all mixtures, the optimum number of adjustable parameters is ascertained from an examination of the variation in standard errors, δ , as given by[16]

$$\delta=(Y^E)=\left[\frac{(Y^E_{obs}-Y^E_{cal})^2}{N-P}\right]^{1/2} \text{ ------(5)}$$

Where N represents the number of experimental points and P is the number of adjustable parameters. The values of these parameters, Aj , along with the standard errors, δ are listed in table (5). Excess molar volume of isobutanol with methylacetate and ethylacetate figures (1-2) , are positive over the whole range of mole fraction and become more positive as temperature increase. On the other hand excess molar volume of isobutanol with

propylacetate are negative figure (3) over the whole range of mole fraction and become more negative as temperature increase.

The observed excess molar volume values in the present investigation may be discussed in terms of several factors which may be divided into physical, chemical and geometrical contributions.The physical interactions involve mainly dispersion forces, giving a positive contribution to V^{E}[17].

In the case of methylacetate the V^{E} is positive due to the strong intera- molecular hydrogen bond between the methylacetate molecules, so for isobutanol , the interaction between them is very weak . In Ethylacetate the V^{E} is less positive, which mean that ethylacetate is slowly dissolve in isobutanol because the molecular interaction between the two compounds through the H – bond is stronger than the self – association of them. In n-propylacetate the V^{E} is negative which mean that interaction between propylacetate and isobutanol molecules is strong due to breaking of intra – H – bond and formation of inter –H – bond with isobutanol [18], the net of isobutanol molecules breaking through the interference of propylacetate molecules and because of it's large molecule will force isobutanol series to expand and give negative V^{E}. Values of V^{E} for all binary systems increase with increase of temperature .this is attributed to decreased ester – ester and alkanol – alkanol contacts with an increase in temperature.

Figures (4- 6) shows that the deviations in viscosity are negative in all the systems and become more negative with an increase in chain length of acetate.

Refrences:

1-Agnieszka Borun , Malgorgata Zurada , and Adam Bald , Journal of Thermal Analysis and Calorimetry , 163. 90-236(2009).

2-Pandharinath S. Nikam , Tukaram R . Mahale , and Mehdi Hasan , J. Chem. Eng . Data, 41, 1055-1058(1996).

3-Rvi M . Pires , Henriqve F. Costa , Abel O. M. Ferreira and Isabel M. A. Fonseca , J . chem. Eng. Data , 52. 1240- 1245, (2007).

4-Doolittle,A.K. "The technology of solvents and plasticizers", New York, John wiley and sons, (1954), pp.644-645.

5-Aminabhavi, T. M ; Aralagvppi, M. I ; shivapvtrappa, B,; Harogoppad, B.; Balvndgi, and R. H ., J. Chem., Eng Data, 38, 31 -39 (1993).

6-Jose M. Resa, Cristina Gon galag , Jose M. Goenaga, and M Iglesias, , J. Chem.. Eng . Data , 49, 804 -808(2004).

7-Kim, E. S . and Marsh, K.N. J . Chem. Eng .Data, 33, 288-292, (1988).

8-Canosa, J and Rodrgvey , A. Tojo, J, J . chem .Eng. Data, 43, 417-421(1998).

9-Ortega, J.; Pena, J. A. ; pa Z-Andrade and M.I, Aust. J . chem.. 39, 1685-1690 (1986).

10-Riddick, J.A; Bunger and W. B sakano. T. K . "organic solvents" , wiley New York (1986).

11-Aminabhavi , T, M, and Banerjee , K .J. Chem. Eng . Data , 39, 529 – 534(1994).

12-Correa , A ; Blanco , A ; Tojo , J ; correa , J . M .; and Arce, A. collect Czech. Chem.. Commun, 56, 2773- 2785(1991).

13-E. Jimeneneg, c. Franjo and M . I PagAndrade, J. Chem. . Eng. Data, 42, 262 (1997).

14-G. Ritzoulis , N. Padonlvs and D. Jannavdakes, J. Chem. Eng . Data, 31 , 14, (1986).

15-O . Redlich and A. T. Kister , Ind , Eng. Chem. , 140, 345 (1948).

16-F. kohler, Monatsh. Chem., 91, 738 (1960).

17-Josef Barthel, H. Krienke, Werner Kunz, " Physical chemistry of electrolyte solutions", springer, 1998, 401.

18-Dabir S.viswanath,Tushar K. Ghosh, "Viscosity of liquids", springer, 2006, 66.

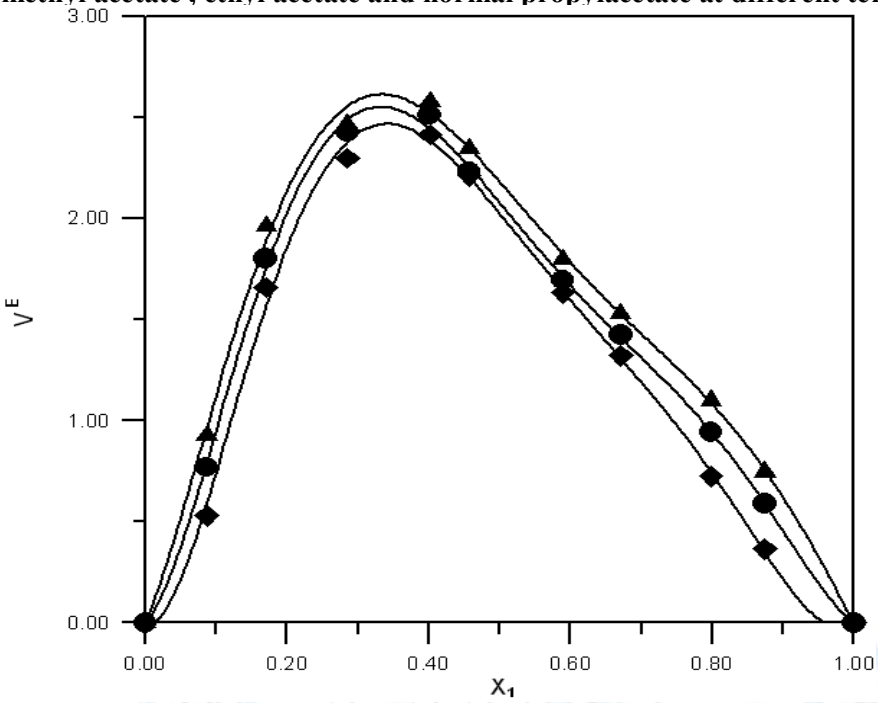

Figure -1-Excess molar volume,V^E,of (X_1 isobutanol + X_2 methylacetate) at different temperatures:♦,298.15; ● ,303.15,▲308.15 K.

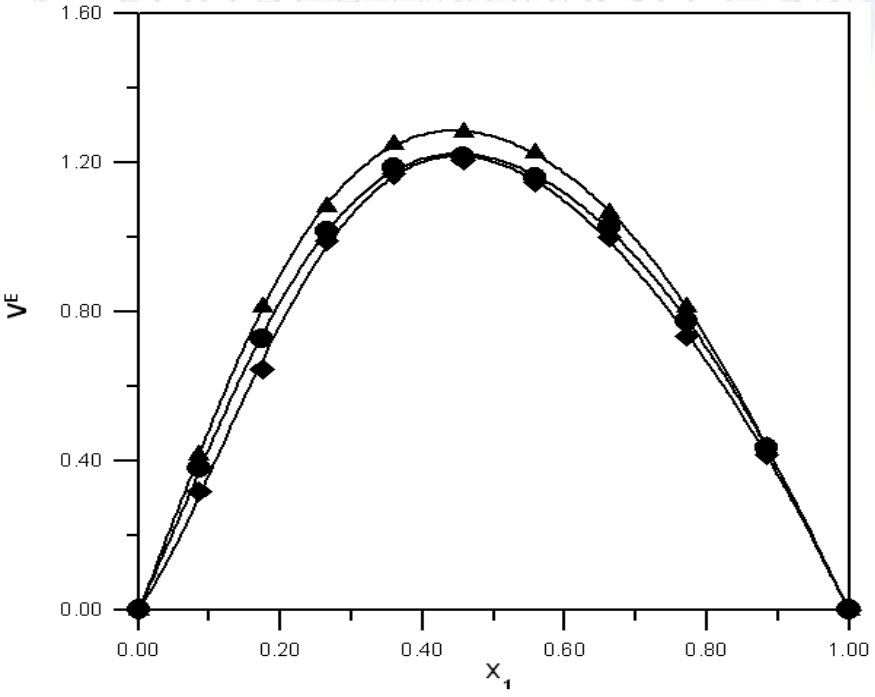

Figure -2-Excess molar volume,V^E,of (X_1 isobutanol + X_2 ethylacetate) at different temperatures:♦,298.15;● ,303.15,▲308.15 K

شيماء باسم خلف

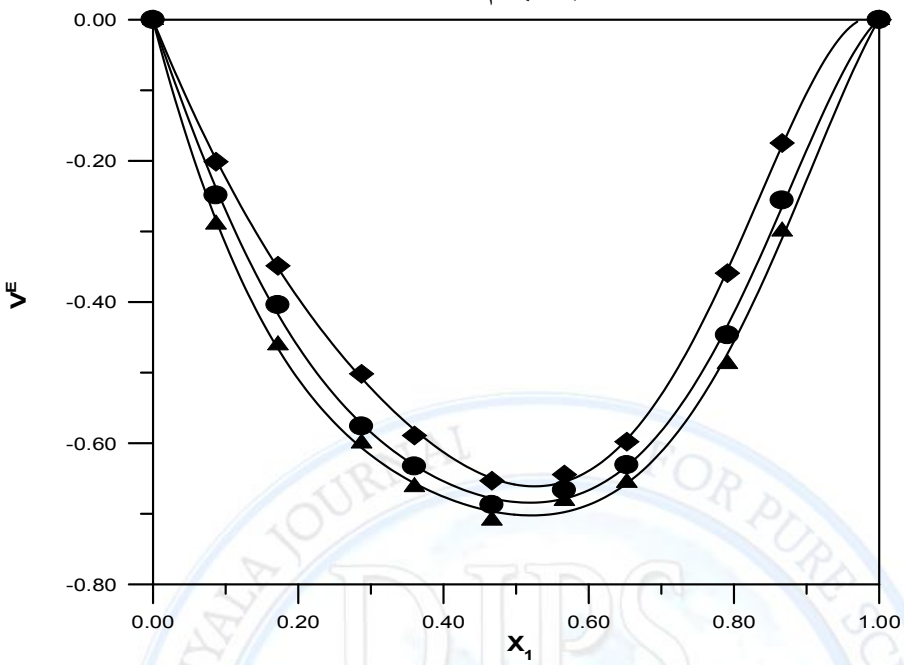

Figure -3-Excess molar volume,V^E,of (X_1 isobutanol + X_2 n- propylacetate) at different temperatures:♦,298.15; ●, 303.15, ▲308.15 K.

Study of Molecular interactions in binary mixture of isobutanol with methyl acetate , ethyl acetate and normal propylacetate at different temperatures

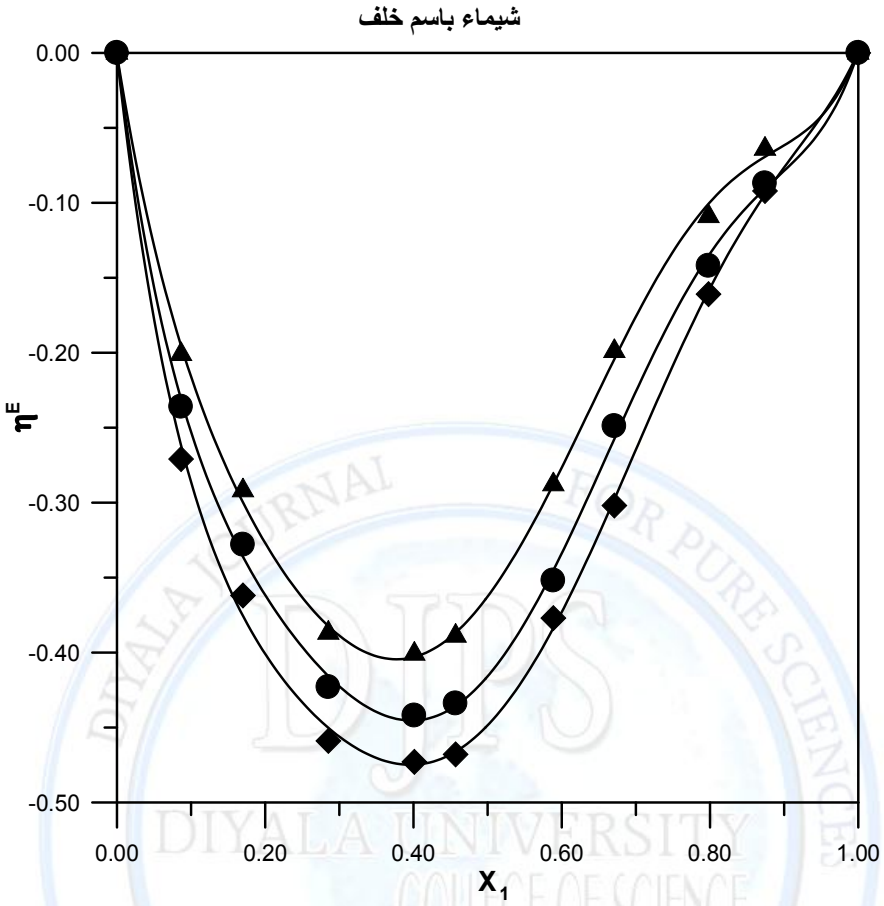

Figure -4-Excess viscosity,η^E,of (X_1 isobutanol + X_2 methylacetate) at different temperatures:♦,298.15; ●,303.15,▲308.15 K.

Study of Molecular interactions in binary mixture of isobutanol with methyl acetate , ethyl acetate and normal propylacetate at different temperatures

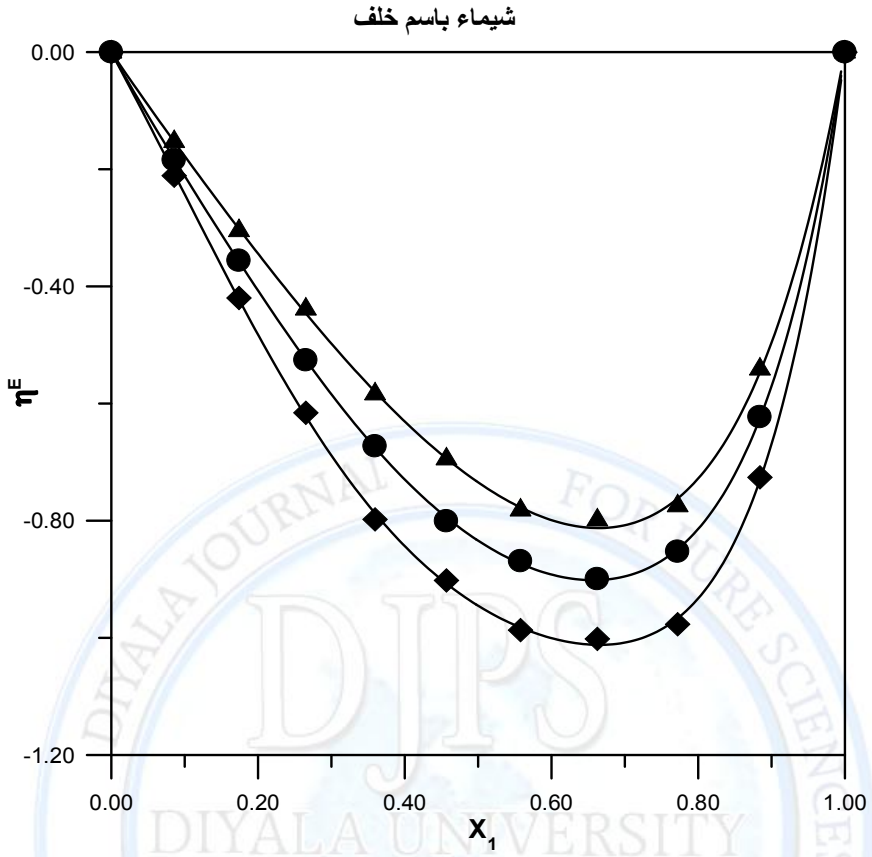

Figure -5-Excess viscosity,η^E,of (X_1 isobutanol + X_2 ethylacetate) at different temperatures:♦,298.15;●,303.15,▲308.15 K.

Study of Molecular interactions in binary mixture of isobutanol with methyl acetate , ethyl acetate and normal propylacetate at different temperatures

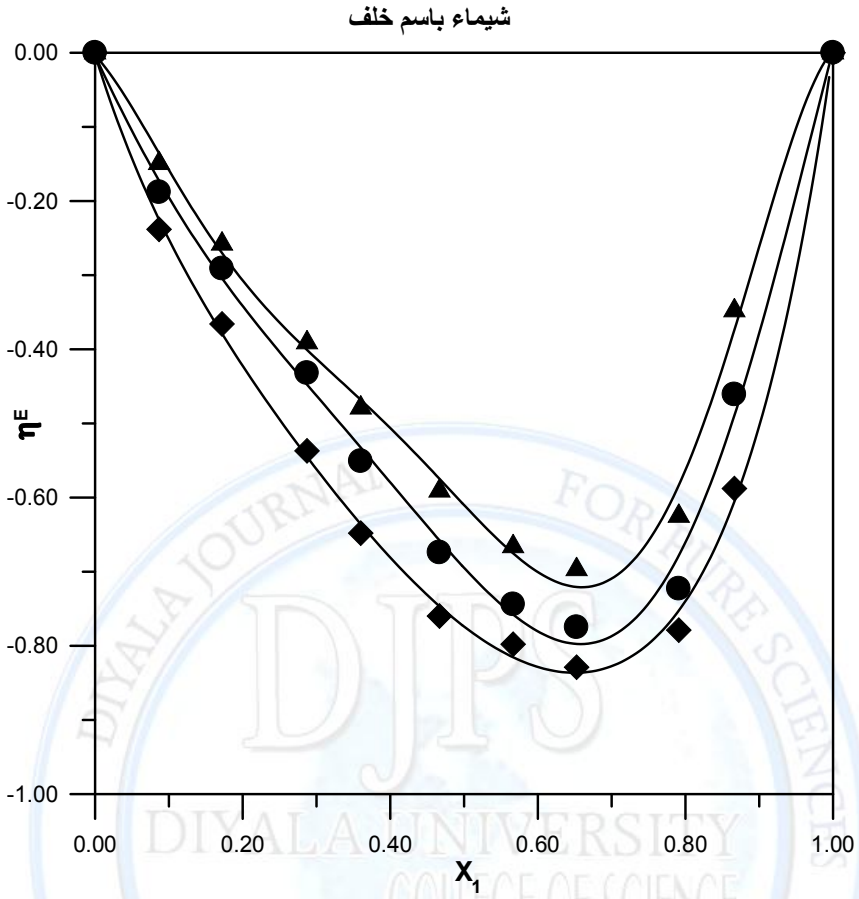

Figure -6-Excess viscosity,η^E,of (X_1 isobutanol + X_2 n- propylacetate) at different temperatures:♦,298.15; ●, 303.15, ▲308.15 K.

Table -2- Experimental values of density ρ,excess molar volumes V^E, viscosity η and excess viscosity η^E for Binary mixture of X_1 isobutanol +X_2 methyl acetate at different temperatures.

X1	ρ/g.cm^{-3}	V^E/cm^3.mol^{-1}	η \cp	η^E\cp
T=298.15 K				
0.0000	0.9284	0.0000	0.384	0.000
0.0865	0.9095	0.5297	0.485	-0.271
0.1699	0.8853	1.6594	0.620	-0.362
0.2851	0.8633	2.2985	0.900	-0.459
0.4011	0.8472	2.4120	1.130	-0.473
0.4568	0.8422	2.2095	1.527	-0.468
0.5888	0.8313	1.6319	1.783	-0.377
0.6711	0.8243	1.3212	2.202	-0.302
0.7981	0.8147	0.7236	2.685	-0.161
0.8743	0.8091	0.3648	3.001	-0.092
1.0000	0.7980	0	3.350	0.000
T=303.15 K				
0.00000	09218	0.0000	0.365	0.000
0.0865	0.9006	0.7677	0.459	-0.236
0.1699	0.8781	1.8013	0.568	-0.328
0.2851	0.8576	2.3259	0.807	-0.423
0.4011	0.8413	2.4972	1.005	-0.442
0.4568	0.8371	2.2199	1.360	-0.434
0.5888	0.8261	1.6942	1.589	-0.352

0.6711	0.8189	1.4222	1.997	-0.249
0.7981	0.8085	0.9431	2.407	-0.142
0.8743	0.8030	0.5899	2.682	-0.087
1.0000	0.7941	0	2.997	0

T=308.15 K

0.0000	09152	0.0000	0.349	0.000
0.0865	0.8927	0.9257	0.418	-0.201
0.1699	0.8706	1.9632	0.491	-0.292
0.2851	0.8508	2.4663	0.669	-0.387
0.4011	0.8355	2.5791	0.832	-0.401
0.4568	0.8310	2.3472	1.127	-0.389
0.5888	0.8205	1.7991	1.348	-0.288
0.6711	0.8134	1.5284	1.687	-0.199
0.7981	0.8029	1.1004	2.024	-0.109
0.8743	0.7975	0.7472	2.249	-0.064
1.0000	0.7902	0	2.499	0

Table -3- Experimental values of density ρ,excess molar volumes V^E, viscosity η and excess viscosity η^E for Binary mixture of X_1 isobutanol +X_2 ethylacetate at different temperatures.

X1	ρ/g.cm^{-3}	V^E/cm^3.mol^{-1}	η \cp	η^E\cp
T=298.15 K				
0.0000	0.8946	0.0000	0.424	0.000
0.0856	0.8839	0.3174	0.551	-0.211
0.1739	0.8728	0.6433	0.671	-0.420
0.2651	0.8730	0.9881	0.795	-0.616
0.3594	0.8508	1.1674	0.919	-0.798
0.4568	0.8413	1.2056	1.111	-0.902
0.5579	0.8321	1.1467	1.311	-0.987
0.6626	0.8232	0.9981	1.572	-1.002
0.7720	0.8146	0.7324	1.864	-0.977
0.8843	0.8061	0.4144	2.373	-0.726
1.0000	0.7980	0	3.350	0
T=303.15 K				
0.00000	0.8884	0.0000	0.400	0.000
0.0856	0.8774	0.3783	0.516	-0.184
0.1739	0.8664	0.7258	0.636	-0.356
0.2651	0.8556	1.0153	0.750	-0.526
0.3594	0.8455	1.1841	0.875	-0.673
0.4568	0.8362	1.2162	1.009	-0.801
0.5579	0.8272	1.1601	1.194	-0.869

0.6626	0.8184	1.0256	1.409	-0.899
0.7720	0.8100	1.7741	1.692	-0.853
0.8843	0.8019	0.4348	2.151	-0.623
1.0000	0.7941	0	2.997	0

T=308.15 K

0.00000	0.8825	0.0000	0.385	0.000
0.0856	0.8714	0.4146	0.476	-0.153
0.1739	0.8602	0.8106	0.561	-0.305
0.2651	0.8498	1.0792	0.659	-0.439
0.3594	0.8399	1.2489	0.735	-0.584
0.4568	0.8308	1.2808	0.838	-0.695
0.5579	0.8220	1.2240	0.957	-0.782
0.6626	0.8136	1.0650	1.139	-0.799
0.7720	0.8054	0.8124	1.356	-0.775
0.8843	0.7978	0.4361	1.777	-0.541
1.0000	0.7902	0	2.499	0

Table -4- Experimental values of density ρ ,excess molar volumes V^E, viscosity η and excess viscosity η^E for Binary mixture of X_1 isobutanol +X_2 n-propylacetate at different temperatures.

X1	ρ/g.cm^{-3}	V^E/cm^3.mol^{-1}	η \cp	η^E\cp
T=298.15 K				
0.0000	0.8830	0.0000	0.551	0.000
0.0866	0.8785	-0.2013	0.686	-0.238
0.1719	0.8735	-0.3487	0.844	-0.291
0.2870	0.8662	-0.5018	0.986	-0.537
0.3599	0.8612	-0.5891	1.113	-0.648
0.4668	0.8532	-0.6533	1.283	-0.760
0.5676	0.8446	-0.6445	1.544	-0.798
0.6526	0.8368	-0.5980	1.771	-0.775
0.7911	0.8220	-0.3591	2.089	-0.779
0.8664	0.8131	-0.1746	2.519	-0.588
1.0000	0.7980	0	3.350	0
T=303.15 K				
0.00000	0.8779	0.0000	0.512	0.000
0.0866	0.8734	-0.2488	0.655	-0.188
0.1719	0.8686	-0.4040	0.773	-0.258
0.2870	0.8615	-0.5761	0.943	-0.432
0.3599	0.8565	-0.6327	1.035	-0.551
0.4668	0.8485	-0.6872	1.163	-0.674

0.5676	0.8401	-0.6663	1.358	-0.744
0.6526	0.8327	-0.6559	1.586	-0.697
0.7911	0.8184	-0.4469	1.846	-0.723
0.8664	0.8096	-0.2559	2.320	-0.461
1.0000	0.7941	0	2.997	0

T=308.15 K

0.0000	0.8718	0.0000	0.483	0.000
0.0866	0.8682	-0.2901	0.603	-0.149
0.1719	0.8628	-0.3450	0.646	-0.258
0.2870	0.8565	-0.6002	0.792	-0.391
0.3599	0.8516	-0.6621	0.875	-0.479
0.4668	0.8438	-0.7096	0.966	-0.591
0.5676	0.8354	-0.6817	1.107	-0.666
0.6526	0.8317	-1.1010	1.223	-0.697
0.7911	0.8144	-0.4877	1.527	-0.625
0.8664	0.8058	-0.2999	1.976	-0.348
1.0000	0.7902	0	2.499	0

Table (5) - Redlich-Kister coefficients A_i and standard deviations, σ ,for the excess molar quantities of solution of (x_1 isobutanol+ x_2 acetates mixtures) at different temperatures.

System	property	T/K	a_0	a_1	a_2	a_3	σ
Isobutanol+methylacetate	$V^E/cm^3.mol^{-1}$	298.15	-0.491	0.050	-0.149	0.491	0.003
		303.15	-0.528	0.027	-1.171	0.660	0.004
		308.15	-0.580	-0.109	-0.092	1.175	0.011
	Δη/mPa.s	298.15	-0.176	0.160	-0.131	0.034	0.001
		303.15	-0.191	0.120	-0.122	0.217	0.001
		308.15	-0.204	0.068	-0.107	0.453	0.003
Isobutanol+ethylacetate	$V^E/cm^3.mol^{-1}$	298.15	1.169	0.412	-0.228	-0.367	0.005
		303.15	1.295	0.496	-0.153	-0.544	0.004
		308.15	1.405	0.594	0.006	-0.683	0.005
	Δη/mPa.s	298.15	-0.967	0.459	-0.209	0.349	0.005
		303.15	-0.882	0.537	-0.249	0.085	0.005
		308.15	-0.882	0.537	-0.249	0.085	0.003
Isobutanol+propylacetate	$V^E/cm^3.mol^{-1}$	298.15	0.757	-0.460	-0.148	0.320	0.004
		303.15	0.962	-0.488	-0.125	0.209	0.005

		308.15	1.107	-0.420	0.184	0.237	0.004
	Δη/mPa.s	298.15	-2.279	1.625	-1.015	0.316	0.002
		303.15	-1.981	1.443	-0.789	0.105	0.008
		308.15	-1.711	1.276	-0.686	-0.094	0.010

Volumetric and Viscometric behavior studies for ternary system of cycloheptane with three isomeric dimethyl benzene at different temperatures.

Ahmed Najem Abd

College of Veterinary Medicine - University of Diyala

Receiving Date: 2011/11/21 - **Accept Date:** 2012/2/7

Abstract:

This study concerned with measurement the densities ρ and viscosities η. Over the range of temperatures (293.15, 303.15, 313.15, and 323.15 k) for ternary mixtures cycloheptane + m-xylene + o-xylene and cycloheptane + m-xylene + p-xylene. From experimental data of densities and viscosities, the excess molar volumes, V^E, and excess viscosities, η^E , were calculated for ternary mixtures. The Flory theory has been extended for the theoretical prediction of excess molar volume of ternary mixtures studied here depending on the pure component liquid parameters. In this study Heric-Coursey equation was used to calculate the excess viscosities for ternary mixtures studied here.

Key words: Ternary system, Cyclohptane , dimethyl benzene isomer, Volumetric and Viscometric of Ternary system.

Introduction:

Dimethyl benzene or xylene is one of the top 30 chemicals produced in the United states in terms of volume. It is used as a solvent in the printing, rubber, and leather industries. Along with other solvents, xylene is also used as a cleaning agent, a thinner for paint, and in varnishes[1]. It is found in small amounts in airplane fuel and gasoline. xylene is used as a material in chemical, plastics, and synthetic fiber industries and as an ingredient in the coating of fabrics and papers. Isomers of xylene are used in the manufacture of certain polymers, such as plastics[2].

Many industrial processes use mixtures of solvents and knowledge of chemical and physical properties of pure liquids and their mixtures is critical to the efficient utilization-preparation development and economic design of appropriate equipment for these processes are only possible if the chemical and physical properties of the solvent or substances to be processed are known. For this reason, many attemps have been made to correlate these data using semi-empirical or theoretical approaches considerable programs have also been made in the development of statistical theories. The calculation of physical properties using statistical theories is still not yet possible for complicated molecules such as xylene and long chain molecules, because of the range of different conformations, which can occur and the effect of these various structures on the intermoleculer interactions[3]. Recently, few equations for estimating the excess thermodynamic and other physicochemical properties of multicomponent systems from the observed properties of their various contributory of the components has been developed and applied to various multicomponent liquid systems[4,5] computer-stimulated calculations and neutron-scattering experiments[6] have been insight into the relations between molecular structure and macroscopic behavior considerable progress has also been made in the development statistical theories over recent years[7].

Experimental:

(a) Materials: All the chemicals used were supplied by BDH and Fluka. Company.

The purities of all substances were better than 99 mass% as found by GLC analysis.

The purity of the chemicals was checked by comparing the densities and viscosities of the components with those reported in the literature[12].

(b) Measurements:

(1) Densities measurement:- Densities were measured at 293.15, 303.15, 313.15, and 323.15 k with an Antopaar digital densimeter (Model DMA 60/601) Densities were measured with a precision of 2×10^{-5} g.cm^{-3}. The maximum uncertainty in the excess molar volumes is expected to be less than 3×10^{-3} cm^3.mol^{-1}.

(2) Viscosities Measurements:- In the present work, the viscosity (η) of the solution was measured using (cannon-ubbelohde semi micro) viscometer. The temperature of the

solution was brought to the desired value by immersing the test viscometer in a controlled temperature water bath with a precision of ± 0.01k

Results:

Experimental results of the densities ρ_m of the ternary mixtures cycloheptane + m-xylene + o-xylene and cycloheptane + m-xylene + p-xylene at (293.15, 303.15, 313.15, and 323.15k) are listed in Table (1).

The excess molar volumes for ternary mixtures studied here were calculated from the measured, densities using the following equation:-

$$V_{123}^{E}(cm^3.mol^{-1}) = \left[\frac{X_1M_1 + X_2M_2 + X_3M_3}{\rho_m}\right] - \left[X_1\frac{M_1}{\rho_1} + X_2\frac{M_2}{\rho_2} + X_3\frac{M_3}{\rho_3}\right] \quad \text{.....(1)}$$

Where $X_{(1,2,3)}$, $M_{(1,2,3)}$ and $\rho_{(1,2,3)}$ are respectively the mole fraction, molar mass and density of the pure component liquid (1,2,3), $\rho_{(m)}$ is the density mixture. The obtained results of V_{123}^{E} are listed in table (3) and a plotted as a function of the mole fraction X_1, X_2 , and X_3 for the three components at four temperatures in figures (1 and 2).

The statistical mechanical concept of Flory theory[13] has been extended for the theoretical prediction of excess molar volume of the ternary mixture from the properties of pure component. The excess molar volumes (V^E) calculated directly from characteristic and reduced volumes and the segment fraction using thermal expansion coefficient (α) of the pure three component, and using the equation.

$$V^{E} = (X_1V_1^* + X_2V_2^* + X_3V_3^*)[\tilde{V} - (\phi_1\tilde{V}_1 + \phi_2\tilde{V}_2 + \phi_3\tilde{V}_3)] \quad \text{.....(2)}$$

Where ϕ_1, ϕ_2 and ϕ_3 are the segment fractions of components 1, 2, and 3 defined by the relations:-

$$\phi_1 = [1 - \phi_2 - \phi_3] \quad \text{.....(3)}$$

$$\phi_2 = \frac{X_2}{X_2 + X_3\left(\frac{V_3^*}{V_2^*}\right) + X_1\left(\frac{V_1^*}{V_2^*}\right)} \quad \text{.....(4)}$$

$$\phi_3 = \frac{X_3}{X_3 + X_2\left(\frac{V_2^*}{V_3^*}\right) + X_1\left(\frac{V_1^*}{V_3^*}\right)} \quad \text{.....(5)}$$

$\tilde{V}$ in equation (6) is the reduced volume of ternary mixture which is obtained by the following equation:-

$$\tilde{V}=V/X_1V_1^* + X_2V_2^* + X_3V_3^* \quad .....(6)$$

Where V is the molar volume of the mixture, given by:-

$$V = (X_1M_1 + X_2M_2 + X_3M_3)/\rho_m \quad .....(7)$$

Where ρ_m is the density of the mixture.

By using the equation of state parameters of pure liquids, table (2) and applied equation (2-7), we calculated the excess molar volumes for the ternary mixtures studied here. Table (3) present the theoretical prediction of V^E values at 293.15k with experimental values for comparison for ternary mixtures studied here. The maximum percent average deviation is less than 0.95% which means that Flory theory for predicting the excess molar volumes of ternary mixtures studied here is quite reasonable, evident from this excellent agreement in both sign and magnitude.

The absolute viscosity (η_m) was calculated for ternary mixtures in this study by measuring the flow time (τ) and using the densities values shown in table (1) at the range of degrees of temperature (293.15, 303.15, 313.15 and 323.15 k) and by using equation (8).

$$\eta = c.\tau.\rho_m \quad .....(8)$$

Where (c) the viscosity constant

Table (4) presents the experimental values of absolute viscosities for ternary mixtures studied here at the range of degrees of temperature.

Excess viscosities, $\eta^{E}_{1,2,3}$ for ternary mixtures at the range of degrees of temperature were calculated from measurements of the viscosity of the mixture and the pure liquid by the following equation:

$$\eta^{E}_{1,2,3} = \eta_{mix.} - X_1\eta_1 - X_2\eta_2 - X_3\eta_3 \quad \text{.....(9)}$$

Where X_1, X_2, X_3 , η_1. η_2 , and η_3 are the mole fractions and the viscosities of components 1,2, and 3 respectively, η_{mix} is the viscosity of the mixture.

The obtained result of $\eta^{E}_{1,2,3}$ are listed in table (5) and plotted as a function of the mole fractions X_1, X_2, and X_3 for the three components at four temperatures in figures (3 and 4).

Several empirical equations have been proposed to calculate excess viscosity of multi component systems based on the available experimental results of viscosities of mixture and pure components, the equation of Heric and coursey [14] was used:

$$\eta^{E} = \ln \eta_{mix} - \sum_{xi} xi \ln \eta_i \quad \text{.....(10)}$$

Where η_{mix} is the viscosity of the mixture, X_i and η_i are mole fraction and viscosity for pure component respectively. Table (5) shows the experimental result of $\eta^{E}_{1,2,3}$ and the predicted values of excess viscosity from equation [10] for comparison for ternary mixtures studied here at (293.15, 303.15, 313.15 and 323.15k).

Discussion:

The experimental excess molar volume $V^{E}_{1,2,3}$ for the ternary mixtures studied here at 393.15, 303.15, 313.15 and 323.14k are positive deviation from ideality over the whole mole fraction, table (3) and figures (1 and 2). Such volumetric behavior may be explained by the globular molecules of cycloheptane disturb the orientational order in isomers of xylene. It means that cycloheptane molecules are interstitial accommodate between isomers of xylene molecules and result less packed structure which is responsible about the positive $V^{E}_{1,2,3}$ for ternary mixtures studied here.

The Flory theory [13] has been extended for the theoretical prediction of excess molar volume of ternary mixtures studied here depending on the pure component liquid parameters, the obtained excess molar volumes $V^{E}_{1,2,3}$ by extended Flory theory for the ternary mixtures studied here at 293.15k are presented in table (3) with the experimental data for comparison. The theory predicted the volumetric behavior and magnitudes of $V^{E}_{1,2,3}$ well.

The researcher conclude that Flory theory could be extended to multi component liquid mixtures based on the pure component liquid parameters[15].

Experimental data of mixture viscosity η_m and excess viscosity $\eta^E_{1,2,3}$ are listed in tables (4 and 5) and a plotted as a function of the mole fractions X_1, X_2, and X_3 for the three components at four temperature in figures (3 and 4) for the ternary mixture studied here. The viscometric behavior for the ternary mixture studied here show a similar volumetric behavior. Heric and Coursey equation was used to calculated excess viscosity of ternary mixtures studied here from experimental results of viscosities of mixtures and pure components. Table (5) shows good agreement between the experimental values of the excess viscosities for the ternary mixtures studied in this work with the predicted values from Heric and Coursey equation.

References:

1. Krishnan K.M., Rambabu K, Raman G.K.V., J. Chem. Eng. Data no, 128 (1995).
2. AL-Azzawi S.F., Awwad A.M., Aurab Bulf J. Scient. Res. Math physc Sci. A6 (3) 351 (1988).
3. Awwad A.M., AL-Dujaili A.H. and Kareem E.T. "Volume of mixing of hydrocarbons mixtures: Coparison with theory" VDM publishing House Ltd. Meldrum Court 17.(2011).
4. Salman H. E., J. Kerbala University, 5, 114 (2007).
5. Awwad A.M. and Farhane A.M., J. Chem. Thermodynamics 41, 205(2009).
6. Sarhan S.T., M.Sc. Thesis, Baghdad University (2007).
7. Salman H.E. National J. of Chemistry 35, 467, (2009).
8. Dhillon M.S.,Chaugh H.S.,J.Chem.Eng.Data 22,262, (1977).
9. Dhillon M.S.,Chaugh H.S.,J.Chem.Eng.Data 23,263, (1977).
10. Murrieta-Guevara F.,Rodriguez , A. T. , J.Chem. Eng. Data , 29 , 204 , (1984).
11. Jannelli L. Pansini M., Jalenti, R. , J. Chem. Eng. Data, 29 , 263, (1984).
12. Habibullah M.,Kamalendra N., Ismail M. , Rhman H.,Ashraf M., and Kaled S., J. Chem. Eng. Data , 55 ,11, (2010).
13. Gupta A.K., Xaday C.K.J. Chem. 9, 112(1997).
14. Shukla R.K., Shukla A.K. and pandey J.D.J. phys. Chem. 93, 4627 (1989).
15. Heiric E.L. and Coursey B.M., J. Chem. Eng. Data, 17, (41-44), (1974).

دراسة السلوك الحجمي واللزوجي للنظام الثلاثي المكون من السايكلوهبتان مع الايزومرات الثلاثة للداي مثيل بنزين عند درجات حرارية مختلفة

أحمد نجم عبد
كلية الطب البيطري – جامعة ديالى

الخلاصة:

تتضمن هذه الدراسة قياس الكثافة واللزوجة على مدى اربع درجات حرارية للمخاليط الثلاثية المكون والتي تتضمن :
cycloheptane + m-xylene + o-xylene and cycloheptane + m-xylene + p-xylene.
ومن النتائج العملية لقياس الكثافة واللزوجة تم حساب الحجوم المولارية الفائضة V^E ، واللزوجة الفائضة η^E للمخاليط الثلاثية قيد الدراسة.
تم تطبيق نظرية فلوري لحساب الحجوم المولارية الفائضة للمخاليط الثلاثية المكون. هذه الدراسة استخدمت معادلة (Heric-Coursey) لحساب اللزوجة للمخاليط الثلاثية المكون.

Table (1) Experimental values of the densities (ρ) for ternary mixtures at four temperatures.

X1 cycloheptane + x2 m-xylene + x3 o-xylene					
X1	X2	ρ ($g.cm^{-3}$) 293.15k	ρ ($g.cm^{-3}$) 303.15k	ρ ($g.cm^{-3}$) 313.15k	ρ ($g.cm^{-3}$) 323.15k
0.2848	0.3715	0.7898	0.7687	0.7501	0.7412
0.2860	0.3534	0.7576	0.734	0.7239	0.7125
0.2909	0.3395	0.7155	0.7025	0.7004	0.6988
0.2923	0.3214	0.6913	0.6832	0.67	0.6667
0.3097	0.3080	0.6609	0.6415	0.6346	0.6223
0.3271	0.2928	0.6412	0.6227	0.6052	0.5974
0.3460	0.2718	0.6334	0.5944	0.5838	0.5781

0.3679	0.2440	0.6147	0.5863	0.5742	0.5509
0.3846	0.2225	0.585	0.5574	0.5459	0.5345
0.3960	0.2155	0.5539	0.5385	0.511	0.5037
0.4286	0.2088	0.5422	0.5293	0.5003	0.4889
0.4302	0.1942	0.5319	0.5011	0.4871	0.479

X1 cycloheptane + x2 m-xylene + x3 p-xylene .I					
X1	X2	ρ ($g.cm^{-3}$) 293.15k	ρ ($g.cm^{-3}$) 303.15k	ρ ($g.cm^{-3}$) 313.15k	ρ ($g.cm^{-3}$) 323.15k
0.2739	0.3585	0.77321	0.74984	0.72089	0.71977
0.2741	0.3209	0.74564	0.72531	0.70785	0.6951
0.2869	0.3035	0.71083	0.69158	0.68665	0.67083
0.2890	0.2700	0.68547	0.67484	0.66807	0.65312
0.2970	0.2412	0.65331	0.63097	0.62515	0.61774
0.3091	0.2278	0.63402	0.60553	0.5819	0.57002
0.3265	0.2100	0.59984	0.58568	0.56571	0.55519
0.3498	0.1624	0.57039	0.56001	0.53432	0.52132
0.3769	0.1363	0.56445	0.54131	0.51009	0.49748
0.4000	0.1200	0.54387	0.5222	0.49781	0.46312
0.4244	0.0885	0.52334	0.49921	0.47321	0.45078
0.4789	0.0563	0.50792	0.4751	0.45112	0.43662

Table (2) Parameters for the pure liquids according to the Flory Theory at 298.15k.[8-11]

Liquid	$V/cm^3.mol^{-1}$	$V^*/cm^3.mol^{-1}$	$\tilde{V}$	T^*/K	$\tilde{T}$	$P^*/J.cm^{-3}$ *	$\alpha \times 10^{-3}/k^{-1}$ *	S/A^{o-1*}
cycloheptane	119.4511	95.2462	1.2542	4942.07	0.1658	٥٤٨	1.109	0.89
o- xylene	123.4552	76.311	1.6178	3312.10	0.1111	٣٧٠	0.588	0.79
m-xylene	123.7427	99.207	1.2473	5276.02	0.1770	٣٨٨	0.998	0.82
p-xylene	124.1725	111.839	1.1103	9822.03	0.3294	٣٦٧	٠.392	0.78

Table (3) Experimental and theoretical prediction values of the (V^E_{123}) for ternary mixtures at four temperatures.

X1 cycloheptane + x2 m-xylene + x3 o-xylene						
X1	**X2**	$V^E_{123}\,exp.$ **($cm^3.mol^{-1}$) 293.15k**	$V^E_{123}pred.$ **($cm^3.mol^{-1}$) 293.15k**	V^E_{123} **($cm^3.mol^{-1}$) 303.15k**	V^E_{123} **($cm^3.mol^{-1}$) 313.15k**	V^E_{123} **($cm^3.mol^{-1}$) 323.15k**
0.2848	0.3715	0.1826	0.1832	0.2149	0.2112	0.1800
0.2860	0.3534	0.2943	0.3117	0.3428	0.3124	0.2931
0.2909	0.3395	0.4551	0.4367	0.4691	0.4087	0.3497
0.2923	0.3214	0.5566	0.5719	0.5527	0.5441	0.4928
0.3097	0.3080	0.6920	0.6628	0.7471	0.7141	0.7122
0.3271	0.2928	0.7856	0.7638	0.8415	0.8700	0.8480
0.3460	0.2718	0.8223	0.8554	0.9961	0.9923	0.6904
0.3679	0.2440	0.9178	0.9640	1.0399	1.0481	1.1328

0.3846	0.2225	1.0853	1.1147	1.2189	1.2316	1.2445
0.3960	0.2155	1.2808	1.1825	1.3461	1.4870	1.4777
0.4286	0.2088	1.3541	1.3359	1.4046	1.5644	1.5936
0.4302	0.1942	1.4273	1.4713	1.6229	1.6762	1.6803

X1 cycloheptane + x2 m-xylene + x3 p-xylene .II						
X1	X2	V^{E}_{123} exp. (cm^3.mol^{-1}) 293.15k	V^{E}_{123} *pred.* (cm^3.mol^{-1}) 293.15k	V^{E}_{123} (cm^3.mol^{-1}) 303.15k	V^{E}_{123} (cm^3.mol^{-1}) 313.15k	V^{E}_{123} (cm^3.mol^{-1}) 323.15k
0.2739	0.3585	0.2374	0.2380	0.2822	0.3222	0.3272
0.2741	0.3209	0.3374	0.3269	0.3769	0.3782	0.3432
0.2869	0.3035	0.4723	0.4864	0.5149	0.4677	0.4510
0.2890	0.2700	0.5806	0.5908	0.5898	0.5540	0.5378
0.2970	0.2412	0.7289	0.7321	0.8030	0.7679	0.7212
0.3091	0.2278	0.8237	0.8327	0.9390	1.0129	1.0013
0.3265	0.2100	1.0071	0.9557	1.0517	1.1120	1.0965
0.3498	0.1624	1.1814	1.1703	1.2096	1.3247	1.3381
0.3769	0.1363	1.2145	1.2828	1.3312	1.5030	1.5240
0.4000	0.1200	1.3481	1.3419	1.4653	1.5975	1.8271
0.4244	0.0885	1.4916	1.4564	1.6412	1.8076	1.9450
0.4789	0.0563	1.5986	1.6078	1.8355	2.0056	2.0803

Table(4) Experimental values of the absolute viscosity (η) for ternary mixtures at four temperatures.

X1 cycloheptane + x2 m-xylene + x3 o-xylene					
X1	X2	η (293.15k)	η(303.15k)	η(313.15k)	η (323.15k)
0.2848	0.3715	1.9531	1.8743	1.6911	1.5423
0.2860	0.3534	1.9295	1.8535	1.6674	1.5209
0.2909	0.3395	1.8982	1.8323	1.6587	1.5018
0.2923	0.3214	1.8843	1.8099	1.6367	1.4929
0.3097	0.3080	1.8522	1.7891	1.621	1.4741
0.3271	0.2928	1.8313	1.7603	1.6048	1.4557
0.3460	0.2718	1.8051	1.7594	1.5889	1.4369
0.3679	0.2440	1.7836	1.7345	1.5753	1.4178
0.3846	0.2225	1.7678	1.7254	1.5559	1.4083
0.3960	0.2155	1.7463	1.7042	1.5483	1.3992
0.4286	0.2088	1.7259	1.6873	1.5348	1.37
0.4302	0.1942	1.7047	1.6775	1.5055	1.3534

X1 cycloheptane + x2 m-xylene + x3 p-xylene					
X1	X2	η (293.15k)	η (303.15k)	η(313.15k)	η (323.15k)
0.2739	0.3585	1.8952	1.8697	1.6132	1.5224
0.2741	0.3209	1.8713	1.8442	1.5959	1.5119
0.2869	0.3035	1.8601	1.8251	1.5715	1.5007
0.2890	0.2700	1.8419	1.7936	1.5543	1.4892
0.2970	0.2412	1.8278	1.7789	1.5112	1.4712
0.3091	0.2278	1.8159	1.7542	1.5034	1.4534
0.3265	0.2100	1.7986	1.7364	1.4987	1.4397
0.3498	0.1624	1.7791	1.7119	1.4772	1.4229
0.3769	0.1363	1.7556	1.6828	1.4583	1.4101
0.4000	0.1200	1.7384	1.6709	1.4211	1.4074
0.4244	0.0885	1.7002	1.6667	1.4102	1.3998
0.4789	0.0563	1.6887	1.6583	1.4032	1.3902

Table(5) : Experimental and the predicted excess viscosities (η^E) for ternary mixtures at 29٣.15k, 30٣.15k, 313.15k,and 323.15k.

(Cycloheptane + x_2 m- xylene + x_3 o- xylene)									
x_1	x_2	$\eta^E_{exp.}$	$\eta^E_{Pred.}$	$\eta^E_{exp.}$	$\eta^E_{Pred.}$	$\eta^E_{exp.}$	$\eta^E_{Pred.}$	$\eta^E_{exp.}$	$\eta^E_{Pred.}$
		293.15k		303.15k		313.15k		323.15k	
0.2848	0.3715	0.8488	0.8485	0.8115	0.8112	0.6934	0.6931	0.6062	0.6058
0.2860	0.3534	0.8233	0.8217	0.7893	0.7890	0.6686	0.6682	0.5836	0.5832
0.2909	0.3395	0.7858	0.7843	0.7627	0.7622	0.6551	0.6544	0.5602	0.5601
0.2923	0.3214	0.7698	0.7699	0.7386	0.7376	0.6318	0.6315	0.5500	0.5511
0.3097	0.3080	0.7162	0.7154	0.6976	0.6954	0.5984	0.5974	0.5156	0.5153
0.3271	0.2928	0.6738	0.6733	0.6487	0.6477	0.5646	0.5632	0.4816	0.4810
0.3460	0.2718	0.6242	0.6231	0.6259	0.6251	0.5295	0.5299	0.4458	0.4453
0.3679	0.2440	0.5756	0.5755	0.5758	0.5745	0.4939	0.4930	0.4072	0.4069
0.3846	0.2225	0.5391	0.5372	0.5474	0.5470	0.4576	0.4569	0.3827	0.3825
0.3960	0.2155	0.5036	0.5021	0.5130	0.5124	0.4384	0.4377	0.3634	0.3624
0.4286	0.2088	0.4434	0.4447	0.4582	0.4589	0.3917	0.3911	0.3051	0.3047
0.4302	0.1942	0.4199	0.4186	0.4466	0.4461	0.3609	0.3613	0.2870	0.2873

(Cycloheptane + x_2 m- xylene + x_3 p- xylene)									
x_1	x_2	$\eta^E_{exp.}$	$\eta^E_{Pred.}$	$\eta^E_{exp.}$	$\eta^E_{Pred.}$	$\eta^E_{exp.}$	$\eta^E_{Pred.}$	$\eta^E_{exp.}$	$\eta^E_{Pred.}$
		293.15k		303.15k		313.15k		323.15k	
0.2739	0.3585	0.8054	0.8052	0.3631	0.3625	0.6333	0.6328	0.5995	0.5991
0.2741	0.3209	0.7802	0.7811	0.3099	0.3092	0.6154	0.6151	0.5883	0.5879
0.2869	0.3035	0.7530	0.7527	0.2632	0.2627	0.5778	0.5775	0.5655	0.5652
0.2890	0.2700	0.7313	0.7315	0.2048	0.2041	0.5581	0.5579	0.5517	0.5511
0.2970	0.2412	0.7068	0.7062	0.1598	0.1590	0.5065	0.5054	0.5261	0.5260
0.3091	0.2278	0.6799	0.6785	0.1113	0.1117	0.4862	0.4853	0.4974	0.4968
0.3265	0.2100	0.6409	0.6401	0.0602	0.0609	0.4635	0.4631	0.4679	0.4680
0.3498	0.1624	0.5918	0.5913	-0.0261	-0.0263	0.4178	0.4175	0.4297	0.4291
0.3769	0.1363	0.5348	0.5339	-0.1057	-0.1055	0.3710	0.3716	0.3924	0.3927
0.4000	0.1200	0.4891	0.4892	-0.1563	-0.1558	0.3100	0.3108	0.3689	0.3691
0.4244	0.0885	0.4205	0.4208	-0.2119	-0.2109	0.2739	0.2733	0.3391	0.3388
0.4789	0.0563	0.3420	0.3417	-0.3071	-0.3062	0.2110	0.2107	0.2805	0.2803

A New Keystream Generator Based on Swarm Intelligence

Ismail K. Ali / ismailkhlil747@yahoo.com

Abdulelah I. Jarullah /Abdul567@yahoo.com

Receiving Date: 2011/7/24 - **Accept Date:** 2011/9/13

Abstract

Advances in the design of keystream generator using swarm intelligence techniques are reported.In this paper particle swarm optimization algorithm for generating random keystream with large complexity is presented. Particle swarm technique is adapted to locate the requirements(larg period ,larg linear complexity, good randomness and high order of correlation immunity). The definitions for some cryptographic properties are generalized, providing a measure suitable for use fitness function in a particle swarm algorithm, seeking randomness that satisfy both correlation immunity and the large linear complexity. Results are presented demonstrating the effectiveness of the proposed method.

Keywords: Particle Swarm Optimization, Stream Cipher, Keystream Generator, Randomness, and Linear Complexity.

الخلاصة

يهدف البحث إلى تقديم طريقة تصميم متقدمة في أنظمة حماية البيانات لمولد مفاتيح انسيابي باستخدام تقنية الحشود الذكية حيث تم استخدام خوارزمية أمثلية حشد الجريئة لتوليد متتابعات مفاتيح انسيابية تمتلك عشوائية جيدة وتعقيد كبير. تم تكيف دالة تقيم مناسبة لخوارزمية حشد الجريئة لتحقيق المتطلبات العامة بمتتابعات المفتاح الانسيابي من حيث (عشوائية جيدة ، دورة متتابعة كبيرة ، تعقيد خطي كبير ، ممانعة ارتباط عالية).

1. Introduction

Protecting secret data from interception is the large problem of communication and computer security. It is well known that the designers and users of encryption algorithms used in cipher systems needed the ways to find a systematic approach in examining their ciphers prior to use, to ensure that they are safe from various forms of cryptoanalytical attack. [٣]

A stream cipher denotes the process of encryption where binary plaintext is encrypted one bit at a time. The simplest and most often used stream cipher for encrypting binary plaintext is where the bit at time interval t of a pseudo random sequence K(t), is combined using XOR (modulo two addition) with plaintext bit, P(t), at time interval t to produce the ciphertext bit at time interval t, denoted by C(t). The sequence K(t) is called the keystream for the stream cipher (See Figure 1). The encryption process can be expressed as:

$$C(t) = P(t) \oplus K(t) \qquad (1)$$ [٧]

Where $\oplus$ denotes modulo two addition. The decryption process can be expressed as:

$$P(t) = C(t) \oplus K(t) \qquad (2)$$

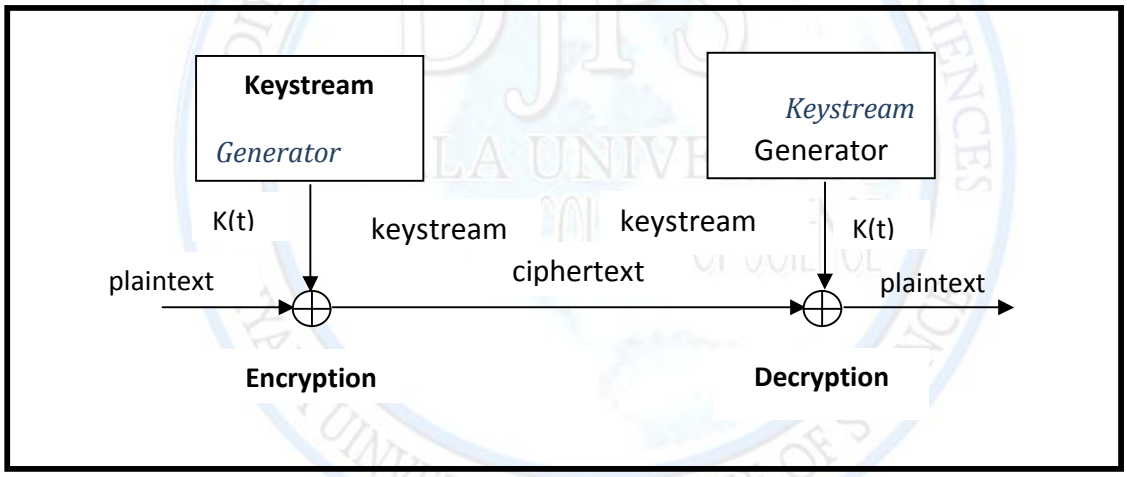

Figure 1: Stream Cipher

It should be noted, as indicated by equations 1 and 2, that both the encryptor and decryptor need to able to generate the same key stream sequence K(t). The key k for the stream cipher is the initial seed to start the generator. Both the encryptor and dycryptor need to process this key. The crypto key used for encryption is changed randomly so that the ciphertext produced is mathematically impossible to break. The changing of random keys will not allow any pattern to be repeated which would give a clue to the cracker to break the ciphertext. The stream cipher can be either hardware [1, 2, 4] or software [8]. It is clear, that the security of the stream ciphers depends entirely on the keystream generator and can be analyzed in terms of randomness, linear complexity, and correlation immunity [3, 7].

In general there are four basic properties in designing the keystream of figure 1. [7]

1. The period of K(t) should be large.
2. The linear complexity of K(t) should be large.
3. The sequence K(t) should have good randomness.
4. The sequence K(t) should have a high order of correlation immunity.

This paper build a new keystream generator using a new approach based on application of an optimization technique inspired by social behavior observable in nature, such as flocks of birds and schools of fish [6], the proposed approach makes use of a Particle Swarm Optimization (PSO) to generate keys needed for encryption. It will generate a keystream sequence that satisfies the general basic properties (large period, good randomness, large linear complexity, and high order degree of correlation immunity).

2. Particle Swarm Optimization (PSO)

Particle Swarm Optimization (PSO) is a population based stochastic optimization technique developed by Dr. Eberhart and Dr. Kennedy in 1995 [5], inspired by social behavior of bird flocking or fish schooling and swarm theory.

The basic PSO model consists of a swarm of particles, which are initialized with a population of random candidate solutions. They move iteratively through the d-dimension problem space to search for the new solutions, where the fitness, f, can be calculated as the certain qualities measure. Each particle has a position represented by a position-vector $\mathbf{x}_i$ (i is the index of the particle), and a velocity represented by a velocity-vector $\mathbf{v}_i$. Each particle remembers its own best position so far in a vector i-th, and its d- dimensional value is **pbest**(p_{id}). The best position-vector among the swarm so far is then stored in a vector i-th, and its d-th dimensional value is **gbest**(p_{gd}). During the iteration time t, the update of the velocity from the previous velocity to the new velocity is determined by Eq. 3. The new position is then determined by the sum of the previous position and the new velocity by Eq. 4.

$$v_{id} = w * v_{id} + c_1 * r_1 * (p_{id} - x_{id}) + c_2 * r_2 * (p_{gd} - x_{id}) \quad (3)$$

$$x_{id} = x_{id} + v_{id} \quad (4)$$

where, i =1,2,…..,N; w is the inertia weight, r_1 and r_2 are the random numbers, which are used to maintain the diversity of the population, and are uniformly distributed in the interval [0,1] for the d-th dimension of the i-th particle. c_1 is a positive constant, called as coefficient of the self-recognition component; c_2 is a positive constant, called as coefficient of the social component. From Eq. 3, a particle decides where to move next, considering its own experience, which is the memory of its best past position, and the experience of its most successful particle in the swarm. In order to guide the particles effectively in the search space,

the maximum moving distance during one iteration must be clamped in between the maximum velocity $[-v_{max}, v_{max}]$.

3. The Proposed Algorithm

The following is an algorithmic description of the generating keystream sequences using particle swarm optimization (PSO):

Input: Length of plaintext(denoting the particles keystream length), the algorithm parameters (c_1, c_2, w, v_{max}, Swarm_Size, Max_Iter).

Output: The key having the highest fitness as found by PSO.

Step 1: Randomly generate the initial particles (keys) and velocities to form a swarm, as clarified in subsection (3.1).

Step 2: Calculate the fitness function of each of the particles (keys) as shown in subsection (3.2)

Step 3: If the current position of the particle is better than the previous history, update the particles to indicate this fact.

Step 4: Find the best particle of the swarm. Update the positions of the particles by using equations 3 and 4:

$$v_{id} = w * v_{id} + c_1 * r_1 * (p_{id} - x_{id}) + c_2 * r_2 * (p_{gid} - x_{id})$$

$$x_{id} = x_{id} + v_{id}$$

Step 5: If the maximum number of iterations has exceeded or if the key with very high fitness value is found, then go to step 6 or else go to step 2.

Step 6: Copy the best key obtained so far in the output key variable and exit.

3.1 Representation (Initialization)

To apply the PSO algorithm for generating a keystream sequence, a representation of solutions to the problem must be appropriately chosen first. The standard stream cipher uses the binary representation in which each solution (keystream) coded as a binary string.

3.2 Fitness Function Calculation

The objective function (fitness function) value for each sequence is calculated by examining the keystream. The objective function used is related to the required properties. Thus, the objective function calculation includes the following:

- Since the required sequence should pass the frequency test, we check that an equal proportion of ones and zeros in the bit stream.

Then:

Error_Frequency = $|n_0 - n_1|$ (5)

- Since the required sequence should pass the binary derivative test, then this test is applied to the sequence by taking the overlapping two-tupels in the original bit stream, thus:

01 becomes 1

10 becomes 1

00 becomes 0

11 becomes 0

We check that an equal proportion of ones and zeros in the new bit stream.

Then:

Error_B-Derivative = $|(count\_n_0 - count\_n_1) - 1|$ (6)

- Apply the change point test; by checking the change point which is the maximum difference between the proportions of ones including the point and the proportion of ones after the point is noted, thus:

n = the total bit in the stream.

S [n] = the total number of ones in bit stream.

t = the change point.

S [t] = the total number of ones to bit t.

U[t] = n. S[t]-t. S[n]

M = the maximum of ABS (U [t]), for t=1…n.

Where ABS denotes the absolute value

Error_C-point = exp (-2M^2 /n.S[n]. (n-S[n])) (7)

- Since required sequence should pass the serial test, we check the probability of a consecutive entry being equal or different is about the same. This will then give same level of confidence that each bit is independent of its predecessor i.e. from the fact that in random sequence $n_{00}=n_{01}=n_{10}=n_{11}= n/4$.

Then:

Error_Serial=$|(n_{00} - n/4) + (n_{01} - n/4) + (n_{10} - n/4) + (n_{11} - n/4)|$ (8)

- Since required sequence should pass the run test, then the run test counts the number of runs of ones (blocks) and runs of zeros (gaps) for each possible run length. Which is $1/2^i * n_r$ runs in the sequence are of length i, where n_r is the number of runs in the sequence, M is maximum run length i, and n_i is the number of runs of length i.

Then:

$$\text{Error\_Run}=\sum_{i=1}^{M}\left|\left(\frac{1}{2^i} * n_r\right) - n_i\right| \qquad (9)$$

- **Furthermore, the linear complexity of a keystream sequence can be included in the objective function value using the BerleKamp-Massy algorithm.**

Then:

Error_L_complexity = L – n / 2 **(10)**

The summation error of every test is calculated, and then the objective function for algorithm is:

Fitness_Function = 1 / ∑ Error **(11)**

4. Results

The work reported in this paper has shown how one of the swarm intelligence techniques called (PSO) can be used to generate a keystream sequence that has (good statistical properties, long period, large linear complexity, and highly order degree of correlation immunity).

During the implementation of the algorithm, the technique has different principle parameters (See Table 1).

Table 1: Parameters selection of keystream generator

Parameters	Symbol	Value
Self confidence	c_1	1.5 – 2.0
Swarm Confidence	c_2	1.5 – 2.0
Inertia weight	w	1.2
Number of particles in the swarm	Swarm_Size	20-40
Maximum number of iteration	Max_Iter	100-500

The PSO algorithm for keystream sequence generator is run a number of times for different parameters values has shown in Table 1. At each factor, ten runs were performed. The results of applying our technique (PSO) algorithm to produce a keystream sequence that satisfies the requirements, for the PSO components the search was terminated when maximum number of iteration is reached. The results of maximizing the objective function values,are also show.

The algorithm performance of algorithm is applied on the sequence of length (2000-5000) bits. The maximum number for each iteration to find the solution is calculated. The statistical tests are applied for the best solution of each iteration that generated from applyed PSO algorithm to decide whether a sequence has passed or failed the test. So there must be a statistical values corresponding to truly random sequences and then set a pass mark. As an illustration, if the pass mark is 95%. This means that a given sequence passes the test if its value lies in the range in which there is exception to find 95% of all sequence. It is usual to denote the pass mark as (100-α), where α is called the significance level of the test. Throughout the tests that applied are (frequency test, binary derivative test, change point test, serial test, poker test, run test, and autocorrelation test).

Table 2 gives iterations that have the best solution which passed the statistical tests. Further more these results passed the statistical tests were applied by Berle_Kamp Massey algorithm [٧] for each best solution of each iteration and the solutions give the perfect linear complexity.

Table 2: Test results with (2000 bits, Swarm_Size = 20, Max_Iter=100)

Run No.	C_1=1.5, C_2=1.5	C_1=1.5, C_2=2	C_1=2, C_2=1.5	C_1=2, C_2=2	Statistical Tests
	Best Value	Best Value	Best Value	Best Value	
1	53	80	66	64	Pass
2	54	57	51	73	Pass
3	92	63	89	66	Pass
4	67	66	72	52	Pass
5	50	34	44	83	Pass
6	52	58	70	47	Pass
7	61	62	72	55	Pass
8	75	82	83	66	Pass
9	65	74	51	80	Pass
10	88	80	63	52	Pass

This approach reduces the encryption time and also the keystream length will always increase in each iteration until a solution is obtained. Figure.2 shows the comparison between the times consuming by encryption using PSO algorithm for a keystream with varying plaintext bits length.

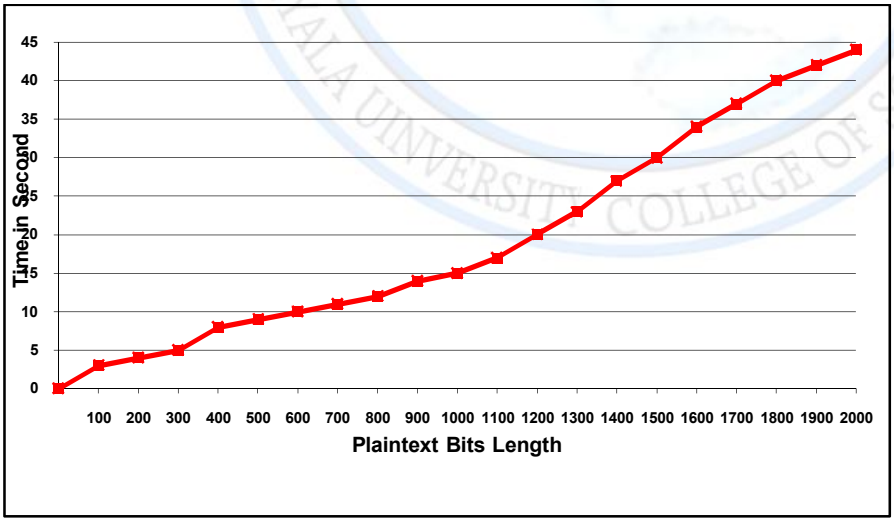

Figure 2: Results for time consumed with varying plaintext bits length

5. Conclusion

Heuristic approach to the design of cryptographiclly strong keystream have been presented. These pseudo random techniques provide a suitable alternative to systematic methods for the construction of cryptographiclly strong random key generator. From studying the solutions of iterations by applying our new generator and according to randomness level and degree of complexity, it is easy to notice that the new generator has generated a large number of solutions that satisfied our requirements (large period, good randomness, large linear complexity, and high order degree of correlation immunity).

The algorithm is robust, since under the generation mechanism and acceptance criterion rules, it's find solution that does not strongly depend on the choice of the initial state, for this reason it can be public.

The best values of the PSO parameters may depend not only the problem being solved, but also on the type and size of instance at hand. Generally to get best results, long iterattions runs must be allowed.

Designing of cryptosystem using this new approach does depend on the number of parameters that considered the secret key of the algorithm. Thus, that increases the complexity of the algorithm against the cryptanalytic attack.

References

1. Deepthi.P.P,Deepa Sara John,P.S.Sathidevi,"**Design and Analysis of a Highly Secure Stream Cipher Based on Linear Feedback Shift Register**", Computers and Electrical Engineering, Volume 35, Issue 2, pp 235-243, March 2009.
2. Good T. and Benaissa M., "**Hardware Results for Selected Stream Cipher Candidates**". State of the Art of Stream Ciphers (SASC 2007), pp 191-204, 2007.
3. Gustafson H.,"**A Computer Package Measuring the Strength of Encryption Algorithms**", Elsevier Science Ltd, 1994.
4. Hell.M, Johansson.T, Maximov.A. Meier.W." **A Stream Cipher Proposal: Grain**". IEEE International Symposium on Information Theory, pp 1614 – 1618, July 2006.
5. Kennedy J. and Eberhart R., "**Particle Swarm Optimization**", in Proceedings of the IEEE International Conference on Neural Networks, pp. 1942-1948, 1995.
6. Reynolds C.W,"**Flocks, Herds and Schools: a distributed behavioral model**", In Computer Graphics, volume 21, pp: 25–34, 1987.
7. Schneier B.,"**Applied Cryptography, Protocols, Algorithms, and Source Code in C Language**", John Wiley and Sons, 1996.
8. Common wealth Office of technology, Monthly cyber security tips, Volume 3 Issue 5, May 2008.

Effect of Apple- Lite Contained of Apple Fibers and Apple Gel Pectin on Body Weight, Lipid Profiles, Kidney Function and Histological Structure of Kidney in Male Albino Rats.

Nusaibah Amer *

Jabbar H.Yenzeel Al-Hilfy

Mustaffa A.K. AL-Taie

Department of Biology, College of Science, University of Baghdad, Baghdad, Iraq

*nusaiba_histo@yahoo.com

Receiving Date: 2011/9/18 **- Accept Date:** 2012/2/7

Abstract

In this study, we evaluated the effect of Apple- lite for 4 weeks on body weight, lipid profiles, kidney functions and histological structure of kidney in male rats. Twenty adult male albino rats (240 - 250 gm) were divided into 2 groups: The first group was considered as control group. The second group was treated orally with Apple- lite (55 mg/kg b.w) by use of intragastric tube. Different physiological parameters were performed including recording of the body weight and measuring lipid profiles, creatinine and urea levels. Body weight gain, total cholesterol, triglyceride, LDL cholesterol, and VLDL cholesterol levels were significantly ($p< 0.05$) reduced in Apple- lite treated rats when compared with the control rats. Urea level was significantly ($p< 0.05$) increased in Apple- lite treated rats, but HDL cholesterol and creatinine levels were none significantly ($P >0.05$) increased when compared with the control rats. Histological examination of Apple- lite treated rat's kidney showed aggregation of inflammatory cells (monocytes) around glomerulus, fibrosis around Bowman's capsule, and congestion of blood vessels. From these results it can be conclude that the treatment with Apple-lite produced a significant reduction in body weight and lipid profiles, but it is incapable of improving the kidney functions. Also there are histopathological effects on kidney tissue in treated rats.

Key Words**:** Apple- lite, Apple fibers, Lipid profile, Kidney Function, Rats.

DIYALA JOURNAL FOR PURE SCIENCES

Effect of Apple- Lite Contained of Apple Fibers and Apple Gel Pectin on Body Weight, Lipid Profiles, Kidney Function and Histological Structure of Kidney in Male Albino Rats.

Nusaibah Amer - Jabbar H.Yenzeel Al-Hilfy -Mustaffa A.K. AL-Taie

تاثير المستحضر ابل لايت الحاوي على الياف التفاح وبكتين تفاح جيلاتيني في وزن الجسم ومستويات الدهون ووظائف الكلى والتركيب النسيجي للكلية في ذكور الجرذان البيض.

نسيبه عامر

جبار حميد ينزيل

مصطفى عبدالخالق الطائي

قسم علوم الحياة، كلية العلوم ، جامعة بغداد، بغداد ، العراق

الخلاصة

في هذه الدراسة تم تقييم تأثير تناول مستحضر الابل لايت لمدة اربعة اسابيع في وزن الجسم ومستويات الدهون ووظائف الكلى ، وفي التركيب النسجي للكلى في ذكور الجرذان البيض.استعملت عشرون من ذكور الجرذان البيض البالغة تراوحت اوزانها مابين 240 الى 250 غرام قسمت الى مجموعتين: الاولى عوملت كمجموعة سيطرة ، وتلقت المجموعة الثانية جرعة من مستحضر الابل لايت مقدارها 55 ملغرام / لكل كيلوغرام من وزن الجسم عن طريق الفم باستخدام انبوب المعدة.تم قياس عدة معايير فسلجية تضمنت وزن الجسم ومستويات الدهون ومستوى اليوريا والكرياتنين. اظهرت النتائج وجود انخفاض معنوي في معدل اكتساب وزن الجسم ومستويات الكوليستيرول والدهون الثلاثية والكوليستيرول واطئ الكثافة والكوليستيرول واطئ الكثافة جدا في دم الجرذان المعاملة بمستحضر الابل لايت عند المقارنة بالسيطرة، في حين لوحظ ارتفاع معنوي في مستوى اليوريا وارتفاع غيرمعنوي في مستويات الكوليستيرول عالي الكثافة والكرياتنين عند المقارنة بالسيطرة . اظهرت نتائج الفحص النسجي لنسيج كلى الجرذان المعاملة بمستحضر الابل لايت تجمع الخلايا الأحادية النواةِ حول اللمة الكبيبية، التهاب النسيج الليفي حول محفظة بومان، كما اظهرت أحتقان في الاوعية الدموية.ومن نتائج الدراسة يتضح ان مستحضر الابل لايت له تاثير واضح في خفض وزن الجسم ومستويات الدهون ، لكن ليس له القدره على المحافظة على وظائف الكلى، كذلك ظهرت له تاثيرات امراضيه نسيجية في نسيج الكلى في الجرذان.

كلمات مفتاحية : ابل لايت ،الياف التفاح، مستويات الدهون ،وظائف الكلى ، الجرذان.

Effect of Apple- Lite Contained of Apple Fibers and Apple Gel Pectin on Body Weight, Lipid Profiles, Kidney Function and Histological Structure of Kidney in Male Albino Rats.

Nusaibah Amer - Jabbar H.Yenzeel Al-Hilfy -Mustaffa A.K. AL-Taie

Introduction:

The use of medicinal plants for treatment and management of diseases has been gaining prominence worldwide especially in the developing countries where 80 % of the population still depends on traditional healing methods [1].Apple lite is food supplement during weight loss programs; it's composed of Apple fibers and Pure Apple Gel Pectin. Apple reduces inflamation of gut and is useful in children and infant's diarrhea, entrocolitis, dysentria, chronic gastroentrities and Thyphoidal fever. Alpona (apple powder) has pectin and reduces blood cholesterol, defecate harmful bacteria from gut (desinfecting effect). Among fruit apples are an excellent source of soluble fiber, pectin and polyphylic compounds [2]. Pectin is a soluble fiber found in the cell walls of many plants. Some studies describe the healthy properties of this fiber. Apple pectin has demonstrated a better cholesterol-lowering effect than other pectins including orange pectin. Pectins are a family of complex polysaccharides that contain 1, 4-linked α-Dgalactosyluronic residues [3].

Three pectic polysaccharides, homogalacturonan, rhamnogalacturonan-I and substituted galacturonans, have been isolated from primary plant cell walls. Pectins also carry nonsugar substituents essentially methanol, acetic acid, phenolic acids and occasionally amide groups.[4] .High methoxy pectin have the ability to form gels with sugar and acid, so-called low water activity gels or sugar-acid-pectin gels. Such a gel is considered a 2-dimensional network of pectin molecules in which the solvent (water) with the co-solutes sugar and acid are immobilized. Several physiological responses, such as lowering of plasma cholesterol level, modification of the glycemic response, improving large bowel function, and lowering nutrient availability, have been associated with isolated fiber fractions or diets rich in fiber-containing foods. In mediating these responses, it is clear that the physical properties of dietary fibers affect the function of gastrointestinal tract and influence the rate and site of nutrient absorption [5].The fiber in apples, which is thought to play a major role in its lipid-lowering capacities, is not found in especially high concentration (2–3 g/100 g), and soluble fibers such as pectin represent 50% of the fiber in apples. Nevertheless, it has been reported that this fraction probably contributes to the effects of apples on lipid metabolism [6]. Several dietary fibers significantly decrease serum cholesterol concentration in human and thereby reduce the risk for coronary heart disease [7]. Apple dietary fiber and rice bran, a predominantly insoluble fiber source was reported to show hypocholesterolic effect in hamsters [8]. Apple fiber is among top five high fiber diets rich in cellulose, hemicellulose, lignin, pectin contents with potentials of hypcholesterolemic effect [2]. For example, eating two apples a day contributes 2 g of pectin to the diet, which can reduce blood cholesterol by 0·10 mmol/l during the period of consumption. [9].The lower energy intake associated with the consumption of fiber leads to a modest reduction in body weight. Howarth etal., [10] concluded that the intake of approximately 12 g fiber per day for 4 months in an ad libitum diet is associated with a decrease of 10% in energy consumption and a weigh loss of approximately 2 kg. The aim of this study was to investigate the effects of daily oral consumption of Apple-lite on body weight, some kidney functions, lipid profiles and histological structures of kidney in rats.

Effect of Apple- Lite Contained of Apple Fibers and Apple Gel Pectin on Body Weight, Lipid Profiles, Kidney Function and Histological Structure of Kidney in Male Albino Rats.

Nusaibah Amer - Jabbar H.Yenzeel Al-Hilfy -Mustaffa A.K. AL-Taie

Materials and methods

Animals and experimental design

Twenty adult 16 weeks old, male albino rats (Rattus *norvegicus*), weighing 240-250 gm were obtained from animal's house of the College of Science, University of Baghdad, Iraq. They were housed in standard plastic cages. The animals were kept in a well ventilated room, temperature of 24-28°C with 12 hrs natural light and 12 hrs darkness. The rats had free access to tap water and dry rat pellets obtained from local market *ad libitum*. The rats were allowed to acclimatize for ten days and then divided into 2 groups; (10 per group) as follows: untreated control group, and Apple- lite treated group which received 55 mg/kg b.w. Apple- lite orally by use of intragastric tube for 4 weeks. (Apple-lite produced by the Arab Company for Pharmaceuticals and Medical plants MEPACO-Egypt), compositions: Apple fibers (from Apple cuticle) 500mg and pure Apple gel pectin (from apple pulp) 50mg.

Collection of blood samples and biochemical analysis

At the end of the experiment, blood samples were taken by cardiac puncture and blood was collected in clean EDTA tubes, then plasma was separated by centrifugation (3000 rpm for 15 min.) and stored at -20°C. Triglycerides level was estimated by use of Randox kit according to [11]. Cholesterol level was estimated by Randox kit according to [11]. The HDL Cholesterol (HDL-C) was estimated by BioMaghreb kit according to [12]. VLDL composition and LDL cholesterol can be calculated with reasonable accuracy by the Friedewald formula [13]. Kits of creatinine, and urea were purchased from Spinreact, S.A. Ctra. Spain. Creatinine was determined by kinetic method described by [14], determination of urea was according to the enzymatic method of [15].

Histological examination

Animals were killed and small piece of kidney tissue taken from experimental animals were fixed in 10% neutral formalin, alcohol-dehydrated, paraffin-embedded and then sectioned to mean thickness of 4 µm. The histological examination was evaluated by assessing the morphological changes with Hematoxylin and Eosin (H&E) stains [16].

Statistical analysis

Data are expressed as the mean ± SE. The statistical significance was carried out using one- way analysis of variance test followed by Duncan's Multiple Range Test (SPSS statistical software package) [17]. A possibility of *P* value ($p < 0.05$) was considered as significant difference between means.

Results and Discussion: Changes in body weight.

Table 1, shows a significant ($p < 0.05$) decrease in the mean body weight of the Apple-lite treated rats (from 244±3.80 g to 262±7.61 g) when compared with normal control group (from 245.8 ± 4.26 g to 297.8±4.65 g). According to Adams et al., [18] the reduction in body weight observed in animals fed highly methoxylated pectins suggests that these fibers can be used as aids in weight management, helping to control obesity. The rationale for the potential role of an increased consumption of fruit in the prevention of overweight and obesity is related to relatively high content of dietary fibers. Dietary fibers and, in particular, viscous dietary fiber, which are present in fruit in considerable amounts, have been shown to increase postprandial satiety and to decrease subsequent hunger [10]. In the long term, this may lead to decreases in energy intake and, thereby, in body weight.

The delay in gastric emptying and unstirred layer thickness formed in the intestine due to pectin viscosity are the causes of a decreased intestinal absorption of glucose [19]. Most soluble fibers create a sense of fullness in the stomach and may therefore result in lesser intake of calories thus helping weight management and obesity. Fiber can affect energy balance and, as a result, body weight through

a variety of mechanisms that lead to both decreased energy intake and increased energy losses. It has been shown that the intake of sufficient amounts of fiber reduces the sensation of hunger. In fact, the presence of fiber in the diet effectively decreases its energy density, and short-term studies show that a lower energy density increases satiety and decreases intake [20]. Additionally, high-fiber foods require greater mastication, which can contribute to the feeling of satiety because the speed of intake is reduced. Likewise, the intake of viscous fiber or foods that are rich in this sort of fiber forms a gel that increases gastric distension and reduces the rate at which the stomach is emptied. This mechanism has been proposed as an explanation for the sensation of fullness and increase in satiety after viscous fiber intake [21]. In turn, soluble fiber decreases the postprandial secretion of insulin [22], which may contribute to satiety. Soluble fiber can also delay or reduce the intestinal digestion and absorption of macronutrients, thus increasing feacal energy losses. In fact, there is a negative relationship between fiber intake and the digestibility of fats and proteins [10]. Finally, fiber may also affect the energy balance through its effects on release of intestinal hormones, such as Glucagon-Like Peptide 1, which favors satiety and weight loss, although the mechanisms are only theoretical [23].

Lipid profiles:

Table 1, shows the effect of Apple-lite on the levels of plasma lipid profile. Apple-lite produced a significant ($p< 0.05$) decrease in plasma levels of cholesterol (76.2±2.03 mg /dl), triglycerides (61.2±2.86 mg /dl), VLDL (12.04±0.38 mg /dl) and LDL-cholesterol (17.94±2.10 mg /dl) when compared with normal rats plasma levels of cholesterol (91.2±4.49 mg /dl), triglycerides (77.2±2.94 mg /dl), VLDL (15.44±0.58 mg /dl) and LDL-cholesterol (32.14±4.32 mg /dl). But plasma HDL-cholesterol level shows non significant ($P > 0.05$) increase (46.22±0.76 mg /dl) when compared with normal group (43.62±2.05 mg /dl). The lipid-lowering capacity of pectin has been reported previously in rats [24].Similar effects were observed when apple supplemented diets were used [25]. It has been recently proposed that polygalacturonic acid in the pectin molecule is responsible for the cholesterol-lowering properties of pectin, and that viscosity could be an important factor in determining the lipid-lowering potency of pectin [26] The metabolic effects of fiber (reduction of blood cholesterol and postprandial glucose peaks) can be attributed solely to soluble fiber and, more specifically, to viscous fiber [21], Viscosity is the ability to form gels.

It is clear that the physical properties of dietary fibers affect the function of gastrointestinal tract and influence the rate and site of nutrient absorption [6]. In regard to the mechanisms of action of dietary fibers, in vitro studies have demonstrated that some but not all types of dietary fiber bind bile acids [27], leading to the hypothesis that bile acid binding, interference with absorption of bile acids or nutrients in the intestine and excretion of bile acids are mechanisms whereby certain types of dietary fiber lower plasma cholesterol. One possibility is that the soluble dietary fibers are producing short chain fatty acids. Short chain fatty acids serve as a source of metabolizable nutrients for the rat and it has been proposed that the sustained production and delivery of short chain fatty acids to the rat liver and systemic circulation in some way modulates blood levels of cholesterol, triacylglycerol and glucose [28]. The production of short chain fatty acids from fermentation of soluble dietary fiber over time might also explain the observed lower energy intake of the rats fed high levels of soluble dietary fiber perhaps by suppression of a hunger sensation. Because the distal ileum is the absorptive site for bile acids, increasing viscosity as water is progressively removed from the luminal contents will hamper bile acid absorption. This effect, together with physical binding of bile acids to the fiber, causes increased faecal bile acid loss and is the principle mechanism by which fiber may reduce serum cholesterol [27].

Creatinine and urea:

Apple-lite produced a significant ($p< 0.05$) increase in plasma levels of urea (37.2±1.30 mg /dl) and a non significant ($P > 0.05$) increase in plasma levels of creatinine (0.584±0.05 mg /dl), when compared with normal control group (urea: 29.8±2.38 mg /dl and creatinine: 0.502±0.04 mg /dl) and as shown in Table 1. No available study has reported the effect of Apple-lite on kidney function parameters, but the results of histological examination in this study may support these results because they showed negative effects on kidney tissue, and this may affect kidney functions. [29] Goetz, showed degenerative changes in the renal tubules of mice treated with pectin. It has been said that pectin, a mixture of large carbohydrate molecules of different constitutions, is probably not metabolized by the mammalian organism, since a large proportion of the injected material is excreted unchanged by the kidneys. The presence of casts of various kinds within the tubules can lead to degenerative changes in the tubular epithelium is a well known fact.

Table 1: Body weight and levels of plasma lipids, creatinine, and urea in rats treated with 55 mg/kg b.w. Apple- Lite.

Groups / Parameters	Normal control group	Apple-Lite group (treated with Apple- Lite 55 mg/kg b.w.)
Initial body weight. g	245.8 ± 4.26	244±3.80
Final body weight. g	297.8±4.65	262±7.61*
Cholesterol mg /dl	91.2±4.49	76.2±2.03*
Triglyceride mg /dl	77.2±2.94	61.2±2.86*
HDL cholesterol mg /dl	43.62±2.05	46.22±0.76
LDL cholesterol mg /dl	32.14±4.32	17.94±2.10*
VLDL cholesterol mg /dl	15.44±0.58	12.04±0.38*
Creatinine mg /dl	0.502±0.04	0.584±0.05
Urea mg /dl	29.8±2.38	37.2±1.30*

Values are expressed as mean ± S.E of 10 animals.

* Values are statistically significant $P <0.05$ when compared with normal control.

Effect of Apple- Lite Contained of Apple Fibers and Apple Gel Pectin on Body Weight, Lipid Profiles, Kidney Function and Histological Structure of Kidney in Male Albino Rats.

Nusaibah Amer - Jabbar H.Yenzeel Al-Hilfy -Mustaffa A.K. AL-Taie

Histological examination

The present study shows some histopathologicl findings of kidney tissues. Histological examination of both Apple-lite- treated and non- treated rat group shows tissues with normal histology (Fig. 1). Renal tissues of Apple-lite treated rat shows aggregation of inflammatory cells (monocytes) around glomerulus, fibrosis around Bowman's capsule and congestion of blood vessels (Fig. 2) and (Fig.3). Consistent with the result of Goetz [29], this showed degenerative changes in the renal tubules of mice. It has been said that pectin, a mixture of large carbohydrate molecules of different constitutions, is probably not metabolized by the mammalian organism, since a large proportion of the injected material is excreted unchanged by the kidneys. As to the changes in the renal tubules, the anatomical evidence points to stasis of pectin may be as a cause. That the presence of casts of various kinds within the tubules can lead to degenerative changes in the tubular epithelium is a well known fact. Our results may be due to the effect of secondary metabolites result from biodegradation of pectin which may have side effects on kidney tissue. From these results it can be concluded that there are negative side effects of Apple-lite on histology of kidney, so as a further study is needed in this respect.

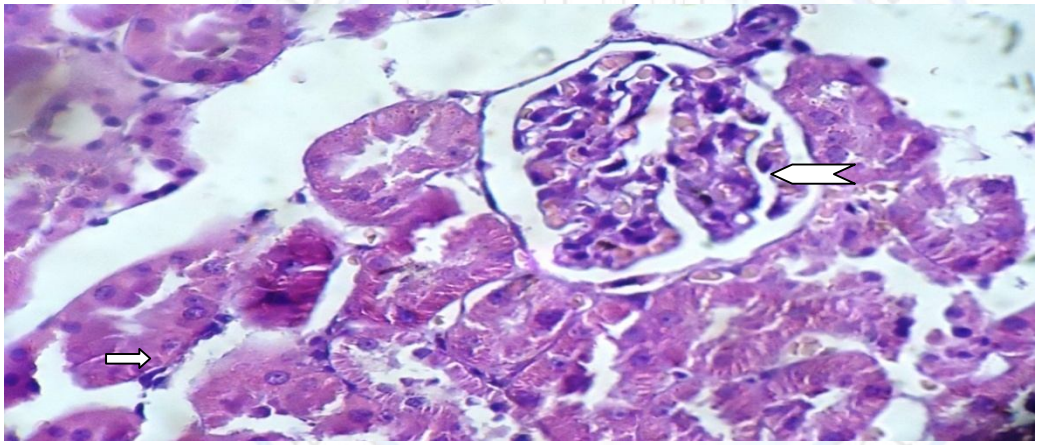

Figure (1): Section in kidney tissue belongs to normal control rat showing normal Bowman's capsule ( ) mal convoluted tubules ( ) (H&E, 400X.

Effect of Apple- Lite Contained of Apple Fibers and Apple Gel Pectin on Body Weight, Lipid Profiles, Kidney Function and Histological Structure of Kidney in Male Albino Rats.

Nusaibah Amer - Jabbar H.Yenzeel Al-Hilfy -Mustaffa A.K. AL-Taie

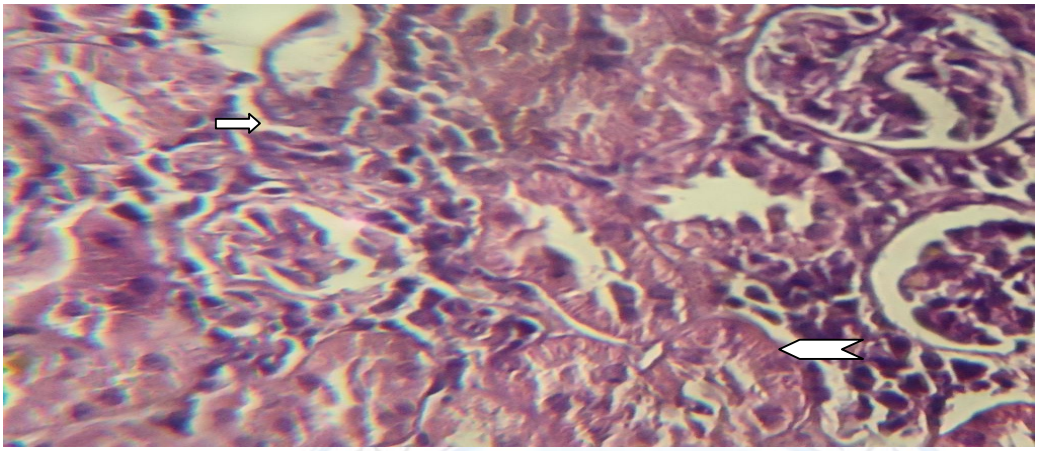

Figure (2): Section in kidney tissue belongs to rat treated with Apple-Lite showing aggregation of inflammatory cells (monocytes) around glomerulus (⇨) fibrosis around Bowman's capsule (⇦) (H&E) 400X.

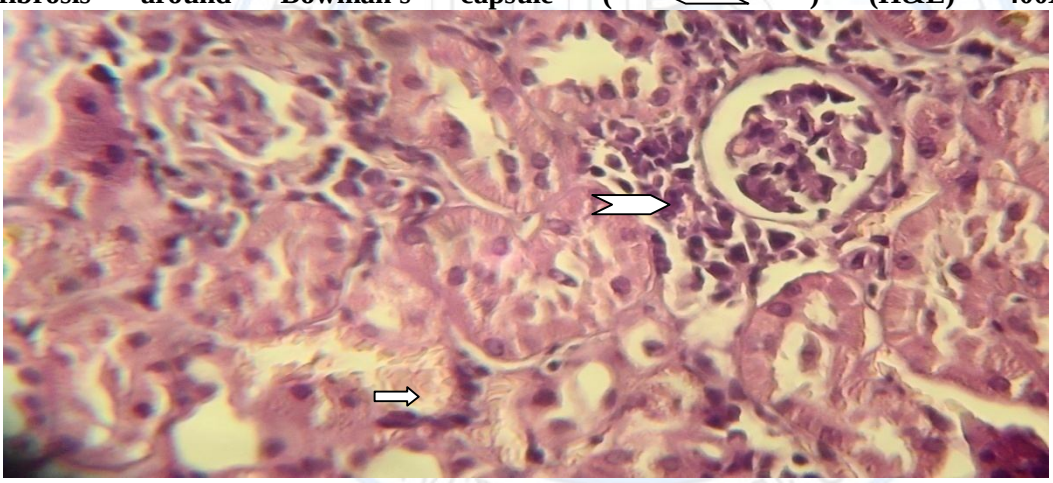

Figure (3): Section in kidney tissue belongs to rat treated with Apple-Lite showing aggregation of inflammatory cells (monocytes) around glomerulus (⇨) congestion of blood vessels (⇨) (H&E) 400X.

References

[1]- Lin, B. H. and Morrisson, R. M. (2002). Higher fruit consumption linked with lower body mass index. Food Review, **25,** 28–32.

[2] -Aprikian O, Levrat-Vemy M, Besson C, Busserolles J, RemesyJ, and Demigne C. (2001). Apple favorably affects parameters of cholesterol metabolism and of antioxidative protection in cholesterol-fed rats. Food Chem. 75: 445-452.

[3] -Ogino Y, Osada K, Nakamura S, Ohta Y, Kanda T, Sugano M.(2007). Absorption of dietary cholesterol oxidation products and their downstream metabolic effects are reduced by dietary apple polyphenols. Lipids. Mar.42 (2):151-61.

[4]- Ridley, B., O'Neill, M.A., Mohnen, D. (2001). 'Pectins: structure, biosynthesis and oligogalacturonide- related signalling', Phytochemistry, 57, 929-967.

[5]- Sembries S, Dongowski G, Mehrländer K, Will F, Dietrich H. (2006). Physiological effects of extraction juices from apple, grape, and red beet pomaces in rats.J Agric Food Chem. Dec 27; 54(26):10269-80.

[6]- Osada K, Suzuki T, Kawakami Y, Senda M, Kasai A, Sami M, Ohta Y, Kanda T, Ikeda M. (2006).Dose-dependent hypocholesterolemic actions of dietary apple polyphenol in rats fed cholesterol. Lipids, Feb; 41(2):133-9.

[7]- Gralak M. A., Leontowicz H., Leontowicz M., Stryczek A., Czerwiñski J, Gorinstein S., Dêbski B.(2006). Effect of apple pulp on calcium, magnesium and manganese content in organs of rats fed atherogenic diets. Pol. J. Food Nutr. Sci. 15/56, SI 2, 55-58.

[8]- Leontowicz H., Gorinstein S., Lojek A., Leontowicz M., Ci¿ M., Soliva- ortuny R., Park Y. S., Yung S. T., Trakhtenberg S., Martin-Belloso O. (2002).Comparative content of some bioactive compounds in apples, peaches and pears and their influence on lipids and antioxidant capacity in rats. J. Nutr. Biochem. 13, 603-610.

[9]- Anderson J.W, Allgood L.D, Lawrence A, Altringer LA, Jerdack G.R, Hengehold D.A & Morel J.G. (2000). Cholesterol-lowering effect of psyllium intake adjunctive to diet therapy in men and women with hypercholesterolemia: meta-analysis of 8 controlled trials. Am J

[10]- Howarth, N.C, Saltzman E & Roberts S.B. (2001.) .Dietary fiber and weight regulation. Nutr. Rev 59, 129–139.

[11]- Allain, C. C.; Poon, L. S.; Chan, C. S.; G. and Richmond, W. F. C. (1974).The Merk manual of diagnostic and therapy, Merk Co. Clin. Chem., 20 (4): 470 – 475.

[12]- Demacherp, N. M. (1980).Chemical and diagnostic specificity of laboratory tests. Clin. Chem., 26: 1775.

[13]- Friedewald, W.T. Levy, R.I. Fredrickson, D.S. (1972). Estimation of the concentration of low-density lipoprotein cholesterol in plasma without use of the ultracentrifuge.Clin Chem. 18:499-502.

[14]- Hare, R.S.(1950).“ Endogenous creatinine in serum and urine” Pro.Soc. Exp. Biol. Med. 147-148.

[15] -Patton, C.J.; Crouch, S.R. (1977). “Enzymatic determination of urea”. Anal. Chem. 49, 464 -469.

[16]- Humason,G.L. (1967). “AnimalTissue Techniques”; 2nd edn.,W.H. Freman Company, San Francisco.

[17]- Duncan, R.C.;Knapp,R.G.; Miller,M.C. (1983). “Introdutory Biostatistics of health science”; Wileg Medical publication, John Wiley and Sons, Lendon,1161-179.

[18]- Adams, K. F.; Schatzkin, A.; Harris, T. B.; Kipnis, V.; Mouw, T.; Ballard-Barbasj, R.; Hollenbeck, A.; Leitzmann, M. F.(2006). Overweight, obesity, and mortality in a large prospective cohort of persons 50-71 years old. N. Engl. J. Med, 355, 763–8.

[19]- Leontowicz M., Gorinstein S., Leontowicz H., Krzemiñski R., Lojek A., Katrich E., M., Martin-Belloso O., Soliva-Fortuny R., Haruenkit R., Trakhtenberg S.(2003).Apple and pear peel and pulp and their influence on plasma lipids and antioxidant potentials in rats fed cholesterol containing diets. J.Agric.Food Chem.51, 5780 -5785.

[20]-Bell E.A. & Rolls B.J. (2001). Energy density of foods affects energy intake across multiple levels of fat content in lean and obese women. Am. J. Clin. Nutr. 73, 1010–1018.

[21]- Jenkins DJA, Kendall CWC, Axelsen M, Augustin LSA & Vuksan V. (2000).Viscous and nonviscous fibres, nonabsorbable and low glycaemic index carbohydrates, blood lipids and coronary heart disease. Curr Opin Lipidol.11,49-56.

[22]- Libuda, L., Alexy, U., Sichert-Hellert, W., Stehle, P., Karaolis-Danckert, N., Buyken, A. E. and Kersting, M. (2008).Pattern of beverage consumption and long-term association with body weight status in German adolescents. British Journal of Nutrition, **99,** 1370–1379.

[23]- Aprikian O, Busserolles J, Manach C, Mazur A, Morand C, Davicco M, Besson C, Rayssiguie Y, Remesy C. and Demigne C. (2002) .Lyophilized apple counteract the development hypercholesterolemia, oxidative stress and renal dysfunction in obese zucker rats. Nutr. 132(7): 1969-1976.

[24]- Leontowicz, M.; Gorinstein, S.; Bartnikowska, E.; Leontowicz,H.; Kulasek, G.; Trakhtenberg, S.(2001). Sugar beet pulp and apple pomace dietary fibers improve lipid metabolism in rats fed cholesterol. Food Chem., 72, 73–78.

[25]- Aprikian, O.; Duclos, V.; Guyot, S.; Besson, C.; Manach, C.; Bernalier, A.; Morand, C.; Rémésy, C.; Demigné, C. (2003).Apple pectin and a polyphenol-rich apple concentrate are more effective together than separately on cecal fermentations and plasma lipids in rats. J. Nutr. 133, 1860–1865.

[26]- Terpstra, A. H., Lapre, J. A., de Vries, H. T. & Beynen, A. C. (2002). Intact pectin and its polygalacturonic acid regions have similar hypocholesterolemic properties in hybrid F1B hamsters. Nahrung 46: 83–86.

[27]- Abeywardena MY. (2003). Dietary fats, carbohydrates and vascular disease: Sri Lankan perspectives. Atherosclerosis. 171: 157-161.

[28] -Erkkila A.T. and Lichtenstein A.H.(2006). Fiber and cardiovascular disease risk: how strong is the evidence? J Cardiovasc. Nurs. 21(1): 3-8.

[29]- Goetz,W. Richter, M.D.(1949). Parenchymatous Lesions of liver and kidney of mice due to pectin.American Journal of pathology.V: 31: 379-387.

The Separation Particle Size and Strain by the Scherrer Analysis Method

K.H.Harbbi

Department of physics , College of education , Ibn-AL-Haitham, University Baghdad

Receiving Date: 2011/5/2 - **Accept Date:** 2011/6/7

Abstract

The Variation of crystallite size and strain of calcium oxide powder with the carbonate temperature of calcium carbonate is studied applying Scherrer analysis method for (111),(200) and (220) reflections .

The results show that size of the crystalline increases and strain decreases with increasing the rang 1100℃ to 1200 ℃ , but the changes are dependent on the crystallographic direction .

DIYALA JOURNAL FOR PURE SCIENCES

The Separation Particle Size and Strain by the Scherrer Analysis Method

K.H.Harbbi

الفصل بين المقاس الحبيبي و الانفعال باستعمال طريقة شيرر في التحليل

خالد هلال حربي
قسم الفيزياء، كلية التربية ابن الهيثم، جامعة بغداد

الخلاصة

تم دراسة مقاس الحبيبة والانفعال لمسحوق اوكسيد الكالسيوم المحضر بطريقة حرق كاربونات الكالسيوم بتطبيق طريقة تحليل شيرر لخطوط الانعكاس (111)،(200) و(220).

واظهرت النتائج انة بزيادة درجة حرارة الحرق من 1100°C الى 1200°C يزدادالمقاس للحبيبة ويقل الانفعال ولكن التغييريعتمد على تلك التجاهات.

The Separation Particle Size and Strain by the

Scherrer Analysis Method

K.H.Harbbi

Introduction

Though the Scherrer method or half maximum breadth method is a frequent measure of mathematical distributions, its use has been limited in the field of X-ray diffraction. The applicability of this method to the analysis of the line broadening of Scherrer powder pattern peaks has been clearly demonstrated by Wilson [1] and developed by Klug and Alexander [2].

The oxide Mo, where M=Ca,Sr,Ba,….,etc are best obtained by calcinating . The carbonates, dehydration of the hydroxide at red heat offers an altimate route [3, 4]. CaO is produced on an enormous scale in many countries. Its major end is used as a flux in steel manufacture, in the production of Ca chemicals, in the treatment of municiptl water supplies, in industrial wasts, in paper industry and in non-ferrous metal production[5]. It is very well know that the chemical reactivity of solids is strongly dependent on both crystallite size and construction of strains. These two facts explain the importance of the mechanical treatments of the materials in chemical technology in order to enhance the reactivity of solid. Thus , it has been report[6]that is possible to carryout, by grinding at room temperature, solid state reactions which to occur would ordinarily require much higher temperature.

Also the study of solid state reaction mechanism is usually approached either through kinetic investigations [7-9].

This paper present for the first time , according to our knowledge the effect of calcinations temperature on the crystallite size and crystal distortion (strain) in CaO powder derived from the thermal decomposition of $CaCo_3$ powder for 30 minutes. The calcinations temperature is ranged from 1100℃ to 1200℃ .

Scherrer Analysis of Line β breadth

The first treatment of crystallite size broadening was due to Scherrer who investigated the case of crystals of regular cubic. The angular breadth (β) at half maximum intensity of a diffraction line produced by the powder method is given by [10]

$$\beta = k\lambda/L\cos\theta \qquad \ldots\ldots\ldots \quad (1)$$

Where L is the crystallite size, $\lambda$is the wave length of the radiation, β is the corrected breadth (in radians), and θ is the Bragg angle, k is the Scherrer constant whose value 0.94 [11]. This constant depends on the definition of breadth β [12].

Also the Scherrer constant depends on the crystal shape and the diffraction line indices, and in all cases to be not for from unity.

In a distorted crystal the interplaner spacing d will not be constant throughout and different parts of the crystal will reflect at different angles. The broadening of the lines in the powder pattern of in aggregate of such distorted crystals may be estimated from Bragg equation.

If the maximum strain in the crystal is ϵ the spacing will vary from $d(1+\epsilon)$ to $d(1-\epsilon)$, and θ will vary in a range numerically equal to $2\epsilon\, tan\theta$. Since the deviation of the rays is 2θ , the range of angle over which the reflexion is appreciable will be [13]doubled:

$$\epsilon = \frac{\beta}{4tan\theta} \qquad \text{……(2)}$$

Where ϵ the crystal distortion (strain).

To find the correct crystallite size, correction for instrumental factor has to be applied on the breadth of the diffraction line. A number of methods have been proposed, some assume the shape of the line, while others donot.

The two most commonly assumed line shapes are the Cauchy and Gaussian functions. For Cauchy profile, originally made by Scherrer in his original analysis of crystallite size effects, the correct crystallite size breadth is given by [14]:

$$\beta = \beta_{meas} - \beta_{instr} \qquad \text{……..(3)}$$

Where β_{meas} is the half width of the experimentally measured breadth and β_{instr} is the half width of the instrumental breadth.

For Gaussian profile, which is more correctly represent the actual reflection profile and instrumental profile, and the relation for the correct size as [12]:

$$\beta^2 = \beta^2_{meas} - \beta^2_{instr} \quad \ldots\ldots\ldots\ldots\ldots\ldots (4)$$

The relationship is holding for both – maximum and integral breadth. Since the actual profiles are never pure Gaussian or pure Cauchy [15]. These simple formulae have only limited practical value.

Since in the present case the full width at half the maximum, $\frac{W}{\beta} > 1$, the Gaussian assumption seems to be valid Decouvolution was accomplished with the relation [4].

Results and Discussion

Broadening of an X-ray diffraction profile is normally caused by small crystallite size, non-uniform strain within the crystallites and faulting on certain crystal planes.

The peak breadth of broadened line can be expressed interms of the crystallite size, hence measurement of the peak breadth gives method for determining crystallite size. An additional broadening termed "instrumental "arising from effects such as slit widths and wavelength widths must be corrected for in order obtain the correct size.

Figure (1) show X-ray diffraction spectra for CaO powder at 1100℃ to 1150℃ and 1200 ℃ [16]. Table (1)shows the half width β_{meas} for line profiles and β for corrections line profile with calcinations temperature for three reflections (111),(200), and 220 the half width decreases with temperatures increases from 1100℃ to 1200℃ . The crystallite size at different temperatures was determined from equation (1). The strain values are obtained from equation (2) and listed an lsion Table (2). It is apparent that the temperature of calcinations has a significant effect on the half width specially above 1100℃ when the conversion is at its beginning .the values of β for curves (111),(200),and (220) reflections in CaO obtained at 1100℃ to 1150℃ and 1200℃ look different. This means that there is an amount of distortion in directions perpendicular to the (111),(200),and (220) planes. This indicates the anisotropic of the crystallites in there directions. Moreover as the temperature of calcinations increases from 1100℃ to 1200℃ , the crystallite size increases progressively for the above

reflections simultaneously and the broadening between the of (111) and other reflections becomes smaller which leads to larger crystallite size (94.677 nm).

The results in this table (2) show that as temperature increases the crystallite size perpendicular to (111),(200), and (220) planes increases when as, inverse behavior it observed for strains. The above behavior could be understood by assuming that the particles of the powder samples are formed by small crystallite welded in a mosaic structure and that the corresponding grain boundaries constitute the main contribution to the particle the lower the size of the crystallite.

Conclusion

1- The crystallites are highly an isotropic in nature and this an isotropic cannot be removed until temperature of 1200℃ is reached
2- Temperature has a prominent effect on the size of the crystallites and the strain of sample
3- There is a considerable amount of distortion in directions perpendicular to the (111), (200) and (220) plans. This indicates the an isotropic nature of crystallites in these diractions.
4- However, increases in strain can explain this broadening of the profile.

The Separation Particle Size and Strain by the

Scherrer Analysis Method

K.H.Harbbi

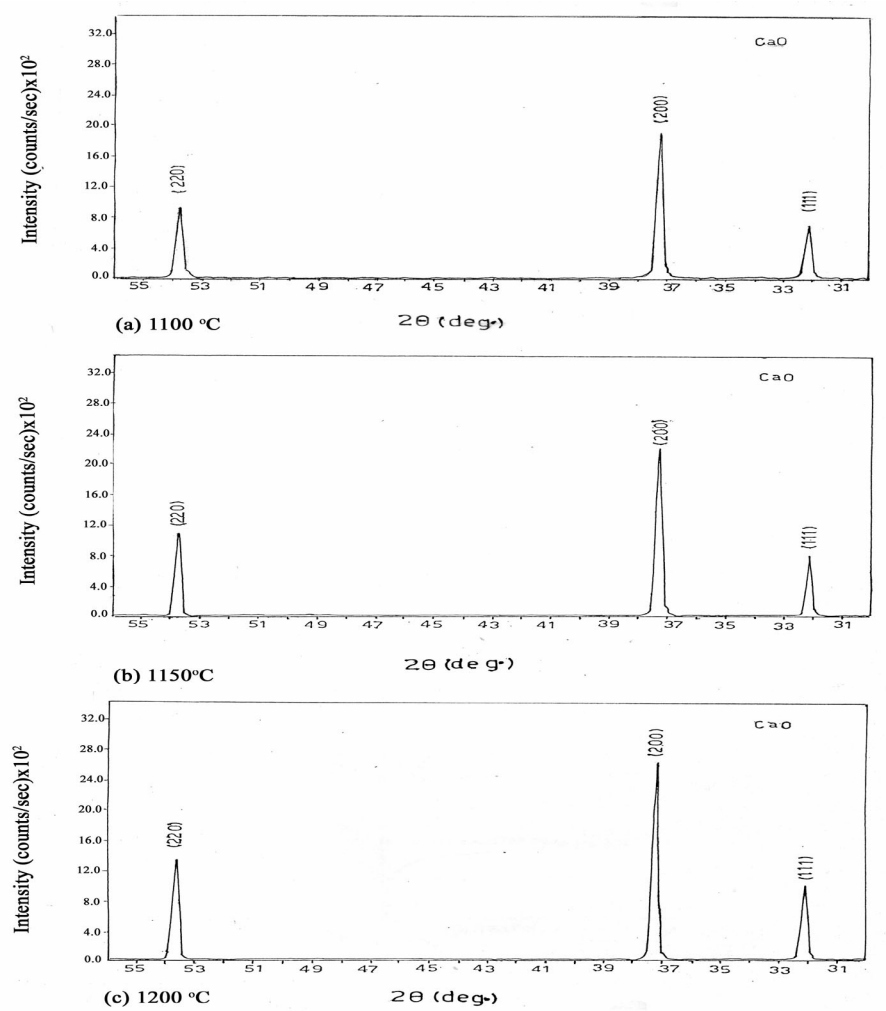

Figure (1): X-ray diffraction spectra for CaO powder at 1100℃ to 1150℃ and 1200℃

Table (1) Experimental measured breadth β_{meas} and crystallite breadth β for CaO obtained at 1100℃ to 1150℃ and 1200℃ for (111), (200), and (220) planes

Reflection	Temperature(℃)	$\beta_{meas} \times 10^{-3}$ (rad)	$\beta \times 10^{-3}$ (rad)
111	1100	3.962	3.107
	1150	3.141	2.027
	1200	2.879	1.591
200	1100	3.455	2.486
	1150	2.879	1.591
	1200	2.617	1.045
220	1100	3.402	2.412
	1150	2.792	1.428
	1200	2.530	0.803

Table (2) Crystallite size and strain for CaO for three planes at different temperatures.

Reflection	Temperature(℃)	Crystallite size(nm)	Strain $\times 10^{-3}$
111	1100	48.481	2.699
	1150	74.312	1.761
	1200	94.677	1.382
200	1100	61.457	1.841
	1150	96.029	1.178
	1200	146.203	0.774
220	1100	67.268	1.191
	1150	113.621	0.705
	1200	202.057	0.396

References

1- Wilson, A.J.C. (1963). Mathematical theory of X-ray powder diffractometry. Eindhoven;Phillips. pp 91-94.
2- Klug, H.P. and Alexander,L.E. (1974). X-ray Diffraction Procedures for Polycrystal Line and Amorphous Materials. 2nd, John Wiely&Sons, Inc. pp 687-692.
3- Everest,D.A.(1973). Comprehensive inorganic chemistry, Pergman Press, Oxford; 1:531-590.
4- Goodenough, R.D and Stenger,V.A.(1973). Magnisium calcium, Stontium, Barium and Radium; 1:591-604.
5- Green Wood,N.N. and Earnshaw, A.(1998). Chemistry of the Elements, University of leeds, U.K; second Edition, pp 119-121.
6- Harbbi,K.H.(2007). Thermo gravimetric Method for Accurate Determination of Thermodynamic Quantities at High Temperatures , Ibn-Al-Haitham, J. for Pure and Applied,Sci; 20:38-45.
7- Ray,S.(1982). The Kinetic Compensation Effect in the Decomposition of Calcium Carbonate, J.Ther.Anal;24:35-41.
8- Barrgia,C. etal.(1986). Changes in the Vaterite-Calcite Transformation with Temperature and Sample Crystallinity, J.M.Sc;21:947-952.
9- Harbbi,K.H.(2005). The Differential Thermal Analysis For Locally Producted Of Calcium Carboniteas a Raw Material, Ibn-Al-Haitham, J. for Pure and Applied,Sci; 18:63-70.
10- Shull,C.G.(1946). The Determination of X-ray Diffraction Line Widths . No 70:679-684.
11- Fievet,F. etal.(1979). Lattice Parameter, Micro strains and Non-Stoichiometry in NiO, Comparsion between Mosaic Microcrystal, J. Appl.cryst.No12:387-394.
12- Delhes,R. etal .(1982). Determintion of Crystallite Size and Lattice Distortions Through X-ray Diffraction Line Profile Analysis, Fresenine Z Anal Chem. No 312:1-16.
13- Wilson,A.J.C.(1962). X-ray optics, London, Methnen and Coltd. New York, John Wiely&Sons, Inc. pp 1-5.
14- Achaya,B.S. and Pradhan,L.D.(1986). Determination of Crystallite Size and Strain in Manganese Dioxide An X-ray Diffraction Study, J.Appl.Cryst:19:214-216.
15- Lsngford,J.(1978).A Rapid Method for Analysis the Breadths of Diffraction and Spectral Lines using the Voigt- Function, J.Appl.Cryst; 11:10-14.
16- Harbbi , K.H(2006). Studing the connection between particles size and lattice distribution , Ibn-Al-Haitham, j. for pure and applied ,Sci;19:41-47.

تحديد الإصابة بداء المقوسات لدى النساء الحوامل في محافظة ديالى

Evaluation of infection with Toxoplasmosis for pregnant women in Diyala province

د.محمد خليفة خضير

كلية العلوم /قسم علوم الحياة

جامعة ديالى

تاريخ استلام البحث:2011/2/26 - **تاريخ قبول النشر: 2011/3/30**

الخلاصة

Toxoplasmosisتضمنت الدراسة التحري مصليا عن داء المقوسات(داء القطط)

كأحد مسببات الاجهاض *Toxoplasma gondii* الذي يسببه طفيلي

لدى النساء الحوامل اللواتي تراوحت أعمارهن (20-50) سنة وللفترة بين (كانون أول)سنة 2009 ولغاية (نيسان) من سنة 2010 ، واللواتي راجعن مستشفى بلدروز

للتشخيص (LAT)العام في محافظة ديالى .تم استخدام اختبار تلازن اللاتكس المباشر

تضمنت الدراسة (50) عينةدم لنساء حوامل ممن لديهن أكثر من إسقاط و (10) عينة دم لنساء حوامل ليست لديهن إسقاط سابق وغير مصابات بداء المقوسات كمجموعة .(control) سيطرة

أظهرت النتائج عدد النساء الحوامل المصابات بداء القطط (27) 54% امراة من مجموع (50). (11) امراة حامل ممن لديهم إسقاط لمرة واحدة وبنسبة (40.7%) و(8) امراة حامل ممن لديهن إسقاط لمرتين وبنسبة (29.6%) .أظهرت النتائج إن الفئة العمرية (20-30) سنة شكلت أعلى نسبة من الإصابات بلغت (72%) كما بينت ان الإصابة في الريف اعلى من المدينة آذ بلغت النسبة (32%)

Abstract:

The study included sera diagnosis of toxoplasmosis which causes by T*oxoplasma gondii* parasites which one causes of apportion for pregnant women with age between(20-50) years. This study performed in period between (December 2009) to(April 2010), who visited the General hospital of Balddrose of Diyala province. We used direct latex agglutination method for diagnosis.

The study included(50) blood samples for pregnant women had been more than one apportion .(10) blood samples for pregnant women which had no apportion and without infection with toxoplasmosis as a healthy group for control.

The result appeared the number of pregnant women infection with toxoplasmosis is (27)(54%) from (50) .(11) pregnant women(40.7%)with one apportion and (8) pregnant women with two apportions (29.6).

The study showed the age group(20-30)year consisted the high percentage of infection (72%) and showed the infections in rural higher than city infection (32%)

(Introduction)

المقدمة

من الاوالي الطفيلية الداخل خلوية *Toxoplasma gondii* يعد طفيلي المقوسات

سنة (1900)، وقد وصف Laveran والذي اكتشف لأول مرة من قبل الباحث

سنة (1908)(1) يصيبMance &Nicolleu الطفيلي وصفا دقيقا من قبل الباحثين

هذا الطفيلي معظم الحيوانات الفقرية وكذلك الإنسان مسببا مرضا يدعى داء المقوسات

أو داء القطط. Toxoplasmosis

أكثر الطرق شيوعا للاصابة بداء المقوسات هو استهلاك اللحوم النيئة أو غير المطبوخة جيدا و الحاوية على الاكياس النسيجية للطفيلي أو عن طريق التلامس مع القطط المصابة التي تعد المضيف النهائي له، اذ تطرح مع خروجها كميات كبيرة من للطفيلي(2).(Oocysts) أكياس البيض

يعد داء المقوسات من الإمراض الشائعة في العالم وخصوصا في المناطق الحارة الرطبة، وقد أكدت جميع البحوث والدراسات على أن لهذا المرض اثأرا سلبية على الأجنة في حالة إصابة النساءخلال فترة الحمل ،اذ أن الإصابة بهذا الطفيلي في فترة الحمل قد تودي الى عبورة إلى الجنين عن طريق المشيمة مسببا خطورة للجنين تكمن بحدوث إسقاط او موت الجنين داخل الرحم (3)، اذ ان إصابة المشيمة يعد سببا اساسياً في تسهيل عبوره الى الجنين فقد وجد ان (30-40%) من النساء المصابات اثناء الحمل يقتحم الطفيلي فيهن المشيمة ويصيب الجنين وتختلف نسبة العبور الى الجنين فيما اذا كانت الام مصابة قبل الحمل او إثناءة اذ لا تتجاوز نسبة العبور(1%) في حالة الاصابة قبل الحمل، لتزداد وتصل (90%) اثناء الحمل وحسب مراحل الحمل اذ تبلغ (15%) في الأشهر الثلاثة الأولى و(30%) في الأشهر الثلاثة الوسطى

و(60%) في الأشهر الثلاثة الاخيرة أي يزداد معدل العبور بتقدم الحمل متعمداً على الانسياب الدموي المشيمي حيث يودي هذا العبور إلى الجنين الى إنجاب طفل مصاب بداء المقوسات الولادي(4)و(5)

أما الإصابة خارج فترات الحمل فليس للطفيلي تأثيرا سلبيا على المراة المصابة الا إن عند حدوث الحمل في النساء المصابات قبل الحمل قد يحدث

للطفيلي داخل جسم المرأة المصابة نتيجة لقلة (Reactivatiion) إعادة تنشيط

المناعة اثناء الحمل او في المرضى المثبطين مناعيا مما يودي الى عبور الطفيلي الى الجنين وحدوث الآثار السلبية المذكور أنفاً للجنين في حالة عدم البدء بالعلاج المناسب للام في مراحل الاصابة الاولية للمرض(6) .إشارة دراسات عديدة في الوطن العربي و العراق ان هذا المرض ينشر بمعدلات عالية .اذ اضهرت دراسة في الكويت أجريت عام 1986 ان نسبة الاصابة بين النساء الحوامل بلغت 58% والذين لديهن اسقاط سابق كذلك سجلت دراسة اجريت في المملكة العربية السعودية ان نسبة 37% من النساء الحوامل قيد الدراسة مصابات بداء المقوسات(7).

اجريت دراسة عام 2000 في محافظة نينوى بأستخدام طريقة التلازن المباشربينت ان نسبت الاصابة بهذا الطفيلي بلغت 39.2% (8,7).

MATERIALS AND METHODS

المواد وطرائق العمل

اجريت الدراسة الحالية في قضاء بلدروز للفترة من كانون الاول عام 2009 الى نيسان عام 2010 شملت النساء الحوامل المراجعات الى العيادة الستشارية للمستشفى العام في القضاء. تم اخذ 60 عينة دم لنساء حوامل ،50 عينة لنساء حوامل ممن لديهن اكثر من اسقاط ، و10 عينة دم لنساء حوامل ليس لديهن اسقاط سابق وغير مصابات بداء المقوسات بعد اجراء الفحوسات المختبرية اللازمة.

الفحص: اختبار تلازن اللاتكس المباشر لداء المقوسات

Latex agglutination test

الاسبانية (Biokit-Sa)من انتاج شركة (Kit) استخدم في هذا الاختبار عدة

للكشف عن وجود الاضداد المتخصصة ضد طفيلي Toxo-Cell-latex وتسمى

(IgM,IgG) المقوسات الكوندية في مصل المريض

من المكونات الاتية: (Kit) تتألف العدة

(Latex reagent) 1- معلق حبيبات اللاتكس

(Polystyrene) هو عبارة عن معلق من حبيبات اللاتكس المصنوعة من مادة

والمغطاة بالمستضد الذائب للطفيلي في محلول دارئ ذي حامضية (8) ويحتوي

بتركيز (0.1%).ان حبيبات (Sodium azide)على مادة حافظة ازايد الصوديوم

اللاتكس تجعل التلازن الناتج من تفاعل بين الضد و المستضد واضح بالعين المجردة أو تحت المجهر بقوة التكبير الصغرى (10*)،اذا يظهر التلازن في حالة وجود الأضداد المتخصصة في المصل المراد فحصة.

2positive control- كاشف السيطرة الموجب

للارنب ويحويIgG مصل بشري مخفف يحوي الأضداد المتخصصة من نوع

على (0.1%) من المادة الحافظة أزايد الصوديوم.

3Negative control- كاشف السيطرة السالب

أي خال من الأضداد المتخصصة (non reactive) مصل بشري مخفف غير فعال

Sodium azide ضد الطفيلي ، ويحوي على (0.1%) من المادة الحافظة

تحفظ العدة بكامل محتوياتها في الثلاجة وفي درجة تتراوح ما بين (2-8) م لحين الاستعمال.

Results &Discussion

النتائج و المناقشة

تم عزل العينات في الدراسة و البالغة (60) عينة مصل دم نساء حوامل مشتبه إصابتهن بداء المقوسات المراجعات العيادة لاستشارية في مستشفى بلدروز العام حيث شملت العينات على 50 عينة مصل دم لنساء حوامل مصابات بداء المقوسات و(10) عينة ثم(control) مصل دم لنساء غير مصابات بداء المقوسات كمجموعة سيطرة

شخصت الإصابات بطريقة اختبار التلازن اللاتكس المباشر (LAT).IgG, IgM

جدول (1) الفئات العمرية للنساء الحوامل

الفئات العمرية	العدد الكلي	النسبة المئوية
20-30سنة	36	%72
31-40سنة	13	%26
41-50سنة	1	%2
المجموع	50	%100

الجدول (1) بين النتائج التالية إن 36 امراة حامل ضمن الفئة العمرية (20-30) سنة شكلت نسبة 72%و13 امرأة حامل تمثل الفئة العمرية (31-40)سنة 26%. والفئة العمرية (41-50) سنة 2% من مجموعة النساء الحوامل قيد الدراسة

جدول (2) عدد النساء الحوامل المصابات بداء القطط حسب عدد مرات الإسقاط

عدد مرات الاسقاط	العدد الكلي	النسبة المئوية%
0	4	%14.8
1	11	%40.7
2	8	%29.6
3	2	%7.5
4	1	%3.7
6	1	%3.7
المجموع	27	%100

يوضح الجدول (2) النسب المئوية لحالات الإسقاط حسب عدد مرات الإسقاط للنساء الحوامل قيد الدراسة اذ بلغت عدد حالات الإصابة للنساء الحوامل ممن لديهن إسقاط لمرة واحدة (40.7%) و(29.6%) لمرتين و(7.5%) لثلاث مرات ، وبذلك تكون أعلى نسبة اللاصابة بين النساء اللواتي حدث لهن إسقاط لمرة واحدة او مرتين

ربما يعود السبب في ازدياد الإصابة بين النساء اللواتي حدث لهن إسقاط لمرة واحدة هو تزايد عدد المراجعات إلى المستشفيات و العيادات الطبية حال حدوث الإسقاط لهن لأول مرة مما يودي إلى تشخيص المرض مع اول اسقاط فتزداد نسبة المصابات بالمرض من الناحية الإحصائية اذ لربما النساء اللواتي حدث لهن اسقاط لمرتين او أكثر قد يكن مصابات مع أول إسقاط لأول نتيجة للجهل بالمرض وتدني درجة التثقيف الصحي (9)

في سنة (1989) في دراسة وبائية حول الإصابة بداءCarter أكدت الباحث

المقوسات على ان درجة التثقيف الصحي للمرأة الحامل لها اثر بالغ في تقليل الإصابة وحصر المرض في مراحله الأولى(10). ايضاً يعود السبب إلى عدم وجود علامات والذي تعتبر من العوامل المهمة في(sub cilinical) واضحة للاصابة بهذا المرض

انتشار المرض لصعوبة تشخيصه في المراحل المبكرة إلا بعد حدوث الإسقاط او موت الجنين (11)

جدول (3) عينات البحث موزعة على الموقع السكني

العينة	positive	النسبة المئوية%	Negative	النسبة المئوية%	العدد الكلي
المدينة	11	%22	10	%20	21
الأرياف	16	%32	13	%26	29
العدد الكلي	27	%54	%23	%46	50

يوضح الجدول (3) النسب المئوية للاصابة بداء المقوسات للنساء الحوامل قيد الدراسة ،إذا بلغت الحالات الموجبة (22%) بينما اعطت (20%) من الحالات نتيجة سالبة بالنسبة للمدينة وبلغت الحالات الموجبة (32%) بينما اعطت (26%) من الحالات نتيجة سالبة بالنسبة للارياف وهذا يوضح ان نسبة الإصابة في الريف أكثر من المدينة.

يشير عدد من الباحثين الى ان من الأسباب المهمة في نقل الإصابة وانتشارها يعود إلى تدني الوعي الصحي الثقافي في الريف مقارنة مع المدينة كذلك طبيعة الحياة في الريف عنة في المدينة حيث تعيش الحيوانات الناقلة للطفيلي دور السكن مما يزيد من خطر الإصابة بهذا الطفيلي لإفراد العائلة ايضأ عدم المعرفة الصحية بدور هذه الحيوانات وخاصة القطط في نقل الإصابة وانتشارها بين النساء الحوامل بشكل خاص(14,13,12)

جدول (4) عدد الإصابات لدى النساء الحوامل وحسب الفئات العمرية

الفئات العمرية بالسنين	عدد العينات	عدد المصابات Positive	النسبة المئوية%	عدد غير المصابات Negative	النسبة المئوية %
30-20	36	21	58.3%	15	41.6%
40-31	13	6	46.1%	7	53.8%
50-41	1	0	0%	1	10%

يوضح الجدول (4) النسب المئوية للفئات العمرية المصابة بالمرض في طوره الفعال إذ بلغت الإصابة (58.3%) لدى الفئة (30-20) سنة في حين بلغت نسبة الإصابة (46.1%) لدى الفئة العمرية (31-40) سنة.

ان زيادة نسبة الإصابة الفعالة في الأعمار التي تتراوح ما بين (20-30) سنة تتفق مع سنة (1999)، اذ إن أعلى نسب الإصابة التي حصل عليها كانتJenum نتائج الباحث

في الفئة العمرية التي تتراوح ما بين (20-30) سنة،وقد أوضحت دراسة للباحثة عبد الله وفريقها سنة (2003) إن أعلى نسب الإصابة كانت لدى فئة العمرية ما بين (20-24) وبنسبة إصابة بلغت(32.8%)، إلا إن هذة النسب لا تعني بالضرورة ان الإصابة محصورة على فئة عمرية دون أخرى بل ربما يعود السبب في زيادة الإصابة لهذه الفئة العمرية إلى إن معظم حالات الزواج في مجتمعنا تقع ما بعد سن العشرين وان سن الإنجاب هو في هذة الفترة من العمر.من هنا نرى ان أكثر المراجعات الحوامل للمستشفيات و العيادات هن اللواتي تجاوزت أعمارهن سن العشرين (16,15،)

المصادر العربية

1-عبد الله ،بسمة احمد ،(2001)، دراسة حول إصابة النساء الحوامل المعرضات للخطورة بداء المقوسات ، مجلة علوم الرافدين ،مجلد 13 العدد 1

2-الخفاف، فرح حازم عمر (2001) . عزل ودراسة مصلية وبائية لداء المقوسات في النساء في سن الإنجاب في محافظة نينوى. رسالة ماجستير ، كلية العلوم ، جامعة الموصل

3- عبد الله ،باسمة احمد ،حسن .شهلة عبد الله . الخفاف ، فرح حازم (2003)، استخدم اختبار اللاتكس في تشخيص داء المقوسات في النساء بسن الإنجاب في محافظة نينوى ، مجلة علوم الرافدين .مجلد 14 ، العدد 3،ص 110-11

4-السمعاني، روید غانم کورکیس ابلحد،(2000) ، دراسة مصلية لتشخيص داء المقوسات اللاغنام و الإنسان في محافظة نينوى .رسالة ماجستير ، كلية الطب البيطري، جامعة الموصل

Reference:

1-Lappalainen M, Koskiniemi M, Hiilesmaa, v,Ammala P,

Teramo K,Koskela P,Lebech M, Raivo KO, Hedman K.

(1995).The study Group .Outcome of children after maternal primary *Toxoplasma* infection during pregnancy with emphasis on avidity of specific IgG. Pediatr infect Dis J, 14,354-61.

2- Jackson MH, Hutchinson WM,(1989). The prevalence and source of *Toxoplasma* infection in the environment.Advances parasitol. 28 , 55-105.

3- Joss AWL , Ho-Yen DO.(1997).The effects of samle storage on polymerase chain reaction –based detection of *Toxoplasma gondii* in amniotic fluid .J Med Microbiol , 46, 92-6.

4- Roizen N,Swisher CN, Stein MA ,Hopkins J,Boyer KM,Holfels E,Mets MB,stein L,Patel D,meier P, Withers S, Remington.

J, Mack D, Heydemann PT,Patton D,McLeod R.(1995) Neurologic and developmental outcome in treated congenital toxoplasmosis .Pediatrics , 95,11-20.

5- Tristran J, Danieal B,Abbal T.(2001).Medical immunology Alange medical book.10th.P.750-56.

6-Ruthlynfield R.and Nicholas G.(1997) Toxoplasmosis . Pediat.

In Rev., 18(3): 75-85

7- Tristran J,Danieal B.Abbal T.(2001).Medical immunology.

Alange medical book.10th ed.P. 750-56.

8- Ho-Yen DO.(1992).Clinical features.In D.0.Ho-Yen, and A.

W.L.Joss(ed), Human toxoplasmosis . Oxford Medical Pubications, oxford. United, Kingdom, 56-78.

9- Ljunstrom I Gille E, Nokes J, Linder E, Forsgren M.(1995) Seroepidemiology of *Toxoplasma gondii* among pregnant women parts og Sweden . Eur J Epidemiol , 11,149-56.

10-Remington JS,McLeod . and Desmonts G (1995) Toxoplasmosis .In Remington ,J.S.and Klein, J.O.(ed). Infectious disease of the fetus and newborn infant, The W.B.saunders Co., Philadelphia th ed.,, P.140-

11- Carter AO, Gelmon SB, Wells GA, Toepell AP.(1989). The effectiveness of a prenatal education programme for the prevention of congenital toxoplasmosis . Epidem infect, 103,539-45.

12-HO-Yen DO , Chatterton JMW.(1990). Congenital Toxoplasmosis – why and how to screen Rev Med Microbiol, 1, 229-35

استخدام المربعات السحرية في بناء الأنظمة الشفرية

Using Magic Squares To Create Cipher System

خلف صالح يوسف* مجيد حميد علي* نسيبه توفيق إبراهيم*

*كلية علوم الحاسبات والرياضيات- جامعة تكريت

تاريخ استلام البحث:2011/3/7 - تاريخ قبول النشر: 2011/5/3

الملخص

تمت دراسة المربعات السحرية (Magic Square) والاستفادة منها في توليد مفاتيح عشوائية "Random Key" لتشفير البيانات والمعلومات ذات الطابع السري، وتنفيذها حاسوبيا باستخدام البرنامج "Matlab"

Abstract

We study Magic Squares, and it uses to generate random keys to cipher the Data and secret information, by using Matlab programming.

المقدمة

أن الغاية الأساسية من تشفير المعلومات هي الحفاظ على سريتها، وهنالك عدة طرق للحفاظ على سرية المعلومات، منها استخدام أنظمة التشفير (Cipher Systems)، والعلم الذي يهتم بتصميم هذه الأنظمة يسمى علم التشفير (Cryptography)، وهنالك عملية أخرى مضادة لعملية التشفير إلا وهي عملية تحليل الشفرة (Cryptanalysis) التي هي عملية استخدام كافة الطرق الممكنة لمهاجمة الشفرة وإيجاد النص الصريح[3] . لذلك العلاقة بين التشفير والتحليل تناسبية. فالمشفر يحاول قدر الإمكان زيادة أمنية الشفرة التي يستخدمها في إرسال المعلومات السرية أما محلل الشفرة فيحاول باستخدام كل الطرق المعروفة في التحليل للوصول إلى النص الواضح. وتعتمد قوة الشفرة على المفتاح المستخدم " Key ". وسنتطرق في بحثنا هذا إلى استخدام المربعات السحرية (Magic Squares) كمفاتيح شفرية.

استخدام المربعات السحرية في بناء الأنظمة الشفرية

خلف صالح يوسف مجيد حميد علي نسيبه توفيق إبراهيم

الهدف من البحث:

لغرض بناء نظام تشفير رصين يصعب كسره ، تم توليد مفاتيح عشوائية من المربعات السحرية وعلى شكل أرقام عشرية (Decimal) يتم تحويلها إلى النظام الثنائي (Binary System) ، حيث يتم تحويل النص الواضح إلى شفرة الاسكي (ASCII) ونعاملها مع المفتاح "Key " المتولد من المربعات السحرية بعملية " XOR " لنحصل على النص المشفر[4].

(Plain text +Key = Cipher text)

ويعرف المربع السحري على انه مصفوفة مربعة تكون مدخلاتها أعداد صحيحة غير متساوية (مختلفة) (من 1 الى n^2) بحيث يكون مجموع المدخلات في كل سطر وعمود وكذلك الأقطار الرئيسية منها مساوية لمقدار ثابت يسمى بالثابت السحري (The Magic Constant)[2] ($\frac{n(n^2+1)}{2}$)، ونستفاد من المربعات السحرية لتوليد عدد هائل من المفاتيح العشوائية[1]. إن عدد المربعات السحرية (4×4) باستخدام الأعداد من 1 الى 16 بالثابت (34) هي 880 مربع سحري، وعدد المربعات السحرية (5×5) باستخدام الأعداد (من 1 الى 25) هو (275305224) ومسالة المربعات السحرية (6×6) فما فوق فإنها تحتاج الى كم هائل من العمليات الحسابية بحيث انه لايمكن استخدام الحاسوب العادي اليوم للتوصل للإجابة وتوجد بعض التقديرات المثبتة هو عدد المربعات السحرية (6×6) باستخدام الإعداد (من 1 الى 36) وبحسب هذه التقديرات فان العدد يفوق(1.7745×10^{19}) من خلال عمليات تبديل اسطر وأعمدة وانعكاسات متعددة ،ان الشكل العام للمربع السحري (4×4) هو

A	B	C	2S-A-B-C
D	2S-A-B-D	2S-A-C-D	2A+B+C+D-2S
3S-2A-B-C-D	A+C+D-S	A+B+D-S	S-D
A+B+C-S	S-C	S-B	S-A

حيث ان (A,B,C,D,S) هي متغيرات حرة وشكل المربع سوف يعتمد على هذه المتغيرات وهو يحتوي على عدد غير منتهي من الحلول للمربع، ولو فرضنا ان (A=16,B=2,C=3,D=5,S=17) فإننا نحصل على المربع السحري التالي:

16	2	3	13
5	11	10	8
9	7	6	12
4	14	15	1

الجانب النظري:

الخطوة الأولى

في البداية يتم تحويل النص المراد تشفيره إلى رمز الاسكي (ASCII code) وهي إلترميزه الأمريكية القياسية لتبادل المعلومات وهي رمز بطول (8) بت بحيث يمكن تشغيل (128) رمز مختلف وهي كافية للأحرف الكبيرة والصغيرة والأعداد والرموز الأخرى . وفي هذه الشفرة تمثل الأعداد العشرية من (65)إلى (90) (في النظام الثنائي من 1000001 إلى 1011010) للحروف الإنكليزية الكبيرة (منA إلىZ) وتستخدم الأعداد الأخرى لتمثيل علامات الترقيم والحروف الصغيرة والأرقام[5] .

الأحرف	ASCII	الأحرف	ASCII	الأحرف	ASCII
A	01000001	J	01001010	S	01010011
B	01000010	K	01001011	T	01010100
C	01000011	L	01001100	U	01010101
D	01000100	M	01001101	V	01010110
E	01000101	N	01001101	W	01010111
F	01000110	O	01001111	X	01011000
G	01000111	P	01010000	Y	01011001
H	01001000	Q	01010001	Z	01011010
I	01001001	R	01010010		

الخطوة الثانية

نولد أرقام عشوائية من المربعات السحرية وبأبعاد (n×n) .وبأخذ (mod 128) ، ثم نقوم بتحويلها إلى النظام الثنائي.

الخطوة الثالثة

نقوم بعملية جمع النص المشفر بالاسكي مع الأرقام العشوائية (Key) المتولدة من المربعات السحرية وبطريقة (XOR)المنطقية وجدولها كآلاتي :

X	Y	XOR
0	0	0
0	1	1
1	0	1
1	1	0

وبذلك نحصل على النص المشفر .

أما عملية حل الشفرة: فنقوم بجمع النص المشفر مع المفتاح (Key) للحصول على النص الواضح حيث إن المفتاح يكون معروفا لدى الطرفين (المرسل والمستلم).

الجانب العملي : إذا أردنا تشفير النص الواضح (UNIVERSITY) وباستخدام المربع السحري (13×13)

الحل: نحول النص الواضح إلى رمز ال(ASCII)، نقوم بتوليد المربع السحري (13×13) باستخدام برنامج ال(Matlab)

93	108	123	138	153	168	1	16	31	46	61	76	91
107	122	137	152	167	13	15	30	45	60	75	90	92
121	136	151	166	12	14	29	44	59	74	89	104	106
135	150	165	11	26	28	43	58	73	88	103	105	120
149	164	10	25	27	42	57	72	87	102	117	119	134
163	9	24	39	41	56	71	86	101	116	118	133	148
8	23	38	40	55	70	85	100	115	130	132	147	162
22	37	52	54	69	84	99	114	129	131	146	161	7
36	51	53	68	83	98	113	128	143	145	160	6	21
50	65	67	82	97	112	127	142	144	159	5	20	35
64	66	81	96	111	126	141	156	158	4	19	34	49
78	80	95	110	125	140	155	157	3	18	33	48	63
79	94	109	124	139	154	169	2	17	32	47	62	77

لو أخذنا المجاميع العشرة الأولى (المستخدمة كمفاتيح للتشفير) وباستخدام (mod 128) ثم نقوم بتحويلها إلى النظام الثنائي فتصبح كالأتي.

Key	Key (mod 128)	Binary
93	93	01011101
108	108	00011011
123	123	00101111
138	10	00101000
153	25	01001100
168	40	00001010
1	1	01000000
16	16	00000100
31	31	01111100
46	46	00111010

اختبار عشوائية المفاتيح المتولدة من المربعات السحرية:

تم إجراء عدة اختبارات إحصائية على السلسلة المتولدة من المربعات السحرية والتي استخدمت كمفاتيح بعد تحويلها الى النظام الثنائي وهي

01011101, 00011011, 00101111, 00101000, 01001100, 00001010, 01000000, 00000100, 01111100, 00111010

ومن هذه الاختبارات:

1-اختبار التردد (frequency test): القانون الرياضي

حيث (n_0) عدد الاصفار في السلسلة

(n_1) عدد الواحدات في السلسلة

(n) طول السلسلة (المفتاح)

علما" بان الاختبار يكون ناجحا" اذا كان $\chi^2 < 3.84$ لدرجة حرية واحدة حيث ان $\chi^2_{0.05} = 3.84$ (من جدول χ^2) وعليه فان الاختبار ناجح لان $3.2 < 3.84$.

1- **اختبار التسلسل (Serial test):** القانون الرياضي

01=10 ,10 = 10 , 00 = 13 ,11 = 17

$\chi^2 = 3.2$ علما" بان قيمة χ^2 الجدولية هي لدرجتي حرية هي (5.99) وعليه $3.2 < 5.99$

فان السلسلة قد اجتازت الاختبار.

2- اختبار بوكر (Poker test): القانون الرياضي

نفرض (m=4) طول المقطع، $F = \frac{n}{m}$ عدد المقاطع من التطبيق أعلاه $\chi^2 = 2$ $\frac{\text{طول الرسالة}}{\text{طول المقطع}}$

علما" بان الاختبار يكون ناجحا" إذا كان اقل من قيمة χ^2 الجدولية لدرجة حرية (2^m-1) قيمة χ^2لدرجة حرية (2^4-1=15) تساوي *25* ، الاختبار ناجح لان $25 < 2$.

وكذلك اجتازت اختبار الجريان (Run test)، واختبار التطابق الذاتي (Autocorrelation)

ألان نقوم بعملية جمع النص المرمز بالاسكي مع الأرقام العشوائية المتولدة والتي تم تحويلها إلى النظام الثنائي

Text	X=Plain Text	Y=Key	Cipher Text
U	01010101	01011101	00001000
N	00111001	00011011	00100010
I	01001001	00101111	01100110
V	00110101	00101000	00011101
E	01010001	01001100	00011101
R	00100101	00001010	00101111
S	01100101	01000000	00100101
I	01001001	00000100	01001101
T	00010101	01111100	01101001
Y	01001101	00111010	01110111

يصبح النص المشفر كالأتي:

00001000 00100010 01100110 00011101 00011101

00101111 00100101 01001101 01101001 01110111

ويمكن تقطيعه إلى مجاميع خماسية جاهزة للإرسال وكما يلي:

00001, 00000,10001,00110,01100,00111,01000,11101,

00101, 11100,10010,10100,11010,11010,01011,10111

أما إذا أردنا حل النص المشفر أعلاه فنتبع الخطوات التالية:

الخطوة الأولى: نحول النص المشفر الأتي:

00001, 00000,10001,00110,01100,00111,01000,11101,

00101, 11100,10010,10100,11010,11010,01011,10111

إلى مجاميع ثمانية

0001000 0100010 1100110 0011101 0011101

0101111 0100101 1001101 1101001 1110111

الخطوة الثانية: نعامل النص المشفر مع المفتاح المستخدم (المتولد في المربعات السحرية) بعملية XOR ثم نستخدم شفرة الASCII لنحصل على النص الواضح.

Cipher Text	Y=Key	X=Plain Text	Text
00001000	01011101	01010101	U
00100010	00011011	00111001	N
01100110	00101111	01001001	I
00011101	00101000	00110101	V
00011101	01001100	01010001	E
00101111	00001010	00100101	R
00100101	01000000	01100101	S
01001101	00000100	01001001	I
01101001	01111100	00010101	T
01110111	00111010	01001101	Y

فنحصل على النص الواضح : University

الاستنتاجات والتوصيات:

الاستنتاجات:

1- باستخدام المربعات السحرية تكون خيارات التوليد كثيرة ومختلفة، حيث ان المربع السحري الذي أبعاده (5×5) يكون عدد المفاتيح المتولدة منه(275) مليون حيث يصعب كسره[4].

2- باستخدام المربعات السحرية حصلنا على أرقام عشوائية اجتازت الاختبارات الإحصائية الخاصة بالعشوائية.

التوصيات:

1-برمجة خوارزمية التشفير بأكملها والحل حاسوبيا" اختصارا" للوقت والجهد

وسرعة المعلومات للاستفادة منها.

2-التوسع في استخدام المربعات السحرية ذو الرتب العليا .

3-مكننة الخوارزمية لصنع جهاز يقوم بعملية التشفير والحل .

المصادر:

1- الأشهب، سليم شفيق، 2000، **نظرية المربعات السحرية برمجيا ورياضيا**، ط1،سلسلة للبحوث العلمية (1) الأردن.

2- ألآمري، مجيد حميد، **دراسة حول الفضاء الصفري للمربعات السحرية المركبة**،رسالة ماجستير، الأردن، 2008.

3- الحمداني، وسيم عبدالامير، **أنظمة التشفير**، الجامعة التكنولوجية، 1997.

4-K. Pinn and C. Wieczerkowski, **Number of Magic Squares From Parallel Tempering Monte Carlo**, ar Xiv:cond-mat/984109v1, Germany, 9 Apr. 1998.

5-Stallings, William, **Cryptography and Network Security Principles and practice**, third edition, prentice-Hall of India, New Delhi, 2005.

إنتاج إنزيم الهيمولايسين Hemolysin مـــن العـــزلـــة المحـلية لبكـتريا *Vibrio cholerae* المعزولة من مرضى مصابين بالإسهال

***محمد ابراهيم نادر **مثنى عبد القادر صالح المهداوي *ايناس يوسف**

*فرع التقنية الاحيائية–معهد الهندسة الوراثية والتقنيات الاحيائية للدراسات العليا.

** قسم علوم الحياة –كلية العلوم–جامعة ديالى

تاريخ استلام البحث:2010/9/20 - **تاريخ قبول النشر:** 2011/11/20

الخلاصة

شخصت 26 عزلة بكترية تعود لبكتريا الكوليرا *V. cholerae* المعزولة من أشخاص مصابين بالإسهال، اختبرت قابلية العزلات لإنتاج إنزيم الهيمولايسين Hemolysin. أظهرت النتائج المتحصل عليها من الغربلة شبة الكمية على وسط اكار الدم المغذي المضاف له 7% من دم الانسان، إن جميع العزلات لها القابلية على إنتاج إنزيم الهيمولايسين، و باعتماد مقايسة الحالة الدموية Hymolytic assay ظهر ان العزلة المحلية AMK6 هي الأكفأ في إنتاج الهيمولايسين.

حددت الظروف المثلى لإنتاج إنزيم الهيمولايسين باستخدام الوسط الغذائي مرق نقيع القلب و الدماغ الحاوي على 3% كليسرول والملح بـ 2% من اللقاح البكتيري بتركيز $3x10^8$ cell / ml عند رقم هيدروجيني 8 و بدرجة حرارة35مْ في حاضنة هزازة بسرعة 120 rpm لمدة 24 ساعة.

Abstract

Diagnosed 26 isolate of *vibrio cholera* was isolated from clinical sources responsible of causing diarrhea. All isolates showed high productivity of hemolysin by different efficiency. Semi quantitative screening on a selective solid medium (blood ager additive 7% blood) showed that all isolates have the ability to produce hemolysin as indicated by the formation of clear zone around the colonies.

The selected isolate characterized as *Vibrio cholera* AMK6 based on its high production of enzyme and used in the present study. The optimum conditions for hemolysin production by submerged cultures (brain heart infusion containing 3%Glycerol) with an inoculums size of $3x10^8$ CFU at an initial pH of 8 with shaking incubation at 35°C, 150 cycle/min for 24 hours.

Vibrio cholera , hemolysin production

إنتاج إنزيم الهيمولايسين Hemolysin مـــن العـــزلـــة المحـلية لبكـتريا *Vibrio cholerae* المعزولة من مرضى مصابين بالإسهال

محمد ابراهيم نادر- مثنى عبد القادر صالح المهداوي -ايناس يوسف

المقدمة

الكوليرا من أهم الأمراض الخطيرة المنتشرة بشكل واسع في أنحاء العالم وخاصة الدول النامية. يسبب الوفاة لإعداد كبيرة من المصابينسنوياً وخاصة في حالات الإصابة الشديدة وغير المعالجة. إذ تعتمد ا قابلية بكتريا الكوليرا على إحداث الإصابة إلى وجود العديد من العوامل الإضافية التي تميزها عن البكتريا غير المرضية وتدعى بعوامل الضراوة Virulence Factor، التي يوجد بعضها ضمن التركيب الخلوي وبعضها الآخر يفرز إلى خارج الخلية مثل الإنزيمات والذيفانات المختلفة، هذه العوامل قد تكون نوعية أو مشتركة لعدد من البكتريا المختلفة. كما انه من النادر أن يعمل أي عامل من عوامل الضراوة بشكل منفرد أو مستقل عن البكتريا نفسها، أما الذيفانات البكتيرية فتعد من عوامل الضراوة الأهم لقدرة أنواع عديدة منها على إحداث المرض بشـكل ذاتـي مباشر [1].

تمتلك بكتريا الكوليرا العديد من عوامل الضراوة التي تؤهلها للإصابات المعوية و إحداث المرض، منها قابليتها على الالتصاق بالخلايا الطلائية المبطنة للأمعاء الدقيقة، و إنتاجها للعديد من الذيفانات الداخلية Endotoxins و الذيفانات الخارجية Exotoxins و التي تتضمن أنواع عديدة أهمها الذيفانات المعوية Enterotoxins المتمثلة بذيفان الكوليرا Cholera toxin(Choleragen) و الذي يعد من أهم عوامل ضراوة بكتريا الكوليرا، و كذلك ذيفانات Cytotoxin و Hemolysin، إضافة لأنواع أخرى من الذيفانات [2].

يلعب الهيمولايسين، الذي يعد من الذيفانات الخارج خلوية Exotoxins، دورا" واضحا" في إحداث الإمراضيه من خلال تأثيره على أغشية الخلايا وتحللها عن طريق إحداث الثقوب فيها، من أهم هذه الخلايا هي خلايا الدم الحمراء Erythrocyte للإنسان وللحيوان [3]. لهذه الذيفانات فعاليات حيوية إضافة للفعالية التحليلية للدم Hemolytic activity من أهمها Enterotoxicity و Cardiotoxicity [4].نظراً لتفشي مرض الكوليرا في بلدنا هدفت هذه الدراسة إلى التحري عن إنتاج إنزيم الهيمولايسين من بكتريا الكوليرا، وتحديد الظروف المثلى لإنتاج إنزيم الهيمولايسين و الذي يلعب دورا" مهما" في إحداث الإمراضية.

المواد وطرائق العمل

مصادر العزلات

تم الحصول على 26عزلة من بكتريا Vibrio cholerae من مختبر الصحة المركزي مشخصة تشخيص اولي. أعيد تشخيص العزلات البكتيرية اعتماداً على تصنيف Bergey's الوارد في Holt *et al* [5] وفقا" للطرائق المستخدمة من قبل منظمة الصحة العالمية [6]. وبالاعتماد على الصفات المظهرية والاختبارات الكيموحيوية في التشخيص.

التحري عن قابلية الضمات لإنتاج الهيمولايسين

اختبر 26 عزلة من بكتريا الكوليرا لتحديد العزلة الأكفاء في قابلية إنتاج إنزيم الهيمولايسين عن طريق الغربلة.

الغربلة شبه الكمية للعزلات

تمت غربلت العزلات البكترية للتحري عن قابليتها في إنتاج الهيمولايسين بنقل جزء من مستعمراتها النامية على وسط الاكار المغذي إلى إطباق حاوية على وسط الدم باستخدام عود خشبي Stick، ثم حضنت لمدة (24) ساعة بدرجة حرارة (37)ْ تحت ظروف هوائية، وبعد انتهاء مدة الحضن لوحظ ظهور مناطق تحلل الدم حول المستعمرات النامية بحيث كان التحلل واضحاً ومن نوع بيتا (β–hemolysin)، إذ يدل ذلك على قابلية هذه البكتريا على تحلل خلايا الدم الحمراء لإنتاجها إنزيم الهيمولايسين و قيست أقطار التحلل حول المستعمرات النامية.

تقدير فعالية الإنزيم

عملت مقايسة الحالة الدموية لكل نموذج لتحديد العزلات الأكثر إنتاجاً للهيمولايسين باستخدام عالق خلايا الدم الحمراء للإنسان. و حسب الطريقة المتبعة من قبل الكرخي [7].

تقدير فعالية إنزيم الهيمولايسين

اعتمدت طريقة Namdari و Bottone [8] لتقدير فعالية الإنزيم بأضافة 1 مليلتر من عالق كريات الدم الحمر إلى 0.5 مليلتر من المستخلص (مزروع خلايا بكتريا الكوليرا النامية في وسط نقيع القلب والدماغ بدرجة 37مْ)، وحضن في درجة حرارة 37 مْ مدة 60 دقيقة، ثم قرئت بجهاز المطياف الضوئي وبطول موجي 544 نانومتر لقياس الخلايا المتحللة من كريات الدم الحمر. حضر المحلول الكفء (Blank) بإضافة عالق كريات الدم الحمر مع 0.5 مليلتر من محلول دارئ الفوسفات الملحي (PBS)، وسجلت الفعالية التحللية (Haemolytic unit) على إنها الحد الأدنى من النموذج اللازم لإنتاج 50% من التحلل.

تحديد العزلة البكتيرية الأكفأ إنتاجا" للهيمولايسين

بالاعتماد على الغربلة الشبة الكمية و على مقايسة الحالة الدموية تم اختيار العزلة الأكثر إنتاجا" لإنزيم الهيمولايسين اذ أظهرت اعلى فعالية نوعية مقارنة ببقية العزلات.

تحديد الوسط الزرعي الامثل لإنتاج الهيمولايسين

اختبرت كفاءة العزلة المختارة في إنتاج الهيمولايسين وذلك باستعمال ستة أوساط زرعيه وهي وسط المرق المغذي، وسط مرق نقيع القلب و الدماغ، وسط إنتاج الهـيمولايسين (Minimal media(MM، وسط إنتاج الهيمولايسين (MGmedia)، وسط MM +Blood(1%) و وسط MG+Blood(1%).

حضرت الأوساط الزراعية السابقة بحجم 100 مليلتر في دوارق مخروطية سعة 250 مليلتر، ثم لقحت الدوارق بحجم2 مليلتر من اللقاح البكتيري بتركيز $3x10^8$ cell/ml و حضنت الدوارق بالحاضنة بدرجة حرارة 37مْ لمدة 24ساعة، ثم نبذ المزروع بسرعة (7000 دورة/دقيقة) لمدة 15 دقيقة، جمع رائق كل عزلة في أنبوبة اختبار معقمة لتقدير فعالية الإنزيم.

تعيين الرقم الهيدروجيني الامثل لإنتاج الهيمولايسين

استخدم وسط مرق نقيع القلب والدماغ للإنتاج، حضر الوسط بأرقام هيدروجينية متدرجة -8 -7.5 -7 -6.5 -6) (8.5 لتحديد الرقم الهيدروجيني الأمثل لإنتاج الهيمولايسين.

تحديد زمن الحضن الامثل لإنتاج الهيمولايسين

لقح وسط مرق نقيع القلب والدماغ ذو رقم هيدروجيني 8 بنسبة 2% من اللقاح البكتيري بتركيز $3x10^8$ cell/ml وحضنت الأوساط بالحاضنة بدرجة حرارة37مْ لمدة (72-48-24) ساعة، ثم نبذ المزروع بسرعة (7000 دورة/دقيقة) لمدة 15 دقيقة، جمع رائق كل عزلة في أنبوبة اختبار معقمة لتقدير فعالية الإنزيم.

تحديد مصدر الكاربون الامثل لإنتاج إنزيم الهيمولايسين

اختبرت كفاءة المصادر الكربونية (Glucose-Sucrose-Dextrose-Maltose-Glycerol) بتركيز 3% لإنتاج إنزيم الهيمولايسين. لقح وسط مرق نقيع القلب والدماغ ذو رقم هيدروجيني 8 بنسبة 2% من اللقاح البكتيري بتركيز $3x10^8$ cell/ml وحضنت الأوساط بالحاضنة بدرجة حرارة37مْ لمدة24 ساعة، ثم نبذ المزروع بسرعة (7000 دورة / دقيقة) لمدة 15 دقيقة ، جمع رائق كل عزلة في أنبوبة اختبار معقمة لتقدير فعالية الإنزيم

تحديد التركيز الامثل للمصدر الكاربوني

اختبرت تراكيز مختلفة من الكليسرول في وسط الإنتاج تضمنت (3-2.5-2-1.5-1-0.5)% لتحديد أي منها الأمثل لإنتاج الإنزيم.

تحديد المصدر النتروجيني الامثل لإنتاج الهيمولايسين

اختبرت اربع مصادر للنتروجين تضمنت (Pepton-Trypton-Urea-NH3) و بتركيز 3% لإنتاج إنزيم الهيمولايسين.

تحديد التركيز الامثل للمصدر النتروجيني

اختبرت تراكيز مختلفة من البيتون في وسط الإنتاج تضمنت (3-2.5-2-1.5-1-0.5)% لتحديد تاثيرها في إنتاج الهيمولايسين

تعيين درجة الحرارة المثلى لإنتاج الهيمولايسين

حضن وسط الإنتاج الملقح بالعزلة المنتجة لإنزيم الهيمولايسين بدرجات حرارة مختلفة تضمنت (25-30-35-37-40-45) لتحديد درجة الحرارة المثلى لإنتاج الهيمولايسين.

تاثير التهوية في إنتاج الهيمولايسين

لقح دورقان مخروطيان حاويان على وسط الإنتاج بالعزلة المنتجة لإنزيم الهيمولايسين ثم حضنت بدرجة حرارة 37مْ، الأول في حاضنة هزازه(Shaking incubator) بسرعة 120rpm ، والثاني بحاضنة غير متحركة Stationary incubator لتحديد تاثير التهوية في إنتاج الهيمولايسين.

النتائج والمناقشة

العزل و التشخيص

تم الحصول على 26 عزلة بكتيرية من مختبر الصحة المركزي مشخصة اوليا" على انها ضمات الكوليرا *Vibrio cholerae*، أعيد تشخيص العزلات للتأكيد اعتمادا" على تصنيف Bergey's الوارد في [2] و الطرائق المستخدمة من قبل منظمة الصحة العالمية و استخدام نظام Api E 20 للعائلة المعوية.

التحري عن قابلية البكتريا على إنتاج إنزيم الهيمولايسين

اختبرت قابلية جميع العزلات البكتيرية الـ26 على إنتاج إنزيم الهيمولايسين بتنميتها على أطباق حاوية على أكار الدم الأساس المضاف له 7% دم بشري و حضنها بدرجة حرارة 37مْ لمدة 24 ساعة. أظهرت جميع العزلات قابلية على تحلل الدم بشكل

كامل متمثلا بظهور هالة شفافة حول المستعمرات دلالة على قابلية هذه العزلات على إنتاج إنزيم الهيمولايسين من نوع بيتا. كانت نتائج قطر المنطقة الشفافة التي أحدثتها هذه العزلات كما موضحة في الجدول(1).

الجدول(1) اقطار التحلل التي احدثها إنزيم الهيمولايسين

رقم العزلة ورمزها	قطر منطقة التحلل (mm)
AMK 1	1
AMK 2	1
AMK 3	2
AMK 4	3
AMK 5	3
AMK 6	6
AMK 7	1
AMK 8	1
AMK 9	2
AMK 10	1
AMK 11	2
AMK 12	4
AMK 13	5
AMK 14	4
AMK 15	3
AMK 16	2
AMK 17	5
AMK 18	4
AMK 19	2
AMK 20	3
AMK 21	6
AMK 22	6
AMK 23	4
AMK 24	6
AMK 25	5
AMK 26	6

اختيار العزلة الاكثر إنتاجا" للهيمولايسين

بالاعتماد على الغربلة شبة الكمية و على مقايسة الحالة الدموية تم اختيار العزلة الاكثر إنتاجا" لإنزيم الهيمولايسين، و هي العزلة AMK6 اذ أظهرت اعلى فعالية مقارنة ببقية العزلات الاخرى وكانت الفعالية 640 وحدة/مليلتر (الجدول 2).

تعيين الظروف المثلى لإنتاج الهيمولايسين

تم تعيين الظروف المثلى لإنتاج الهيمولايسين من خلال اختيار متطلبات النمو التالية:

إنتاج إنزيم الهيمولايسين Hemolysin مـــن العـــزلـــة المحـلية لبكـتريا

Vibrio cholerae المعزولة من مرضى مصابين بالإسهال

محمد ابراهيم نادر- مثنى عبد القادر صالح المهداوي -ايناس يوسف

جدول(2) فعالية الهيمولايسين المنتج من العزلات باستخدام مقايسة الحالة الدموية

رقم العزلة ورمزها	الفعالية (وحدة/مليلتر)
AMK 1	80
AMK 2	80
AMK 3	80
AMK 4	160
AMK 5	320
AMK 6	640
AMK 7	80
AMK 8	80
AMK 9	160
AMK 10	80
AMK 11	80
AMK 12	320
AMK 13	320
AMK 14	320
AMK 15	160
AMK 16	80
AMK 17	160
AMK 18	160
AMK 19	80
AMK 20	160
AMK 21	640
AMK 22	320
AMK 23	160
AMK 24	320
AMK 25	320
AMK 26	320

إنتاج إنزيم الهيمولايسين Hemolysin مـــن العـــزلـــة المحـلية لبكـتريا

***Vibrio cholerae* المعزولة من مرضى مصابين بالإسهال**

محمد ابراهيم نادر- مثنى عبد القادر صالح المهداوي -ايناس يوسف

اختيار الوسط الزرعي الامثل لإنتاج الإنزيم

اختيرت أربع أوساط زرعيه مختلفة في محتوياتها من المصادر الكربونية و النتروجينية لتحدد الوسط ألزرعي الأمثل لإنتاج الهيمولايسين من العزلة رقم AMK6 لبكتريا *V. cholerae*. بينت النتائج الموضحة في الشكل(1) إن الوسط ألزرعي مرق نقيع القلب و الدماغ يعطي أعلى إنتاجية لإنزيم الهيمولايسين اذ بلغت قيمة الفعالية 640 وحدة/مليلتر وهو الوسط الأمثل للإنتاج، ثم يليه وسط Minimal Media المضاف له 1% من دم بشري وبفعالية قدرها 80 وحدة /مليلتر في حين انخفضت إنتاجية الإنزيم في الأوساط (MG+1%Blood; MM; Nutrient broth)، إذ بلغت الفعالية 40 وحدة/ مليلتر.

تحديد الرقم الهيدروجيني الأمثل لإنتاج الإنزيم

بينت اختبارات قدرة العزلة رقم AMK6 على إنتاج إنزيم الهيمولايسين باستخدام وسط نمو بقيم أرقام هيدروجينية مختلفة تراوحت بين (6-9) إن أعلى فعالية لإنزيم الهيمولايسين من العزلة المحلية AMK6 بلغت 640 وحدة/مليلتر عند الرقم الهيدروجيني 8. و تلاشت فعالية الإنزيم عند ارتفاع قيمة الأس الهيدروجيني في وسط النمو إلى 8.5 و 9 حيث بلغت الفعالية 0 وحدة/مليلتر. في حين كانت الفعالية 320 وحدة/مليلتر عند قيم الأس الهيدروجينية 7 و7.5 و انخفضت الفعالية مع انخفاض قيمة الاس الهيدروجيني اذ وصلت الى 160 وحدة/مليلتر عند الاس الهيدروجيني6 و 6.5 ، كما موضح في الشكل (2).

مدة الحضن

اختبرت إنتاجية إنزيم الهيمولايسين من قبل العزلة رقم AMK6 و في مدد زمنية مختلفة تراوحت بين 24-72 ساعة كما مبين في الشكل (3). و أظهرت النتائج إن مدة الحضن المثلى لإنتاج الإنزيم كانت بعد 24 ساعة من الحضن إذ بلغت قيمة الفعالية 640 وحدة/مليلتر، و ربما يرجع السبب إلى إن إنزيم الهيمولايسين يعد من مواد الايض الاولي التي تنتج وتفرز في الطور اللوغارتمي المتأخر. لذا تكون أعلى فعالية للإنتاج بعد 24 ساعة و بزيادة فترة الحضن يتعرض الإنزيم للتحلل من خلال فعالية إنزيم البروتيز الذي يفرز في نهاية الطور اللوغارتمي و بداية طور الثبوت من النمو، كما مسجل في بكتريا الـ *A. hydrophila*، وهذا ما أشارت إليه الدراسات التي قام بها بعض الباحثون و التي أوضحت إن مدة الحضن المثلى هي 20 ساعة [9] [10,11].

مصدر الكاربون و التركيز الأمثل للإنتاج

تؤثر مكونات الوسط ألزرعي في نمو و تكاثر الكائن ألمجهري و قدرته على إنتاج الإنزيمات، إذ درس تأثير إضافة المصادر الكربونية المختلفة (الكلوكوز ،السكروز ، الدكستروز ، المالتوز والكليسرول) كمصادر وحيدة للكربون في الوسط ألزرعي. و أظهرت النتائج إن الوسط ألزرعي المحتوي على الكليسرول كان الأفضل في إنتاج الهيمولايسين، وكما موضح في الشكل (4)، اذ بلغت الفعالية 2560 وحدة/مليلتر. وانخفضت الإنتاجية عند استخدام مصادر الكربون الأخرى، التي تشمل الدكستروز ، السكروز ، المالتوز و الكلوكوز و بفعالية قدرها 1280، 640,640 و320 وحدة/مليلتر على التوالي.

لغرض تثبيت التركيز الأمثل للمصدر الكربوني (الكليسرول) انتخبت التراكيز الآتية 0.5 و1و1.5 و2و 2.5و3% و أظهرت النتائج المبينة في الشكل (5) حصول زيادة تدريجية في إنتاجية إنزيم الهيمولايسين مع زيادة تركيز الكليسرول، اذ سجلت أعلى فعالية تحليلية للإنزيم والتي بلغت 2560 وحدة /مليلتر عند قيمة 2.5 و3 %. وبذلك اعتبر التركيز 2.5% من الكليسرول التركيز الأمثل لإنتاج إنزيم الهيمولايسين.

مصدر النتروجين و التركيز الامثل للإنتاج

درس تأثير المصادر النتروجينية المختلفة (ببتون، تربتون، يوريا و امونيا) في إنتاج الهيمولايسين من العزلة رقم AMK6 لبكتريا الكوليرا بتركيز 3%لكل منها. و قد بينت النتائج الواردة في الشكل (6) إن أعلى فعالية للهيمولايسين و بلغت 2560 وحدة/مليلتر كانت في الوسط المحتوي على الببتون اذ اعتبر مصدر النتروجيني الامثل للإنتاج ، بينما كانت الفعالية للهيمولايسين عند استخدام اليوريا و التربتون و الامونيا هي 1280 ، 640 ، 320 وحدة/مليلتر على التوالي.

إنتاج إنزيم الهيمولايسين Hemolysin مـــن العـــزلـــة المحـلية لبكـتريا

***Vibrio cholerae* المعزولة من مرضى مصابين بالإسهال**

محمد ابراهيم نادر- مثنى عبد القادر صالح المهداوي -ايناس يوسف

لغرض تثبيت التركيز الأمثل للمصدر النتروجيني (البيتون)انتخبت التراكيز الاتية 0.5 و1و1.5 و2و 2.5و3% و أظهرت النتائج المبينة في الشكل (7) حصول زيادة تدريجية في إنتاج الهيمولايسين عند زيادة في تركيز البيتون اذ سجلت النتائج فعالية قدرها 640 وحدة /مليلتر عند التراكيز 0.5و1 %من البيتون و فعالية قدرها 1280 وحدة/مليلتر عند التركيز 2% كما ان اعلى قيمة للفعالية قد سجلت عند التراكيز2و2.5و3% و التي بلغت 2560 وحدة /مليلتر و اعتبر التركيز 2% التركيز الامثل لإنتاج الهيمولايسين.

الحرارة المثلى لإنتاج الإنزيم

نميت العزلة رقم AMK6 من بكتريا الكوليرا بدرجات حرارة مختلفة بين 25- 45م لإنتاج إنزيم الهيمولايسين و أشارت النتائج المبينة في الشكل (8) حصول زيادة تدريجية في إنتاج الهيمولايسين عند زيادة درجات الحرارة إلى حد معين ثم تعود لتنخفض الإنتاجية، فقد بلغت فعالية الهيمولايسين 320 و1280 وحدة/مليلتر عند درجة حرارة 25 و30مْ على التوالي. وان أعلى إنتاجية لإنزيم الهيمولايسين كانت عند درجات الحرارة 35 و37مْ إذ بلغت قيمة الفعالية 2560 وحدة/مليلتر، ثم عادت لتنخفض الإنتاجية عند درجات الحرارة 40و 45مْ لتصل الفعالية إلى 80 و0 وحدة/مليلتر على التوالي.

تأثير التهوية في إنتاج الهيمولايسين

بينت هذه الدراسة تاثير التهوية و التحريك في إنتاج إنزيم الهيمولايسين فقد أظهرت النتائج كما في الشكل (9) زيادة إنتاج إنزيم الهيمولايسين من العزلة المحلية AMK6 باستخدام التحريك بسرعة 120 دورة/دقيقة، إذ بلغت الفعالية 5120 وحدة/مليلتر في حين كانت الفعالية عند الثبات 2560 وحدة/ مليلتر.

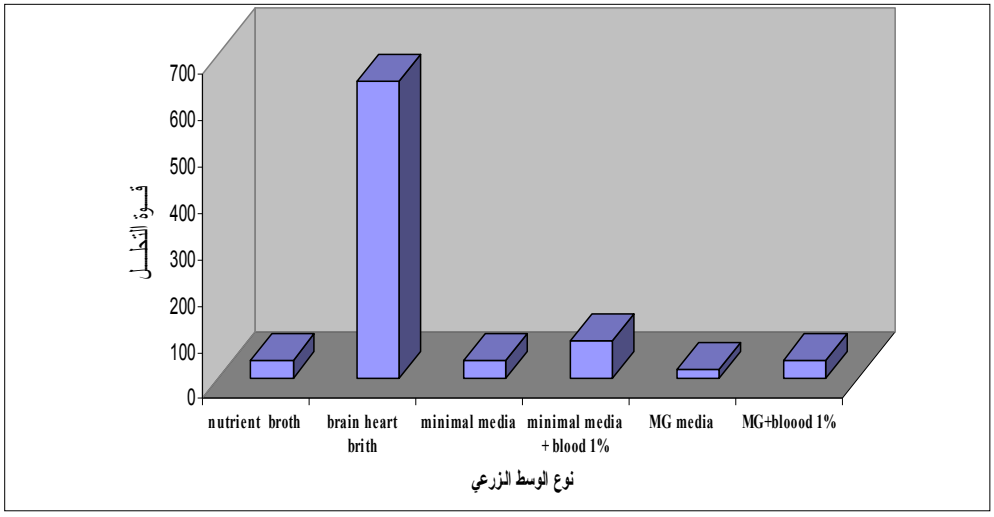

الشكل(1) تحديد الوسط الزرعي الامثل لإنتاج إنزيم الهيمولايسين من العزلة المحلية لبكتريا الكوليرا AMK6

إنتاج إنزيم الهيمولايسين Hemolysin مـــن العـــزلـــة المحـلية لبكـتريا

Vibrio cholerae المعزولة من مرضى مصابين بالإسهال

محمد ابراهيم نادر- مثنى عبد القادر صالح المهداوي -ايناس يوسف

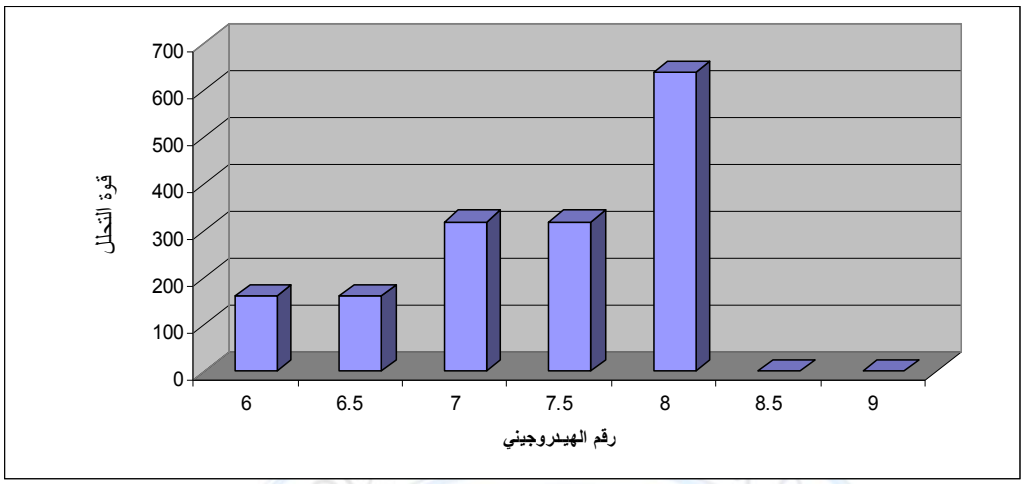

الشكل رقم (2) تأثير الرقم الهيدروجيني في إنتاج إنزيم الهيمولايسين.

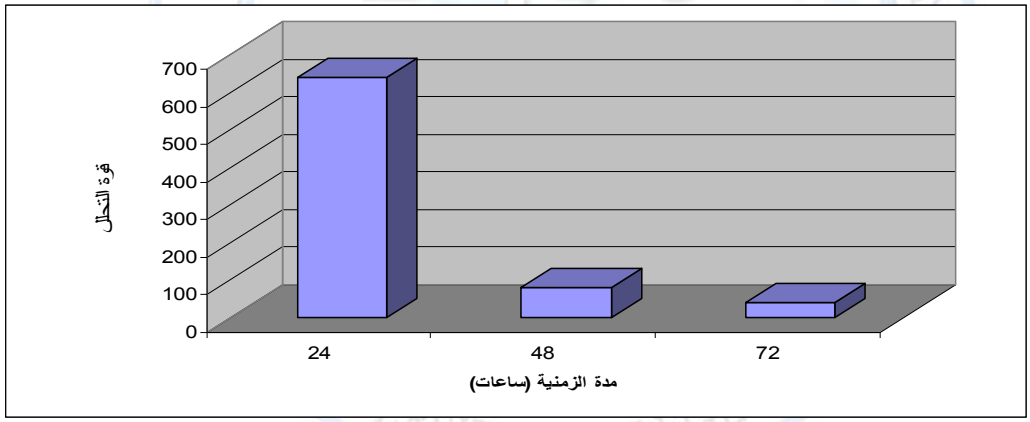

الشكل (3) مدة الحضن المثلى لإنتاج الهيمولايسين

إنتاج إنزيم الهيمولايسين Hemolysin مـــن العـــزلـــة المحـلية لبكـتريا

Vibrio cholerae المعزولة من مرضى مصابين بالإسهال

محمد ابراهيم نادر- مثنى عبد القادر صالح المهداوي -ايناس يوسف

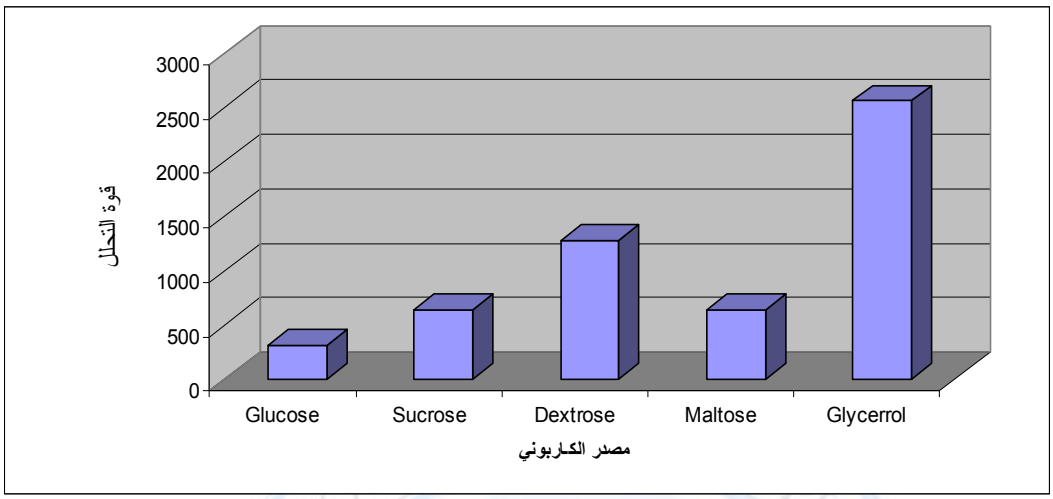

الشكل (4) تأثير المصادر الكربونية المختلفة في إنتاج إنزيم الهيمولايسين من العزلة المحلية لبكتريا الكوليرا AMK6

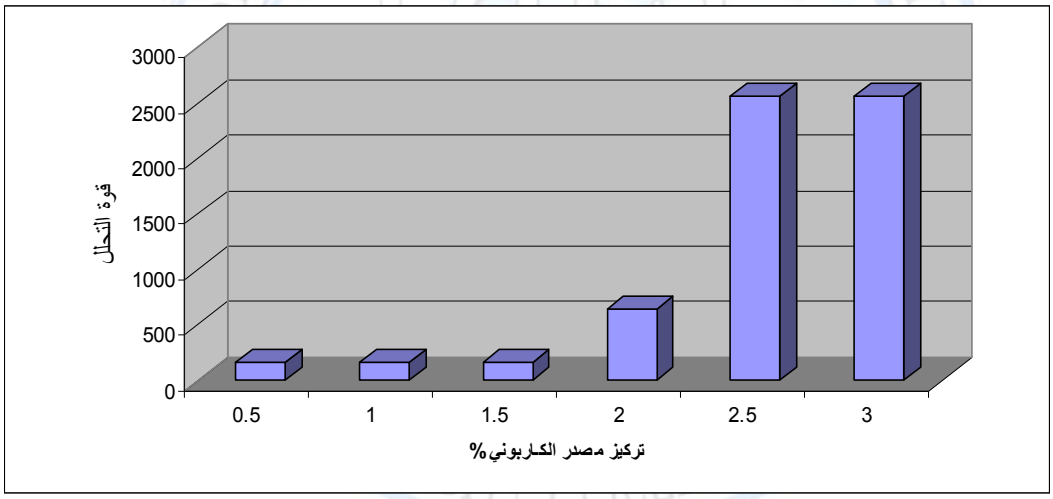

الشكل (5) تأثير التراكيز المختلفة للكليسرول كمصدر كربوني في إنتاج إنزيم الهيمولايسين

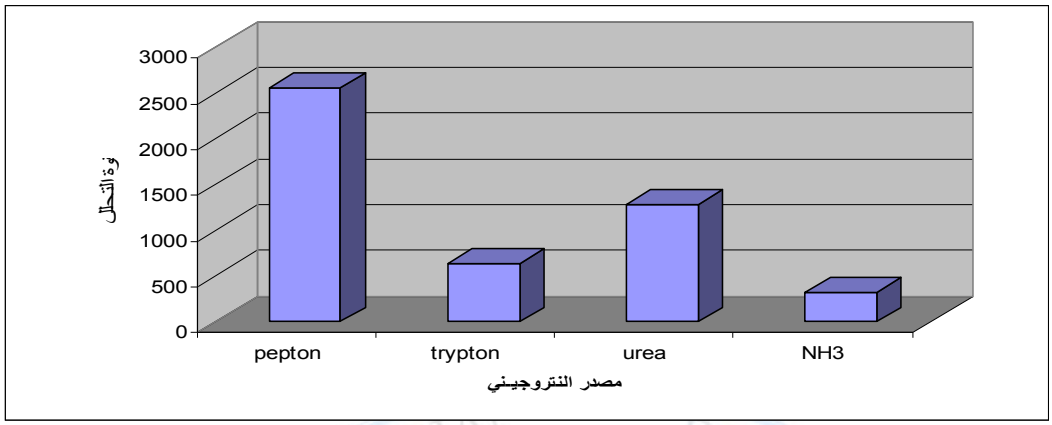

الشكل (6) تأثير المصادر النتروجينية المختلفة في إنتاج إنزيم الهيمولايسين من العزلة المحلية لبكتريا الكوليرا AMK6

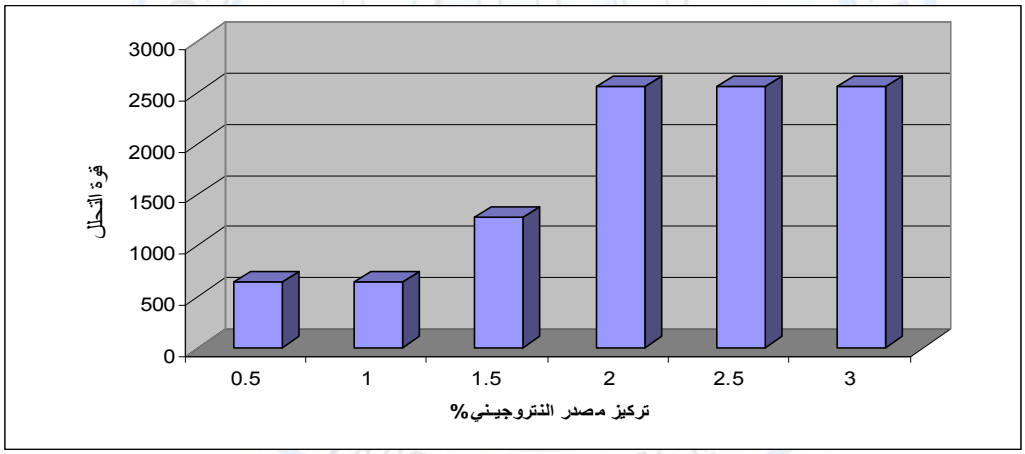

الشكل (7) تأثير تراكيز مختلفة من البيتون في إنتاج إنزيم الهيمولايسين من العزلة المحلية لبكتريا الكوليرا AMK6

إنتاج إنزيم الهيمولايسين Hemolysin مـــن العـــزلـــة المحـلية لبكـتريا

Vibrio cholerae المعزولة من مرضى مصابين بالإسهال

محمد ابراهيم نادر- مثنى عبد القادر صالح المهداوي -ايناس يوسف

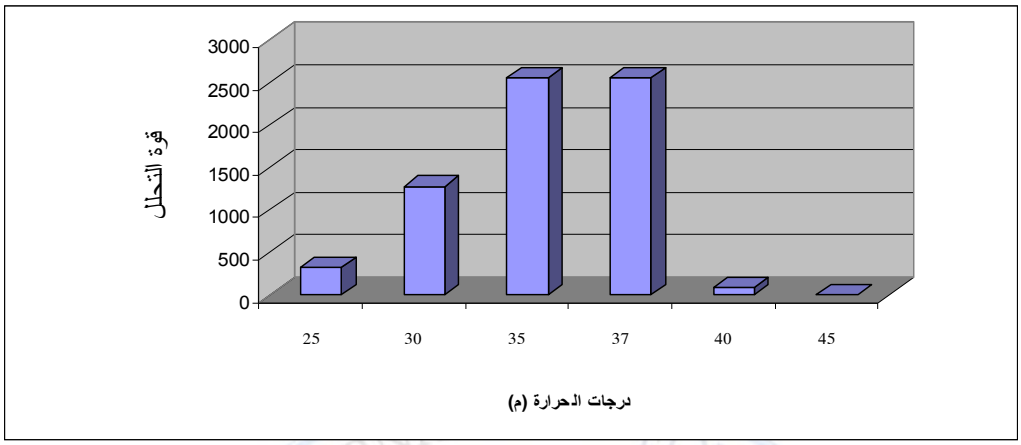

الشكل (8) تأثير درجة الحرارة في إنتاج إنزيم الهيمولايسين من العزلة المحلية لبكتريا الكوليرا AMK6

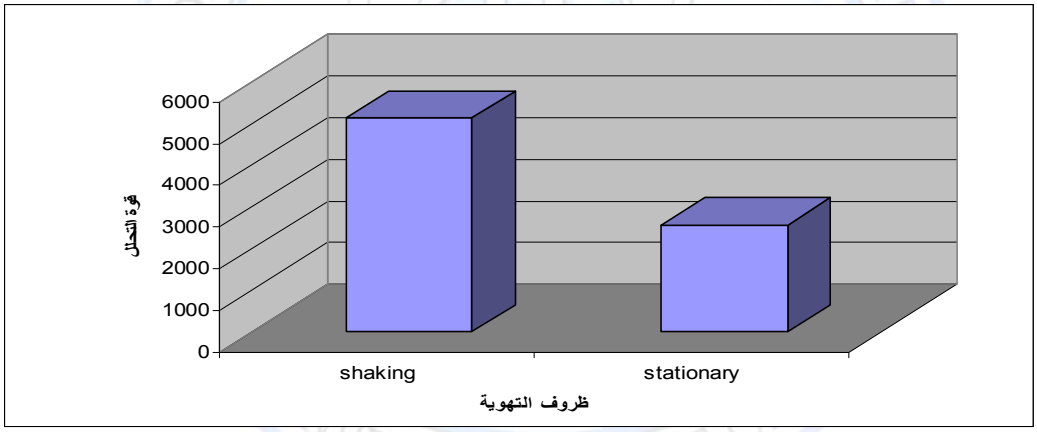

الشكل (9) تأثير التهوية في إنتاج إنزيم الهيمولايسين من العزلة المحلية لبكتريا الكوليرا AMK6

المصادر

1- الزعاك، علي عبد الرحمن (1994). البيولوجي الجزيئي لضراوة البكتريا. مطبعة القبس. بغداد _ العراق.

2- نادر، محمد ابراهيم. (2009). دراسة تأثير السمي للإنزيم البروتيز المنقى من عزلة محلية لبكتريا *Vibrio cholerae* باستخدام الحيوانات المختبرية. معهد الهندسة الوراثية و التقنيات الاحيائية . جامعة بغداد.

3- Tomita, T. and Kamio, Y. (1997). Molecular Biology of pore–forming cytolysine from *Staphylococcus aureus*, alpha and gamma–hemolysin and leukocidin. Biosci. Biotechnol. Biochem. Vol 61 (4) : 565 .

4- Takahashi, Y.; Sato, Y. ; Shiomi , V. V.; Cantraelli, T. (2000). Mechanisms of chloride secretion induced by thermostable direct haemolysin of *Vibrio parahaemolyticus* in human colonic tissue and a human intestinal epithelial cell line. J. Med.Microbiol. (49) : 801 – 810 .

5- Holt, J. G.; Krieg, N. R.; Sneath, P. H; Staley, J. T. and Williams, S. T. (1994). Bergey's Manual of Determinative Bacteriology. (9th ed.). Williams & Wilkins, U.S.A. PP: 190-191,254-255.

6- World Health Organization. (1997). Guide lines for cholera control. WHO Regional. Office for the Eastern Mediterranean

7- الكرخي ، كفاح أحمد جاسم . (2001) . عزل وتشخيص السلالات النمطية وغير النمطية لبكتريا *V.cholerae* من المرضى وحساسيتها للمضادات الحيوية. رسالة ماجستير . كلية العلوم .الجامعة المستنصرية .

8- Namdari, H., and E. J. Bottone. 1990. Microbiologic evidence supporting the role of *Aeromonas caviae* as a pediatric enteric pathogen. J. Clin. Microbiol. 28:837-840

9- Oreilly , T.and Day ,D.F. (1983). Effect of cultural conditions on protease production by *Aeromonas hydrophila* .Appl.Environ. Microbiol.Vol 45 (3) :1132-1135 .

10- Honda,T.and Finkelstein,A.R.(1979).Purification and Characterization of a Hemolyin Produced by *Vibrio cholera* Biotype El Tor :Another Toxic Substance Produced by Cholera Vibrios.J. Infection and Immunity.Vol 26(3):1020-1027.

11- Yamamoto,K.;Ichinose, Y.;Naksone,N.;Tanabe ,M. ;Nagahama,M.;Sakurai,J.and Iwanaga,M. (1986) .Identity of Hemolysins Produced by *Vibrio cholera* Non-o1 and V .cholerae O1,Biotype El Tor . J.Infection and Immunity .Vol51(3):927-931.